ARISTOTLE UNIVERSITY OF THESSALONIKI
FACULTY OF SCIENCES
SCHOOL OF GEOLOGY
DEPARTMENT OF METEOROLOGY AND CLIMATOLOGY

VASILEIOS PAVLIDIS

Physicist

MSc: Meteorology and Climatology

Estimating error and uncertainty of cloud-aerosol-radiation interactions in regional climate model simulations

DISSERTATION THESIS

THESSALONIKI

2020

This research is co-financed by Greece and the European Union (European Social Fund- ESF) through the Operational Programme «Human Resources Development, Education and Lifelong Learning» in the context of the project "Strengthening Human Resources Research Potential via Doctorate Research" (MIS-5000432), implemented by the State Scholarships Foundation (IKY)

ΑΡΙΣΤΟΤΕΛΕΙΟ ΠΑΝΕΠΙΣΤΗΜΙΟ ΘΕΣΣΑΛΟΝΙΚΗΣ
ΣΧΟΛΗ ΘΕΤΙΚΩΝ ΕΠΙΣΤΗΜΩΝ
ΤΜΗΜΑ ΓΕΩΛΟΓΙΑΣ
ΤΟΜΕΑΣ ΜΕΤΕΩΡΟΛΟΓΙΑΣ ΚΑΙ ΚΛΙΜΑΤΟΛΟΓΙΑΣ

ΒΑΣΙΛΕΙΟΣ ΠΑΥΛΙΔΗΣ

Φυσικός

MSc: Μετεωρολογίας-Κλιματολογίας

Εκτίμηση σφαλμάτων και αβεβαιότητας αλληλεπιδράσεων νεφών-αερολυμάτων-ακτινοβολίας σε κλιματικές προσομοιώσεις περιοχικής κλίμακας

ΔΙΔΑΚΤΟΡΙΚΗ ΔΙΑΤΡΙΒΗ

ΘΕΣΣΑΛΟΝΙΚΗ

2020

Το έργο συγχρηματοδοτείται από την Ελλάδα και την Ευρωπαϊκή Ένωση (Ευρωπαϊκό Κοινωνικό Ταμείο) μέσω του Επιχειρησιακού Προγράμματος «Ανάπτυξη Ανθρώπινου Δυναμικού, Εκπαίδευση και Διά Βίου Μάθηση», στο πλαίσιο της Πράξης «Ενίσχυση του ανθρώπινου ερευνητικού δυναμικού μέσω της υλοποίησης διδακτορικής έρευνας» (MIS-5000432), που υλοποιεί το Ίδρυμα Κρατικών Υποτροφιών (ΙΚΥ)

Ευρωπαϊκή Ένωση
Ευρωπαϊκό Κοινωνικό Ταμείο

Επιχειρησιακό Πρόγραμμα
Ανάπτυξη Ανθρώπινου Δυναμικού,
Εκπαίδευση και Διά Βίου Μάθηση
Με τη συγχρηματοδότηση της Ελλάδας και της Ευρωπαϊκής Ένωσης

ΕΣΠΑ 2014-2020
ανάπτυξη - εργασία - αλληλεγγύη

VASILEIOS PAVLIDIS

Physicist

MSc: Meteorology-Climatology

Estimating error and uncertainty of cloud-aerosol-radiation interactions in regional climate model simulations

Completed in the Department of Meteorology and Climatology, School of Geology, Aristotle University of Thessaloniki (AUTh)

Submitted in the School of Geology, Aristotle University of Thessaloniki on March 2020

Date of presentation and defense: 13/02/2020

Annex Number of the Scientific Annals of the School of Geology N^{o}: 196

Thesis supervisory committee

Eleni Katragkou, Assistant Professor, Supervisor

Prodromos Zanis, Professor

Theodoros Karacostas, Emeritus Professor

Examining committee

Eleni Katragkou, Assistant Professor, School of Geology, AUTh

Prodromos Zanis, Professor, School of Geology, AUTh

Theodoros Karacostas, Emeritus Professor, School of Geology, AUTh

Dimitrios Balis, Professor, School of Physics, AUTh

Petros Katsafados, Associate Professor, Department of Geography, Harokopio University

Andreas Kazantzidis, Associate Professor, Department of Physics, University of Patras

Stylianos Kazadzis, Senior Researcher, Physics and Meteorology Observatory Davos, World Radiation Center, Switzerland

ΒΑΣΙΛΕΙΟΣ ΠΑΥΛΙΔΗΣ

Φυσικός

MSc: Μετεωρολογίας-Κλιματολογίας

Εκτίμηση σφαλμάτων και αβεβαιότητας αλληλεπιδράσεων νεφών-αερολυμάτων-ακτινοβολίας σε κλιματικές προσομοιώσεις περιοχικής κλίμακας

Εκπονήθηκε στον Τομέα Μετεωρολογίας και Κλιματολογίας του Τμήματος Γεωλογίας Α.Π.Θ.

Υποβλήθηκε στο Τμήμα Γεωλογίας Α.Π.Θ. τον Μάρτιο του 2020

Ημερομηνία Προφορικής Εξέτασης: 13/02/2020

Αριθμός Παραρτήματος Επιστημονικής Επετηρίδας Τμήματος Γεωλογίας N°: 196

Τριμελής Συμβουλευτική Επιτροπή

Ελένη Κατράγκου, Αναπληρώτρια Καθηγήτρια, Επιβλέπουσα

Πρόδρομος Ζάνης, Καθηγητής

Θεόδωρος Καρακώστας, Ομότιμος Καθηγητής

Εξεταστική Επιτροπή

Ελένη Κατράγκου, Επίκουρη Καθηγήτρια, Τμήμα Γεωλογίας, Α.Π.Θ.

Πρόδρομος Ζάνης, Καθηγητής, Τμήμα Γεωλογίας, Α.Π.Θ.

Θεόδωρος Καρακώστας, Ομότιμος Καθηγητής, Τμήμα Γεωλογίας, Α.Π.Θ.

Δημήτριος Μπαλής, Καθηγητής, Τμήμα Φυσικής, Α.Π.Θ.

Πέτρος Κατσαφάδος, Αναπληρωτής Καθηγητής, Τμήμα Γεωγραφίας, Χαροκόπειο Πανεπιστήμιο

Ανδρέας Καζαντζίδης, Αναπληρωτής Καθηγητής , Τμήμα Φυσικής, Πανεπιστήμιο Πατρών

Στυλιανός Καζαντζής, Κύριος Ερευνητής, Physics and Meteorology Observatory Davos, World Radiation Center, Switzerland

Εκτίμηση σφαλμάτων και αβεβαιότητας αλληλεπιδράσεων νεφών-αερολυμάτων-ακτινοβολίας σε κλιματικές προσομοιώσεις περιοχικής κλίμακας. – Διδακτορική Διατριβή

Estimating error and uncertainty of cloud-aerosol-radiation interactions in regional climate model simulations. – *Ph.D. Thesis*

Citation:

Παυλίδης Β., 2020. Εκτίμηση σφαλμάτων και αβεβαιότητας αλληλεπιδράσεων νεφών-αερολυμάτων-ακτινοβολίας σε κλιματικές προσομοιώσεις περιοχικής κλίμακας. Διδακτορική Διατριβή, Τμήμα Γεωλογίας Α.Π.Θ., Αριθμός Παραρτήματος Επιστημονικής Επετηρίδας Τμ. Γεωλογίας Νο 196, 176 σελ.

Pavlidis. V., 2020. – Estimating error and uncertainty of cloud-aerosol-radiation interactions in regional climate model simulations. Ph.D. Thesis, School of Geology, Aristotle University of Thessaloniki, Annex Number of Scientific Annals of the School of Geology No 196, 176 pp.

Contents

Introductory Note

The aim of this study is to explore the role of aerosol effects on regional climate simulations over Europe, using the Weather Research and Forecasting Model (WRF). We mainly explore the impact of aerosol-radiation interactions (direct and semi-direct effect) but also the implementation of aerosol-cloud interactions (indirect effect) is explored in the model.

This study comprises of two main parts. Part 1 (chapter 1) consists of sensitivity experiments with the WRF model using different aerosol parameterizations and datasets covering the period 2004-2008. In this part we explore the different aerosol options and datasets used and identify the impact of aerosol over Europe. Part 2 (chapter 2) consists of WRF simulations of historical (1971-2000) and future climate (2021-2050) under the Rcp8.5 scenario. The model in these experiments is being driven by the CESM1 global climate model. In this part we assess the impact of aerosol over Europe in a larger (30year, historical) period over Europe and explore their impact in the trends for both the historical and the future period. Detailed discussion of the results from both main parts is presented in the chapter "Summary and Discussion" (chapther 3) whereas the main conclusions are presented in chapter 4 "Conclusions.

The author would like to thank all the people that helped in this thesis, especially the supervisory committee and the supervisor professor Eleni Katragkou. Detailed acknowledgements are given in the end of this thesis.

A. Abstract

Aerosols play a very important role in the climate. This study tries to examine the impact of aerosols, especially the direct aerosol effect, in regional climate simulations over Europe. This study consists of two main parts. The first part consists of sensitivity experiments using the WRF model and implementing different aerosol datasets and climatologies. Results indicate a severe impact on radiation components as well as on temperature. Indications of aerosol induced changes in atmospheric circulation are also presented. The second part of this study focuses on the impact of aerosol on regional climate simulations of the future European climate. Results indicate that the decreasing trend of aerosol concentrations clearly impacts the future temperature trends and increases the impact of global warming.

B. Introduction

What are aerosols

Aerosols are microscopic particles of solid or liquid phase suspended in the atmosphere. They can have varying shapes and occupy a large range of sizes, from nanometers to several micrometers with a typical range being between 0.001 to 10μm (Haywood et al., 2000). The sources of aerosol can be both natural as well as anthropogenic. Natural aerosol include sea salt from the oceans, dust particles as a result of wind action, volcanic sulfate aerosol as well as organic aerosol like spores, pollen and bacteria. Human sources are mainly fossil fuel combustion and biomass burning that produce sulfates, organic carbon, black carbon and nitrates, whereas several human activities that change the land surface may contribute to the dust particle concentrations. Anthropogenic emissions of sulfates, organic and black carbon can be larger than the natural emissions on a global scale (Ramanathan et al., 2001). The vast majority of aerosol reside within the troposphere, close to the sources of production, whereas higher in the stratosphere only aerosols of volcanic origin can be found. Typical aerosol life time is short in the troposphere, between one day and two weeks. However in the stratosphere, aerosols can remain for much longer time scales, typically for around a year (IPCC AR5, 2014). An important characteristic of aerosols, is that their concentrations can have significant spatial and temporal variability. Large aerosol amounts usually are to be found downwind of the sources of production and confined within the troposphere. Therefore beside their important role to the global climate, aerosol impact can be considerably more pronounced and thus of particular significance to the local scale. Volcanic aerosols on the other hand can have a much more widespread effect. Volcanic eruptions are one of the most significant natural sources of aerosol. The large plume of a volcanic eruption can inject aerosols of sulfate origin high into the stratosphere where they can be transferred large distances away from the initial source and remain aloft for an increased amount of time considerably reducing solar radiation at the surface. It is characteristic that some of the largest historical eruptions have clearly impacted the global temperature cooling the entire planet (McCormick et al., 1995).

Aerosol impact

Aerosol, especially the finer particles, can affect human health and thus have been traditionally considered an atmospheric pollutant and their concentrations have been closely monitored. Apart from their effect on human health aerosol can also play a significant role in the atmosphere and generally the climate of our planet (Ramanathan et al., 2001) through different ways. Firstly they can intensely interact with the solar radiation, which lies in the shortwave spectrum, through scattering and absorption. The aerosol-radiation interaction is called the aerosol direct effect. Moreover aerosols can act as cloud condensation nuclei, thus affecting cloud formation, lifetime and albedo. This is called the aerosol indirect effect. Finally aerosol through radiation absorption can change the thermodynamic profile of the atmosphere and as a result affect again cloud formation. This is called the aerosol semi-direct effect. It is therefore clear that aerosol can affect key components of the climatic system like radiation and clouds (Hansen et al., 1997).

Aerosol optical parameters

The aerosol interaction with radiation is described by three main parameters. The most prominent parameter is the aerosol optical depth (AOD) and consists of the integration of the aerosol extinction coefficient along an atmospheric path. It describes the total extinction caused by the aerosol load. The single scattering albedo (SSA) is the ratio of the scattering coefficient to the extinction coefficient and describes the relative significance of the scattering process to the whole aerosol-induced extinction. The asymmetry factor (ASY) is the mean cosine of the scattering angle and describes the mean direction of radiation scattering (American Meteorological Society, 2019).

Direct effect

The direct aerosol effect is quite well understood scientifically (IPCC AR5, 2014). The scattering and absorption of solar radiation by aerosols clearly decreases the radiation that reaches the surface, thus producing a negative radiative effect at the surface. Anthropogenic aerosol mainly interact with the solar radiation while only dust mineral aerosol have a significant interaction with the longwave spectrum of radiation (Dufresne et al., 2002; Ramanathan et al., 2001). Naturally, larger aerosol optical depth leads to larger decreases in shortwave radiation at the surface. Thus the large spatial and temporal variability of aerosol can produce a strong direct radiative effect at a regional scale. For example, in the comprehensive regional climate modeling study of Nabat et al. (2015a), an average annual direct radiative effect of -19 W/m^2 was seen over Europe, that could exceed -40 W/m^2 over specific areas in the south during summer. However, the overall effect of aerosol-radiation interactions depends not only on the immediate scattering and absorption of radiation, but also on the inflicted change in the cloud cover (semi-direct effect).

Semi direct effect

Aerosol semi-direct effect strongly depends on the aerosol absorptivity (IPCC AR5, 2014). Absorption of radiation heats the atmospheric layer and can evaporate cloud droplets or

modify atmospheric stability and as a result it may affect cloud cover. Previously it was considered that the semi-direct effect resulted in cloudiness reduction. However the impact on cloudiness is more complex and depends on the relative position of aerosols to the cloud and the cloud type (Koch and Del Genio, 2010). For example absorbing aerosols below the cloud base may enhance convection and increase cloud cover. On the other hand aerosols above the cloud top can stabilize the atmosphere and may decrease cumulus clouds but increase stratiform ones. Since the semi-direct effect can impact cloudiness, and often reduce it, it has the ability to produce a positive radiative effect at the surface. It is important to note that for absorbing aerosol the positive semi-direct radiative effect due to cloud cover decrease might completely counterbalance the negative direct radiative effect leading to a positive overall aerosol radiative effect at the surface (Johnson et al., 2004).

Indirect effect

The indirect aerosol effect can be considerably impactful on cloudiness and therefore on radiation levels. The role of aerosols as cloud condensation nuclei enables them to impact the size and quantity of cloud droplets. In general, larger aerosol concentrations lead to increased numbers of cloud droplets that are smaller in size, causing an increase in cloud albedo thus leading to larger amounts of solar radiation scattering (first indirect effect). Moreover the decreased size of cloud droplets reduces precipitation leading to cloud lifetime increase (second indirect effect). These two facets of indirect effect are estimated to be of around the same magnitude, around -0.5 to -1.5 W/m^2 on a global average (Lohmann and Feichter 2005).

The theoretical knowledge of the indirect effect however is not as solid as in the case of the direct effect. Aerosol cloud interactions are complex and may occur through numerous pathways. Moreover the impact of the indirect effect is accompanied with a large uncertainty. It is characteristic that aerosols and especially the indirect and semi direct effects are considered one of the main factors of uncertainty regarding the climate and climate change (IPCC 2007, 2014).

Aerosol and Regional Climate Models

Because of their considerable impact, aerosols are an important physical facet of the climate that needs to be considered in any attempts to model the climatic system. Especially due to their impact on radiation, aerosol representation is considered essential in solar energy applications (Gutiérrez et al., 2018).

Since aerosols play an important role all over the globe, there are RCM studies exploring their role over several regions. For example, Qian and Giorgi (1999) used one of the first coupled RCM-aerosol systems to study the effect of sulfate aerosol over eastern Asia. Qian et al. (2003) also explored the regional climate effect of aerosol over China using the MM5 model. Ji et al. (2016) explored the aerosol radiative effect over the Tibetan Plateau and the Himalayas using RegCM4. Sarangi et al. (2018) studied the impact of aerosol-cloud interactions in the Indian summer monsoon using WRF and also over India, the WRF-Chem

study of Kedia et al. (2016) explored the aerosol impact on summer rainfall. Over Africa studies usually have explored the impact of dust aerosol (Solmon et al., 2008, 2012). However Mbienda et al. (2017) used RegCM4 to also assess the impact of anthropogenic aerosol over Central Africa. Our study focuses over Europe, and there are several aerosol studies over this domain (described later in this section) that present a significant impact of aerosol on the regional climate.

However, despite their intense regional effects, the implementation of aerosol in regional climate simulations has not been given sufficient emphasis and attention. Global climate models have been more comprehensive regarding the incorporation of aerosols compared to the regional models. Aerosols, at least the direct effect, are usually considered by the majority of GCM simulations. Unfortunately this is not always the case with RCMs and aerosol representation is in many cases not given the proper attention it deserves. Regional climate models with interactive chemistry (chemistry-coupled) do certainly include detailed aerosol implementation, however these models are extremely computationally demanding, and the bulk of the conducted simulations lack such a detailed representation of atmospheric chemistry.

Indicative of the low attention to the role of aerosols in RCMs, is the fact that even in the context of large ensemble experiments like the regional climate model experiments of the Coordinated Regional Climate Experiment (CORDEX), aerosol implementation presents varying levels of completeness since no specific guide lines are usually addressed (Giorgi and Gutowski, 2015). In the framework of EURO-CORDEX it is characteristic that there are simulations, though a small number, that do not even take at all into account aerosol effects[1]. The majority of the EURO-CORDEX simulations implement aerosol by using aerosol climatologies. These climatologies can be either a completely static aerosol field or can present monthly variations, whereas in limited cases inter-annual trends are also taken into account and are incorporated in the climatological aerosol field. A small number of simulations uses more complex prognostic aerosol schemes with natural and anthropogenic aerosol emission considered. Regarding the aerosol effects represented, the majority of the experiments takes into account only the direct effect. The indirect effect is rarely considered and is usually confined only to simulations using prognostic aerosol.

As said previously, the majority of RCM simulations over Europe implement only aerosol-radiation interactions by using climatological aerosol data. The aerosol climatologies used may vary considerably. Some simulations use relatively old datasets (Tegen et al. 1997 ,Tanre et al. 1984) and not always state of the art information. Using COSMO-CLM over Europe, Zubler et al. (2011) have recommended the RCM community to use updated aerosol climatologies since it has been demonstrated that the use of newer products can have a considerable impact on the simulated climate, especially on shortwave radiation amounts at the surface. A more recent study (Schultze and Rockel, 2018) also concluded that the use of more recent aerosol climatologies is preferable. Some of the newer products of aerosol climatologies are the MACC climatology from the ECMWF (European Center of Medium Weather Forecast) and the MAC-v1 and the more recent MAC-v2 climatologies of the Max-

[1] https://docs.google.com/document/d/1UCCv-DU8hLlZaSPkcndnM0SrJHoX4cvG-yqxbIDZlRc/edit

Planck Institute. A study that compared the use of different climatologies, including MACC and MAC-v1, in satellite remote sensing algorithms, concluded that the MACC data resulted in the highest accuracy of the retrieved solar radiation (Mueller and Träger-Chatterjee, 2014). Another recent aerosol climatology is that of (Nabat et al. 2015). It provides optical depth, for the European-Mediterranean region, including the vertical dimension in the atmosphere, and has been constructed with the use of various remote sensing as well as modeled aerosol products.

RCM studies over Europe

The European region is an area that is affected by aerosols and presents considerable spatial and temporal aerosol load variability (Basart et al., 2009). Dust aerosol coming from Northern Africa frequently reaches large parts of the region, especially those of southern Europe. Moreover since Europe presents substantial industrial and agricultural activities and is in large part a densely populated area, considerable amounts of anthropogenic aerosol (industrial, urban, biomass burning) are also present, even though anthropogenic aerosol concentrations regarding sulfates are decreasing in the last decades.

For the region of Europe, despite that aerosols have not been given primary focus by the bulk of the regional climate model (RCM) simulations, a number of interesting and comprehensive studies has been conducted the recent decades, primarily focusing on the direct and semi-direct aerosol effects. Zanis (2009) in a RegCM study regarding the direct effect of anthropogenic aerosols for the summer of 2000 found a significant aerosol impact on surface temperature that amounts up to 1.2C. Moreover aerosol induced changes in the atmospheric circulation are observed and particularly a southward shift of the subtropical jet stream. In a later RegCM study, of 12 years, (Zanis et al., 2012) the aerosol induced cooling in annual mean temperature was largest over the Balkan Peninsula amounting to -0.2^{o}C. Moreover changes in the atmospheric circulation have also been observed. However the changes in both circulation and temperature have been in the verge of statistical significance in this study, indicating a constrained feedback of aerosol direct effect on the European climate. Another RegCM study over Europe, that of (Huszar et al., 2012), found intense regional seasonal perturbations of surface temperature with the introduction of aerosols in the range of ±1.5^{o}C. It is interesting that all the above studies do not find a clear spatial correlation between the aerosol load, and consequently radiative forcing, and the induced changes in temperature. This is a clear indication of the complexity and non-linearity of aerosol impact on the climate system.

A CNRM study of dust aerosols for the 2012 summer (Nabat et al. 2015b) over the Mediterranean concluded that the use of a prognostic aerosol scheme was superior to the use of monthly averaged AOD means. The prognostic scheme succeeded in simulating the dimming associated with dust events and improved the representation of surface temperature compared to the use of AOD means.

Nabat et al. (2015c) conducted a comprehensive study of aerosol direct effect on the climate of the EURO-Mediterranean region. Using CNRM with aerosols taken into account as inter-

annual AOD climatologies. Aerosol direct effect produced a negative surface radiative forcing (-14.7 W/m2 average over Europe). Interestingly the semi-direct effect calculated on the other hand was positive and responsible for partially offsetting the direct effect impact, due to changes in cloudiness and atmospheric circulation. However the overall aerosol radiative effect was negative and produced an average temperature decrease of -0.4^{o}C over Europe, including sea surface. One of the major conclusions of this study indicated the importance of coupling an RCM with an ocean model over the Mediterranean. If the sea surface temperature cannot be modified, the aerosol induced feedbacks and overall impact are attenuated (or are not shown to their full extent).

Schultze and Rockel (2018) conducted a long term COSCO-CLM study over Europe covering a 60 year period. They used different aerosol climatologies and concluded that the older default climatology used by the model (Tanre et al. 1984) should be replaced with newer more up to date datasets. Moreover this study also showed a widespread shortwave radiation reduction at the surface that was larger during summer that led to a modest seasonal mean cooling. The vertical profile of temperature changes is characterized by a near surface cooling that is shallow, while warming happens higher in the troposphere. This results is the stabilization of the atmosphere which in turn leads to the decrease of cloud fraction and precipitation.

The study of Alexandri et al. (2015) assessed the ability of the RegCM4 model to simulate solar radiation at the surface over Europe. It highlighted the importance of aerosol impact on radiation concluding that aerosol optical depth is one of the most important parameters affecting solar radiation levels and variability, besides of course cloud cover and cloud optical depth.

Aerosol-cloud interactions (indirect effect) have not been usually implemented in RCM simulations over Europe. In order to capture both aerosol-radiation (ARI) and aerosol-cloud (ACI) interactions these is a need to use models that have online aerosol estimation. This is usually done with complex coupled meteorology-chemistry models. Such modeling studies focusing on the effects of both aerosol-radiation and aerosol-cloud interactions have been conducted over Europe. However since these models are computationally very expensive, the studies focus mainly on specific events and case studies and usually do not cover periods larger than several months. For example, Forkel et al. (2012), used WRF-Chem over Europe to simulate June and July of 2006 and assess the impact of including aerosol-radiation and aerosol-cloud interactions. They found a mean solar radiation reduction over central Europe around 3-7 W/m^2. However changes in the cloud cover due to the semi-direct aerosol effect had a much greater regional impact, and the semi-direct effect dominating over the aerosol-radiation interactions. Moreover an intense response in precipitation was seen with regional changes between ±100%. Another study by Forkel et al. (2015) used an ensemble of eight WRF-Chem simulations over Europe for the year 2010. Focusing on a Russian wildfire episode for the summer of that year, the study found a large reduction of mean seasonal solar radiation by 20 W/m^2 and a reduction of mean temperature drop of 0.25^{o}C. The same wildfire episode was also studied with the WRF-Chem model by Péré et al. (2014) who found

a large reduction of solar radiation over Eastern Europe and a decrease in temperature between 0.2 and 2.6°C. Baró et al. (2017) conducted an evaluation of an ensemble of coupled meteorology-chemistry models that simulated online aerosol concentrations, in order to assess the aerosol impact on regional temperature. Two case studies were examined for the year 2010 over Europe. They concluded that the inclusion of aerosol-radiation interactions did not clearly improve the bias, however the spatial and temporal correlation and variability were improved. Tuccella et al. (2019) used the WRF-CHIMERE coupled meteorology-chemistry model to simulate aerosol-cloud interactions over Belgium and the Netherlands for May 2008. They concluded that aerosol indirect effect had a positive radiative effect at the surface for both shortwave and longwave radiation, with the overall net increase being around +1W/m^2. Moreover they found strong impacts on local scale temperature and precipitation.

Finally, an interesting study of Da Silva, Mailler, and Drobinski (2018) explored the effects of aerosol-cloud interactions on summer precipitation over Europe. However they did not use a meteorology-chemistry coupled model. They used the ordinary WRF model and the Thompson aerosol-aware microphysics scheme (Thompson and Eidhammer, 2014). This scheme presents a computationally efficient way of simulating aerosol-cloud interactions. They concluded that increased aerosol loads lead to precipitation reduction both in the low resolution (50km) simulations as well as in the convection permitting high resolution simulations (3.3km).

Weather Research and Forecast Model

Among the various regional climate models, the Weather Research and Forecasting (WRF) model(Powers et al., 2017; Skamarock et al., 2008) is a widely used RCM by many users around the world. Earlier versions of WRF did not provide many options regarding the simulation of aerosol effects. However recent versions (especially after version 3.6 and on) provide several parameterizations that simulate aerosol-radiation as well as aerosol-cloud interactions. Therefore studies with the WRF model have been performed to assess aerosol impact on the weather and the climatic system Ruiz-Arias, Dudhia, and Gueymard (2014) presented a new parameterization regarding aerosol-radiation interactions and investigated the aerosol impact on radiation over the US. They concluded that the parameterization works satisfactory for simulating solar radiation. Furthermore the inclusion of aerosol – radiation interactions considerably enhanced radiation prediction and improved the seasonality of the bias. Aerosol-cloud interaction simulation is also recently available in WRF through a cloud microphysics scheme, the Thompson aerosol-aware scheme (Thompson and Eidhammer, 2014). This scheme is not very computationally demanding so that it can be easily used in weather forecasting and solar applications as well as longer climate projections without considerably increasing simulation run time. As described above Da Silva used the Thompson aerosol-aware scheme to explore the effect of aerosol-cloud interactions over Europe. Jimenez et al. (2016) used both the aerosol-radiation parameterization (Ruiz-Arias et al., 2014) and the Thompson aerosol-aware scheme to simulate solar radiation over North America. The inclusion of aerosol effects resulted in

significant improvement of radiation prediction especially on the direct and diffuse components of solar radiation.

Solar dimming and brightening

The overall aerosol load presents considerable temporal variability, and in several cases long term inter-annual trends have been observed. For example, before the early 1990s a global average increase in aerosol load had been observed which was followed by a decrease in global aerosol concentrations for the more recent decades. It is characteristic of the severe impact of aerosol on radiation that the trends in aerosol load have been linked with observed trends in shortwave surface radiation (Rsds) (Streets et al., 2006). Therefore the global decrease in Rsds (dimming) before the 1990s has been mainly attributed to the aerosol load increase and the subsequent increase of radiation (brightening) to the global aerosol load reduction (Wild 2009). This effect is even more pronounced at regional scales over Europe and North America (Cusworth et al. 2017-for the US). In these two regions it is thought that a stricter environmental legislation has lead to decreased aerosol emissions (Vestreng et al., 2007) thus affecting radiation levels at the surface. For the rest of the world (Mehta et al. 2016-period 2001-2014) decreasing aerosol trends are found also over South America and certain parts of southeast Asia and China that up until recently had been exhibiting increasing aerosol pollution. On the other hand, clear increase of aerosol concentration is present over the Indian subcontinent and the Arabic Penninsula. Over Europe the diming phase has been detected in the period 1950s to mid 1980s with a shortwave radiation trend estimated to be around -2 to -10W/m^2 per decade. After 1990 a clear brightening period is observed whereas estimates for the increase of shortwave radiation between 1 to 5 W/m^2 per decade (Wild 2009). Regarding climate models, both global and regional, the correct simulation of the observed trends in shortwave radiation at the surface (Rsds) proves to be a difficult task, especially for the regional ones. Since many of the regional models use aerosol climatologies that do not evolve with time, the main physical mechanism responsible for the Rsds trends is not taken into account. Moreover since Rsds levels definitely impact near surface temperature, the aerosol induced trends in Rsds can impose a time evolving influence upon temperature. The brightening over Europe of the recent decades, with larger radiation amounts at the surface, tends to increase temperature levels further enhancing the impact of climate change. Therefore the realistic representation of future aerosol trends is considered a very important part of simulations of the future climate, especially regarding heat extremes (Xu et al., 2018). A study by van Oldenborgh et al. (2009) shows that GCMs tend to underestimate the temperature trend in western Europe for the recent decades and incorrect representation of aerosol trends, among other factors, does play a role. However Zubler et al. (2011) using a regional climate model to simulate the European climate from 1958 to 2001 found that the use of static aerosol climatology or time evolving aerosols had a much lesser impact to the Rsds amounts and trends compared to the internal variability of the model. The aerosol effects on clear-sky radiation trend were strong, but for all-sky radiation the role of cloudiness produced less definitive results. However, newer RCM simulations, implementing also a coupling with ocean model, indicate that long-term trends in radiation and temperature over the Euro-

Mediterranean region are definitely linked to trends in aerosol load (Nabat, Somot, Mallet, Sanchez-Lorenzo, et al. 2014). Moreover these trends in temperature and radiation cannot be reproduced correctly without the use of aerosol effects in the RCM simulations. Finally, aerosols might also play a role in shaping the future shortwave radiation amounts at the surface. A study by Bartók et al. (2017) showed large discrepancies in the future (2006-2100) shortwave radiation at the surface, between GCMs and RCMs over Europe. Global models showed an increase in the future compared to the historical period, whereas a decrease was seen in RCMs. These discrepancies were mainly attributed to the different behavior of cloudiness amount between GCMs and RCMs. However, the different representation of aerosol did have some impact in shortwave radiation amounts.

C. The goal of this study

As it can be clearly be seen from the introduction above, aerosols play a complex and significant role in the climate. Some significant studies regarding aerosols in regional climate models have been published the last decade but unfortunately aerosol effects have not been given the proper attention they deserve in atmospheric models especially in regional models. The main goal of this study is to investigate the impact of aerosols in regional climate simulations over Europe. Focus is given in aerosol-radiation interactions but the aerosol-cloud interactions (indirect effect) is also investigated. We aim to assess the role of aerosols on simulations of both the current and the future climate. Since aerosol concentrations present clear trends in their temporal evolution, we also aim to investigate the role of aerosols in the climate change signal. We use a very popular regional climate model, the Weather Research and Forecasting (WRF). As a result a secondary goal is to assess the aerosol parameterizations offered in the RCM and the sensitivity of the model to different aerosol options and datasets. To conclude this study aims to address the following questions:

What is the impact of aerosols on the European Climate?

What are the aerosol parameterizations in the WRF model and what is the sensitivity of the model to different aerosol options and aerosol datasets?

How can aerosol temporal evolution affect the signal of the climate change?

What is the uncertainty aerosols induce in the climate simulation and how does it compare to the uncertainty attributed to other parameterizations?

D. Outline

This study comprises of two main parts. Part 1 consists of sensitivity experiments with the WRF model using different aerosol parameterizations and datasets covering the period 2004-2008. In this part we explore the different aerosol options and datasets used and identify the impact of aerosol over Europe. Part 2 consists of WRF simulations of historical

(1971-2000) and future climate (2021-2050) under the Rcp8.5 scenario. The model in these experiments is being driven by the CESM1 global climate model. In this part we assess the impact of aerosol over Europe in a larger (30year, historical) period over Europe and explore their impact in the trends for both the historical and the future period.

E. Observational data

In this section we present the observational data used in the evaluation of the climate simulations. Data from ground-based measurements as well as satellite data have been used.

Temperature and precipitation

Regarding near surface temperature (2m) and precipitation model simulations are compared to the E-OBS v16 dataset (Haylock et al., 2008). It is a gridded dataset based on ground measurements covering the entire EURO-CORDEX domain. The gridding process is performed in a way so that the value of each grid point is representative of the condition of the whole grid box. This facilitates the use of this dataset in evaluation studies of model simulations. The E-OBs dataset has some limitations. In a comparison against regional datasets of higher station density (Hofstra et al., 2009) it presented a mean absolute error of 0.5^{o}C for temperature whereas in general it underestimated precipitation with differences exceeding in some cases 100%. Moreover gridded precipitation datasets over Europe present in general large uncertainties over mountainous areas and over environments with frequent snow fall.

For trend analysis in near surface temperature, we also use the E-OBS v19.0eHOM dataset. This is a homogenized version of the E-OBS v19.0e dataset (Squintu et al., 2019).

Radiation

We use the Surface Solar Radiation Data Set - Heliosat (SARAH)-Edition1 in order to assess shortwave downwelling radiation at the surface (Rsds) and direct normalized irradiance at the surface (DNI). This is a dataset based on satellite observations from geostationary Meteosat satellites that use the MVIRI and SEVIRI instruments (Müller et al., 2015). It is a gridded dataset with a high spatial resolution of 0.05° x 0.05°. Monthly values of the SARAH dataset have been used.

For Rsds evaluation we have also used another satellite dataset, the CLARA-A1 (Karlsson and Johansson, 2013). This is a dataset with global coverage and includes not only radiation but a number of other products such as cloud cover and characteristics. The CLARA dataset is based on polar orbiting satellites using the Advanced Very High Resolution Radiometer (AVHRR). It is a gridded dataset with a resolution of 0.25^{o}, lower than that of SARAH.

We have obtained both the SARAH and CLARA-A1 datasets from the Satellite Application Facilities for Climate Monitoring (CMSAF) a part of the European Organization for the Exploitation of Meteorological Satellites (EUMETSAT).

For radiation at the surface SARAH is the better product with better accuracy (< 5W/m^2), less estimated uncertainty (<10W/m^2) and less missing data. We have conducted a comparison of the two datasets and found that differences are in general small not exceeding 15% for most regions and seasons. However larger differences are found in north latitudes, especially over Scandinavia during winter. Large latitudes can be challenging for the geostationary satellites (Schulz et al., 2009) (like those used in SARAH dataset) and also areas of extensive snow cover increase measurement uncertainty. To conclude we have chosen to use the SARAH dataset for the radiation (Rsds) evaluation since differences between the two datasets are small and spatial patterns of radiation are very similar (spatial correlation >0.95). The CLARA-A1 dataset however is being used in some cases in order to take into account observational uncertainty.

Cloud fraction

We use the term "cloud fraction" to describe the total column cloud fraction over a grid cell. Cloud fraction is evaluated against the CLARA-A1 satellite dataset (Karlsson et al., 2013) described above. This cloud fraction dataset has been evaluated against global synoptical observations and presented satisfactory results producing a small overestimation of 3.6% (Karlsson and Hollmann 2012). Moreover when compared against measurements from the CALIOP/CALIPSO instrument (satellite based as well) it presented an underestimation of -10%.

Moreover, we also use the CLAAS-2 record of cloud properties (Benas et al., 2017). It is derived by the SEVIRI instruments being carried by the Meteosat second generation (MSG) geostationary satellites. We use monthly mean values on a 0.05^ox0.05^o resolution grid.

Aerosol optical depth

Since several aerosol datasets have been used in this study we wanted to perform an evaluation of the aerosol optical depth (at 550nm) provided by these different sources. For this purpose we use the aerosol optical depth (AOD) at 550nm of the MODIS Level-3 (L3) Atmosphere Monthly Global Product (Platnick et al., 2015; Hubanks et al., 2019). This is a satellite gridded dataset of various atmospheric parameters with a global coverage on a 1x1 degree resolution. It estimates AOD for non cloudy conditions in daytime. We use monthly mean values of AOD.

To improve confidence in the evaluation we also use AOD estimates of the CMSAF climate data record (Clerbaux 2017). This is a satellite based dataset using measurements from the SEVIRI instrument on the Meteosat Second Generation satellites and implementing the Land Daily Aerosol (LDA) algorithm. For our study monthly AOD estimates have been used.

1. PART 1: Sensitivity simulations

1.1 Simulation general characteristics

The model used to perform all the simulations of this study is the Weather Research and Forecasting Model (WRF) version 3.8.1 using the ARW core (Skamarock et al. 2008, Power et al. 2018).

The simulations are forced by the ERA-Interim reanalysis dataset (Dee et al., 2011). Domain setup follows the EURO-CORDEX specifications (Giorgi and Gutowski, 2015). Simulations are performed over Europe with a resolution of 0.44^{o} (~50km) covering the area between 25N-75N and 40W-75E. The domain is partitioned in 131x130 grid points in the horizontal dimension whereas in the vertical dimension 31 vertical levels are used with the top of the atmosphere reaching 50hPa. A 9 grid cell relaxation zone is used at the boundaries. The simulations of the sensitivity study cover the period 2004-2008, while 2003 is used as spin up time. We have selected this time period since it overlaps temporary with several satellite datasets used for the validation process as well as with several aerosol optical depth datasets. The simulations are all conducted with the exact same model setup while they differ only in the aerosol parameterizations and datasets used (see section 1.3). The exception is simulation icloud1 that uses another cloud fraction parameterization from the control simulation.

The basic model parameterizations used:

We use the RRTMG (Iacono et al., 2008) radiation scheme for both shortwave and longwave radiation simulation. We also use the CLM4 (Lawrence et al., 2011; Oleson et al., 2010) land surface model, the revised-MM5 surface layer scheme (Jiménez et al., 2012) the Yonsei University (Hong et al., 2006) boundary layer scheme and the Grell-Freitas cumulus scheme (Grell and Freitas, 2014). For fractional cloud cover the “icloud=3” option in the namelist is used which is based on the relative humidity threshold method of Sundqvist et al. (1989). Also sub-grid cloud fraction interaction with radiation is enabled with the “cu_rad_feedback” option enabled (Alapaty et al., 2012). Finally we use the Thompson microphysics scheme (Thompson et al., 2008) in six simulations and the Thompson aerosol aware microphysics scheme (Thompson and Eidhammer, 2014) in three simulations (Table1). The Thompson aerosol-aware scheme allows for aerosol-cloud interaction (indirect effect), a process that is absent from the 2008 Thompson scheme.

1.2 Aerosol options in WRF model

Aerosol-radiation interactions

The WRF model, when the RRTMG shortwave radiation scheme is used, provides three main aerosol-radiation parameterizations. All of them enable aerosols to interact only with the

solar (shortwave) radiation spectrum. In the case of the RRTMG shortwave scheme, the spectrum covers the range 0.2–12.2 mm.

1. The first option enables the model to use the aerosol optical depth (AOD) climatology of Tegen et al. (1997) to interact with radiation (aer_opt=1 in the namelist). This climatology has a coarse resolution of 5 degrees in longitude and 4 degrees in latitude and includes monthly variations of AOD throughout the year. Five different aerosol types are taken into account: organic carbon, black carbon, sulfate, sea salt, dust. The overall AOD provided in the model is an aggregate of the five aerosol types. It is important to note that the Tegen climatology is 4-D and also provides a vertical dimension in the aerosol optical depth which is thus provided in every vertical level of the model.

2. The second option enabling aerosol-radiation interactions (aer_opt=2 in the namelist) (Ruiz-Arias et al., 2014) permits the user to provide the aerosol data in the model. The user can choose to provide either fixed values of aerosol optical depth and aerosol properties, or aerosol data with spatial and temporal variations through an external file. In the latter case, the user needs to provide the total column aerosol optical depth at 550nm over every grid point. The vertical distribution of aerosol optical depth is parameterized by this option assuming an exponential profile (Ruiz-Arias et al., 2013) (Fig. 5 - middle row). Three other aerosol optical properties, the single scattering albedo (SSA), the asymmetry factor (ASY) and Angstrom exponent (AE) can also be provided by the user from an external data source or they can be parameterized through a selection of “aerosol type” in the model namelist. In the current aerosol parameterization three “aerosol types” are available: rural, urban and maritime. We have experimented with the first two. The “rural” aerosol type represents aerosol that are not heavily affected by industrial or urban sources. It comprises of a mixture of 70% water soluble aerosol and 30% dust aerosol. On the other hand the “urban” type is a mixture of 80% “rural” type aerosol and 20% black-carbon aerosol. Therefore the “urban” type becomes significantly more absorbing than the “rural” one. Finally the relative humidity level is also taken into account for the parameterization of the aforementioned aerosol optical properties.

3. The third option (aer_opt=3 in the namelist) enables the model to use the aerosol data generated by the Thompson aerosol aware microphysics scheme to interact with the radiation. In essence it is based on the second aerosol-radiation interaction option (aer_opt=2) and it uses the total AOD from the generated aerosol field and the “rural” aerosol type to describe the aerosol properties. More information about the Thompson aerosol-aware scheme is given in the next paragraph.

Aerosol-cloud interactions

Aerosol-cloud interactions are possible through the use of the Thompson aerosol-aware cloud microphysics scheme (Thompson and Eidhammer, 2014). The scheme separates aerosol into water-friendly aerosol that act as cloud condensation nuclei (CCN) and ice-friendly aerosol that act as ice nuclei (IN). For the water friendly aerosol category: sea salt, sulfates and organic carbon are taken into account. These aerosol types constitute a large

fraction of the CCN found in clouds all over the world. As ice nuclei only dust particles larger than 0.5 μm are considered. Black carbon is not considered in the scheme. Aerosol number concentrations of the two aerosol types are explicitly predicted by the scheme. The scheme uses an aerosol climatology to initialize the aerosol field and provide boundary conditions. The climatology used is based on the Goddard Chemistry Aerosol Radiation and Transport (GOCART) model (Ginoux et al., 2001) and is constructed from global simulations for the period 2001-2007 (Colarco et al., 2010).

Then the two aerosol categories are advected within the model domain able to act as condensation nuclei in the right conditions whereas a surface emission flux of droplet-nucleating aerosol is added at the surface in every model time step. This emission flux is artificial and is based on the initial aerosol optical depth and the mean wind. In the version 3.8.1 of WRF used in this study no emission flux is available for the ice-nucleating aerosol. With the above mechanisms of aerosol initialization, emissions, sinks and advection the Thompson scheme achieves a 3 dimensional aerosol field that is constantly evolving. In essence what the Thompson aerosol aware scheme tries to achieve with the above way of aerosol description, is to generate an aerosol field that on the long term approximates the GOCART climatology but on the short term changes according to the atmospheric conditions.

Finally as mentioned before, the aerosol generated by the Thompson aerosol-aware scheme can also be enabled to interact with the radiation (aer_opt=3) enabling both aerosol-radiation and aerosol cloud interactions in a model simulation.

1.3 Sensitivity simulations description

We have performed a control experiment and 9 sensitivity experiments based on the original control simulation. For 8 of the simulations the aim of the sensitivity study is aerosols and their implementation in the model. Thus different aerosol sources and datasets have been used. One simulation explores the impact of the cloud fraction scheme parameterization and is examined in a different chapter. All the simulations span the period between 2004 to 2008. Here is a list of the sensitivity experiments conducted:

- The control experiment (CON). It does not take aerosol into account at all, thus neither aerosol-radiation nor aerosol-cloud interactions are included. The basis on which the rest of the sensitivities are performed.

Aerosol-radiation interaction

- The simulation ARI_T that enables aerosol-radiation interactions and uses the Tegen (1997) climatology.

The next four simulations also enable aerosol-radiation interactions and use the parameterization of Ruiz-Arias, Dudhia, and Gueymard (2014) (aer_opt=2):

- ARI_Mv1 uses AOD of the MACv1 climatology and the “rural” aerosol type.

- ARI_Mv1urban uses AOD of the MACv1 climatology and the considerably more absorbing "urban" aerosol type.
- ARI_Mv1full uses AOD, single scattering albedo (SSA) and asymmetry factor (ASY) from the MACv1 climatology. The "rural" aerosol type is used to parameterize only the Angstrom exponent (AE).
- ARI_MC uses AOD of the MACC reanalysis and the "rural" aerosol type.

The implementation of aerosol-radiation interactions in a simulation enables both the direct and semi-direct effects. All of the above simulations described use the Thompson cloud microphysics scheme (mp=8) (Thompson et al., 2008) that does not include aerosol-cloud interactions. The "urban" aerosol type is considerably more absorbing than the "rural". It is characteristic that in our experiments the single scattering albedo (SSA) values for the "rural" type range between 0.92 and 0.98 whereas for the "urban" type they start at 0.6. These values are unrealistically absorbing (Rodríguez et al., 2013; Tombette et al., 2008; Witte et al., 2011) and therefore we treat ARI_Mv1urban as an idealized experiment that showcases the effects of extremely absorbing aerosols.

Aerosol-cloud interaction

These simulations use the Thompson aerosol-aware scheme (mp=28 in the model namelist) that includes aerosol indirect effect. We often refer to the Thompson aerosol-aware scheme as the TE2014.

- Simulation ACI includes only aerosol-cloud interactions.
- Simulation ARCI includes both aerosol-cloud and aerosol-radiation interactions. It presents the most complete representation of aerosol effects in our study.
- Simulation ARCI_no is the same with ARCI except that the microphysics scheme does not pass the calculated effective radii of cloud particles to the radiation scheme. This hinders the full effect of the aerosol-cloud interactions.

Simulation ARCI_no is performed in order to estimate the significance of the process of communication between the radiation and cloud microphysics schemes in terms of cloud particle effective radii. It is not part of the main sensitivity ensemble that assesses and is examined in a different section (1.5.3.11)

- Simulation icloud1 is the same with control CON, thus having no aerosol, except that it uses a different scheme to parameterize cloud fraction amount (icloud=1 in the namelist). It is conducted in order to assess the impact of the cloud fraction scheme and compare it to the sensitivity of the aerosol options and data. It is examined in a different section apart from the main aerosol sensitivity.

It is evident that the simulations are named according to the aerosol effects they implement, either aerosol-radiation (ARI) or aerosol-cloud (ACI) interactions. The simulations that have only aerosol-radiation interactions (ARI in their names) are referred to as the ARI group of

simulations. For the implementation of both aerosol-radiation and aerosol-cloud interactions we use ARCI in the naming.

The simulations conducted for the sensitivity study and information about the aerosol implementation and parameterizations used are presented in Table 1 below.

Table 1: Simulations conducted and aerosol-physics options used in the sensitivity study. Blue header for the main simulations used for the aerosol sensitivity study. Pale pink header for two secondary simulations that are examined at different sections.

Simulation	CON (Control)	ARI_T	ARI_Mv1	ARI_Mv1 urban	ARI_Mv1full	ARI_MC	ACI	ARCI	ARCI _no	icloud1
Mp scheme	Thompson 2008	Thompson 2008	Thompson 2008	Thompson 2008	Thompson 2008	Thompson 2008	Thompson Aerosol 2014	Thompson Aerosol 2014	Thompson Aerosol 2014	Thompson 2008
Aerosol radiation option	-	1	2	2	2	2	-	3	3	-
Aerosol source	-	Tegen	MACv1	MACv1	MACv1	MACC	GOCART	GOCART	GOCART	-
User input data	-	No input by user	AOD, ”rural” aerosol type	AOD, ”urban” aerosol type	AOD,SSA, ASY + ”rural” aerosol type	AOD, ”rural” aerosol type	-	-	-	-
Aerosol interacting with	-	**radiation**	**radiation**	**radiation**	**radiation**	**radiation**	**clouds**	**radiation + clouds**	**radiation + clouds**	-
Eff. Radii passing from microphysics to radiation scheme	yes	yes	yes	yes	yes	yes	yes	yes	no	yes

Cloud fraction scheme	Sundqvist	Sundqvist	Sundqvist	Sundqvist	Sundqvist	Sundqvist	Sundqvist	Sundqvist	Sundqvist	Xu-Randall

1.4 Methodology

In this section we describe the methodology followed in the analysis.

Several variables are analyzed. The main variables are: temperature at 2m, precipitation, shortwave down welling radiation at the surface (Rsds), direct normalized irradiance at the surface (DNI), diffuse irradiance at the surface (DIF), total cloud fraction (CFRACT) and cloud fraction of different level clouds and the wind field at various pressure levels.

In addition to CFRACT we also analyze cloud fraction of low (<2.5 km), medium (2.5<z<6 km) and high (>6 km) level clouds. Calculation of cloud fraction for each cloud category is performed according to the random overlapping method. Thus the total cloud fraction C_{rand} for two layers is considered as: $C_{rand} = c_a + c_b - c_a c_b$ where c_a, c_b are the cloud fraction in each layer (Hogan and Illingworth, 2000).

In order to assess the effect of aerosol on radiation we calculate the metrics below:

i. The radiative effect of aerosol on shortwave radiation at the surface (RE). It is the difference in net shortwave radiation at the surface (netSw) between an aerosol simulation and the control experiment CON. Thus $RE = netSw\_Aerosol - netSw\_Control$

ii. The direct radiative effect of aerosol on shortwave radiation at the surface under clear-sky conditions (DRE). This is the difference in net (downwelling-upwelling) clear-sky shortwave radiation at the surface (netCSw) between an aerosol simulation and the CON experiment. Thus $DRE = netCSw\_Aerosol - netCSw\_Control$. Because the DRE is calculated under clear-sky conditions it accounts only for the direct aerosol effect and not the semi-direct effect.

iii. The effect of clouds on shortwave radiation at the surface (SCRE). It is the difference of the net shortwave radiation at the surface (netSw) and the net clear-sky shortwave radiation at the surface (netCSw) for a given experiment: $SCRE = netSw - netCSw$.

iv. In a similar way the effect of clouds is also calculated at the top of the atmosphere (SCRE_TOA). It is the difference of the net shortwave radiation at the top (netSw_TOA) and the net clear-sky shortwave radiation at the stop (netCSw_TOA) for a given experiment: $SCRE\_TOA = netSw\_TOA - netCSw\_TOA$.

Therefore, $SCRE_{TOA} = (swdt - swut) - (swdtc - swutc)$, where swdt is the shortwave downward radiation at the top of atmosphere, swut is the shortwave upward radiation at top, swdtc is the clear-sky shortwave downward radiation at top and swutc is the clear-sky shortwave upward radiation at the top. Since swdt and swdtc are equal (no clouds and aerosol in space) we have that:

$SCRE_{TOA} = swutc - swut$.

v. In order to assess the impact of the aerosol implementation on the radiative effect of clouds, the difference of SCRE (ΔSCRE) is calculated between an aerosol experiment and CON. Therefore $\Delta SCRE = SCRE_{Aerosol} - SCRE_{Control}$ = $RE - DRE$.

When a simulation that includes only aerosol-radiation interactions is compared against the control experiment CON, the calculated ΔSCRE accounts for the semi-direct effect of aerosols. The change in cloud forcing is also calculated in a similar way for the top of the atmosphere (TOA) as:

$\Delta SCRE\_TOA = SCRE\_TOA_{Aerosol} - SCRE\_TOA_{Control}$.

In general, in order to assess the impact of aerosol effects implementation in the model we compare a simulation that includes aerosol effects against the control experiment CON. In order to assess the impact of aerosol-radiation interaction we compare the simulation family ARI (aerosol-radiation interaction only) to CON. When comparing the simulation ACI (aerosol-cloud interactions only) to CON we assess the impact of the Thompson aerosol-aware microphysics scheme that includes aerosol-cloud interactions (indirect effect). This comparison does not clearly isolate the impact of aerosol-cloud interactions since CON and ACI use different cloud microphysics schemes (Thompson2008 and TE2014 respectively) thus the indirect effect is not just turned on or off. Therefore in our study we assess the impact of indirect effect implementation in the model through the TE2014 scheme.

Lastly, the only situation when we do not compare a simulation against control experiment CON is when we compare ARCI to ACI. Both use the Thompson aerosol-aware scheme and include aerosol indirect effect. The ARCI to ACI comparison indicates the impact of aerosol-

radiation interaction implementation in an environment where the indirect effect is also active.

For the evaluation process we use the metrics: Bias (model-reference), Absolute Bias (|model-reference|) and relative Bias ((model-reference)/reference)*100. The same metrics (named Difference, Absolute Difference and Relative Difference) are also used in the comparison between the simulations themselves when the control experiment (or ACI) is considered as reference data. We use the Mann-Whitney non-parametric test to calculate statistical significance at the 0.05 level since many of the variables examined deviate from a normal distribution. We use mean daily values to calculate statistical significance on a seasonal basis in order to have a sufficient number of data since the sensitivities span only 5 years. The use of the monthly or seasonal values would be problematic for this purpose. In our opinion the use of daily values does not degrade the results of the statistical significance tests. On the contrary we believe that it is an even harder test of significance, than the use of monthly values, since the variables examined present a much larger variability on a day-to-day basis. Thus only a very robust signal of statistical significance can be detected by this method.

In order to be able to compare model results and observational data at a grid point level we remap the data on a common grid. We use the distance weighted average remapping method using the four nearest neighbor values and always remap from the finer resolution grid to the coarser one. As a result, the satellite products are remapped onto the WRF 0.44^{o} grid. On the other hand model temperature and precipitation results are remapped onto the E-OBS 0.44^{o} rotated grid. Moreover, simulated temperature is corrected with respect to the E-OBS elevation, using a temperature lapse rate of 0.65 K/km all over the domain.

Analysis of the results is conducted over the Prudence subregions (Christensen et al., 2007) but mainly over the European domain which we define as the region encompassing all the Prudence subregions but also extends to the east over the Black Sea (Fig. 1). Therefore, it lies between -10^{o} and 40^{o} in longitude and 36^{o} to 70^{o} in latitude. We symbolize the above European domain as “EU” and we refer to it as the EU domain or the EU region. Moreover, all the domain averaged values presented in the study correspond to the EU domain. We use the terms subdomains and subregions in order to refer to the Prudence subregions. Finally, both land and sea points are considered in the domain and subdomain averaging of variables, unless otherwise stated.

Table 2: The Prudence subregions and their boundaries in degrees of longitude (west-east) and latitude (south-north).

Subregion	West	East	South	North
(BI) British Isles	-10	2	50	50
(IP) Iberian Peninsula	-10	3	36	44
(FR) France	-5	5	44	50
(ME) Mid-Europe	2	16	48	55

(SC) Scandinavia	5	30	55	70
(AL) Alps	5	15	44	48
(MD) Mediterranean	3	25	36	44
(EA) Eastern Europe	16	30	44	55

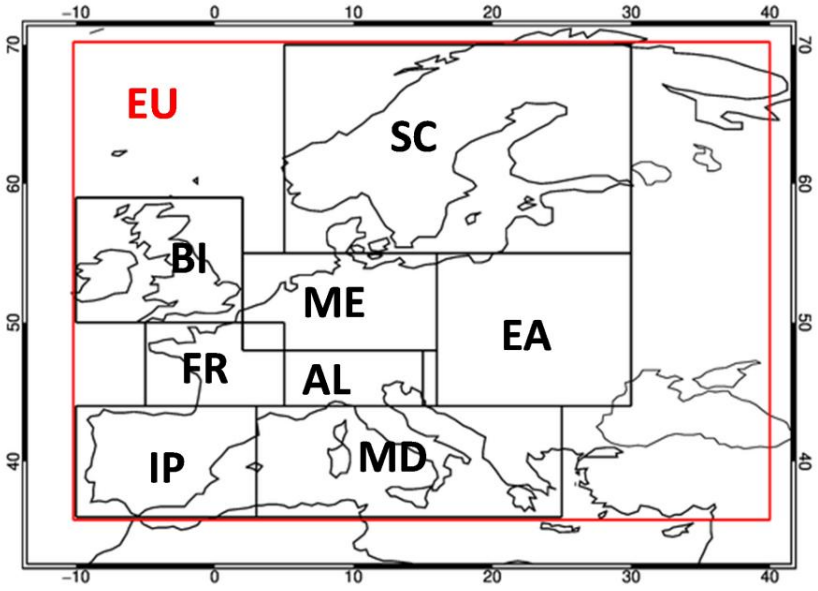

Fig. 1: The Prudence subregions (black line) and the EU region (red line) used in the analysis.

1.5 Results of aerosol implementation

1.5.1 Aerosol Optical Depth

In this study we have used several aerosol datasets in the sensitivity simulations. In order to assess the credibility of each dataset we conduct a quick qualitative comparison of the datasets used against the AOD estimates of the MODIS Terra (Hubanks et al., 2019) and the CMSAF SEVIRI climate data record (Clerbaux et al., 2017). We have used both the MODIS Terra and Aqua products, but since they are very similar for the scope of this evaluation, we present only the Terra product. Fig. 2 depicts the mean seasonal fields of aerosol optical depth at 550nm used for the simulations as well as the satellite estimates. It can be seen that both satellite products do not have consistent coverage over Europe during winter and autumn. Thus, we have only used grid points that had no missing values (monthly means) over the entire 2004-2005 period. Table 3 presents the mean seasonal AOD of all products, only over the grid points where MODIS has valid values. The mean AOD of the products used

in the simulations over the entire EU domain can be seen in (Table 6). In the case of the simulations using the Thompson aerosol aware microphysics scheme, the aerosol field is not prescribed but produced by the scheme itself. Since the fields of all the simulations using the Thompson aerosol aware scheme are quite similar we present only the AOD field of the ARCI simulation.

All the datasets examined present a very similar seasonal variability. Largest AOD values are seen in summer and spring whereas AOD is smallest in winter. Interestingly, the only exception is the AOD of the ARCI simulation, which is produced by the Thompson aerosol-aware microphysics scheme. ARCI has an AOD maximum over Eastern Europe that is persistent throughout the year. Moreover it consistently has larger AOD than all other aerosol products examined, for all seasons.

The satellite datasets, MODIS and SEVIRI, have quite similar AOD fields. However, MODIS presents a slightly larger AOD over continental Europe in summer.

The fields of MACC reanalysis and MAC-v1 climatology have both larger AOD values than the satellite datasets. Interestingly, MAC-v1 has a local AOD maximum over Eastern Europe in summer that is strong and spatially extensive and is not seen in either satellite product. MAC-v1 has also large AOD over central and Eastern Europe during spring. This is an indication that MAC-v1 might overestimate the African dust aerosol over central Europe during spring and summer, since they seem spatially connected to the strong AOD over North Africa present during these seasons. Finally, the climatology of Tegen has the lowest AOD compared to all other products, throughout the year.

Table 3: Mean seasonal aerosol optical depth (AOD) of all datasets examined, only over the grid points where MODIS has valid values.

	DJF	MAM	JJA	SON
MODIS	0,12	0,20	0,20	0,15
Seviri	0,14	0,20	0,21	0,16
Tegen	0,11	0,17	0,18	0,17
Macv1	0,14	0,27	0,24	0,20
MACC	0,15	0,26	0,22	0,20
ARCI	0,20	0,25	0,24	0,22

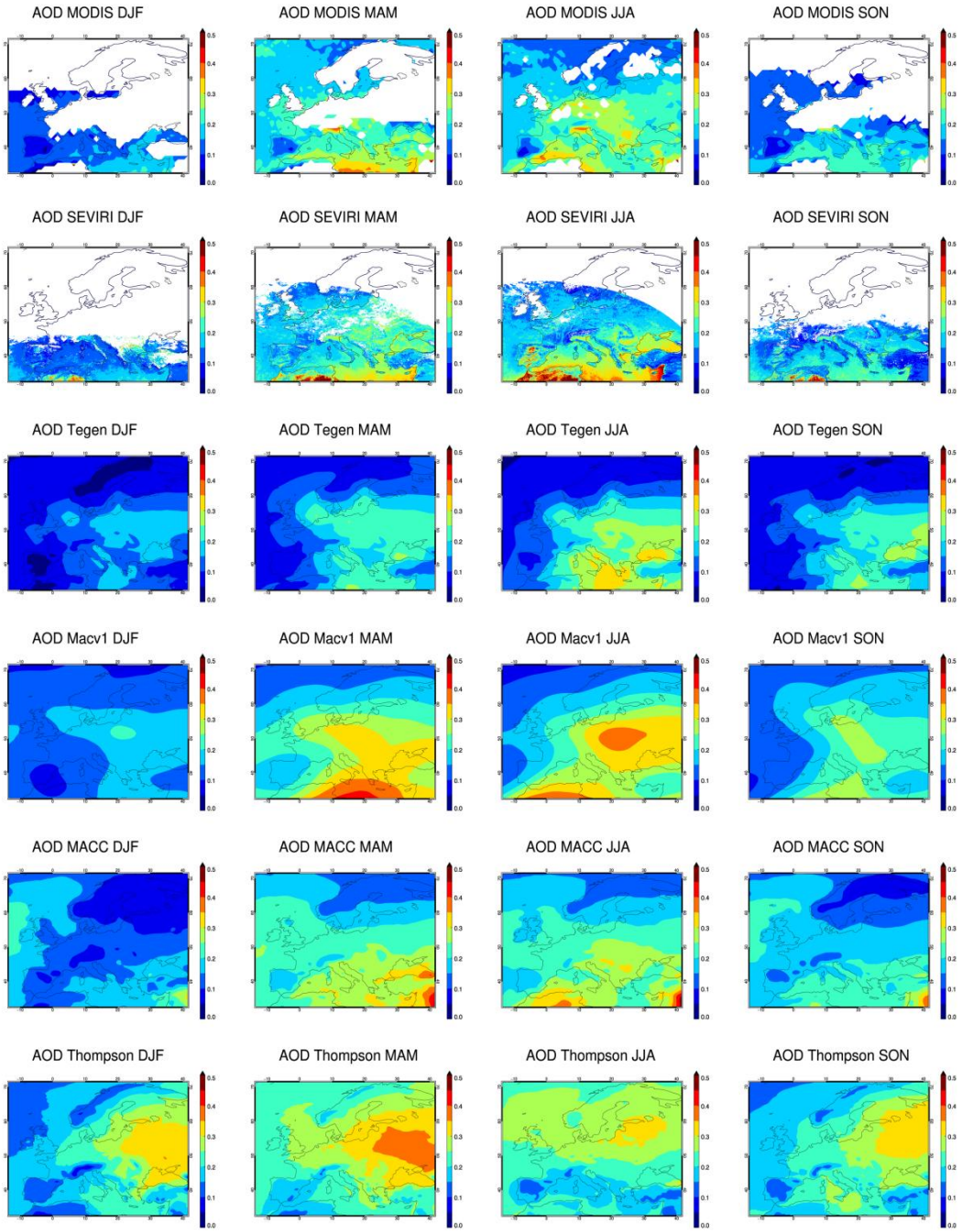

Fig. 2: Mean seasonal aerosol optical depth at 550nm for (top to bottom) the MODIS TERRA satellite dataset, the CM SAF climate record (SEVIRI), the Tegen climatology, the MACv1 climatology, the MACC reanalysis and the ARCI simulation that uses the Thompson aerosol aware microphysics to produce the aerosol field.

Because the Thompson aerosol aware scheme produces the AOD field, as described in the methodology, we have tried to assert its ability to maintain the pattern and levels of the AOD field throughout the 5 year long climate simulations. The trend of domain averaged AOD monthly mean values is slightly negative, showing a decrease of -0.003 or -1.5% over the 5 year period (Fig. 3). In the scope of our study this decreasing trend is negligible since it does not change at all the regime of AOD of each season. In order to put this in perspective,

the mean AOD difference between winter and summer is much higher, 0.06 or 32% whereas between summer and autumn is 0.033 or 17%, more than an order of magnitude larger than the decrease experienced due to the trend. Similar behavior is seen for the concentrations of water friendly and ice friendly aerosols, with the trend of ice friendly aerosols being slightly more negative due to the lack of an emission field for this aerosol category. Regarding the spatial pattern, for a given month or season the AOD field presents some differences due to the inevitable differences in the meteorological conditions throughout the years, but retains the same basic characteristics. Thus we believe that the Thompson aerosol aware scheme can be successfully implemented in short multi-year climate simulations like the ones used in this study. For considerably longer simulations however, the decreasing trend of AOD could lead to larger reductions in aerosol load that might start to deviate from normality. In newer WRF versions (v3.9 and on), the stability of the AOD field is expected to increase even further. This is because of the addition of an emission field for ice friendly aerosols and introduction of monthly variations in the emission fields of both ice friendly and water friendly.

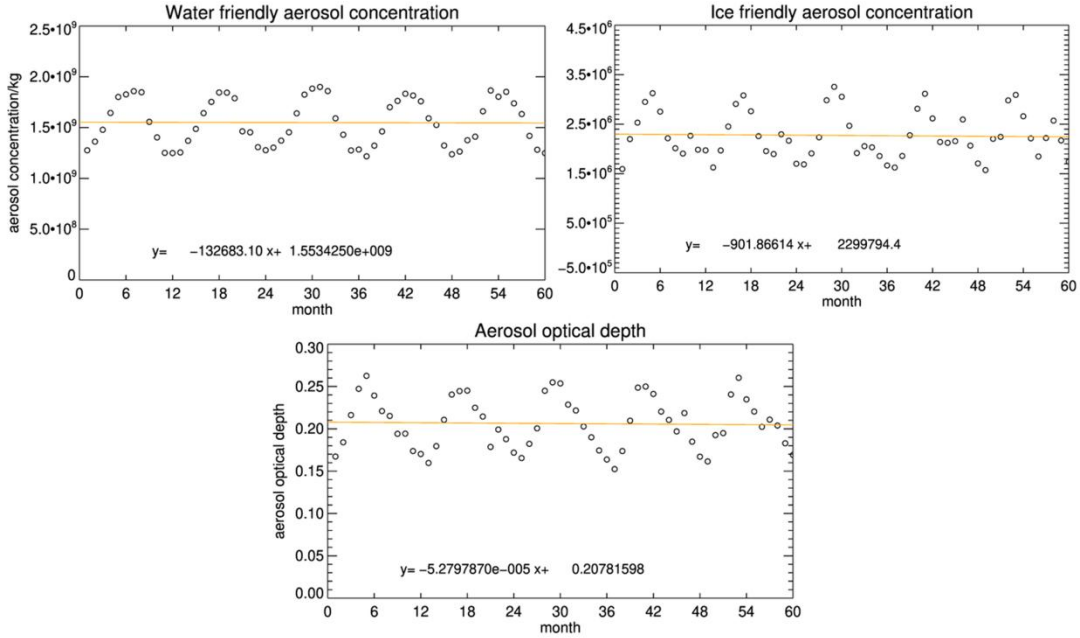

Fig. 3: Domain averaged monthly mean values (circles) of aerosol concentration for water friendly aerosol (top left), ice friendly aerosol (top right) and aerosol optical depth (bottom) together with the linear fit line (yellow). For simulation ARCI using the Thomspon aerosol aware scheme.

Aerosol extinction vertical profile

Besides the total aerosol optical depth (AOD), the vertical profile of the aerosol extinction can also be quite important since it can affect the vertical thermodynamic profile of the atmosphere. This is especially true in the case of absorbing aerosol.

The annual mean vertical profile of the aerosol extinction coefficient (km^{-1}) in each model layer is presented in Fig. 4 for the EU region. It is presented for the first aerosol option (aer_opt=1), the second aerosol option (aer_opt=2) and the Thompson aerosol aware

scheme (TE2014). All aerosol implementations in the model have the same basic characteristics. Maximum values of extinction coefficient are seen near the surface and a decrease of extinction is encountered with increasing altitude. The Tegen climatology used in the first aerosol option has much smaller values of extinction near the surface compared to the aerosol datasets (MAC-v1, MACC) that have been used in the second option. Moreover, the Thompson aerosol-aware scheme has systematically the largest aerosol extinction near the surface.

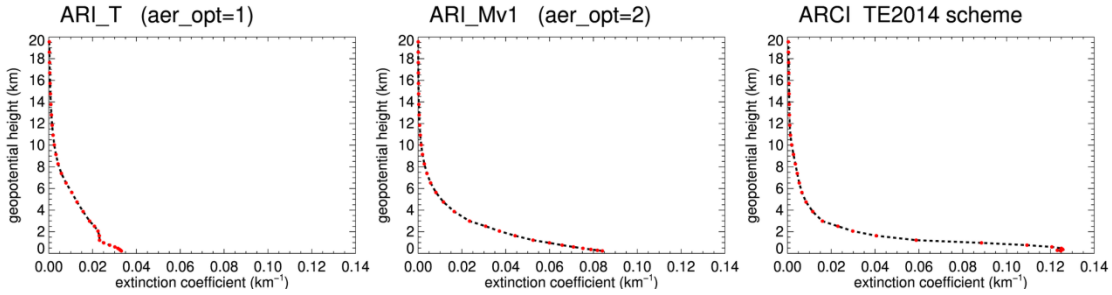

Fig. 4: Domain averaged of annual mean vertical distribution of aerosol extinction coefficient at 550nm (km^{-1}) in each model layer (red dots). For the simulations ARI_T (indicative of aer_opt=1), ARI_Mv1 (indicative of aer_opt=2) and ARCI (indicative of the TE2014 scheme).

We also present in Fig. 5 the total aerosol extinction (in essence the AOD) in each model layer, averaged for the EU region and for all seasons. Top row presents the vertical profile of the aer_opt=1 option that uses the Tegen climatology. Middle row presents the profile of ARI_Mv1. All simulations that use aer_opt=2 (ARI_Mv1, ARI_Mv1full, ARI_Mv1urban and ARI_MC) have an almost identical vertical profile since this is parameterized by the aforementioned option. Bottom row presents the profile of simulation ARCI that uses the Thompson aerosol aware scheme. All simulations using the Thompson aerosol aware scheme (ACI, ARCI, ARCI_no) have similar profiles (however not identical).

In Fig. 5 all simulations have a similar general behavior: Increasing AOD values as we move from the surface up to the maximum AOD, that is relatively low in the troposphere, and then decreasing AOD, close to an exponential decay, as we move in higher altitudes. The maximum AOD per layer is encountered not near the surface but at higher altitudes, despite the aerosol extinction per unit of altitude being larger near the surface. This is because of the varying thickness of model layers. Layers are much thinner near the surface (50-100m) and despite the large extinction coefficients, the total AOD of the layer is moderate. The extinction coefficients considerably decreases with altitude but the layer thickness increases (~500m), thus resulting in maximum AOD values near the lower to middle troposphere .

As said before, the profile of AOD per layer is quite similar for all options used. However discrepancies do exist, mainly regarding the height and shape of the maximum. Simulation ARI_T (top row) has an AOD maximum around 3.5km. ARI_Mv1 (middle row) has a double peak in AOD of equal magnitude, one close to 1.5-2km and the other around 3.5-4km. Finally ARCI (bottom row) has a maximum closer to the surface, 1-1.5 km and a considerably smaller secondary peak higher, around 3.5km.

It must be stated here that the vertical AOD profile in the option aer_opt=2 is prescribed. It is given by the equation $\tau(z) = \frac{\tau_o / Z_h}{e^{-\frac{Z_{sfc}}{Z_h}} - e^{-\frac{Z_{toa}}{Z_h}}} \int_z^{z_{toa}} e^{-\frac{Z}{Z_h}} dz$ where τ(z) is the AOD at height z, τ_o is the total column AOD, z_{toa} the altitude at the top of the atmosphere and z_h a scale height parameter that is set to 2.5 km (Ruiz-Arias et al., 2013, 2014). Therefore the shape of the AOD profile is the same over all grip points of the domain. Moreover this profile is fully representative for all simulations using aer_opt=2 regardless of the AOD dataset implemented.

On the other hand the vertical profile of aer_opt=1 that uses the Tegen climatology is not prescribed. The climatology of Tegen is fully 3-dimensional and the vertical profile of AOD is given for all five aerosol types described (organic carbon, black carbon, sea salt, dust, sulfates) (Fig. 6). The total aerosol optical depth in each vertical level is the sum the aerosol optical depth of all the aerosol types. Therefore the vertical AOD profile can change depending on the region, since the spatial distribution of the aerosol types differs. However in essence, the shape of the vertical profile and the height of the maximum are very similar in all subregions.

Finally the Thompson aerosol aware microphysics scheme creates its own 3-dimensional AOD field since it has mechanisms of aerosol emission, sinking and advection. This means however that the vertical profile has more degrees of freedom to change. Indeed larger differences are seen in the simulations using the Thompson aerosol aware for the different subregions and seasons. In Fig. 7 we see that for a given season (summer) the simulations using aer_opt=1 and 2 (first two rows) do not change the shape of their vertical profile between different subregions. On the other hand, simulation ARCI (bottom row) with the Thompson aerosol aware scheme diversifies to a considerable degree the vertical AOD distribution. It is important to note however that the general behavior of the AOD profile (maximum at a low height and then decrease with altitude) remains remarkably stable. This is an important result regarding the use of the Thompson aerosol aware scheme.

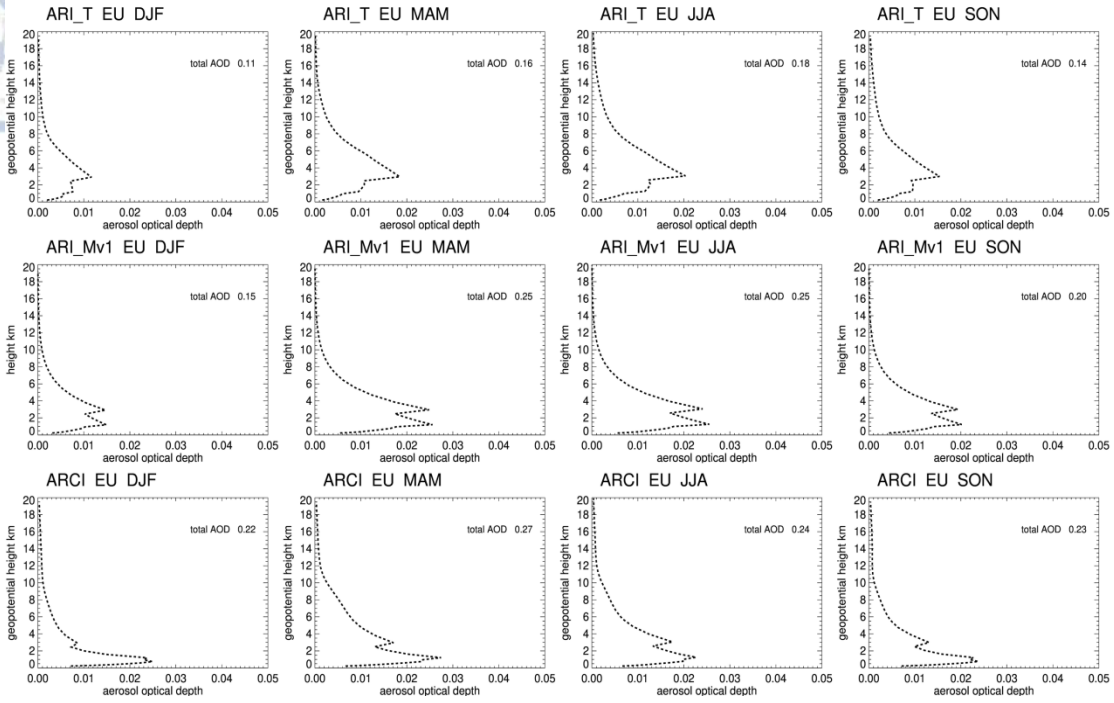

Fig. 5: Aerosol optical depth (AOD) vertical profile averaged for the EU region. For simulation ARI_T (top) that uses aer_opt=1, for simulation ARI_Mv1 (middle) that uses aer_opt=2 and for simulation ARCI that uses the Thompson aerosol aware microphysics scheme. For all seasons. The vertical y-axis presents the geopotential height (km). The horizontal x-axis the aerosol optical depth.

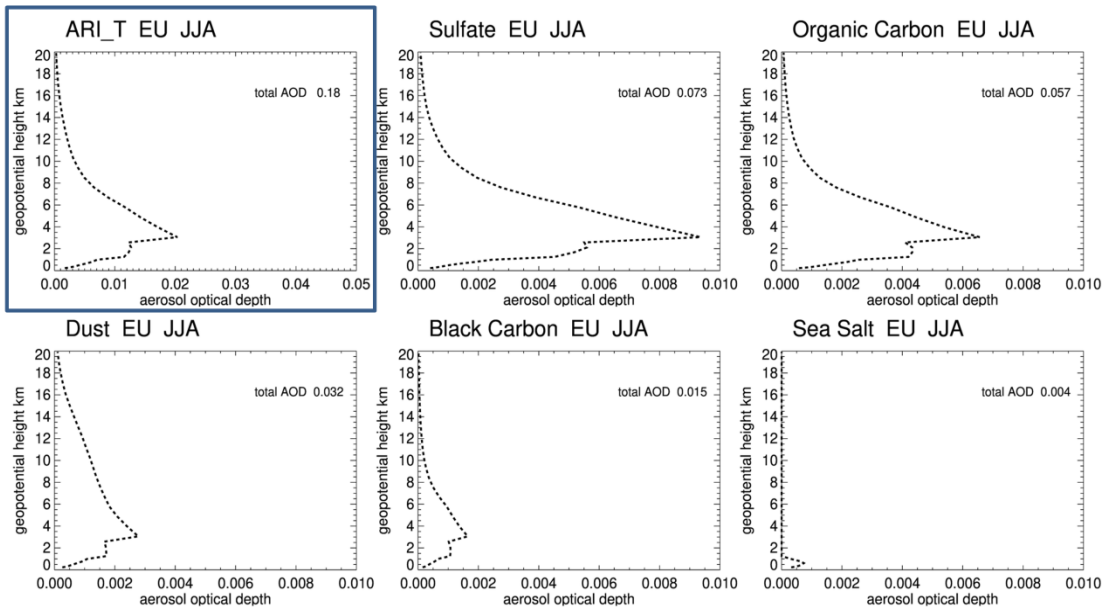

Fig. 6: Total aerosol optical depth vertical profile for ARI_T (aer_opt-=1) in summer (blue box- top row and left) and aerosol optical depth decomposition in each aerosol species. Mind the different horizontal y-axis for the total AOD and the various aerosol species.

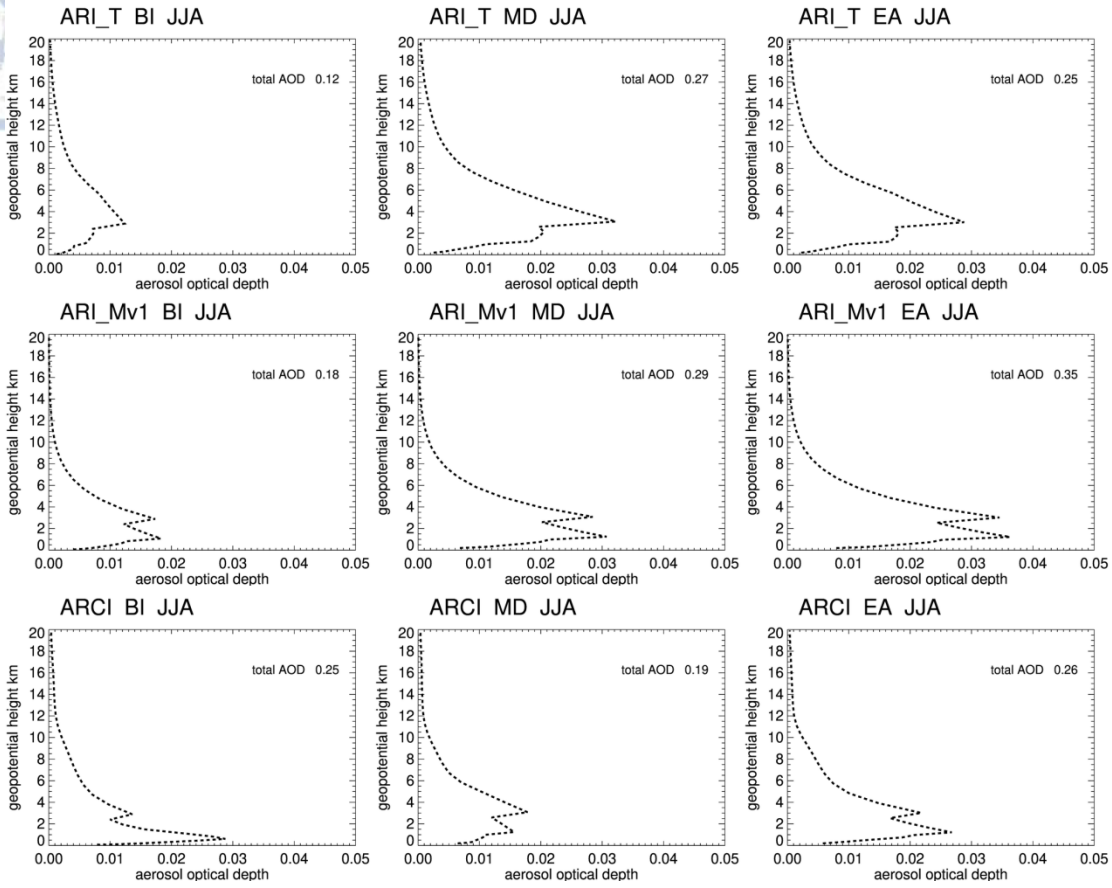

Fig. 7: Aerosol optical depth vertical profile in summer for the subregions: British Isles (BI – left column), Mediterranean (MD – middle column) and Eastern Europe (EA – right column). For simulation ARI_T (aer_opt=1) (top row), ARI_Mv1 (aer_opt=2) (middle row) and ARCI (Thompson aerosol aware scheme) (bottom row).

Single Scattering Albedo

Single scattering albedo (SSA) describes the relative importance of scattering compared to the overall extinction caused by the interaction of aerosols with radiation. The more SSA deviates from 1 the more absorbing the aerosols are. It is a very important characteristic of aerosols especially regarding the semi-direct effect, since the absorption of radiation tends to warm the surrounding air masses, leading to changes in the thermodynamic profile of the atmosphere and thus impacting cloudiness.

We present in Fig. 8 the single scattering albedo in the spectrum 0.4-1.0 μm at the surface. Simulation ARI_T (aer_opt=1,) has values close to 0.9 over large parts of central Europe and even more absorbing aerosol over North Africa with SSA reaching 0.85. On the other hand the Atlantic ocean has intensely scattering aerosol.

The SSA of ARI_Mv1 is depicted in the second row. It presents considerably more scattering aerosol than ARI_T since the SSA values are always above 0.93 over the entire domain. This SSA field is fully representative of all simulations using aer_opt=2 and the “rural” aerosol

type to parameterize aerosol properties (ARI_Mv1, ARI_MC) as well as for simulation ARCI that uses the Thompson aerosol aware scheme. This is because the interaction of aerosol with radiation in the Thompson aerosol aware scheme (aer_opt=3) parameterizes SSA according to the "rural" type of the aer_opt=2 option. Therefore the SSA field has negligible differences in all these simulations.

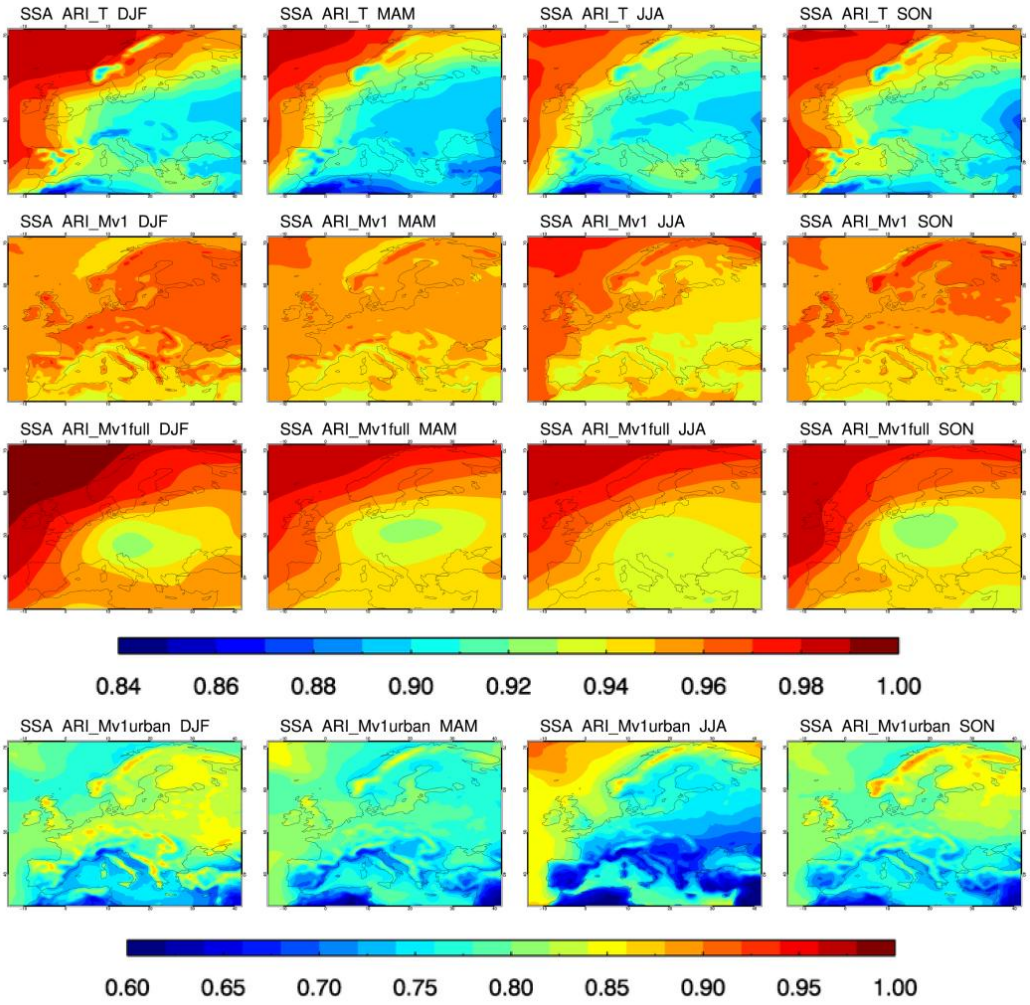

Fig. 8: Single scattering albedo (SSA) in the spectrum 0.4-1.0μm for simulations ARI_T (top), ARI_Mv1 (second row), ARI_Mv1full (third row) and ARI_Mv1urban (bottom). For all seasons. Mind the different colorbar for ARI_Mv1urban.

Simulation ARI_Mv1full uses the single scattering albedo from the MACv1 climatology. In this case a spot of SSA minimum (0.92) is seen over central-eastern Europe (0.92). Therefore over this area ARI_Mv1full has more absorbing aerosol compared to ARI_Mv1, but are still considerably less absorbing than ARI_T. Finally very scattering aerosols are seen over the Atlantic. We must note here that we used from the MACv1 product single scattering albedo at the 550nm. However if the SSA is externally provided in the aer_opt=2 option, as is the case here, it is used without any adjustment for the full spectrum of the RRTMG radiation

scheme. Therefore the SSA field of MACv1 at 550nm is fully comparable with the SSA fields of all the rest simulations, hat have been obtained by the model output for the spectrum 0.4-1.0 μm.

Finally ARI_Mv1urban has way more absorbing aerosols than all the other simulations. SSA values reach as low as 0.6 over North Africa. Values below 0.65 are seen over extensive areas of southern Europe during summer. Moreover continental Europe almost always has SSA values less than 0.85. As said before, these values are unrealistically absorbing (Rodríguez et al ., 2013; Tombette et al., 2008; Witte et al., 2011). Thus we consider ARI_Mv1urban as an idealized experiment exploring the effects of extremely absorbing aerosols.

1.5.2 Evaluation

In this section we present a basic evaluation study, mainly focusing on the control simulation CON. We examine temperature at 2m, precipitation, cloud fraction and shortwave radiation at the surface. Since all the sensitivity experiments are based on CON, it is important to assess the ability of the control experiment to correctly simulate the climate. Large deviations would decrease the credibility of the sensitivity simulations. Results indicate that there are some biases present, but in general the control simulation describes the basic characteristics of the European climate. This indicates that the main physical processes are simulated with a sufficient degree of correctness, therefore increasing the robustness of the sensitivity study.

Quick summary

The control simulation is in general mildly colder (-0.5^{o}C) than the observations in both winter and summer, with colder biases over Scandinavia. Precipitation amount is overestimated during winter and underestimated in summer with the exception of limited areas in the Mediterranean. Total cloud fraction is overestimated all over the domain in winter and in central and northern Europe during summer. Shortwave radiation is affected by the cloud fraction overestimation and is in general slightly underestimated.

The biases of the control simulation are depicted in Fig. 9.

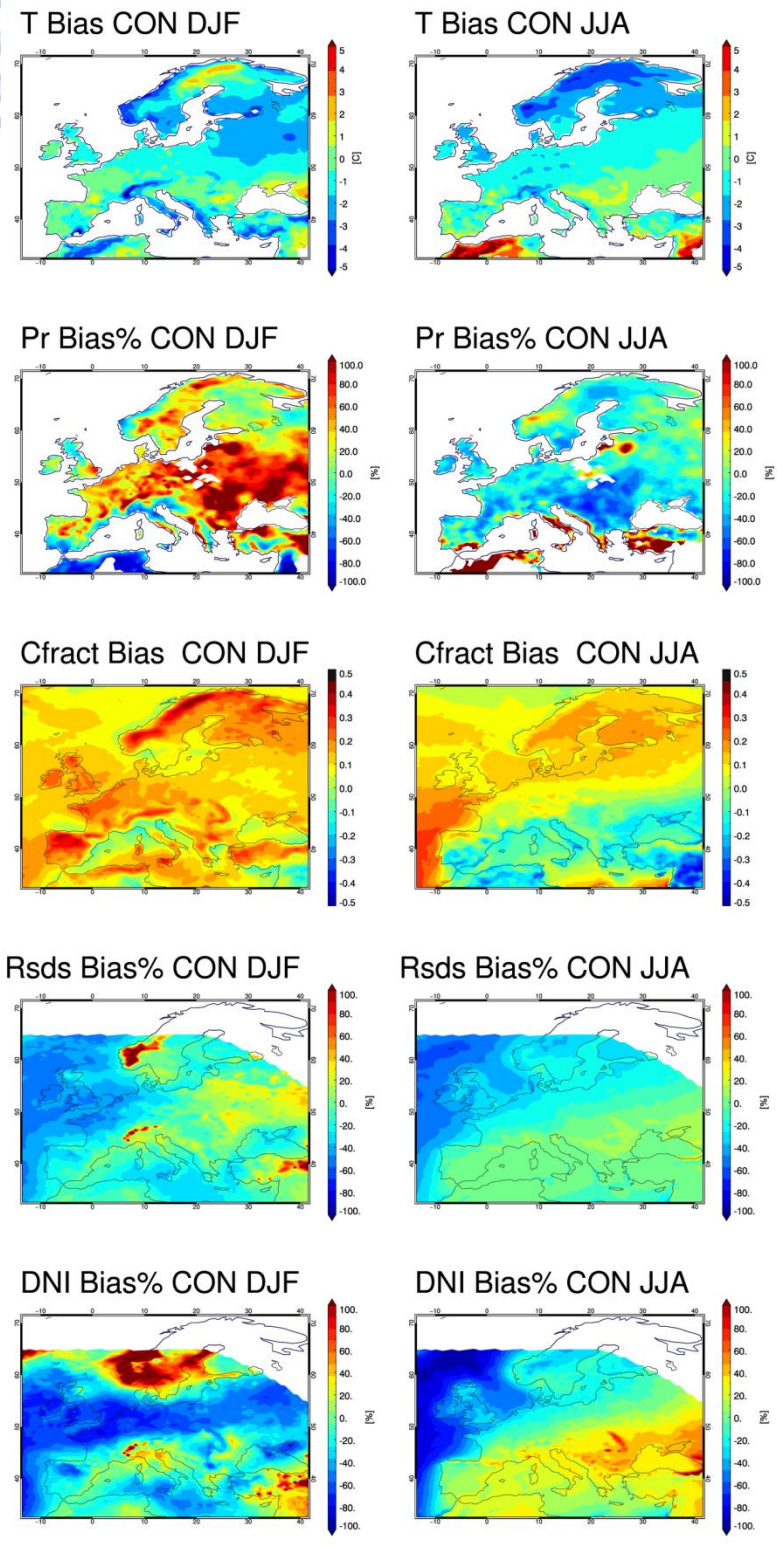

Fig. 9: Bias plots for control simulation CON for winter (DJF-left) and summer (JJA-right). Biases depicted from top to bottom for temperature (T), precipitation (Pr), total cloud fraction (Cfract) ,down welling shortwave radiation to the surface (Rsds) and direct normalized irradiance at the surface (DNI).

1.5.2.1 Temperature

In winter the control simulation is mildly colder than the observations (-0.5^{o}C on average) (Fig. 9-top panel). Larger cold biases, exceeding -1C, can be seen over Scandinavia, parts of the Mediterranean and the Alps. Cold biases during winter, especially over northern Europe, are quite common in EURO-CORDEX simulations (Kotlarski et al., 2014). Interestingly, compared to other WRF hindcast simulations in EURO-CORDEX (Katragkou et al., 2015), the winter cold biases in our study are reduced. Large parts of northern Europe are covered with snow during winter and correct simulation of the snowpack by the land scheme of the model is very important. Interestingly, most of the WRF simulations in EURO-CORDEX use the Noah land surface scheme. Therefore we believe that the use of the CLM land surface scheme in this study plays a significant role in reducing the cold winter bias. Summer presents dual pattern of a cold bias over the largest part of the domain (-5^{o}C domain average) whereas some areas with warm bias are seen in south and eastern Europe. A bias pattern like the above (cold bias in the north and warm in the south) is also present in several other RCM simulations over the European domain (Kotlarski et al., 2014), including different models like CCLM4, HIRHAM and RCA4.

1.5.2.2 Precipitation

The control simulation in winter is considerably more wet than the observations. Precipitation in winter is considerably overestimated all over the domain (43% domain average). Large wet biases exist over central and eastern Europe that may exceed 100% over limited areas. Winter precipitation overestimation over eastern Europe is common in many WRF simulations (García-Díez et al., 2015; Jin et al., 2010; Katragkou et al., 2015; Mooney et al., 2013). Compared to the bibliography this winter wet bias is enlarged in the control simulation of this study.

In summer there is a general precipitation underestimation (-3% domain average) with several areas presenting a dry bias around -20 to -30%. This dry bias during summer is not commonly found in WRF simulations. On the other hand there are some limited areas, mainly in southern Europe, with large wet biases. These must be interpreted with caution since summer precipitation amounts over these regions are quite small, something that can strongly amplify the relative bias. Interestingly the bias patterns described for both summer and winter are present not only in CON but in all the sensitivity simulations, regardless the microphysics scheme used (Thompson2008 or Thompson aerosol-aware). We also conducted an additional simulation using the WDM6 microphysics scheme that produced very similar behavior regarding precipitation bias. Therefore we have a strong indication that the microphysics scheme used is not the main cause of the precipitation bias detected.

1.5.2.3 Cloud fraction

In winter, cloud fraction is considerably overestimated all over the domain with a mean bias of 0.17 or +35%. Larger pronounced biases are common over mountainous areas, as well as over other regions such as the Iberian Peninsula (+60%) (Fig. 9, 3rd panel). In summer there is also cloud fraction overestimation on average but to a lesser degree (0.08 or 12%). There

is however a dual pattern present, with overestimation in north Europe (around 30%) and a small underestimation (-10%) over south Europe and the Mediterranean. Since summer cloud fraction amount over south Europe is small, something that amplifies relative bias, this small underestimation is almost negligible. Interestingly, several other WRF simulations (García-Díez et al., 2015; Katragkou et al., 2015) have presented very similar bias patterns for both winter and summer. Interestingly, the WRF simulations in the study of Katragkou et al. 2015, that had a large cloud fraction overestimation over north Europe, where those using the Grell-Devenyi cumulus parameterization scheme. In this study we use the Grell-Freitas scheme that is closely related to the Grell-Devenyi. Therefore the cloud fraction overestimation seen in our study could be partially connected to the cumulus scheme used. We expect this link to be more pronounced during summer when convection plays a significant role in shaping cloudiness levels. On the other hand, large biases are seen also in winter when convection is less significant and cloudiness is governed mainly by large scale processes. This indicates that the cumulus scheme is definitely not the only factor of cloud fraction bias. The microphysics scheme theoretically could have a large influence on cloud fraction bias, especially in winter. However similar behavior to then control simulation regarding the cloud fraction bias is also seen in the simulations using the Thompson aerosol aware scheme and the one that used the WDM6 microphysics. Thus the large cloud fraction biases in our study do not seem to be connected to the microphysics scheme. However, we show in section 1.5.4 that the cloud cover scheme can have a considerable impact on cloudiness amount and bias.

1.5.2.4 Shortwave radiation and direct component

As expected, shortwave radiation at the surface (Rsds) is strongly influenced by the general cloud fraction overestimation. Therefore Rsds is underestimated over Europe for both winter and summer. In winter, domain averaged bias is small (-4%). There are however areas of central Europe that present considerably larger underestimation (-20 to -40%). In summer the domain averaged bias is larger, around -8%. Radiation underestimation is large over northern Europe and gradually decreases in intensity moving towards the southern parts of the domain, thus following closely the dual cloud fraction bias pattern seen in summer. It is characteristic that for all seasons the bias patterns of cloud fraction and shortwave radiation are very well spatially correlated.

Regarding the direct normalized irradiance (DNI), its bias pattern is similar to the one seen in Rsds, however the bias magnitude is amplified. In winter the domain averaged underestimation is around -13%. However there is an extensive area of large positive bias over southern Scandinavia. In summer, a dual north-south bias pattern is present, like the ones seen in Rsds and cloud fraction, but even more pronounced. Negative biases are encountered in the north (-20%) that change to overestimation (20 to 30%) as we move towards the southern parts of Europe.

1.5.2.5 Sensitivity simulations evaluation

Evaluation results of the sensitivity simulations (Table 4) are quite similar to those of the control experiment, regarding the bias patterns and magnitude. This is the case for most of the variables examined, regardless of the aerosol interactions implemented and aerosol data used. This is a clear indication that aerosol parameterization is not one of the main sources of bias in the simulations of this study. However in the case of shortwave radiation (Rsds and DNI) the introduction of aerosol-radiation interactions does have a considerable impact on bias. Aerosol with their scattering and absorption tend to decrease radiation at the surface. Thus the radiation underestimation seen in the control simulation is amplified when aerosol-radiation interaction is enabled. For example domain averaged Rsds bias for CON in winter is -11% and amplifies to around -17% with aerosol-radiation interactions enabled. This effect is even more pronounced in DNI where a winter underestimation of -13% for CON is enlarged to around -40% for the ARI group of simulations. Therefore we see that the inclusion of an additional physical mechanism in the model, despite providing a more complete representation of the physical processes, does not always improve the bias. On the contrary in some cases, as described above for radiation, it can considerably increase it. It must also be noted here that the simulation ARI_Mv1urban presents the largest bias changes compared to the control simulation. ARI_Mv1urban utilizes the very absorbing "urban" type aerosol that in general have a very intense impact compared to CON for all the variables examined.

Table 4: Domain averaged bias for temperature, precipitation, cloud fraction, shortwave radiation at the surface and direct normalized irradiance. For all seasons.

Temperature (^{o}C)								
	CON	ARI_T	ARI_Mv1	ARI_Mv1full	ARI_MC	ACI	ARCI	ARI_Mv1urban
DJF	-0,5	-0,6	-0,6	-0,8	-0,7	-0,4	-0,6	-0,9
MAM	-1,8	-1,9	-1,9	-2,2	-1,7	-1,5	-1,7	-1,9
JJA	-0,5	-0,8	-0,8	-1,0	-0,7	-0,1	-0,5	-0,6
SON	-0,1	-0,6	-0,3	-0,5	-0,4	-0,2	-0,1	-0,6

Precipitation (%)								
	CON	ARI_T	ARI_Mv1	ARI_Mv1full	ARI_MC	ACI	ARCI	ARI_Mv1urban
DJF	43	41	42	40	41	41	37	36
MAM	22	14	19	20	13	16	21	4
JJA	-3	-9	-4	-1	-7	0	-6	-18
SON	7	10	7	11	8	12	4	2

Cloud fraction (%)								
	CON	ARI_T	ARI_Mv1	ARI_Mv1full	ARI_MC	ACI	ARCI	ARI_Mv1urban
DJF	28	28	29	28	28	27	26	28
MAM	25	25	26	26	25	24	24	24
JJA	12	14	13	15	15	9	10	10
SON	27	29	28	27	29	25	26	29

Rsds (%)								
	CON	ARI_T	ARI_Mv1	ARI_Mv1full	ARI_MC	ACI	ARCI	ARI_Mv1urban
DJF	-11	-16	-16	-15	-14	-6	-8	-21
MAM	-13	-17	-18	-18	-17	-8	-12	-24
JJA	-11	-17	-17	-17	-16	-5	-11	-23
SON	-21	-28	-27	-26	-27	-16	-20	-34

Direct Normalized Irradiance (%)								
	CON	ARI_T	ARI_Mv1	ARI_Mv1full	ARI_MC	ACI	ARCI	ARI_Mv1urban
DJF	-13	-39	-41	-40	-35	-6	-25	-41
MAM	-18	-37	-42	-42	-40	-11	-31	-41
JJA	-2	-31	-32	-32	-30	5	-20	-31
SON	-17	-44	-45	-44	-41	-13	-30	-47

1.5.3 Aerosol treatment Sensitivities

This section is the main part of the sensitivity study. We present the results of aerosol introduction in the model by showing the impact on each variable.

1.5.3.1 Clear sky radiation at the surface and DRE

Clear sky downwelling shortwave radiation at the surface (CRsds) is produced when the radiation scheme of the model does not take into account cloudiness at all. Therefore it is a

variable free of the impact of clouds on radiation. Thus we examine CRsds as a first step in the sensitivity study, since it provides a clear view regarding the impact of aerosol on radiation that is isolated by the impact of cloudiness on radiation.

In general, enabling of aerosol-radiation interactions clearly leads to a reduction in CRsds that is statistically significant, regardless of the aerosol data used (Fig. 10). This decrease is around -5 to -8% (domain average) (Table 5) for all seasons and all the simulations. Exception is simulation ARI_Mv1urban with the heavily absorbing aerosol. In this case the decrease is amplified to -14%.

We have also calculated the direct radiative effect of aerosol (DRE) as the difference of the net CRsds between a simulation having aerosol-radiation interactions and the control experiment CON. Regarding domain averages, the DRE is negative and very similar for all the simulations that enable aerosol-radiation interactions only (ARI group), despite the different aerosol data used. DRE values are around -4 to -5 W/m^2 in winter and -14 to -17 W/m^2 in summer (Table 6). The impact of ARI_Mv1urban is again enlarged and almost double compared to the rest simulations.

When we implement aerosol-radiation interactions in an environment where aerosol-cloud interactions are also present (we calculate the difference ARCI-ARI), the results are very similar to the ones seen in the simulations that have only aerosol-radiation effects. This is the case for both the relative CRsds decrease and the observed DRE values.

Spatially there is a very good correlation between the DRE and the AOD field used in each experiment. The AOD maxima coincide spatially with the DRE minima and vice versa. For the ARI group, the correlation coefficients are very high, between -0.8 and -0.98. However this correlation is considerably weaker for simulation ARCI that implements all aerosol interactions. Coefficients range around -0.7 to -0.8 for most seasons whereas in winter it is considerably lower at -0.4. As stated before, the DRE of ARCI is calculated against ACI. Both of these simulations use the Thompson aerosol-aware microphysics scheme that produces an evolving AOD field. In the correlation analysis we used the mean AOD pattern, an action that has possibly partially responsible for the decreased correlation. Moreover the produced AOD field depends on the meteorological conditions that are not identical on simulations ARCI and ARI something that results in slightly different AOD fields for these two simulations. This effect is also responsible for the decreased spatial correlation.

We have also calculated the ratio of the DRE (decrease in net clear-sky radiation at the surface) to the AOD for all ARI simulations including the ARCI-ACI comparison (Table 7). We see that all simulations that use the second aerosol-radiation option (aer_opt=2) (ARI_Mv1, ARI_Mv1full, ARI_MC) have a similar decrease of clear-sky radiation at the surface (CRsds) per unit of AOD, that is around -50 W/m^2 on an annual basis. These simulations have aerosol datasets (MAC-v1, MACC) with similar AOD values and also make use of similar single scattering albedo (SSA) values. Interestingly, the ARI_T simulation (aer_opt=1, Tegen climatology) leads to a larger (-70 W/m^2) decrease per AOD. This is probably due to the existence of more absorbing aerosol (smaller SSA). The result is that ARI_T presents a similar DRE to the rest ARI simulations (except of course ARI_Mv1urban), despite having smaller AOD values (Tegen), exactly because it tends to decrease clear-sky radiation more strongly

per unit of AOD. Simulation ARI_Mv1urban presents by far the largest CRsds decrease (-100 W/m^2) per AOD due to its extremely absorbing aerosols. Moreover, the ARCI-ACI comparison presents a similar but slightly smaller ratio to that of ARI_Mv1, ARI_Mv1full and ARI_MC, as it shares very similar SSA values with them. Finally, all simulations present a larger DRE/AOD in spring and summer. This must also be connected to the fact that in these two seasons the absorptivity of aerosol is increase (smaller SSA values).

Table 5: Relative difference (%) from control CON for clear-sky shortwave radiation (CRsds), shortwave radiation (Rsds), direct normalized irradiance (DNI) and diffuse radiation at the surface (DIF). For all simulations and seasons.

	DJF			MAM			JJA			SON		
	Rsds	DNI	DIF	Rsds	DNI	DIF	Rsds	DNI	DIF	Rsds	DNI	DIF
ARI_T	-5	-30	7	-4	-22	12	-7	-27	36	-8	-31	16
ARI_Mv1	-5	-33	8	-5	-29	17	-6	-30	38	-7	-34	18
ARI_Mv1urban	-11	-33	-3	-12	-29	0	-13	-29	12	-16	-37	1
ARI_Mv1full	-4	-31	9	-5	-28	17	-7	-29	37	-6	-33	18
ARI_MC	-3	-26	7	-5	-27	15	-6	-29	35	-7	-29	15
ARCI-ACI	-2	-20	6	-4	-23	12	-6	-25	26	-3	-18	14
ACI	7	8	7	7	9	5	9	11	6	8	6	7
ARCI	5	-14	13	2	-16	17	2	-17	31	5	-14	21

Table 6: Domain averaged values of aerosol optical depth (AOD), Radiative effect (RE), direct radiative effect (DRE) and change in shortwave cloud effect at the surface (ΔSCRE) all calculated as differences from control CON. For all experiments and all seasons. At the first column the changes that are being implemented are stated above each group of simulations. For simulation ARCI all the above quantities are also calculated against ACI (e.g. ARCI-ACI) in order to assess the implementation of aerosol-radiation interactions in the Thompson aerosol aware microphysics.

	AOD				RE				DRE				ΔSCRE			
Radiation interacting	DJF	MAM	JJA	SON	DJF	MAM	JJA	SON	DJF	MAM	JJA	SON	DJF	MAM	JJA	SON
ARI_T	0,11	0,16	0,18	0,15	-2	-7	-13	-7	-5	-13	-16	-9	3	7	4	2
ARI_Mv1	0,14	0,24	0,24	0,19	-2	-8	-12	-5	-4	-13	-15	-8	3	5	4	3
ARI_Mv1urban	0,14	0,24	0,24	0,19	-4	-18	-26	-12	-8	-29	-34	-16	4	11	8	4
ARI_Mv1full	0,14	0,24	0,24	0,19	-2	-8	-13	-5	-5	-14	-17	-9	3	6	4	4
ARI_MC	0,13	0,22	0,22	0,17	-2	-6	-11	-5	-4	-12	-14	-7	2	6	3	2
ARCI-ACI	0,22	0,26	0,24	0,23	-1	-6	-11	-3	-5	-13	-14	-8	4	7	4	5
Cloud interacting + cloud microphysics																
ACI	-	-	-	-	2	7	10	3	0	0	0	0	2	6	10	3
Radiation + Cloud interacting + cloud microphysics																
ARCI	0,22	0,26	0,24	0,23	1	0	-1	0	-5	-13	-14	-8	6	13	13	8

Table 7: Ratio of direct radiative effect (DRE) to the aerosol optical depth (AOD) over the domain for all ARI simulations (W/m^2/AOD). The DRE is calculated against the control simulation CON. The ARCI-ACI comparison is also included to examine aerosol-radiation interactions in an environment where the indirect effect is also present.

	DRE/AOD				
	DJF	MAM	JJA	SON	Annual
ARI_T	-46	-82	-91	-60	-70
ARI_Mv1	-32	-56	-64	-43	-49
ARI_Mv1urban	-59	-121	-143	-85	-102
ARI_Mv1full	-33	-59	-70	-46	-52
ARI_MC	-30	-56	-64	-40	-48
ARCI-ACI	-24	-50	-59	-35	-42

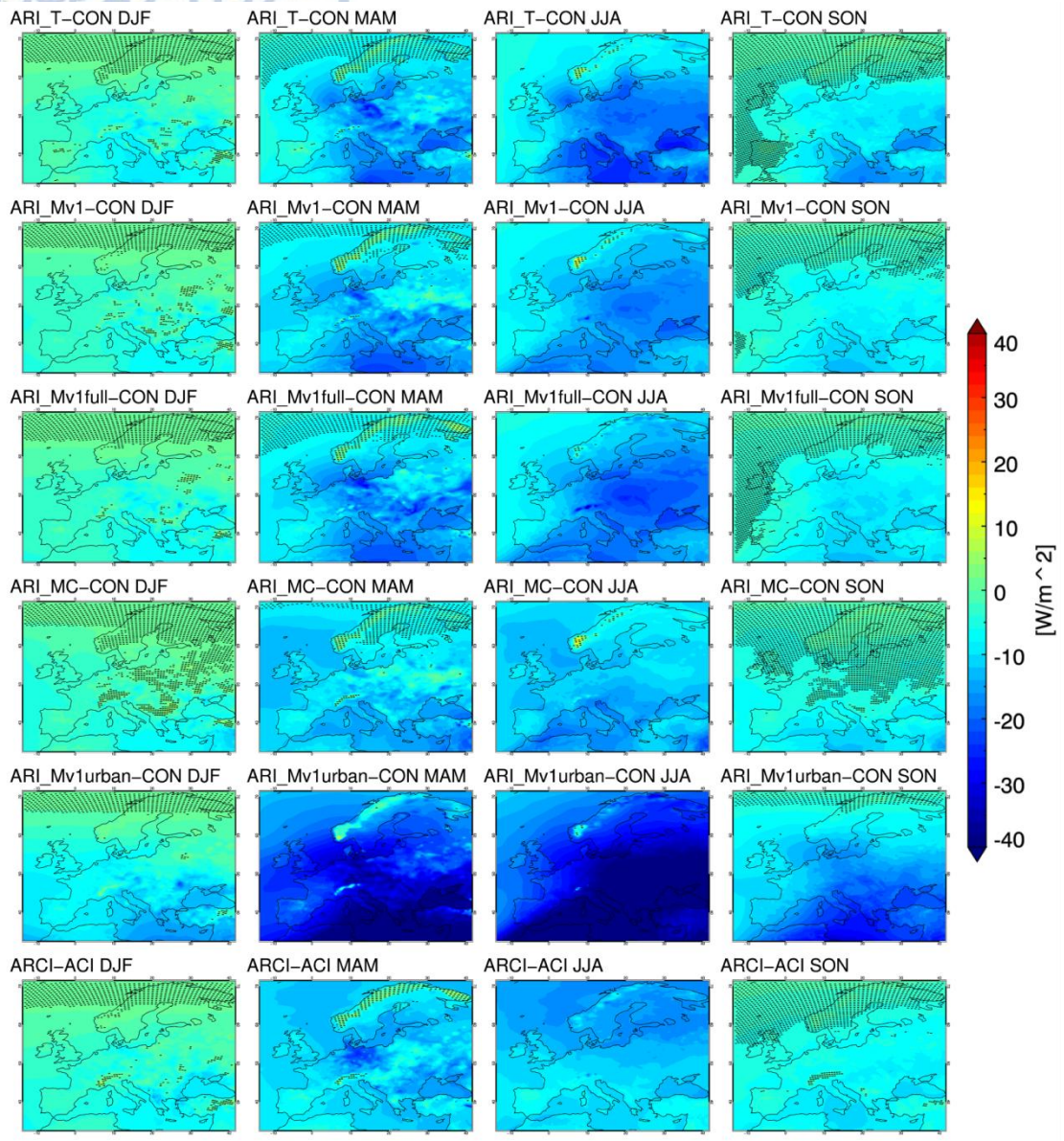

Fig. 10: Direct radiative effect (DRE) at the surface for simulations implementing aerosol-radiation interactions. For all seasons. DRE has been calculated as the difference in net CRsds at the surface from control CON for the ARI group of simulations (rows 1 to 5). The last row depicts the direct aerosol effect in an environment where the indirect effect is also present and displays the difference of experiment ARCI from ACI. Stippling indicates areas where the differences are not statistically significant at the 95% level, according to the Mann-Whitney non-parametric test.

1.5.3.2 Radiation at the surface and RE

With the implementation of aerosol-radiation interactions, shortwave downwelling radiation at the surface (Rsds) is decreased in the ARI group of simulations. This reduction is present throughout the year almost over the entire domain while being statistically significant over extensive large areas. The attenuation of Rsds is around -3 to -8%, regarding domain averages, for all seasons (Table 5). These values are similar to the decrease seen in clear-sky radiation (CRsds). Interestingly, over specific areas an Rsds decrease larger than -10% can be frequently seen (Fig. 11). Similarly to CRsds, simulation ARI_Mv1urban is again an exception since it presents a much larger domain averaged decrease that is around -11 to -16%.

In addition to the relative difference of Rsds, we have calculated the metric of radiative effect (RE) (Fig. 12). RE is the change of the net shortwave radiation at the surface, and it consists of the sum of the direct radiative effect (DRE) and the forcing due to changes in cloud cover and cloud properties (ΔSCRE). Implementation of only aerosol-radiation interactions produces a negative RE of -7W/m^2 as annual domain average. The RE in winter is -2W/m^2 whereas in summer it is considerably stronger, around -11 to -13W/m^2 (Table 6), something to be expected due to the larger amounts of radiation at the surface as well as due to the increased AOD during this season. Simulation ARI_Mv1urban has again a more pronounced effect on radiation with RE values being much more negative, more than double of those seen in the ARI group. RE for ARI_Mv1urban is -15 W/m^2 as annual average, -4 W/m^2 in winter and -26 W/m^2 in summer.

In general, the radiative effect for the ARI group of simulations (except ARI_Mv1urban) is smaller when compared to other studies. The study of Huszar et al. (2012) presented a RE similar to our study in summer (-12 to -15 W/m^2) but had a noticeably larger effect in winter (-7 W/m^2). Zanis (2009), using RegCM3, calculated a RE for the summer of 2000 that is stronger compared to the mean values of our study. Moreover Nabat et al. (2015) presented a RE of -10 W/m^2 as an annual average. Indeed the simulations of our study that implement only aerosol-radiation interactions have a smaller radiative effect both as annual averages as well as on a seasonal basis. The exception of ARI_Mv1urban on the other hand presents values that are larger (more negative) compared to the studies discussed above. Especially during summer ARI_Mv1urban has a way to strong RE (-26 W/m^2) to be considered realistic.

Interestingly, when we implement aerosol-radiation interactions in an environment where aerosol-cloud interactions are also present, the impact on radiation slightly weakens. In order to assess this, we calculate the RE between ARCI and ACI. It presents a similar behavior compared to the RE calculated between the ARI group and CON however, Rsds decrease is smaller and the RE is slightly less negative ranging from -1W/m^2 in DJF to -11W/m^2 in JJA. As it will be shown in section 1.5.3.6, this happens because between ARCI and ACI there is change in the cloud forcing (ΔSCRE) that is positive and increased compared to the ARI simulations. Therefore this is a clear indication that when both aerosol-radiation and aerosol-cloud interactions are introduced, cloudiness responds in a way that tends to counterbalance the radiation decrease seen by aerosol-radiation interactions.

We have seen that ARCI has aerosol-cloud-radiation interactions and uses the Thompson aerosol-aware microphysics. If we compare ARCI to the control simulation CON (and not to ACI as above) the clear-sky radiation decreases as expected due to aerosol scattering and absorption. Interestingly however, the Rsds presents a small increase of 2 to 10% (domain average) whereas RE becomes negligible close to zero. This happens because the simulations using the Thompson aerosol-aware scheme present in general a slightly smaller cloud cover compared to those using the Thompson2008 microphysics (see section 1.5.3.6). This leads to a positive cloud forcing (clouds allow more radiation to reach the surface) that in turn leads to the radiation increase. Therefore when ACI, that has only the indirect effect, is also compared to CON it presents Rsds increase that is around 7 to 9% depending on season. Therefore we see that only the change of the microphysics scheme can lead to a considerable change in shortwave radiation. Back to the comparison of ARCI to CON, we see

that the RE presents both positive and negative values over the domain. The positive RE is more pronounced during spring and summer in the northern and western part of the domain, spatially coinciding with large positive changes in the cloud forcing. However, as we will see in section 1.5.3.6, the significant changes in cloud forcing do not always coincide spatially with large and significant changes in the amount of cloud cover.

By implementing aerosol-radiation interactions only, the spatial correlation between radiative forcing RE (calculated as a difference from CON) and the AOD field is high (-0.6 to -0.9). However, when aerosol-cloud interactions are also included this spatial correlation considerably decreases (-0.2 to -0.4). This is something to be expected and must be attributed to the occurring changes in cloud fraction that blur the link between the AOD field and the overall impact on radiation. These changes in cloudiness can be attributed not only to aerosol-cloud interactions that are enabled effects but also to the different microphysics scheme used.

We must note here that aerosol optical depth (AOD) is of course extremely important in modeling aerosol-radiation interactions, but the other aerosol optical properties, especially the single scattering albedo (SSA), can also have an intense impact on radiation amount. The study of Alexandri et al. (2015), using RegCM4 over Europe, found that AOD is the most important of the aerosol parameters for correctly simulating shortwave radiation but the other aerosol optical properties, single scattering albedo (SSA) and asymmetry factor (ASY), can also play an important role that can be crucial over specific areas and during specific months.
In the case of our study, a nice example is to look at the simulations, ARI_Mv1, ARI_Mv1full and ARI_Mv1urban. All of them use the MACv1 climatology of AOD but have differences in the other aerosol optical properties. Simulations ARI_Mv1 and ARI_Mv1full have similar values of SSA (ranging from 0.92 to 0.98) and also present very similar results in Rsds decrease and radiative effect. Their results are however not identical (e.g. Table 5), showing that small differences in single scattering albedo can have an impact on radiation levels despite using the same AOD. Interestingly, in some cases the differences in radiation between simulations with the same AOD but different SSA values can be as large as the differences between simulations using different AOD fields. Simulation ARI_Mv1urban on the other hand has much lower SSA values (starting from 0.6) compared to all the other simulations in the sensitivity study. Therefore its aerosols are considerably more absorbing leading to a much larger impact on Rsds attenuation that in many cases is more than double compared to that of the rest simulations. This intense effect on radiation is widespread over the domain. It is characteristic that ARI_Mv1urban has a distribution (including all grid points on a given season) of Rsds decrease that is clearly shifted towards more negative values compared to the rest simulations (Fig. 11).

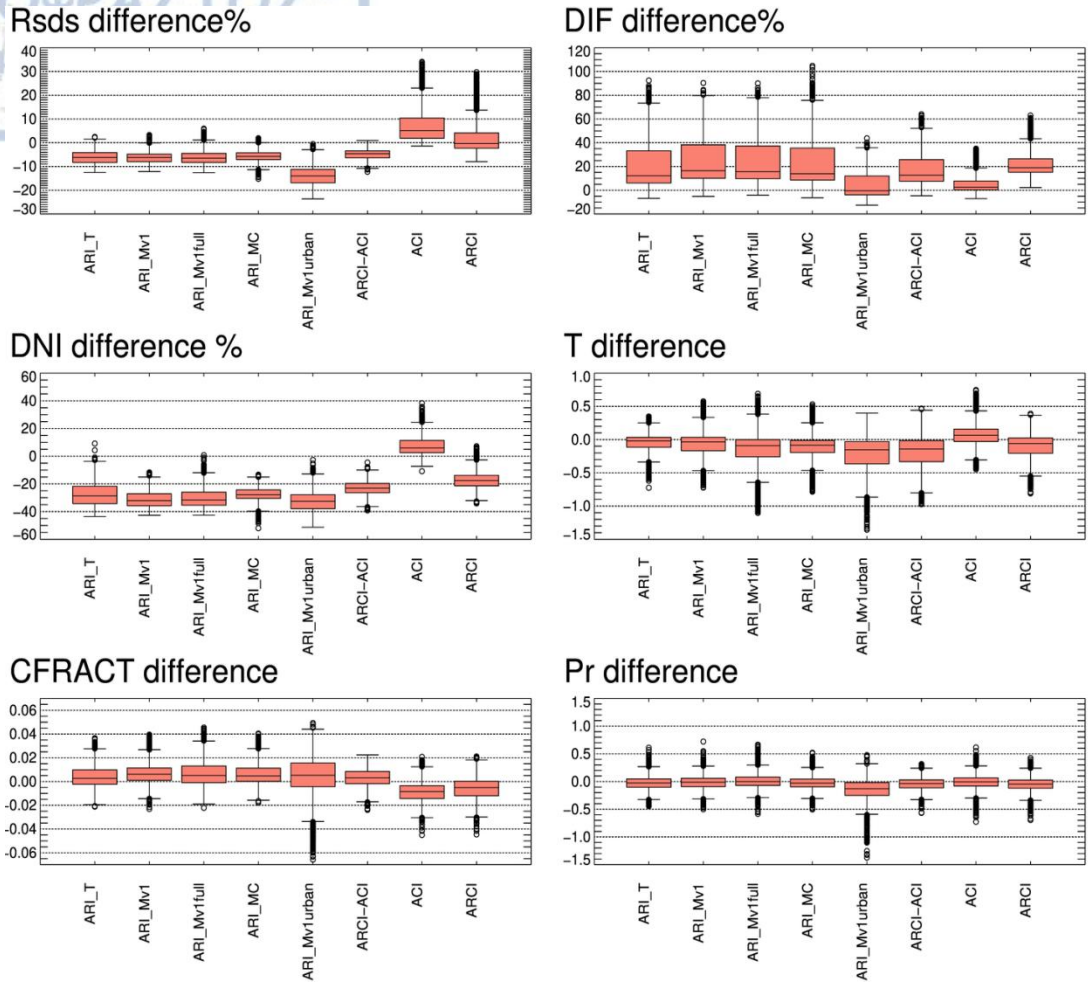

Fig. 11: Box plots regarding annual domain averaged values of the difference of each simulation from control simulation CON. For shortwave radiation at the surface (Rsds), diffuse radiation at the surface (DIF), direct normalized radiation at the surface (DNI), temperature (T), total cloud fraction (CFRACT) and precipitation (Pr). The difference of ARCI-ACI is also included to assess aerosol-radiation interactions in an environment where the indirect effect is also present.

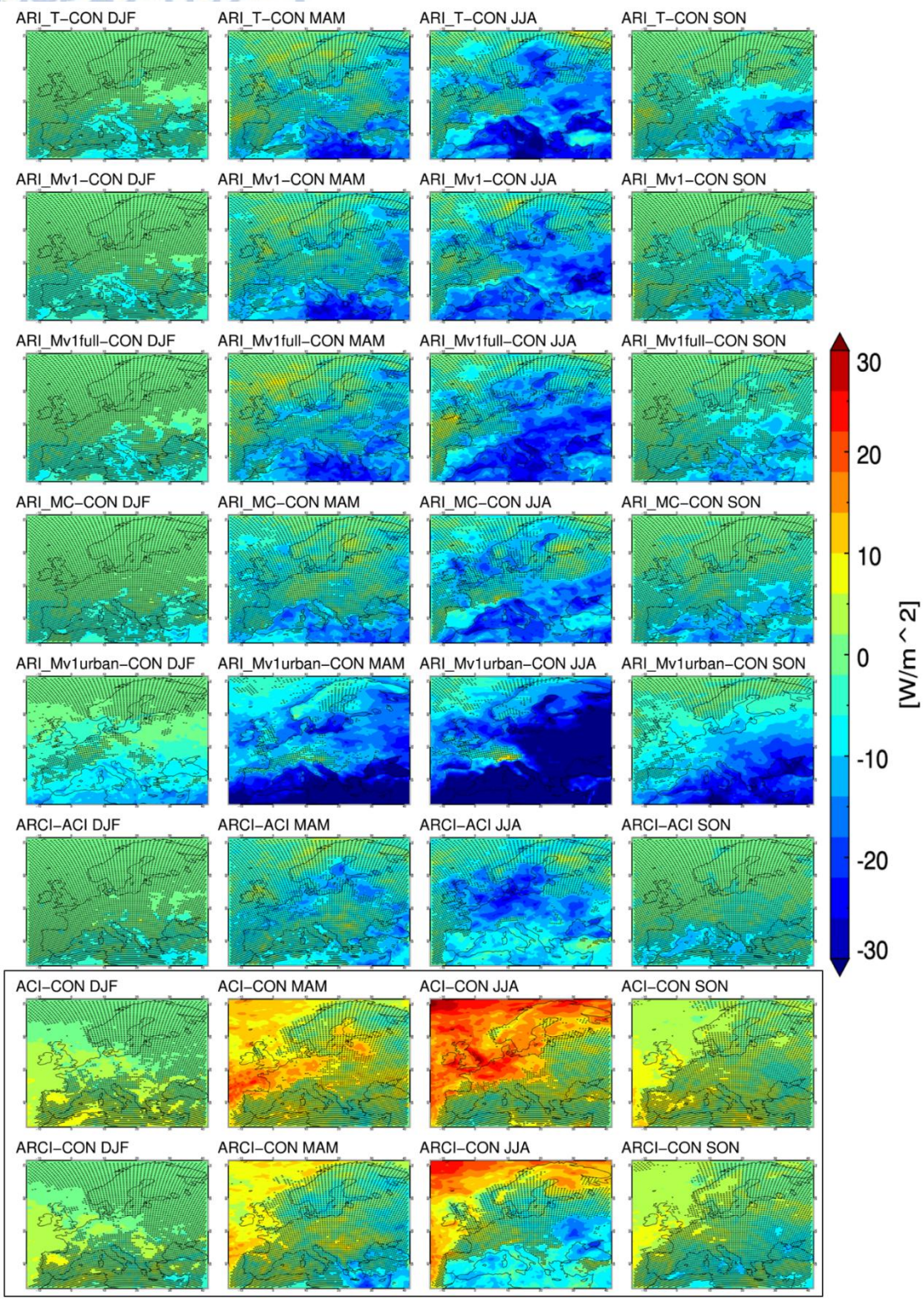

Fig. 12: Radiative forcing (RE) calculated against control CON for all experiments and seasons. Furthermore, the RE of ARCI calculated against ACI (ARCI-ACI) is given to assess aerosol-radiation interaction implementation in the Thompson aerosol aware microphysics that includes the indirect aerosol effect (row six). First six rows present the impact of aerosol-radiation interactions. Last two rows (black box) present the impact of TE2014 with indirect effect against control (row seven) and TE2014 with aerosol-radiation interactions enabled against control (row eight).Stippling indicates areas where the differences are not statistically significant at the 95% level, according to the Mann-Whitney non-parametric test.

1.5.3.3 Overall radiation budget

We have also calculated the change in the overall radiation budget at the surface. The overall budget consists of the sum of the net shortwave (downwelling-upwelling) radiation and net longwave (downwelling-upwelling) radiation at the surface. The change in the overall radiation budget at the surface after aerosol-radiation interactions is negative and has a very similar behavior to the change in shortwave radiation at the surface and the radiative effect (RE) regarding both the spatial pattern (Fig. 13) as well as the domain averaged values (Table 8). However, the change in the overall radiation budget is consistently slightly smaller than the change in the net shortwave radiation. This is because the change in the net longwave radiation at the surface is slightly increased when aerosol-radiation interactions are enabled.

The decrease in the overall radiation budget at the surface is seen almost over the entire domain. The changes are of statistical significance over large parts of the domain, especially during summer. The annual domain averaged change is around -5 to -6W/m^2 for the ARI group of simulations (except ARI_Mv1urban), while on a seasonal basis, domain averaged values are smaller in winter (-1 to -2W/m^2) and largest in summer (-9 to -11W/m^2). Interestingly, if we consider the relative difference (%) from control simulation CON, winter is the season with by far the largest relative decrease (-50%). The small radiation amounts in winter definitely play a role in inflating the relative decrease amount. Again ARI_Mv1urban presents a much stronger impact (-13W/m^2 annual average) that is more than twice as large as the one seen for the other simulations that implement only aerosol-radiation interactions.

Table 8: Domain averaged values of aerosol optical depth (AOD), change (W/m^2) and relative change (%) in overall radiative budget at the surface (net shortwave + net longwave) from control CON simulation. For all experiments and all seasons. For simulation ARCI the change in overall radiation budget is also calculated against ACI (e.g. ARCI-ACI) in order to assess the implementation of aerosol-radiation interactions in the Thompson aerosol aware microphysics.

	AOD				OVERALL RADIATION BUDGET							
					Difference (W/m^2)				Relative Difference (%)			
Radiation interacting	DJF	MAM	JJA	SON	DJF	MAM	JJA	SON	DJF	MAM	JJA	SON
ARI_T	0,11	0,16	0,18	0,15	-2	-6	-10	-5	-59	-7	-8	-19
ARI_Mv1	0,14	0,24	0,24	0,19	-2	-7	-10	-4	-52	-9	-7	-14
ARI_Mv1urban	0,14	0,24	0,24	0,19	-4	-15	-22	-9	-120	-19	-18	-35
ARI_Mv1full	0,14	0,24	0,24	0,19	-2	-7	-11	-4	-53	-9	-8	-15
ARI_MC	0,13	0,22	0,22	0,17	-1	-5	-9	-3	-49	-7	-7	-14
ARCI-ACI	0,22	0,26	0,24	0,23	-1	-5	-8	-2	-59	-6	-6	-8
Cloud interacting + cloud microphysics												
ACI	-	-	-	-	1	5	8	1	18	6	6	6
Radiation + Cloud interacting + cloud microphysics												
ARCI	0,22	0,26	0,24	0,23	-1	-1	-1	-1	-30	-1	-1	-3

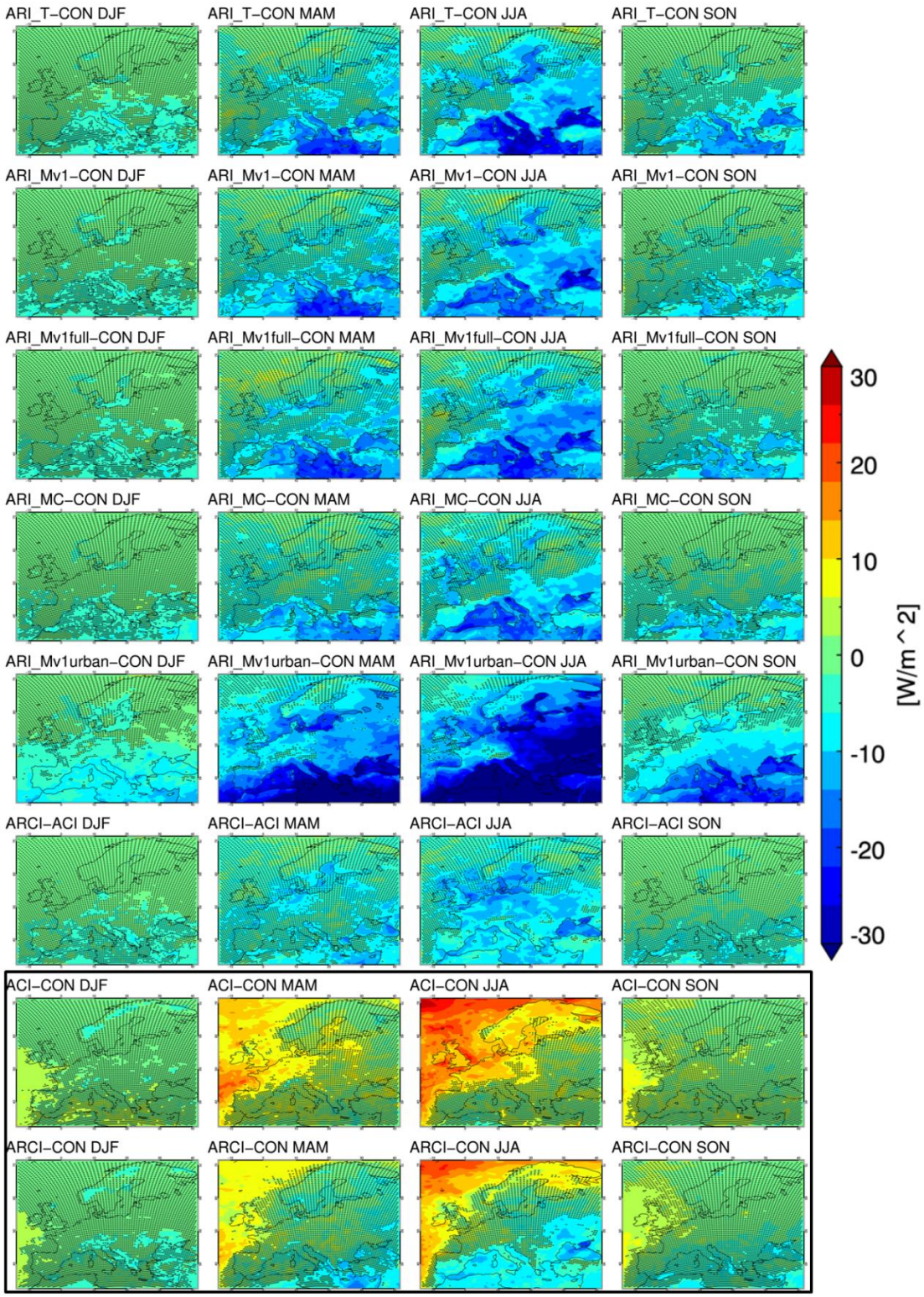

Fig. 13: Change of overall radiative budget at the surface (net shortwave + net longwave) from control simulation CON. Furthermore, the difference of ARCI calculated against ACI (ARCI-ACI) is given to assess aerosol-radiation interaction implementation in the Thompson aerosol aware microphysics that includes the indirect aerosol effect (row six). First six rows present the impact of aerosol-radiation interactions. Last two rows (black box) present the impact of TE2014 with indirect effect against control (row seven) and TE2014 with aerosol-radiation interactions enabled against control (row eight).Stippling indicates areas where the differences are not statistically significant at the 95% level, according to the Mann-Whitney non-parametric test.

1.5.3.4 Direct and Diffuse radiation

The shortwave radiation at the surface comprises of the direct and diffuse components. The direct radiation has not been scattered or absorbed and thus comes from the direction of the sun disk. In this study we examine the direct normalized irradiance (DNI) that is the direct radiation measured on a surface perpendicular to the direction of radiation. The diffuse radiation has been scattered and therefore comes from all angles.

Introduction of aerosol-radiation interactions in the ARI group leads to an intense direct normalized irradiance decrease that is considerably more severe than the decrease seen for Rsds. The domain averaged differences (from control) are around -30% for all simulations and seasons (Table 5). Over specific grid points the DNI decrease can exceed 50% (Fig. 11) especially during winter and autumn when the DNI levels are low due to the extensive cloud cover and small radiation (Rsds) levels.

Introducing aerosol-radiation interactions in an environment where the indirect effect is also present (ARCI-ACI) leads to a smaller decrease of DNI that is around -20% to -25% for all seasons. This is not attributed to cloud fraction changes between ARCI and ACI. This is because cloud fraction changes are not larger compared to the ARI group of simulations and also there is no tendency for a general cloud fraction decrease that could counteract the reduction of DNI by the aerosol. However, as shown in section 1.5.3.6, a general increase of cloud forcing is seen in the ARI group of simulations. Interestingly, this increase in cloud forcing is slightly larger between ARCI and ACI that only have aerosol-radiation interactions. Therefore, since the clouds let even more radiation to reach the surface in the ARCI-ACI comparison, we expect the direct component to be enhanced. This is probably the effect that slightly compensates for the decrease in DNI by aerosol scattering, thus leading to a more moderate reduction of DNI.

We have seen that the experiments with the Thompson aerosol-aware microphysics scheme present in general less cloud fraction values than those with the Thompson2008 scheme. This naturally affects DNI. For example when we compare ARCI (that has aerosol-cloud-radiation interactions) to CON the DNI decrease is less intense than those seen in the ARI group or in the ARCI-ARI comparison, mainly due to the less cloudiness amount ARCI has compared to CON. The same mechanism is seen in the comparison of ACI to CON. ACI does not have aerosol-radiation interactions and since it presents less cloud fraction values it normally shows increased DNI compared to CON. This increase is not negligible, around 6 to 11% regarding domain averages and consistent since it is present over almost 75% of all grid points (Fig. 11). As it was the case for Rsds, we see that only the change of the microphysics scheme can have a considerable and spatially extensive impact on the direct normalized irradiance.

Contrary to DNI, the diffuse radiation at the surface (DIF) consistently increases in all simulations with aerosol-radiation interactions enabled, except ARI_Mv1urban (Table 5). The intensity of the decrease varies noticeably and depends on the season. In winter it is around 7 to 20% whereas in summer it intensifies around 30 to 40%. We see that the impact of aerosol-radiation interaction on DIF is in general more intense over areas with small cloudiness amount, as is the case over the southern part of Europe especially during

summer. It is characteristic that a dual pattern of DIF changes (from control) is seen with the largest increase over the south parts of the domain that becomes less intense as we move towards the north. As said above, one interesting exception to the general increase of diffuse radiation is ARI_Mv1urban. This simulation presents a small domain averaged decrease of DIF in winter (-3%) and zero change in spring that is of course the product of compensation between areas with increased and areas with decreased DIF. Moreover the increase seen in summer and autumn is much smaller compared to the rest ARI simulations. This peculiar behavior of ARI_Mv1urban is probably connected to the changes in cloud fraction seen in this simulation. ARI_Mv1urban has the most pronounced changes (compared to control) in cloud fraction among all the simulations conducted and presents an overall cloud fraction decrease. Therefore, this decrease in cloudiness is partially counterbalancing the diffuse radiation increase due to aerosol scattering.

Ratio of direct to diffuse

We have seen how aerosol-radiation interactions impact radiation amounts. It is interesting to examine how shortwave radiation is distributed to the direct and diffuse components, and how this is differentiated with aerosol implementation. For this reason we examine the ratio of direct to diffuse radiation. We take into account the direct radiation (DIR) that reaches the surface and not direct normalized irradiance (DNI). This is because DIR and diffuse (DIF) both are calculated at the surface with their sum constituting the overall shortwave radiation (DIR+DIF=Rsds).

It is evident that aerosol-radiation interactions clearly impact the direct/diffuse ratio systematically, lowering it for all seasons compared to control CON (Fig. 14). The impact is less pronounced in winter, possibly due to the extensive cloudiness in this season which is dictating the distribution of Rsds to its direct and diffuse components.

The general behavior of the ratio distribution is quite similar for all simulations having aerosol-radiation interactions. For all seasons except summer, the largest part of the DIR/DIF distribution is below 1, indicating that diffuse radiation is usually greater than the direct component when aerosol-radiation interactions are enabled. Moreover the maximum values of the DIR/DIF ratio are small (at most 2-3) indicating that direct radiation never gets overwhelmingly larger than diffuse.

On the contrary, the control simulation CON that has no aerosol, has a DIR/DIF distribution that is clearly shifted towards larger values. Characteristically, in spring and autumn half of the grid points over the domain have larger direct than diffuse radiation, a number that is increased to 75% of the grid points for summer. Moreover in CON there are many cases where direct radiation can become immensely larger than diffuse, even by an order of magnitude (in summer). It must be noted that simulation ACI, which also does not have aerosol-radiation interactions, has an identical behavior to CON.

Finally, the DIR/DIF ratio has also been calculated for the SARAH satellite dataset. SARAH consistently presents direct radiation that is larger than diffuse. It is characteristic that in spring, summer and autumn 75% of the grid points present larger direct than diffuse radiation. In this respect, the distribution of the control simulation CON is closer to that of

the satellite dataset. However the maximum of DIR/DIF ratio is considerably more constrained in SARAH in spring, autumn and especially in summer compared to CON. The very large DIR/DIF values are absent for the satellite data for these seasons.

To sum up, aerosol-radiation introduction clearly affects the DIR/DIF ratio, lowering it and systematically presenting larger diffuse than direct radiation values. However the distribution of the DIR/DIF ratio seems to be closer to the satellite data when aerosol-radiation interactions are not enabled. This is probably related to the calibration of the model and especially the radiation scheme (RRTMG) used.

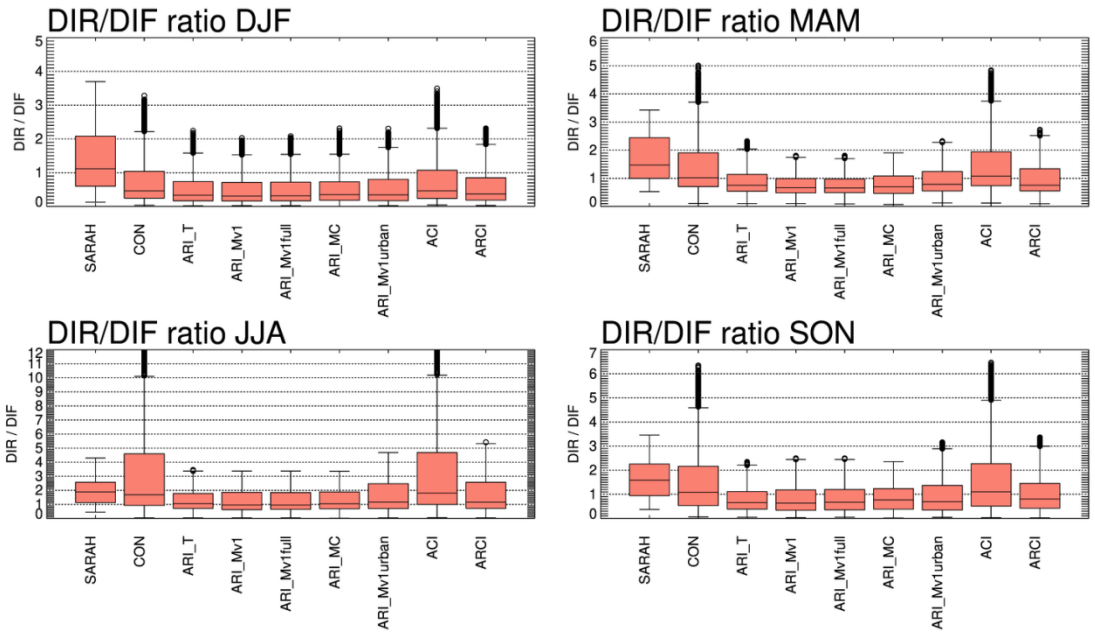

Fig. 14: Box plots of the direct/diffuse radiation at the surface ratio for each season. For all sensitivity simulations and the SARAH satellite dataset. The whiskers extend to the maximum and minimum data, or to 1.5 times either the IQR75 or IQR25, if there is data beyond this range. Outliers are identified with small circles.

1.5.3.5 Spatial and Temporal comparison of radiation with satellite data

In this section we explore how much the spatial and temporal patterns of radiation change in the sensitivity simulations and how well they compare against the satellite data. We have seen that aerosol-radiation introduction does not necessarily improve the radiation bias (1.5.2.5). On the contrary in several cases it may worsen it. Bias however depends on the calibration and overall tuning of the model and its parameterization schemes. Since aerosols have considerable spatial and temporal variability, a more relevant question would be whether the introduction of aerosols improves the spatial pattern and temporal correlation with reference datasets. However due to their highly parameterized nature, satellite datasets might not be adequate to fully assess the spatial pattern of the sensitivity simulations, a matter that is discussed below.

Spatial pattern

We have constructed Taylor plots of the mean spatial pattern (all grid points of EU domain) for each season for clear-sky radiation (CRsds) and shortwave radiation at the surface (Rsds) as well as for the direct normalized irradiance (DNI) and total cloud fraction (CFRACT). We mainly use the SARAH dataset as reference but also present results for the CLARA dataset (for CRsds) and the CLAAS dataset (for CFRACT).

Regarding clear-sky radiation, when compared against the SARAH dataset (Fig. 15, top), correlation is very high for all seasons (above 0.95) and all simulations are tightly grouped together. Exception is summer where correlation is slightly worse (but still quite high, above 0.9) and simulations present a larger spread. Finally all simulations overestimate the variability (standard deviation) of the satellite data. The same overall picture is seen for comparison against the CLARA dataset, with the exception that the correlation coefficients are generally smaller (between 0.8 and 0.95).

For all seasons except summer, introduction of aerosol does not seem to make a considerable difference regarding spatial matching with the reference datasets. Interestingly in summer, introduction of aerosol-radiation interactions slightly worsens the correlation with the SARAH dataset for almost all simulations compared to that of the control simulation CON. Only ARI_MC with the MACC climatology has a similar correlation coefficient with that of CON. On the other hand, in the comparison against the CLARA dataset, the simulations using the MAC-v1 climatology (except ARI_Mv1urban) present a small improvement in correlation. However these results seem to be strongly connected to the parameterized nature of the satellite datasets. It has been a surprise to discover that both the SARAH and CLARA datasets presume the existence of specific aerosol climatologies in order to parameterize radiation. The SARAH use a slightly modified MACC aerosol climatology (Müller et al., 2015), therefore simulation ARI_MC (yellow square in summer), which uses the MACC climatology, presents better correlation with this dataset compared to the other simulations with aerosol-radiation interactions. On the other hand, the CLARA dataset presumes an aerosol climatology that is related to the MAC-v1 (Karlsson et al., 2013). Thus, simulations ARI_Mv1 and ARI_Mv1full that use the MAC-v1 climatology (blue and green squares in summer) have better correlation against CLARA. As a result, the use of these satellite datasets in order to assess spatial pattern correlation, at the fine level that is required for simulations with aerosol-radiation interactions, is definitely dubious.

However we can make a statement about the assessment of the CRsds spatial variability of the simulations. All simulations present systematically larger spatial variability compared to both SARAH and CLARA datasets. Moreover the use of aerosol-radiation interactions tends to slightly reduce the spatial variability and thus leads to a moderate improvement with the satellite datasets.

If we examine all-sky shortwave radiation at the surface (Rsds) and its direct normalized component (DNI) we see that spatial pattern behavior is very similar regarding spatial correlation for all simulations on a given season (Fig. 16). More importantly, simulations are grouped together in the Taylor plots forming clusters for a given season in a way that follows the spatial pattern assessment of simulated cloud fraction against satellite data. Both the

CLARA and the CLAAS (which is more closely related to the SARAH dataset) satellite datasets have been used in CFRACT assessment to improve robustness of results. This indicates that cloudiness is the major factor impacting the seasonal spatial pattern of both Rsds and DNI and aerosol inclusion has little to no difference. However, as is the case in CRsds, the inclusion of aerosol-radiation interactions leads to a reduction of the spatial variability, an effect that is very strong in direct normalized irradiance. Since the control simulation tends to overestimate both Rsds and DNI spatial variability for all seasons except winter, the inclusion of aerosol-radiation interactions constrains the variability and generally improves its matching with the satellite data.

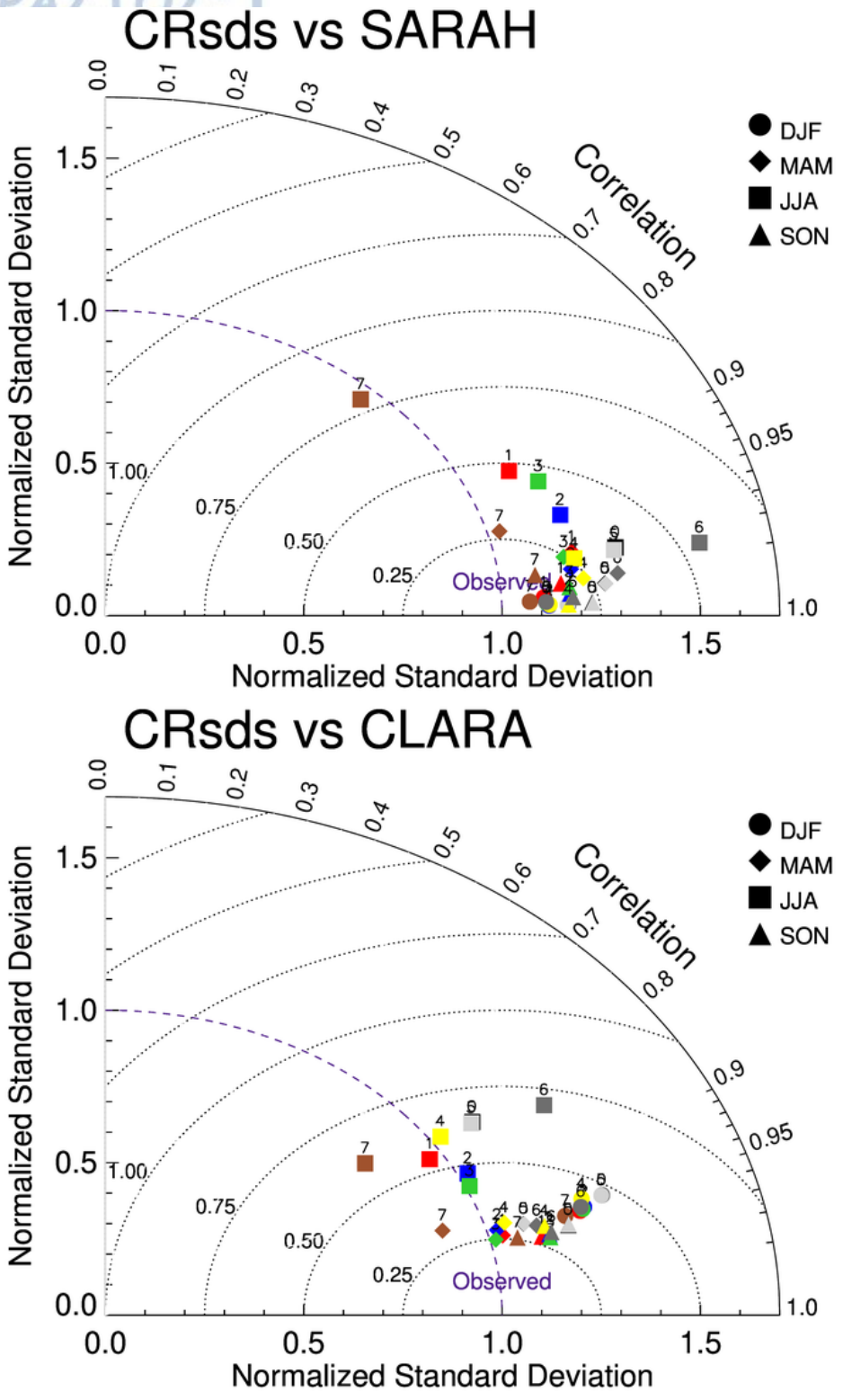

0 CON *1 ARI_T* *2 ARI_Mv1* *3 ARI_Mv1full* *4 ARI_MC* *5 ACI* *6 ARCI* *7 ARI_Mv1urban*

Fig. 15: Taylor plot for the mean seasonal spatial pattern of clear-sky down welling radiation at the surface (CRsds). Comparison against the SARAH satellite dataset (top) and the CLARA satellite dataset (bottom). The seasons are depicted with different symbols. The simulations are depicted with different colors and numbers.

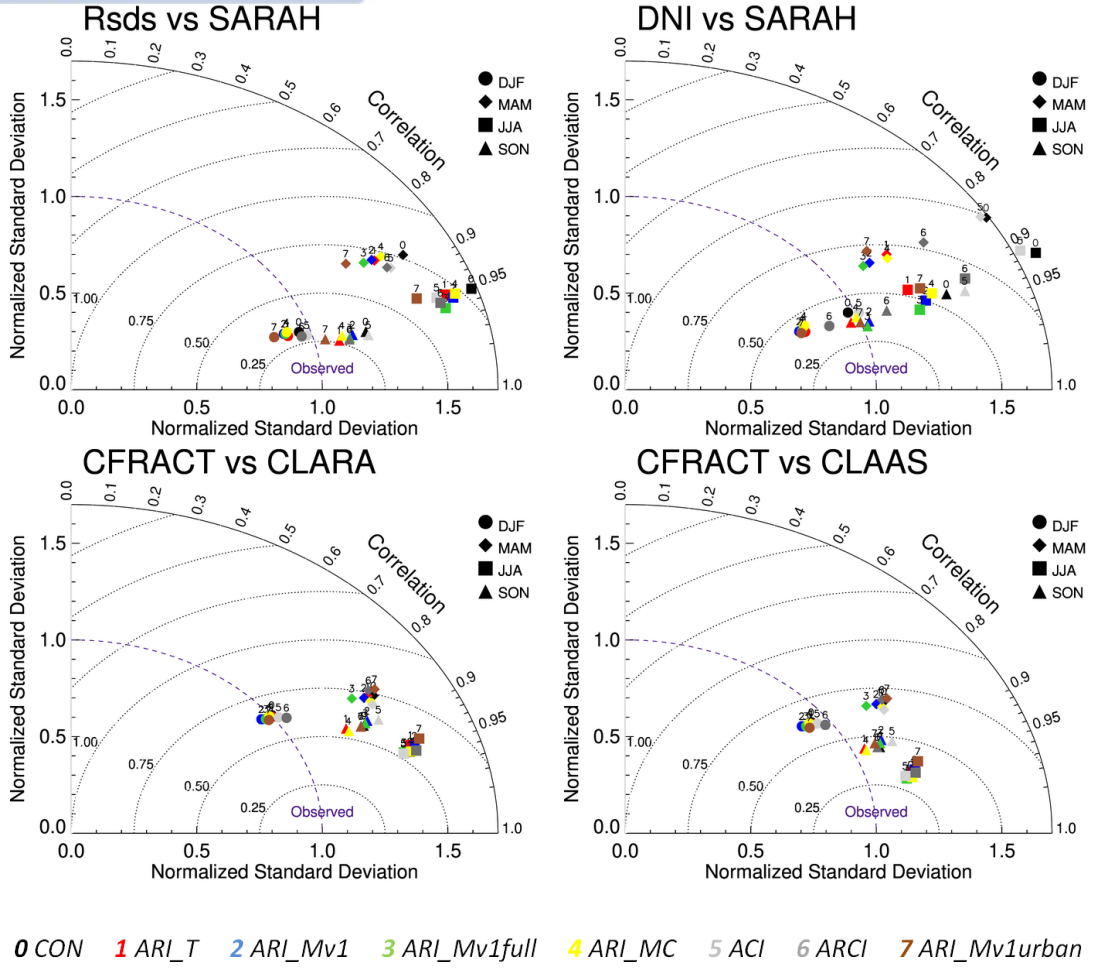

Fig. 16: Top: Taylor plot for the mean seasonal spatial pattern of shortwave down welling radiation at the surface (Rsds) (left) and its direct normalized component (DNI) (right) against the SARAH satellite dataset. Bottom: Taylor plot for the mean seasonal spatial pattern of total cloud fraction (CFRACT) against the CLARA (left) and the CLAAS (right) satellite datasets. The seasons are depicted with different symbols. The simulations are depicted with different colors and numbers.

Temporal matching

We have constructed temporal Taylor plots for CRsds, Rsds and DNI against the SARAH dataset, using as time series the spatial mean for all the Prudence subregions and the EU domain for the entire 2004-2008 period (Fig. 17). Both monthly mean and daily mean values have been used with similar results. We do not put emphasis on the temporal comparison against the satellite data since for all the variables examined the inclusion of aerosol does not have an impact on correlation. Despite the strong seasonal variability of aerosol, the correlation of all radiation variables examined is dominated by the natural seasonal cycle of solar radiation. Thus all simulations present very good correlation with SARAH and no impact of aerosol is seen on temporal correlation. The only impact is seen in the case of DNI where the temporal variability is greatly reduced when aerosol-radiation interactions are used.

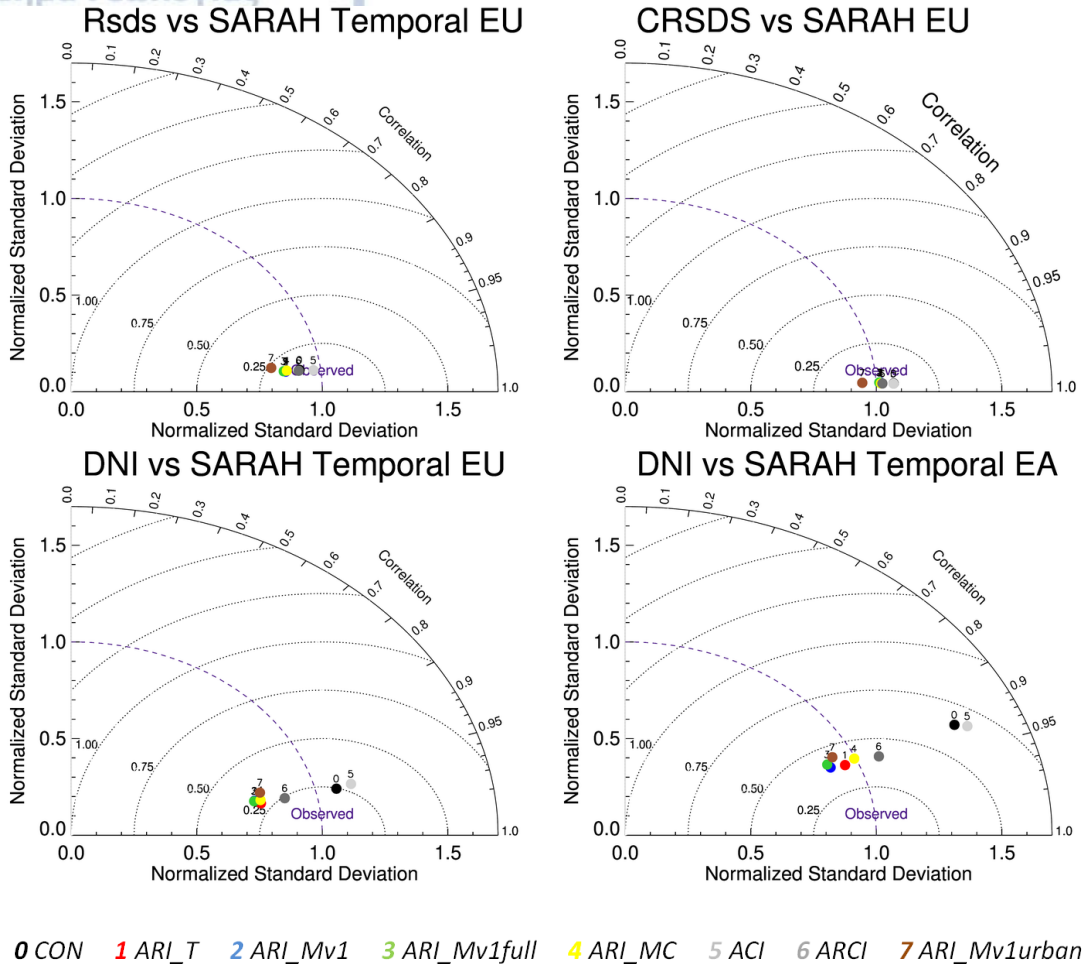

Fig. 17: Temporal Taylor plot using domain averaged values for the EU region and the Eastern Europe (EA) subregion (bottom, right) against the SARAH satellite dataset. For shortwave radiation at the surface (Rsds), clear-sky shortwave radiation at the surface (CRsds) and direct normalized irradiance (DNI).

1.5.3.6 Cloud fraction and cloud forcing

Total cloud fraction

The model calculates cloud fraction at each vertical level. Total cloud fraction (CFRACT) is synthesized by the fraction amount of all the vertical levels and it represents the extent to which the sky is covered with clouds as seen at the surface.

Changes in CFRACT, compared to control CON, are in general very constrained for all simulations, regardless of the aerosol interaction enabled or aerosol data set used. The domain averaged changes are very small, around 0.01 (in a 0 to 1 scale). Of course this is up to a point due to sign compensation since there are CFRACT decreases and increases over different areas of the domain. However even the absolute differences from CON are also small. They range from 0.01 to 0.03, showing that changes in cloudiness are indeed quite

constrained and that the sign compensation described above is not what it keeps the domain averaged values small.

Enabling aerosol-radiation interactions in the ARI group leads to changes that are usually less than 0.01 and at most 0.03 for some subregions. The smallest impact is seen in winter, something to be expected since then the aerosol load is small and also cloudiness is mainly affected by strong synoptic phenomena. In relative values differences of up to 10% can be seen over areas with small cloud amount, such as south Europe during summer (Table 9). The direction of cloudiness change is not very clear, nevertheless a small domain averaged increase in CFRACT is seen for all ARI simulations, except ARI_Mv1urban, in summer and spring. Other studies of aerosol-radiation interactions (Nabat et al., 2015a; Schultze and Rockel, 2018) have shown a general cloud fraction reduction.

Interestingly, we can see from Fig. 19 that all the ARI simulations, including ARI_Mv1urban, share a common area of pronounced cloud fraction increase in autumn that seems to be of statistical significance. This area lies over the Black and the eastern Balkan Peninsula and includes parts of central-eastern Mediterranean and North Africa is some cases. These are probably connected to a cyclonic anomaly found in the upper atmosphere that is present over the region (section 1.5.3.9). It seems that aerosol can have an impact on temperature (section 1.5.3.7) and the overall thermodynamic profile of the atmosphere that can lead to local changes in circulation that in turn can affect cloudiness amount.

The absorbing “urban” aerosol type of ARI_Mv1urban seems to have a more pronounced impact on cloudiness. Areas of central Europe, including France and the Alps present a pronounced decrease in CFRACT during spring and summer that ranges around -2% to -18% (-0.02 to -0.09) and in several grid points can exceed -20% (-0.15). In summer and autumn an intense increase of CFRACT is seen over large parts of eastern and northeastern Europe that reaches 20% in places (exceeds 0.1). In autumn a CFRACT increase (2%) is seen almost all over the domain, except over the Alps. For all seasons except winter there are extensive areas of the domain with CFRACT changes that seem to be of statistical significance. ARI_Mv1urban highlights once again the importance of correctly representing aerosol optical properties such as SSA in climate simulations.

The use of the Thompson aerosol-aware microphysics scheme seems to have an impact on cloudiness, since it presents in general lower cloud fraction amounts compared to the Thompson2008 scheme. It is characteristic that simulation ACI, that uses the aerosol-aware scheme, has smaller CFRACT compared to CON for all seasons and for almost all the subregions of the domain (Table 9). Averaged for the entire domain the CFRACT difference from CON is between -0.7% in winter and -3% in summer. Regarding the subregions the largest difference is seen over central Europe (including ME, FR and AL) in summer, where it reaches -7%. For this extensive area we also have the indication that the differences present statistical significance. Simulation ARCI, that also uses the Thompson aerosol-aware scheme, presents also smaller CFRACT values than CON, but to a smaller extent compared to ACI. Interestingly ARCI does not present an area of significant CFRACT decrease (compared to CON) over central Europe, as is the case with ACI. The implementation of aerosol-radiation interactions in ARCI leads to a significant increase of CFRACT over this area compared to ACI.

Therefore when ARCI is compared to CON the differences over central Europe are negligible. Finally, in addition to CFRACT, the Thompson aerosol-aware microphysics also presents impact on variables that are related to cloudiness such as the liquid water path (LWP) and the ice water path (IWP). Both ARCI and ACI present lower values of both IWP and LWP compared to control CON for all seasons and for the biggest part of the domain. This makes the results on CFRACT even more robust, thus we can clearly state that the Thompson-aerosol aware scheme has a clear tendency of producing less cloudiness compared to the Thompson2008 scheme.

Finally we have a comment regarding the impact on different cloud levels. So far we have only examined the impact on total cloud fraction (CFRACT). We have also categorized cloudiness, according to the height it is encountered, into Low, Medium and High clouds and have calculated a total cloud fraction for each category. For this we used the same algorithm the model uses to derive the total cloud fraction (maximum-random overlap). Investigating the sensitivities for the different cloud categories it becomes clear that the cloud fraction of the Low clouds presents the biggest changes among the three categories, regardless the aerosol-interaction implemented or the aerosol data used. Moreover the patterns of pronounced and statistical significant changes in total cloud fraction are mainly driven by changes in the Low clouds. The changes of Medium level clouds are less intense and less extensive in terms of area, whereas higher clouds are the least impacted by changes in aerosol and/or the microphysics scheme. This is something to be expected since the largest aerosol loads in the model, as well as in nature, are located in the lower parts of the troposphere. Fig. 18 presents two cases (ACI in summer and ARI_T in autumn) where the total cloud fraction differences from control CON are decomposed into the three cloud categories.

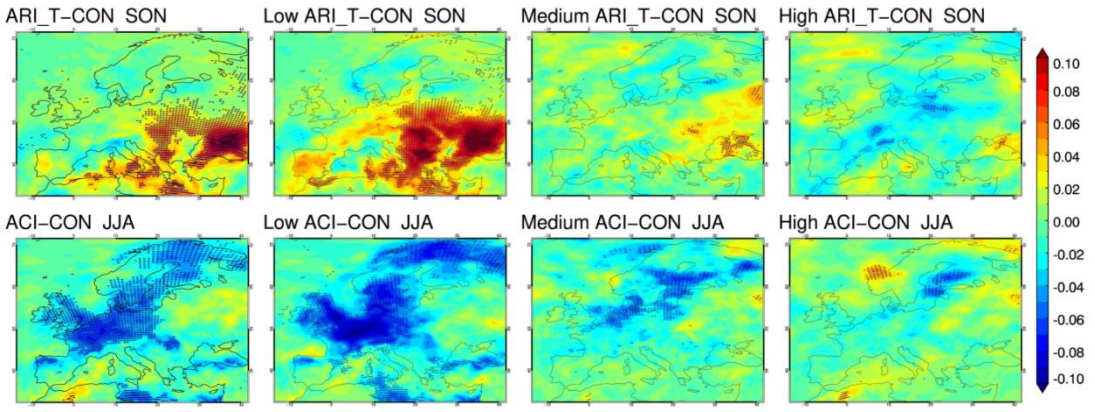

Fig. 18: Difference from control simulation CON regarding total cloud fraction (first column) as well as cloud fraction for Low, Medium and High clouds (second to fourth column respectively) for simulation ARI_T during Autumn (top row) and simulation ACI during summer (bottom row). Stippling indicates areas where the differences are statistically significant at the 95% level, according to the Mann-Whitney non parametric test.

Table 9: Relative differences in total cloud fraction (CFRACT) from control CON. For all seasons and all subregions.

DJF

	ARI_T	ARI_Mv1	ARI_Mv1urban	ARI_Mv1full	ARI_MC	ACI	ARCI	ARCI-ACI
BI	-0,2	0,0	0,1	0,3	-0,2	-0,3	-0,5	-0,2
IP	-0,2	2,2	0,9	0,9	0,4	-1,7	-3,7	-2,0
FR	0,0	1,0	-0,8	0,3	0,2	-0,1	-1,3	-1,3
ME	-0,5	-0,4	-0,9	-1,2	-0,5	-0,6	-1,4	-0,8
SC	-0,1	-0,4	-0,1	-0,4	-0,1	-0,5	-0,4	0,1
AL	-0,3	0,8	-1,4	-0,9	-0,3	-0,2	-1,9	-1,7
MD	0,3	1,9	1,1	1,1	0,3	-1,3	-2,1	-0,9
EA	-0,6	-0,5	-0,7	-0,9	-0,1	-0,8	-1,2	-0,5
EU	-0,1	0,5	0,0	0,0	0,0	-0,7	-1,4	-0,6

MAM

	ARI_T	ARI_Mv1	ARI_Mv1urban	ARI_Mv1full	ARI_MC	ACI	ARCI	ARCI-ACI
BI	0,2	-0,3	0,9	-1,0	0,9	-0,5	-0,5	0,0
IP	-0,3	0,6	1,3	0,3	1,0	-1,1	-1,9	-0,9
FR	-1,1	0,6	-1,8	-1,0	-0,2	-3,4	-2,5	0,9
ME	-0,2	-1,0	-1,5	-0,4	-0,9	-2,3	-1,4	0,9
SC	-1,2	0,2	0,1	-0,1	-0,8	-1,6	-0,1	1,4
AL	-1,1	-0,6	-7,2	-0,3	-0,9	-2,0	-1,7	0,3
MD	0,5	2,0	-2,3	3,8	1,4	-1,4	-1,0	0,4
EA	-1,7	-0,5	-3,9	0,1	-1,1	-2,9	-3,0	-0,2
EU	-0,6	0,3	-1,1	0,5	0,0	-1,5	-1,0	0,5

JJA

	ARI_T	ARI_Mv1	ARI_Mv1urban	ARI_Mv1full	ARI_MC	ACI	ARCI	ARCI-ACI
BI	1,0	1,4	1,7	0,9	2,2	-2,7	0,3	3,0
IP	-0,7	4,5	6,8	1,3	-0,6	-2,0	-2,2	-0,1
FR	-1,1	-0,9	-5,9	-0,3	0,0	-5,4	-1,3	4,2
ME	-1,2	1,7	-1,8	0,8	2,0	-6,8	0,0	6,8
SC	2,6	2,3	0,6	2,0	1,5	-3,1	-1,0	2,1
AL	-3,5	-3,9	-18,0	1,8	1,7	-5,6	-1,9	3,7
MD	5,7	-0,9	-10,5	11,2	7,4	-1,0	-6,7	-5,7
EA	-0,3	1,0	0,1	3,6	2,5	-3,5	-0,1	3,4
EU	1,1	0,9	-2,3	3,2	2,4	-3,0	-1,9	1,2

SON

	ARI_T	ARI_Mv1	ARI_Mv1urban	ARI_Mv1full	ARI_MC	ACI	ARCI	ARCI-ACI
BI	0,6	1,2	1,3	-0,2	0,9	-0,4	-0,8	-0,5
IP	1,3	-1,7	-0,8	-2,0	2,0	-5,9	-1,7	4,6
FR	-0,1	1,8	1,4	-0,2	2,0	0,4	-1,5	-1,9
ME	1,0	2,1	2,6	1,6	-0,7	0,0	-1,4	-1,5
SC	-0,1	0,9	1,0	1,4	0,2	-0,4	-1,1	-0,8
AL	-0,9	-0,2	-2,4	-1,2	-0,8	-1,1	-2,6	-1,6
MD	5,6	1,3	3,4	0,9	6,0	-2,6	1,9	4,5
EA	4,6	3,1	5,0	1,6	3,9	-0,4	1,0	1,3
EU	1,9	1,0	2,0	0,7	2,1	-1,3	-0,5	0,8

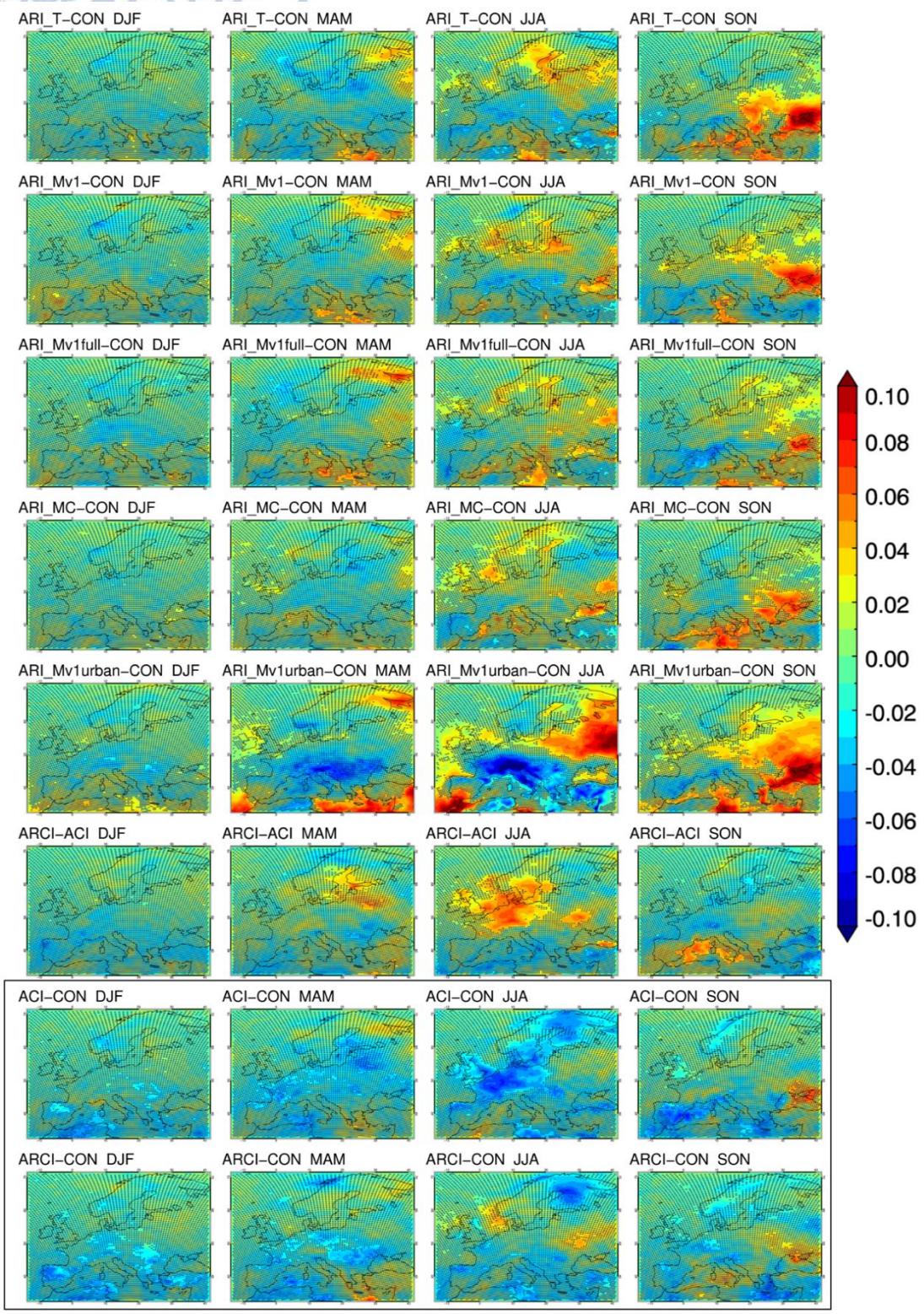

Fig. 19: Total cloud fraction (CFRACT) difference from control simulation CON for all simulations and seasons. Moreover the CFRACT difference of ARCI calculated against ACI (ARCI-ACI) is given to assess implementation of aerosol-radiation interactions in the Thompson aerosol aware microphysics (row six). First six rows present the impact of aerosol-radiation interactions. Last two rows (black box) present the impact of TE2014 with aerosol-cloud interactions against control (row seven) and TE2014 with both aerosol-radiation and aerosol-cloud interactions enabled against control (row eight). Stippling indicates areas where the differences are not statistically significant at the 95% level, according to the Mann-Whitney non-parametric test.

Cloud forcing

We have seen so far that aerosol-radiation interactions can change total cloud fraction over specific areas, whereas the use of the Thompson aerosol-aware scheme produces lower CFRACT amounts compared to the Thompson2008 scheme.

Probably of even greater importance than the changes in cloud fraction is the impact of aerosol on the ability of clouds to interact with radiation. In order to assess this impact we calculated the change in the cloud forcing at the surface regarding shortwave radiation (ΔSCRE). ΔSCRE is the difference between the radiative effect RE and the Direct radiative effect DRE (thus ΔSCRE=RE-DRE). The change in the cloud forcing definitely depends on the change in cloud fraction amount but also depends on the change in the cloud optical properties that lead to changes in the cloud optical thickness. If no changes in the optical properties are made we expect the changes in cloud forcing to be negatively correlated with the changes in CFRACT. For example a decrease (increase) in CFRACT lets more (less) radiation to reach the surface thus presents an increased (decreased) ΔSCRE.

Interestingly, when compared to control CON, all the simulations present an increase in the cloud forcing. Domain averaged ΔSCRE is positive for all simulations (Table 6) while ΔSCRE is also positive over almost the entire domain (Fig. 21). Therefore the introduction of aerosol-radiation interactions and/or the Thompson microphysics with aerosol-cloud interactions leads to situation where cloudiness is enabling more radiation to reach the surface.

For the simulations that have only aerosol-radiation interactions (ARI group), the ΔSCRE represents the impact of semi-direct aerosol effect on radiation. The semi-direct effect is positive with annual average around 3 to 4 W/m^2 and is strongest during spring (5 to 7 W/m^2) (Table 6). The study of Nabat et al. (2015) had calculated a somewhat larger semi-direct effect of 5 to 6 W/m^2 regarding annual averages. The positive semi-direct effect is counteracting the clearly negative direct radiative effect (DRE) of aerosol thus helps to constrain the overall negative total aerosol radiative effect (RE). Compared to the direct radiative effect the magnitude of the semi-direct effect is considerable. For example the semi-direct effect amounts to 60% of the direct radiative effect (absolute value) on radiation in winter, 45% in spring and ranges from 20 to 35% in summer and spring. Therefore the impact of the semi-direct effect plays an important role in the overall effect of aerosol-radiation interaction implementation in the model. Fig. 20 decomposes the overall radiative effect into the direct radiative effect and the change in the cloud forcing (semi-direct effect for ARI group). It clearly displays the counteracting between DRE and ΔSCRE as well as the relative importance of ΔSCRE in the overall radiative effect RE.

When we compare simulation ARCI to ACI (ARCI-ACI) we examine the implementation of aerosol-radiation interactions in an environment where aerosol-cloud interactions are also present. In this case the ΔSCRE represents the combined impact of the semi-direct and indirect effect on cloud forcing. Results show that ΔSCRE slightly increases (4-7 W/m^2) compared to the cloud forcing change seen in the ARI group. The relative importance of ΔSCRE is also larger, reaching 80% of the DRE in winter and 65% in autumn.

In the comparison of ARCI to control CON, the change in cloud forcing is attributed not only to the semi-direct and indirect effects but to the change in the microphysics scheme as well. The ΔSCRE is further increased in this case ranging from 6 to 13 W/m^2. This leads to a ΔSCRE that is equal in magnitude to the DRE and has an increased relative importance in the overall radiative effect RE.

As we have said before, the changes in cloud forcing are the result of: a) changes in cloud fraction amount and/or b) changes in cloud optical properties and characteristics. We would expect that a general positive change in the cloud forcing, seen when aerosol-radiation interactions are enabled, would be attributed to an overall decrease of cloudiness. However, this does not happen in the ARI group of simulations (except for ARI_Mv1urban for most seasons) and there seems to be no clear connection between the change in cloud forcing and the change in cloud fraction amount (Fig. 22). Of course, over the domain areas with considerable cloud fraction changes usually impact cloud forcing. On the other hand there are also areas where a statistically significant CFRACT change does not lead to a significant change in cloud forcing (such as the CFRACT increase near the Black Sea in autumn for the ARI group). Since, the positive change in ΔSCRE is not explained by an overall decrease of cloudiness amount, it must be explained by a change in the cloud optical properties. To examine this, we have also calculated the shortwave cloud forcing at the top of the atmosphere (SCRE_TOA) and its change (ΔSCRE_TOA) with the introduction of aerosol-radiation interactions. The SCRE_TOA is the difference of shortwave upwelling clear-sky radiation at the top (swutc) and the shortwave upwelling radiation at the top (swut), thus SCRE_TOA = swutc – swut (see section 1.4). Since the existence of clouds tends to increase the shortwave upwelling radiation at the top due to scattering (thus swut > swutc) the SCRE_TOA values are negative. An increase of cloudiness amount or/and cloud reflectivity would make SCRE_TOA even more negative whereas a decrease of cloud fraction or/and cloud reflectivity makes SCRE_TOA less negative (positive change). In our study it is characteristic that when aerosol-radiation interactions are introduced, the change in cloud forcing at the top of atmosphere (ΔSCRE_TOA) is clearly positive over the entire domain and for all seasons. Since there is not a general decrease of cloudiness amount, this positive ΔSCRE_TOA must be explained by a decrease in cloud reflectivity. Moreover, the change in cloud forcing at the top of the atmosphere (ΔSCRE_TOA) has very similar values to the change in the cloud forcing at the surface (ΔSCRE). It is impressive that for the different subregions, the ΔSCRE clearly follows the ΔSCRE_TOA for all seasons and all ARI simulations (Fig. 23). This further enhances the notion that clouds tend to let more radiation to reach the surface due to a decrease in their reflectivity.

Finally, there are some areas with a very intense ΔSCRE increase that is accompanied by a very small negligible change in cloudiness that has no indication of statistical significance. This behavior is encountered in the simulations using the Thompson aerosol-aware microphysics and is prominent over the northeastern part of the domain especially over the Atlantic Ocean during spring and summer. In these cases a mean ΔSCRE of around 12W/m^2 is seen over areas with negligible cloud fraction changes (first 5% of the absolute cloud fraction changes). Therefore in these cases, the positive change in the cloud forcing can also be attributed to changes in cloud properties that result in decreased cloud optical depth possibly due to smaller reflectivity. Since the Thompson aerosol-aware scheme enables

aerosol-cloud interactions these changes in cloud properties are a very important indication of the impact of the indirect aerosol effect.

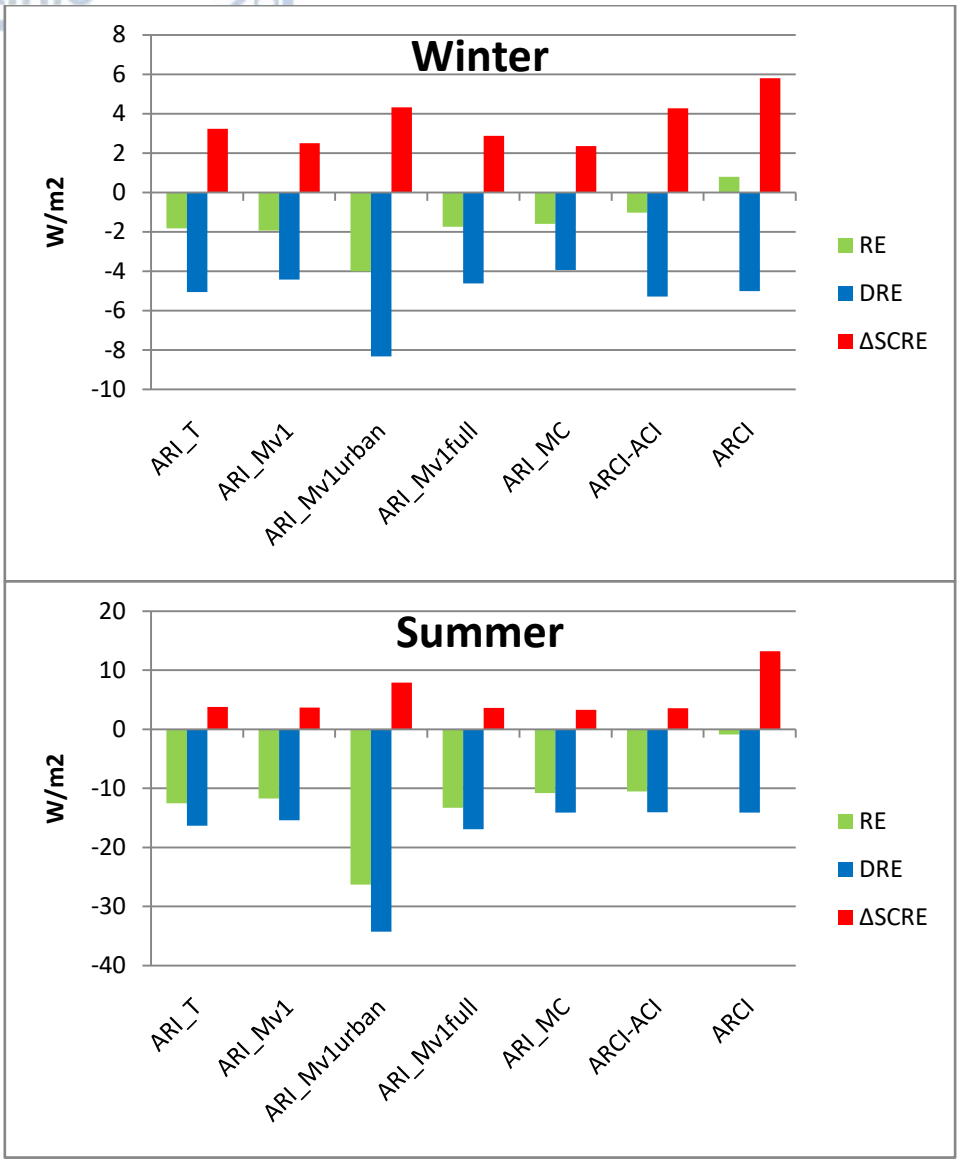

Fig. 20: Radiative effect (RE-green) decomposition into direct radiative effect (DRE-blue) and change in the cloud forcing (ΔSCRE-red) for winter (top) and summer (bottom) regarding domain averaged values.

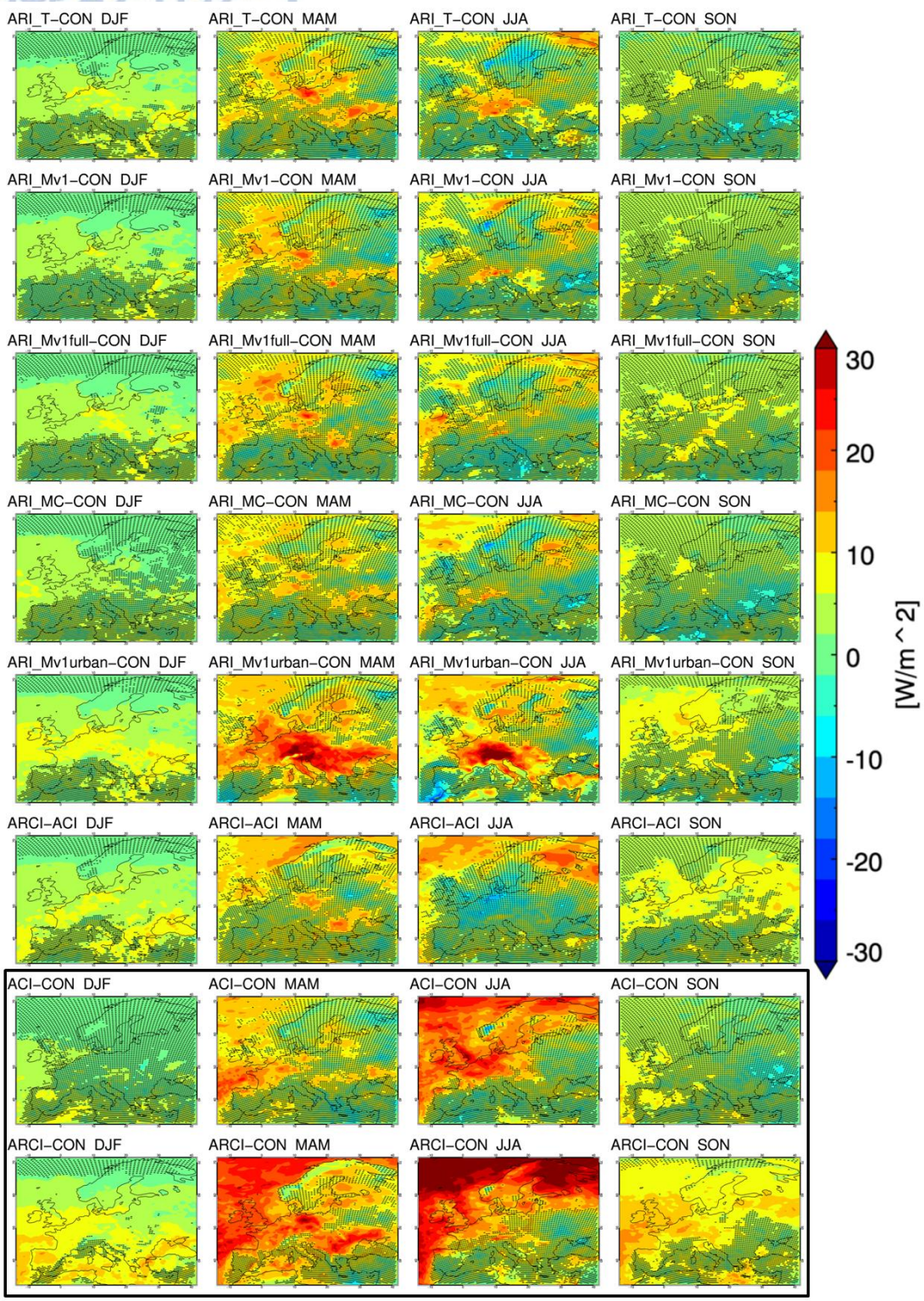

Fig. 21: Shortwave cloud radiative effect difference (ΔSCRE) from control simulation CON for all experiments and seasons. Furthermore the SCRE difference of ARCI calculated against ACI (ARCI-ACI) is given to assess aerosol-radiation interaction implementation in the Thompson aerosol aware microphysics (row six).The last two rows (black box) present the impact of TE2014 with aerosol-cloud interactions against control (row seven) and TE2014 with both aerosol-radiation and aerosol-cloud interactions enabled against control (row eight). Stippling indicates areas where the differences are not statistically significant at the 95% level, according to the Mann-Whitney non-parametric test.

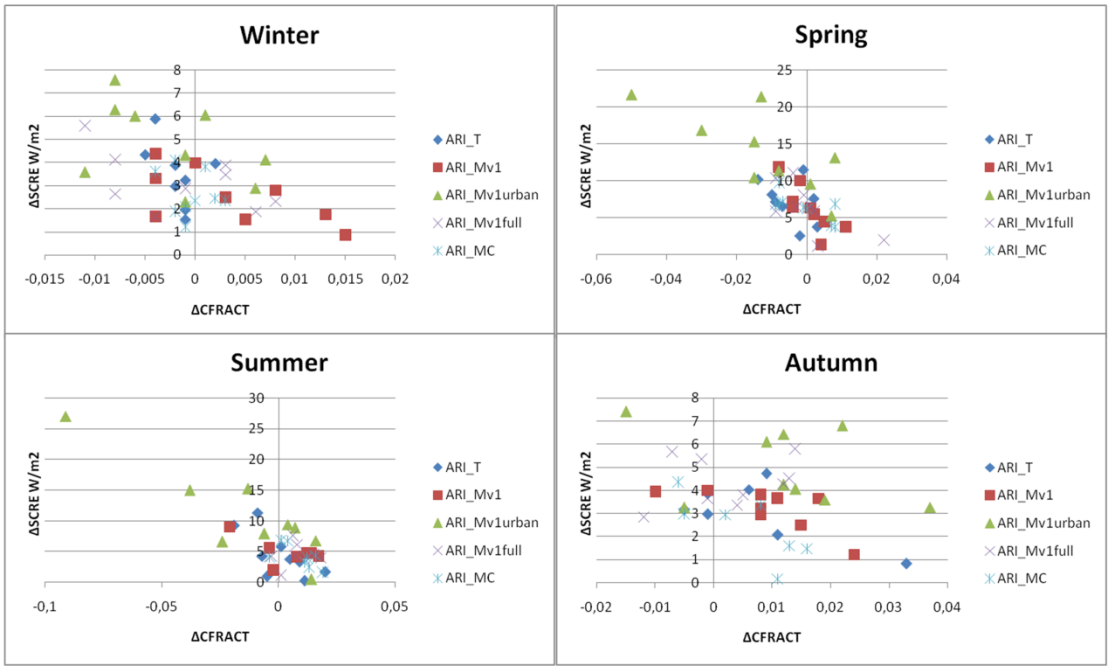

Fig. 22: Change in the cloud forcing at the surface (ΔSCRE) in relation to the change in total cloud fraction (ΔCFRACT) for all ARI simulations and all subregions, compared to control simulation CON. For all seasons. Each simulation is depicted with a different symbol and color. Each point represents a different subregion.

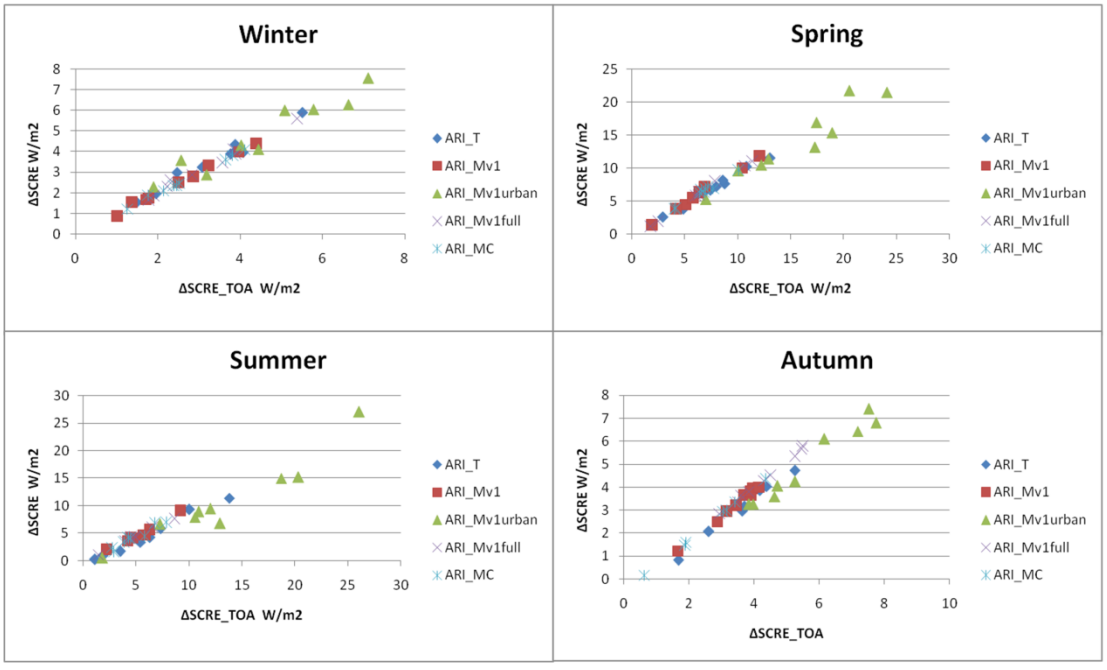

Fig. 23: Change in the cloud forcing at the surface (ΔSCRE) in relation to the change in the cloud forcing at the top of the atmosphere for all ARI simulations and all subregions, compared to control simulation CON. For all seasons. Each simulation is depicted with a different symbol and color. Each point represents a different subregion.

1.5.3.7 Temperature

As we have seen in section 1.5.3.2, introduction of aerosol-radiation interactions in the ARI group leads to considerable shortwave radiation decrease at the surface. This decrease in radiation clearly impacts temperature leading to surface cooling. The ARI simulations present negative domain averaged changes ranging from -0.1 to -0.4^{o}C depending on season. The study of Zanis et al. (2012) presented very similar values of temperature decrease in a RegCM study over Europe. Nabat et al. (2015) however presented a larger cooling of -0.4^{o}C regarding annual average (over land only).

Back to our study, the observed cooling seen in the ARI group, with the exception of ARI_Mv1urban, is spatially extensive. It is characteristic that almost all the subregions present temperature decrease throughout the year. In some cases the subregional averaged decrease can reach -1 ^{o}C (e.g. Eastern Europe in autumn). At grid point level the cooling can be considerably more intense, in cases exceeding -1.5 ^{o}C (Fig. 24).

Spatial correlation of temperature changes with the AOD field is moderate to good (coefficients usually between -0.3 and -0.65 depending on season). Usually the maxima of cooling are collocated or very close to the AOD maxima. In some cases however, (e.g. ARI_Mv1 in autumn) a considerable spatial discrepancy between the two is seen. Temperature decrease is also moderately to well spatially correlated with the pattern of shortwave radiative effect (RE) of aerosol (coefficients range between 0.45 and 0.65 depending on season). In contrast, two RegCM studies over Europe, (Zanis, 2009; Zanis et al., 2012) presented a poorer spatial correlation of temperature decrease with radiative effect.

Table 10: Domain averaged temperature difference (^{o}C) compared to CON for all simulations and seasons. In parenthesis the values when only land points are considered. Where stated, for simulation ARCI the above quantities are also calculated against ACI (ARCI-ACI) in order to assess the implementation of direct effect in the Thompson aerosol aware microphysics.

(^{o}C)	Year		DJF		MAM		JJA		SON	
ARI_T	-0,2	(-0,3)	-0,1	(-0,1)	-0,1	(-0,2)	-0,2	(-0,4)	-0,4	(-0,5)
ARI_Mv1	-0,2	(-0,2)	-0,1	(-0,1)	-0,1	(-0,2)	-0,3	(-0,4)	-0,2	(-0,3)
ARI_Mv1urban	-0,2	(-0,4)	-0,2	(-0,3)	-0,1	(-0,2)	-0,2	(-0,4)	-0,4	(-0,6)
ARI_Mv1full	-0,3	(-0,4)	-0,1	(-0,2)	-0,3	(-0,4)	-0,3	(-0,5)	-0,3	(-0,4)
ARI_MC	-0,1	(-0,2)	-0,1	(-0,1)	0,0	(-0,1)	-0,1	(-0,2)	-0,2	(-0,3)
ARCI-ACI	-0,1	(-0,2)	-0,2	(-0,3)	-0,1	(-0,2)	-0,2	(-0,3)	0,1	(0,1)
ACI	0,1	(0,1)	0,1	(0,1)	0,1	(0,2)	0,2	(0,3)	-0,1	(-0,1)
ARCI	0,0	(0,0)	-0,1	(-0,2)	0,0	(0,0)	0,0	(0,0)	0,0	(0,0)

Interestingly the temperature decrease is not only constrained to the surface but also reaches higher parts of the atmosphere. This can be clearly seen at Fig. 25 that depicts the vertical profile of temperature changes from control (and the difference ARCI-ACI) at a cross-section of 48.25° latitude. This latitude is near the middle of the domain and the cross-section passes over or close to areas of AOD local maxima in eastern Europe. If we examine the ARI group, excluding ARI_Mv1urban, we see that with aerosol-radiation interactions the temperature decrease is largest near the surface and lowers in intensity with height. The vertical profile of temperature decrease is not uniform with longitude and depends heavily on the spatial distribution of aerosol optical depth. The higher altitudes are strongly affected only over spots with intense surface cooling. Over these areas a considerable temperature decrease can easily reach 800hPa. In summer for example we observe a -0.5°C cooling at this level between 20° and 40° longitude that quickly diminishes at higher altitudes. In autumn, a decrease of -0.2 °C reaches up to 400hPa over similar longitudes. This area is located over the Balkans and the Black Sea, coinciding with the cyclonic wind anomaly described at section 1.5.3.9. Winter is the season with the smallest impact regarding both near surface temperature as well as the higher altitudes. Finally when we compare simulations ARI_Mv1 and ARI_Mv1full, that have the same AOD, they present a fairly similar behavior. However in spring and in autumn ARI_Mv1full presents a larger cooling both at the near surface and at the higher levels (reaching 400hPa). Therefore it is an important conclusion that a small differentiation at the aerosol optical properties besides AOD (SSA and ASY) can have a considerable impact on temperature at 2m and temperature profile.

An even larger change in the aerosol absorptivity (SSA) however, can have a dramatic impact on temperature. This is the case of ARI_Mv1urban with the more absorbing “urban” type aerosol. It is characteristic that this is the only simulation with only aerosol-radiation interactions that presents an extensive area (over the Iberian Peninsula, the Alps, Italy and part of the Balkans) with considerable warming at the surface (larger than 1 °C in cases). This warming has the indication of statistical significance and spatially coincides with a decrease in total cloud fraction. On the other hand intense cooling at the surface is encountered over large part of the rest of the domain, especially on the northeastern Europe. Over the warming areas, the absorbing aerosols warm the atmosphere not only near the surface but mainly at higher altitudes. In summer as well as in spring an intense warming of the entire troposphere is seen, reaching up at the tropopause (200hPa), with the maximum of warming near the 700hPa level. In the case of summer this maximum warming exceeds 2 °C. Warming at the surface is also encountered in other studies (Huszar et al., 2012; Zanis, 2009) including the spatial pattern of both warming and cooling seen in summer even though these studies had aerosol with more realistic and less absorbing properties compared to ARI_Mv1urban. Interestingly in our study, the area of considerable cooling in eastern Europe (between 20° and 40°) reaches up to 850hPa, but above that there is an intense upper level warming. The “urban” aerosols warm the atmosphere by absorbing solar radiation but due to this absorption they also limit the radiation that reaches the lower levels and the surface. Moreover the change of the thermodynamic characteristics of the atmosphere can induce changes in the circulation and the cloud fraction. Therefore the final impact on temperature depends of the balance between all of these factors, leading to either cooling or warming.

Implementation of aerosol-radiation interactions in an environment where aerosol-cloud interactions are also present (examining ARCI-ACI) has quite similar results with the ARI group that have only aerosol-radiation interactions enabled. Cooling at the surface is seen over extended parts of the domain for all seasons. Domain averaged temperature decrease is around -0.1 to -0.2^{o}C, roughly the same cooling seen when aerosol-radiation interaction are enable in control CON, with the exception of autumn. In autumn however a warming (around 0.5 ^{o}C) is seen over a large area surrounding the Alps and spatially coincides with a positive change in the cloud forcing. This warming is also seen at higher altitudes with a temperature increase of 0.6 ^{o}C almost reaching the 300hPa level. Therefore we see that if the indirect effect is enabled, the aerosol-radiation interactions (for normal-not extremely absorbing aerosol) do not always lead to the clear temperature decrease at the surface seen in the ARI group. Finally, simulation ACI presents a domain averaged temperature increase (0.1 to 0.2^{o}C) compared to CON. We have seen that the use of the Thompson aerosol-aware scheme in ACI presents decrease cloud fraction and cloud forcing, which is probably the reason for the observed temperature increase.

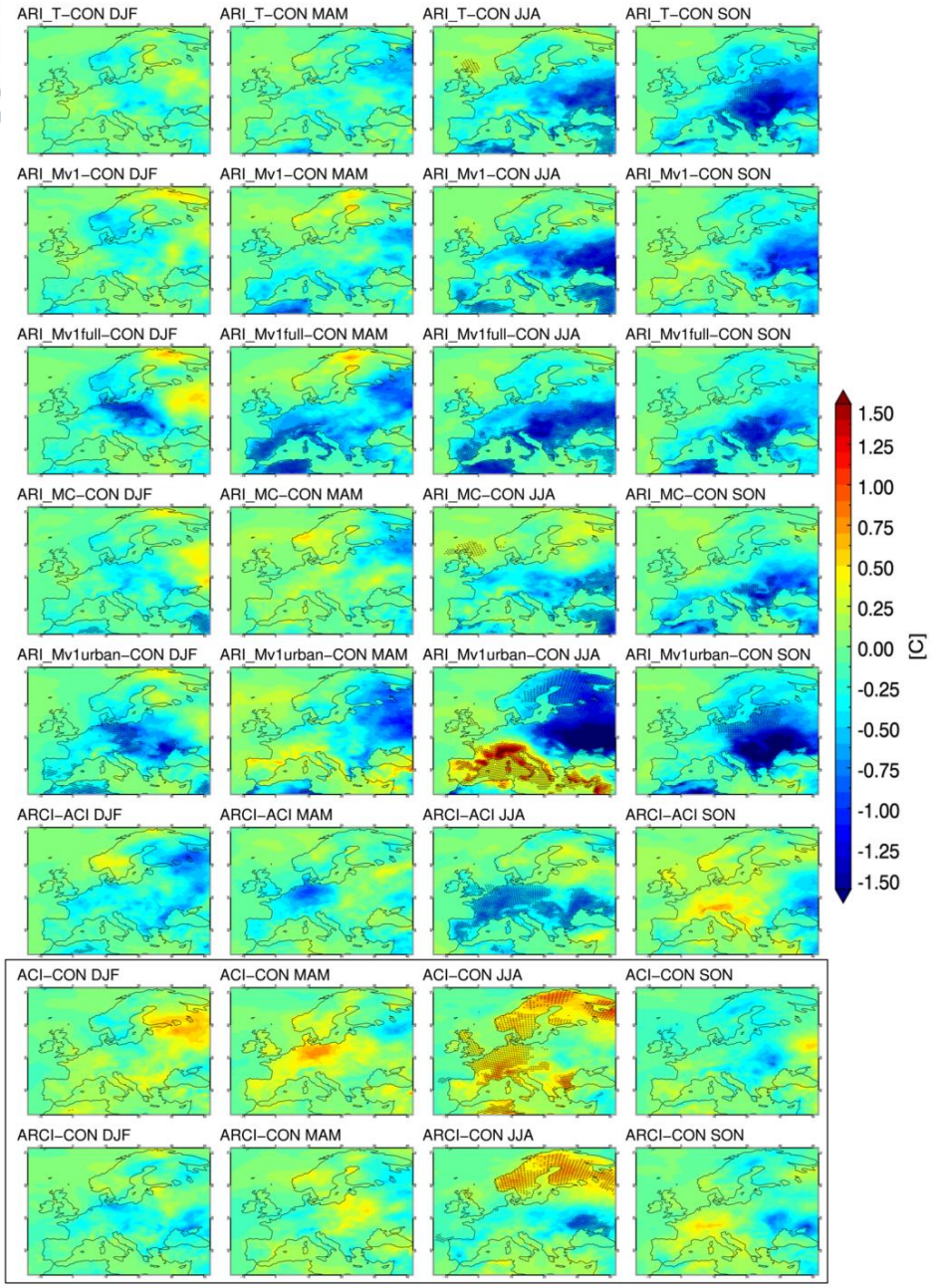

Fig. 24: Temperature at 2m (T) changes from control simulation CON for all simulations and seasons. Furthermore the temperature difference of ARCI calculated against ACI (ARCI-ACI) is given to assess aerosol-radiation interaction implementation in the Thompson aerosol-aware microphysics (row six). First six rows present the impact of aerosol-radiation interactions. The last two rows (black box) present the impact of TE2014 with aerosol-cloud interactions against control (row seven) and TE2014 with both aerosol-radiation and aerosol-cloud interactions enabled against control (row eight). Stippling indicates areas where the differences are NOT statistically significant at the 95% level, according to the Mann-Whitney non parametric test.

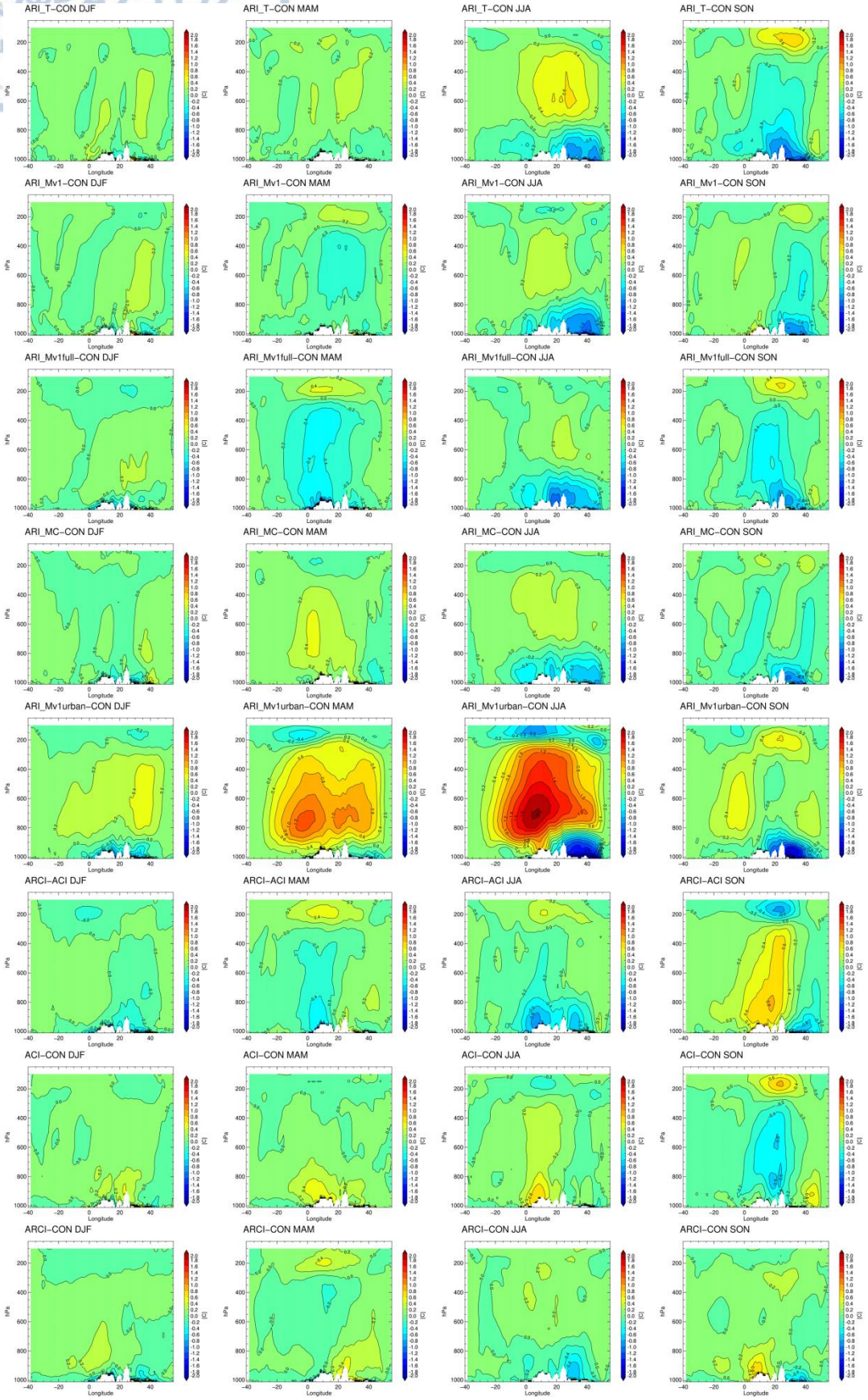

Fig. 25: **Vertical profile of temperature changes from control simulation CON at a 48.25 latitude cross-section. For all simulations and seasons. Furthermore the temperature difference of ARCI calculated against ACI (ARCI-ACI) is given to assess aerosol-radiation interaction implementation in the Thompson aerosol-aware**

microphysics (row six). First six rows present the impact of aerosol-radiation interactions. The last two rows (black box) present the impact of TE2014 with aerosol-cloud interactions against control (row seven) and TE2014 with both aerosol-radiation and aerosol-cloud interactions enabled against control (row eight). Stippling indicates areas where the differences are NOT statistically significant at the 95% level, according to the Mann-Whitney non parametric test.

1.5.3.8 Precipitation

Domain averaged precipitation changes related to aerosol-radiation interaction are small in all simulations (±0.08mm/day) and do not exceed ±5% in relative values, with the exception of ARI_Mv1urban. The small values however are to an extent the product of compensation since the spatial pattern of precipitation differences from control is not uniform but patchy ad presents many small areas with increases and decreases scattered all over the domain (Fig. 26). The changes at grid scale level can exceed ±50%, in many cases. Because the spatial pattern of the changes seems random, this effect is probably related to the internal model variability and not to the aerosol introduction. In general the small impact of aerosol-radiation interactions is seen in winter.

It is quite important that the ARI group of simulations, except ARI_Mv1urban, presents no specific tendency of precipitation change throughout the year. However, in spring and summer most of the ARI group simulations (except ARI_Mv1full) have a small domain averaged precipitation decrease (-2 to -5%, -0.02 to -0.09 mm/day). In general winter is the season which is least impacted by aerosol implementations. Nabat et al. (2015) presented a precipitation decrease over Europe using a coupled atmospheric-ocean model. The decrease in precipitation was attributed to the decrease of sea surface temperature (SST) induced by the reduction of radiation due to aerosol interactions. The decrease in SST led to a decrease in the latent heat fluxes that in turn led to decreased atmospheric humidity and cloud cover finally impacting precipitation amount. For this reason the use of prescribed SST in our study is a limitation that could especially affect precipitation results. Moreover the long term RCM study of Schultze and Rockel (2018) over Europe, presented also precipitation reduction that was attributed to the stabilization of the atmosphere.

Most of the simulations of the ARI group (except ARI_MC) present a common area of precipitation increase over the Black Sea in autumn that has the indication of statistical significance. ARI_T with the Tegen climatology has the most pronounced increase. At this area a significant CFRACT increase and a cyclonic anomaly in the wind field are also present, something that indicates a systematic impact on precipitation. However this area of precipitation increase is also seen in simulations ACI and ARCI, therefore its attribution to aerosol-radiation interactions remains uncertain. Moreover there is no clear spatial correlation between cloud fraction and precipitation changes. In the case over the Black Sea in autumn precipitation increase coincided with cloud fraction increase. However in the case of ACI for example, the spatially extensive and significant CFRACT decrease over central and northern Europe in not accompanied by a respective decrease in precipitation amount.

The more absorbing aerosol of ARI_Mv1urban however definitely have a systematic impact on precipitation. Precipitation amount is decreased for all seasons with the decrease being more pronounced in relative values in spring and summer (-11%). For these two seasons there are also large areas of central Europe that have extensive precipitation decrease with the indication of statistical significance (around -30% in summer, -15 to -25% in spring). It is clear that the absorbing aerosol warm the mid troposphere stabilizing the atmosphere and finally leading to cloud dissolution and the suppression of precipitation.

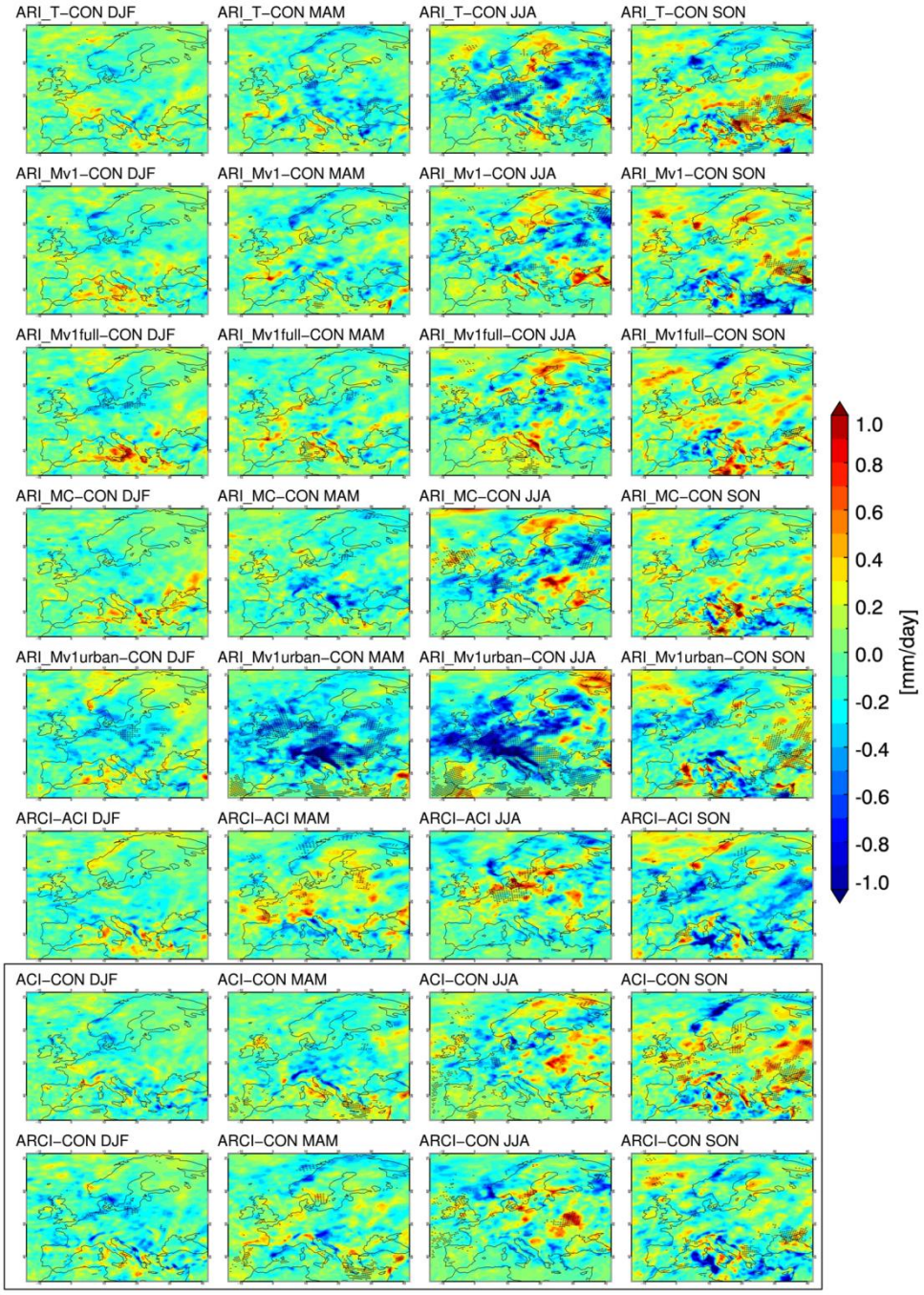

Fig. 26: Precipitation changes from control simulation CON for all simulations and seasons. Furthermore the precipitation difference of ARCI calculated against ACI (ARCI-ACI) is given to assess aerosol-radiation

interaction implementation in the Thompson aerosol-aware microphysics (row six). First six rows present the impact of aerosol-radiation interactions. The last two rows (black box) present the impact of TE2014 with aerosol-cloud interactions against control (row seven) and TE2014 with both aerosol-radiation and aerosol-cloud interactions enabled against control (row eight). Stippling indicates areas where the differences are NOT statistically significant at the 95% level, according to the Mann-Whitney non parametric test.

Table 11: Domain averaged precipitation difference (mm/day) and relative difference (%) compared to CON for all simulations and seasons. Where stated, for simulation ARCI the above quantities are also calculated against ACI (ARCI-ACI) in order to assess the implementation of direct effect in the Thompson aerosol aware microphysics.

	DJF		MAM		JJA		SON	
	mm/day	relative %	mm/day	relative %	mm/day	relative %	mm/day	relative %
ARI_T	0,00	0	-0,08	-4	-0,08	-5	0,04	2
ARI_Mv1	0,00	0	-0,05	-2	-0,02	-2	0,00	0
ARI_Mv1urban	-0,05	-2	-0,24	-13	-0,21	-14	-0,06	-2
ARI_Mv1full	-0,01	0	-0,01	0	0,00	0	0,06	3
ARI_MC	0,01	0	-0,09	-5	-0,03	-2	0,02	1
ARCI-ACI	-0,04	-1	0,02	1	-0,03	-2	-0,13	-5
ACI	-0,04	-2	-0,05	-3	0,00	0	0,07	3
ARCI	-0,08	-3	-0,03	-2	-0,04	-2	-0,06	-2

1.5.3.9 Wind field

At first glance the introduction of aerosol-radiation interactions does not have a visible impact on the wind field. Fig. 27 depicts the wind field at the 850hPa level for control CON, ARI_T and ARI_Mv1urban for all seasons. Colored contours represent the wind velocity. We can see that aerosol implementation has a little to no impact on the general seasonal wind circulation even in the case of the ultra absorbing “urban” aerosol. The same picture is true for higher levels like the 500hPa.

Looking at the wind field anomalies (from control CON) however reveals the existence of a tendency towards specific changes at the circulation. Fig. 28 depicts the wind change compared to control (as well as ARCI-ACI) at the 850hPa level. The colored contours depict the change in the value of the meridional wind component. Red values mean either increased wind speed towards the south or reduction of the wind speed towards the north. Blue values mean increased wind speed towards the north or reduction of the wind speed towards the south. We can observe a general tendency of cyclonic anomalies to form over areas of intense surface cooling. The existence of this cooling also at much higher levels in the troposphere seems to help towards the formation of an anomaly but it does not seem to be absolutely necessary. One other hand we have a few areas with near surface warming and those do not seem to have a considerable impact on the wind field at the lower troposphere. However if this warming is retained at higher levels, considerable anti-cyclonic anomalies form in the same area at the 500hPa level.

A characteristic example is the cyclonic anomaly at 850hPa seen in autumn north of the Black Sea, for all ARI simulations. In autumn these simulations present an area of considerable cooling near the surface that is also clearly observed much higher in the atmosphere up to 400hPa. The cyclonic anomaly is also seen higher, at the 500hPa level. Simulation ARI_MC presents the smallest near surface temperature decrease and also the

least pronounced cyclonic anomaly. On the other hand, ARI_T and ARI_mv1urban that have the largest near surface cooling also present the most intense cyclonic anomalies in autumn. This enhances the notion that there seems to be a connection between the intensity of temperature change and the formed anomaly in circulation. It is important to note for these simulations extended areas of both the zonal and the meridional wind anomalies (in essence the south-east part of the whole cyclonic anomaly) present indications of statistical significance at the 95% level.

In summer the ARI group presents a temperature decrease that is quite similar to autumn with the exception of ARI_Mv1urban. Cooling is seen over similar areas and with comparable magnitude but this time it is more shallow as it ends around 800hPa and does not reach higher altitudes. There are faint traces of a weak cyclonic anomaly at the same area as seen in autumn in some simulations (ARI_Mv1, ARI_MC) but in other simulations it is completely absent. On the contrary an anti-cyclonic anomaly at 850hPa is trying to form at the north part of Eastern Europe, north of the cooling spot. It is also encountered at the 500hPa level. We suspect that it is the change in temperature difference between areas that drives the form of the anti-cyclonic anomaly. Cooling over the Balkans and north of the Black Sea can produce a more intense temperature change as we move more towards the north. Thus the north Eastern Europe seems “warmer” compared to the cooling spot to its south when aerosol-radiation interactions are enabled.

Simulation ARI_Mv1urban has the biggest impact on circulation. A well formed and pronounced cyclonic anomaly is seen in summer and in autumn (at both 850 and 500hPa) above the Balkans and north of the Black Sea, areas that also present intense near surface cooling. This cooling however does not extend in height past of the 800hPa level. On the other hand, the intense warming seen over central Europe in summer does not seem to have a considerable impact on the wind field at 850hPa. At 500hPa however there is a clear anti-cyclonic anomaly probably the attributed to the warming extending up to the tropopause at 200hPa.

Finally, ACI presents another case of a cyclonic anomaly forming over an area of cooling. In autumn an area of moderate cooling over the Balkans is accompanied by a well formed cyclonic anomaly that spreads over the biggest part of the domain at both 850 and 500hPa. The cooling might not be considerable in magnitude, especially compared to the ones seen in the ARI simulations, but it extends way up in the troposphere, exceeding 400hPa.

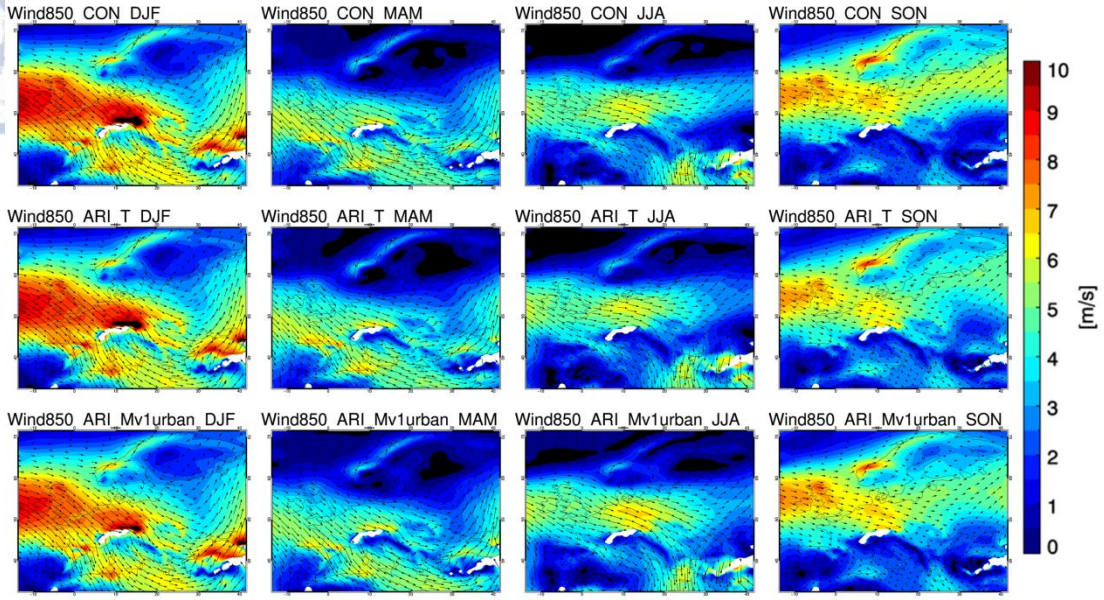

Fig. 27: The wind field (arrows) and wind speed (colored contours) for the control simulation CON (top), ARI_T (middle) and ARI_Mv1urban (bottom). For each season.

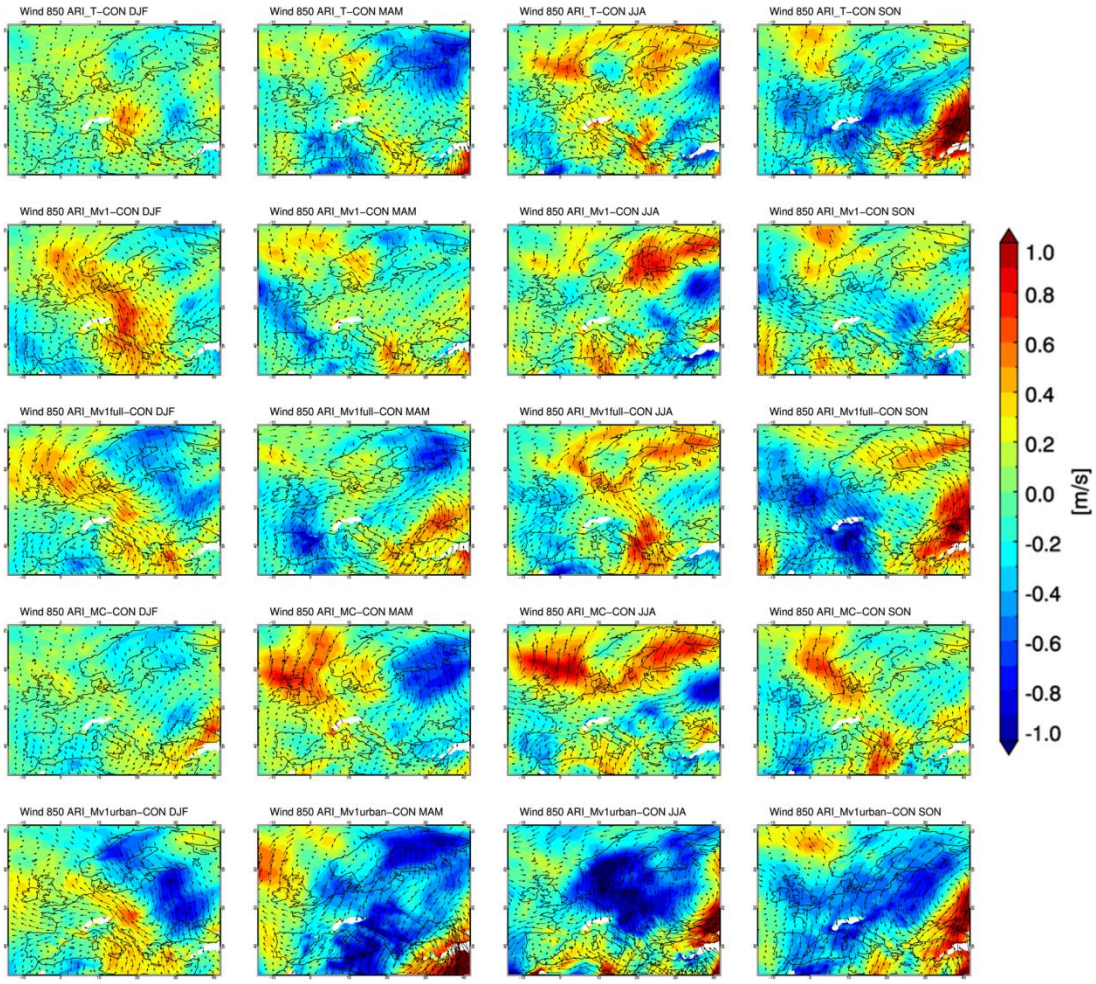

Fig. 28: Wind field difference (arrows) and meridional (v) wind component difference (colors) from control simulation CON. For ARI group of simulations and all seasons.

1.5.3.10 Two examples of aerosol-radiation interaction impact

We have seen so far the impact on each variable separately. In this section we present two cases of strong impact due to aerosol-radiation interactions and offer a more concentrated view of the impact on all the variables of the climate examined. We want to present a more rounded view of the aerosol impact and also address the possible connections and feedback mechanisms between the impacted variables.

Firstly we present the example of simulation ARI_T during autumn. Then we present the example of ARI_Mv1urban in summer.

ARI_T in autumn

A composite analysis for this case can be seen at Fig. 29. Mind that in this figure stippling depicts the areas that HAVE the indication of statistical significance.

Firstly we can see that the aerosol optical depth presents a maximum over the Black Sea and large AOD values are encountered over eastern Europe, the Balkans and eastern Mediterranean. This aerosol field leads to an intense and significant reduction in the shortwave radiation at the surface (negative RE), seen both over land and at sea. The reduced radiation leads to a significant near surface temperature decrease that exceeds 1^{o}C. The cooling spatially coincides with the AOD field but it is seen only over land.

Over the sea the temperature change is negligible. Changes at SST are not expected to be large since the sea has a much larger thermal capacity than land and is therefore more resistant to temperature change. However the use of prescribed SST in this study and the lack of an ocean model does not allow the sea surface to cool at all and thus impact the near surface temperature. Therefore the cooling due to aerosol-radiation interactions does not reach its full potential. This seems to be one of the limitations of this study.

The observed cooling over land is also seen at much higher levels of the troposphere decreasing in intensity with height while spatially coinciding with the surface cooling. At the 850hPa level a cooling of around -0.4^{o}C is seen whereas a decrease of -0.2^{o}C is seen way up at the 400hPa.

Total cloud fraction (CFRACT) is clearly increased over the land area of intense surface cooling but also over the sea, especially over the Black Sea where we have the maximum of cloud fraction increase. It is characteristic that almost all the large CFRACT changes have the indication of statistical significance. The increased cloudiness leads in turn to decreased cloud forcing (ΔSCRE) allowing even less radiation to reach the surface. The ΔSCRE in this case represents the aerosol semi-direct effect. We can therefore identify a positive feedback mechanism where the cooling due to aerosol scattering and absorption (direct effect) leads to cloud fraction increase (semi-direct effect) that in turn leads to further cooling. It seems however that aerosol direct effect is the major driver of reduced radiation and cooling at the surface. The decrease at the radiation levels due to cloudiness increase (semi-direct effect) is

considerably weaker (around 6 times) than then decrease due to aerosol direct effect. It is characteristic that over the areas with negative semi-direct effect (ΔSCRE), (around -2.5W/m^2) the semi-direct effect amounts on average around 16% of the entire radiative effect (direct + semi-direct). Therefore the negative semi-direct effect on radiation seen over and near AOD maxima is not negligible but it is five times smaller than the observed direct effect.

Interestingly changes in the wind circulation are also detected. A clear cyclonic anomaly in the wind field forms near the cooling spot and is seen both at the 850 and 500hPa level. Spatially it is close to the cooling seen at the surface and at the 850hPa but does not coincide completely, since its center lies to the east of the area with maximum cooling. Indications of statistical significance are seen at the south and east part of the anomaly. This change in the circulation could potentially affect cloud fraction. The CFRACT increase over the Black Sea could be partially attributed to the south wind anomaly importing humidity over the area. No change at the vertical wind speed (w) is seen over the Black Sea and the Balkans. However parts of the Mediterranean have positive changes in w especially at the 500hPa, indicating increased upwards speed something that could explain the increased cloud fraction in this area. Regarding the overall situation, it is interesting that despite the cooling of the lower troposphere, the atmosphere is not stabilized and the cyclonic anomaly with cloud amount increase is formatted. Here it also must be noted that during autumn very low wind speeds are present at 850hPa in the area of the cyclonic anomaly, denoting the absence of a severe forcing from the general circulation thus facilitating the impact of the aerosol implementation over the wind field.

Finally the cloud fraction increase is also accompanied with significant precipitation increase over the Black Sea and the Balkans that is considerable and regularly exceeds +30%. We can therefore clearly state that for ARI_T in autumn not only radiation at the surface and temperature are affected, but there is an area where a systematic impact is observed on the wind circulation, cloud fraction and precipitation amount as well.

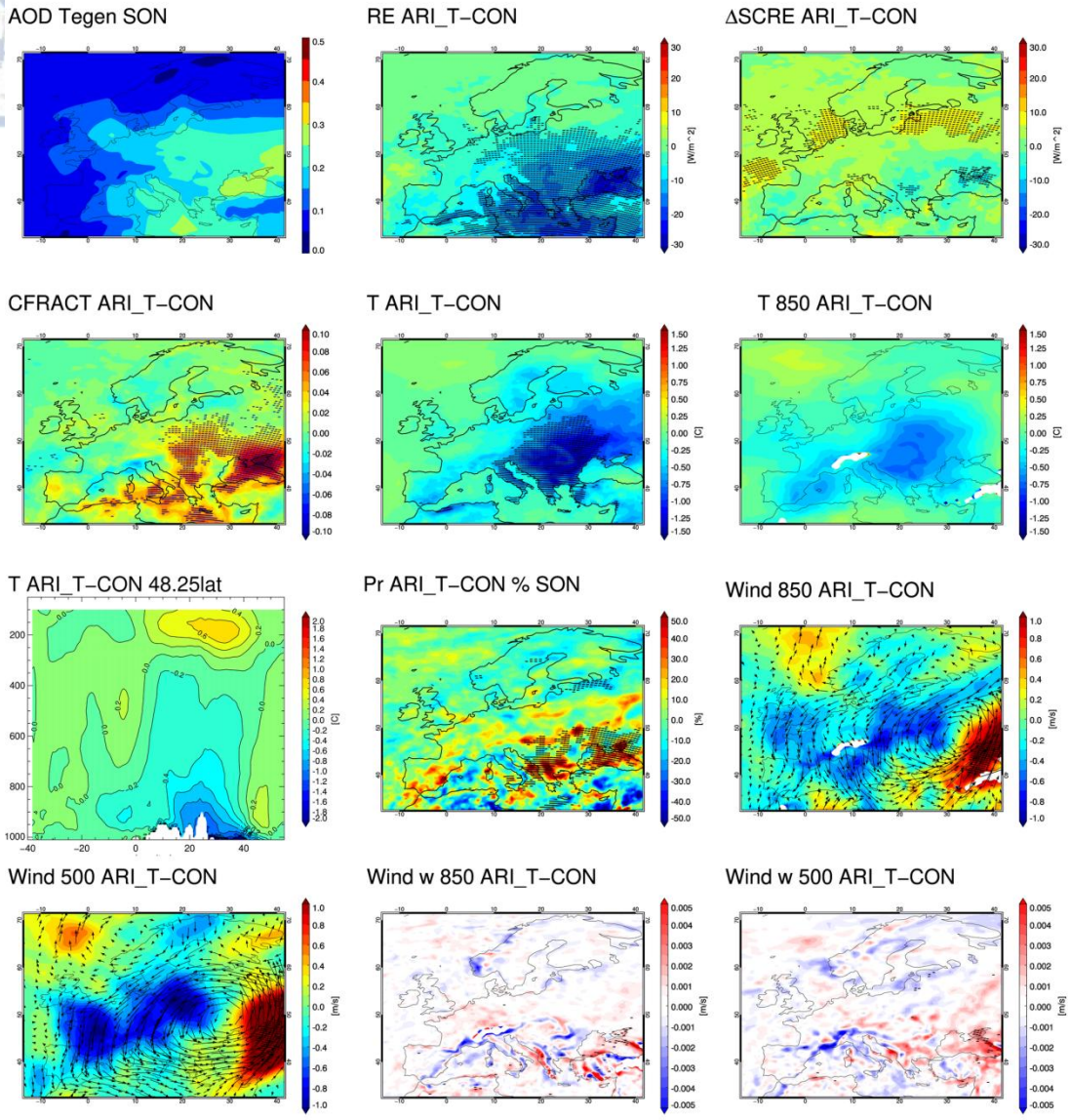

Fig. 29: Composite analysis for simulation ARI_T in autumn. The shown differences are calculated against control CON. Top row, from left to right: AOD field, Radiative forcing RE, differences in cloud forcing (ΔSCRE). Second row: difference in cloud fraction (CFRACT), difference in near surface temperature (T), temperature difference at 850hPa. Third row: cross-section at 48.25 latitude depicting differences in temperature vertical profile, relative difference in precipitation (Pr), differences at the wind field at 850hPa. Bottom row: differences at the wind field at 500hPa, difference in vertical wind speed w at 850hPa (left) and at 500hPa (right). Stippling indicates areas that ARE of statistical significance. Statistical significance has not been calculated for temperature in the upper atmosphere.

ARI_Mv1urban in summer

Simulation ARI_Mv1urban is a good example of the impact of ultra absorbing aerosol. It is reminded that the "urban" type aerosol are extremely absorbing (SSA values starting from 0.6) and thus we consider ARI_Mv1urban as an idealized experiment showing the impact of unrealistically intense absorption. The "urban" type might be suitable for specific limited areas suffering from urban or industrial pollution but not for the entire European domain.

The intense impact of the absorbing "urban" aerosol is seen in almost every aspect of the climate examined, while the indication of statistical significance is present over extended areas of the domain (Fig. 30). The MACv1 climatology used presents the largest AOD values over Eastern Europe and north Africa. The SSA values are lower (thus more absorbing) over the southern half of the domain.

Shortwave radiation is intensely reduced almost over the entire domain. The RE is highly negative and significant and routinely exceeds -30W/m^2. In relative values an Rsds reduction of around 15% (exceeding) is seen over southern Europe whereas over eastern Europe it exceeds 20%.

We could expect that the intense and overall reduction of radiation at the surface would lead to a wide spread cooling at the near surface, as we have seen in all the other sensitivities implementing aerosol-radiation interactions. This indeed happens over a large area over eastern and northeastern Europe with intense temperature dropping over 1^{o}C. Interestingly, on the other hand a large area including the Alps, Italy, parts of the Balkans and the Iberian Peninsula shows a completely different picture with considerable near surface warming that in places exceeds 1^{o}C. One explanation for this peculiar behavior could be that over this exact area we have considerable cloud fraction decrease that significantly increases the cloud forcing (clouds let more radiation to reach the surface). However the direct radiative effect of the absorbing aerosol is so strong in reducing radiation that in most areas compensates for cloudiness decrease. Therefore only an area around the Alps has an overall Rsds increase (positive RE), something that could explain the warming at this specific place. The other areas present a strange combination of shortwave radiation decrease and near surface warming. Therefore the intense surface warming must be attributed to the warming induced by the aerosol absorption of incoming radiation. Highly absorbing aerosol tend to warm the surrounding atmosphere. Therefore the resulting temperature change at the near surface mainly depends on the balance between shortwave radiation reduction (due to aerosol scattering and cloud fraction changes) and the warming due to the aerosol radiation absorption.

Naturally, aerosol radiation absorption also tends to warm higher altitudes in the atmosphere. A considerable warming is seen way up until the tropopause, whereas the maximum of warming is encountered around 800-700hPa and is so intense that exceeds 2^{o}C. It is evident that the absorbing aerosol can dramatically change the thermodynamic profile of the atmosphere. Over the area of near surface warming there is warming encountered at all vertical levels up the tropopause (Fig. 30, 40.25^o latitude cross section). At eastern Europe, the area with near surface cooling, the cooling reaches up to the 800hPa level. However above that level an intense warming is still encountered (Fig. 30, 52.25^o latitude cross section), testament to the warming abilities of absorbing aerosol.

The presence of the maximum warming high in the atmosphere and not near the surface where the aerosol load is larger might seem peculiar. However, we must also take into account that radiation amount decreases from the top of the atmosphere towards the surface, due to interaction with the atmospheric components and especially in this case with the absorbing aerosol. Thus the maximum is seen at an altitude where the balancing

between these two factors is optimum, meaning that there is a considerable aerosol load but also a sufficient shortwave radiation amount for the aerosol to absorb.

As we have already seen, the ultra absorbing aerosol also have a considerable impact on cloud fraction. The intense change of the atmospheric thermodynamic profile leads to a strong semi-direct aerosol effect. A large part of the domain is covered with significant CFRACT changes. We have seen an area above the Alps, Italy and the Balkans with cloud fraction decrease and surface warming. This area also present significant precipitation reduction (ranging from -20% to over -50%). There is also the extended area with surface cooling over eastern Europe that presents considerable cloud fraction increase. This cloudiness increase seems to further aid the temperature reduction at the surface. Moreover a clear impact on the wind circulation is also detected. A clear cyclonic anomaly is formed over eastern Europe, coinciding with the CFRACT increase and near surface cooling. It is present both at the 850hPa and 500hPa level. Some traces of increased upwards vertical speed w do exist at the area and could be partially responsible for the cloudiness increase. Conversely, over the area with CFRACT decrease an anti-cyclonic anomaly in the wind field is seen, but this time only at the 500hPa level. In this case a decrease in the upward wind speed w is also seen over several spots and could be partially responsible for the observed cloudiness reduction.

To sum up, we have strong indications that the absorbing “urban” aerosol have a large impact not only due to their direct effect (warming and radiation reduction due to absorption) but also due to their strong indirect effect that causes significant changes in the wind circulation and cloudiness amount.

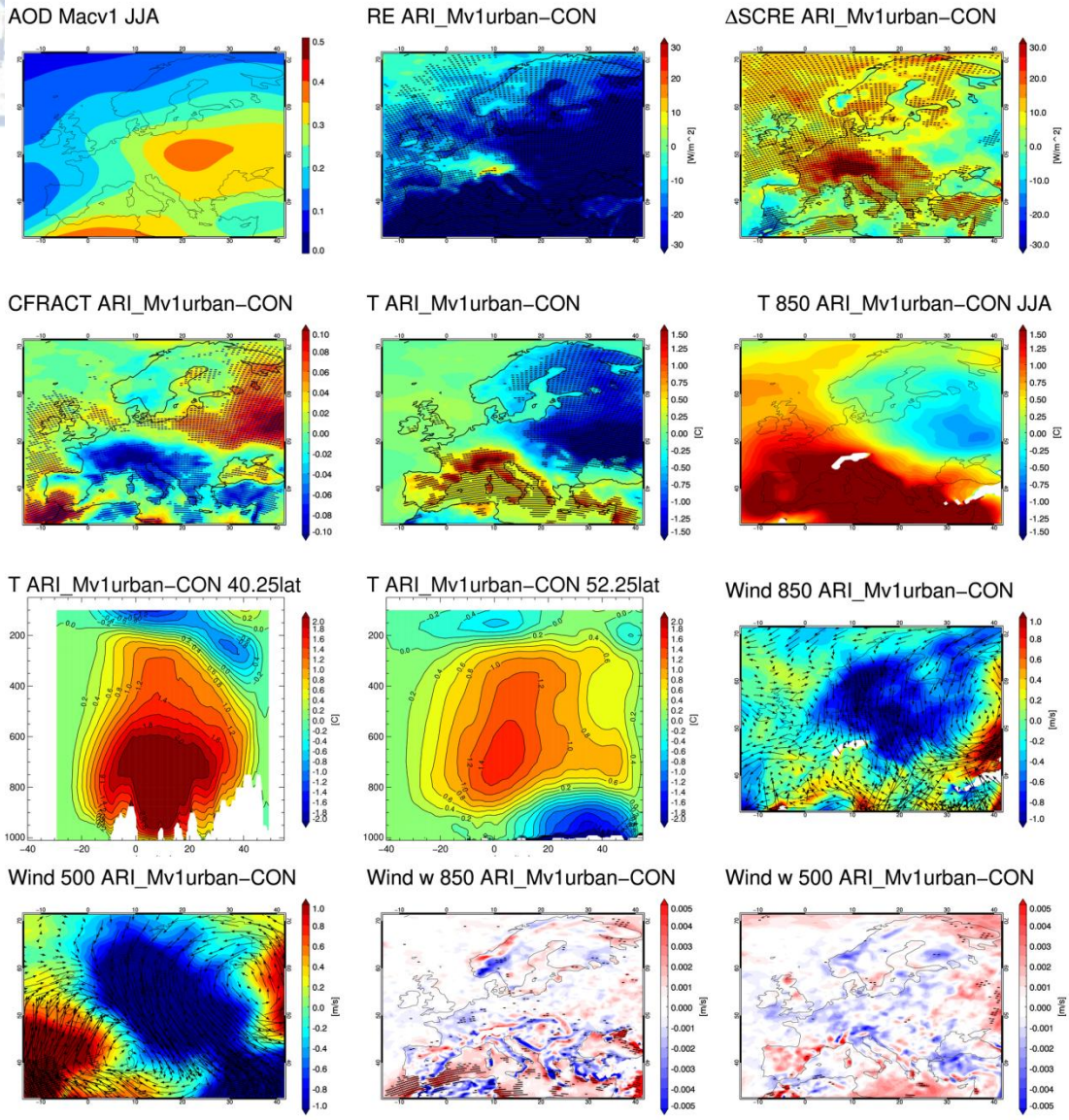

Fig. 30: Composite analysis for simulation ARI_Mv1urban in summer. The shown differences are calculated against control CON. Top row, from left to right: AOD field, Radiative forcing RE, difference in cloud forcing SCRE.. Second row: Difference in cloud fraction CFRACT, Difference in near-surface temperature (TAS), Temperature differences at 850hPa. Third row: Cross-section at 40.25 latitude depicting differences in temperature vertical profile, cross-section at 50.25 latitude depicting differences in temperature vertical profile, difference in the wind field at 850hPa. Bottom row: Difference in the wind field at and 500hPa, difference in vertical wind speed w at 850hPa and at 500hPa. Stippling indicates areas that ARE of statistical significance. Statistical significance has not been calculated for temperature in the upper atmosphere.

1.5.3.11 Effective radii communication between microphysics and radiation schemes

So far, all the simulations examined have a connection between the microphysics and radiation schemes regarding the effective radii of the cloud particles. That is the microphysics scheme that calculates the radii of the cloud particles (either water droplets or ice particles) passes the results to the radiation scheme which uses it to parameterize cloud optical thickness and finally calculate radiation results. Such a communication between the

two schemes obviously improves the physical consistency of the simulation. However this option has only been recently made available (version 3.5.1) and can only be used with the RRTMG radiation scheme and a limited number of microphysics schemes. Otherwise the radiation scheme makes its own simplified assumptions about the effective radii of cloud particles. Since the aerosol-cloud interactions may lead to changes in the cloud particles, the communication of the microphysics and radiation schemes is vital in order to fully and properly simulate the aerosol indirect effect. As said before, the communication between the two schemes is by default enabled in the model (from version 3.5.1). However the user is given the option to turn this off (from version 3.8). In order to assess the impact of the effective radii communication we have performed another simulation, ARCI_no, that has this communication disabled. It is identical to ARCI that has both aerosol-radiation and aerosol-cloud interactions with only the effective radii communication option disabled. ARCI was chosen as the basis of this sensitivity since it is the most complete simulation in terms of the aerosol effects included and it would be interesting to see the impact of removing a vital piece of the physical mechanism that can especially affect the indirect effect.

Results

In order to estimate the impact of radiation-microphysics communication we directly compare the simulation ARCI_no to ARCI. As expected both simulations have almost identical results regarding clear-sky shortwave radiation (CRsds). This is because CRsds is not affected by cloudiness at all and any change in cloud characteristics does not impact it.

However we see that ARCI_no has differences in cloud forcing compared to ARCI. We calculated the change in the cloud forcing (ΔSCRE) between the two simulations. There are large areas with the indication of statistical significant changes (Fig. 31). Some of them are connected with changes in the cloud fraction. Indeed there are some areas (e.g. northeastern Europe in spring and central Europe in autumn) with significant cloud fraction changes that inevitably affect the cloud forcing. In general cloudiness is not affected in a particular way. There are both increases and decreases of cloud fraction over the domain and thus if we average over the domain the changes counterbalance (Table 12).

The interesting characteristic is that there are large areas with significant and considerable increase in cloud forcing that are not accompanied by intense or significant cloud fraction changes. This implies that the change in cloud forcing is attributed to the different cloud optical properties that in turn can be attributed to the different effective radii of cloud particles. This is particularly evident over the sea and especially over the Atlantic at the northwest part of the domain. In general ARCI_no presents a clearly increased cloud forcing over the sea compared to ARCI. This is because in ARCI_no the effective radii of cloud particles are parameterized by the RRTMG radiation scheme and not the microphysics. Moreover the RRTMG makes a clear distinction between cloud water particles over land and over the sea, using different relations to describe the effective radii, leading to a different cloud forcing above the ocean.

Since clouds in ARCI_no allow more radiation to reach the surface, the shortwave radiation at the surface (Rsds) is also increased. The change in net Rsds, in essence the radiative effect (RE) due to microphysics-radiation scheme communication, presents the same extended

areas of considerable changes with the indication of significance (Fig. 31 – 3rd row) as seen in the ΔSCRE. The domain averaged relative change in Rsds ranges between 1% (autumn) and 7% (winter). Similarly to the change in cloud forcing (ΔSCRE), the impact on Rsds is clearly larger over the sea with elevated domain averages ranging between 7% (autumn) and 10% (winter). If we focus on the area of the north Atlantic (-13° west - 10° east, 45° south – 70° north) with the most pronounced changes, we observe an impressive increase of 17% in summer and 13% in spring (over sea only).

Bae, Hong, and Lim (2016) in a WRF study over Korea using the WDM6 microphysics found that the coupling between the microphysics and RRTMG also lead to a shortwave radiation increase at the surface, which in their case was more pronounced over areas with small cloud fraction.

The impact on Rsds in our study is definitely large. If we take into account that aerosol-radiation interactions lead to an Rsds decrease that is around -5% to -7% throughout the year, the coupling of the microphysics-radiation schemes seems quite important. In order to better understand the magnitude of the change we calculate the mean absolute difference for each month. The absolute difference is always positive and therefore we cannot have effects of compensation between positive and negative values. Thus it is a better metric to describe how big the change is. Fig. 32 presents the mean absolute difference ARCI_no-ARCI (red line) on Rsds for each month over the European domain (EU-right) and over the British Isles (BI-left). The same difference but only above the sea is also depicted (red line). Finally to establish the relative importance of the radiation-microphysics coupling we also present the absolute difference ARI_T-CON that represents the aerosol-radiation interaction impact. Firstly we clearly see that the Rsds difference is clearly larger above the sea almost throughout the year for both domains. This is the case for all the Prudence subdomains examined that encompass sea grid points. Secondly it becomes even more obvious that the effective radii coupling impact is comparable to the enabling of the aerosol-radiation interactions. For the European domain (EU) the ARCI_no-ARCI absolute difference is very similar in magnitude to the aerosol-radiation impact for a large part of the year (winter and spring) and becomes smaller but still comparable in summer and autumn. This is usually the case for most of the Prudence subdomains. There are subdomains, like Scandinavia and France, where the ARCI_no-ARCI absolute difference is larger than the aerosol-radiation impact for some months of the year. The most extreme case however is the British Isles (BI) where the effective radii coupling impact is consistently larger throughout the year.

The change in shortwave radiation at the surface does affect temperature but not towards a specific direction. Small increases and decreases are seen all over Europe thus the domain averages become small. In spring there is a large area of warming covering most of the east part of the domain, but it has no indication of significance. The only case where the changes have the indication of statistical significance is in summer over a large part of central Europe and Spain that presents cooling. This is somewhat peculiar since it does not fully coincide spatially with a clear reduction in Rsds. Finally the intense radiation increase over the sea does not impact near surface temperature. This impact is definitely hindered by the lack of an ocean component in the model of our study, that does not let sea surface temperature to change (it uses seasonally changing prescribed values) and in turn affect near surface

temperature. However because of the large thermal capacity of the sea the impact on sea surface temperature would be considerably weaker compared to that on land.

Summary

To sum up, the coupling between the microphysics and radiation scheme is important. It can have a large impact on Rsds, especially over the sea where a clear Rsds increase is observed if the coupling is disabled. The impact of the coupling on shortwave radiation is comparable in many cases with the impact of enabling aerosol radiation interactions.

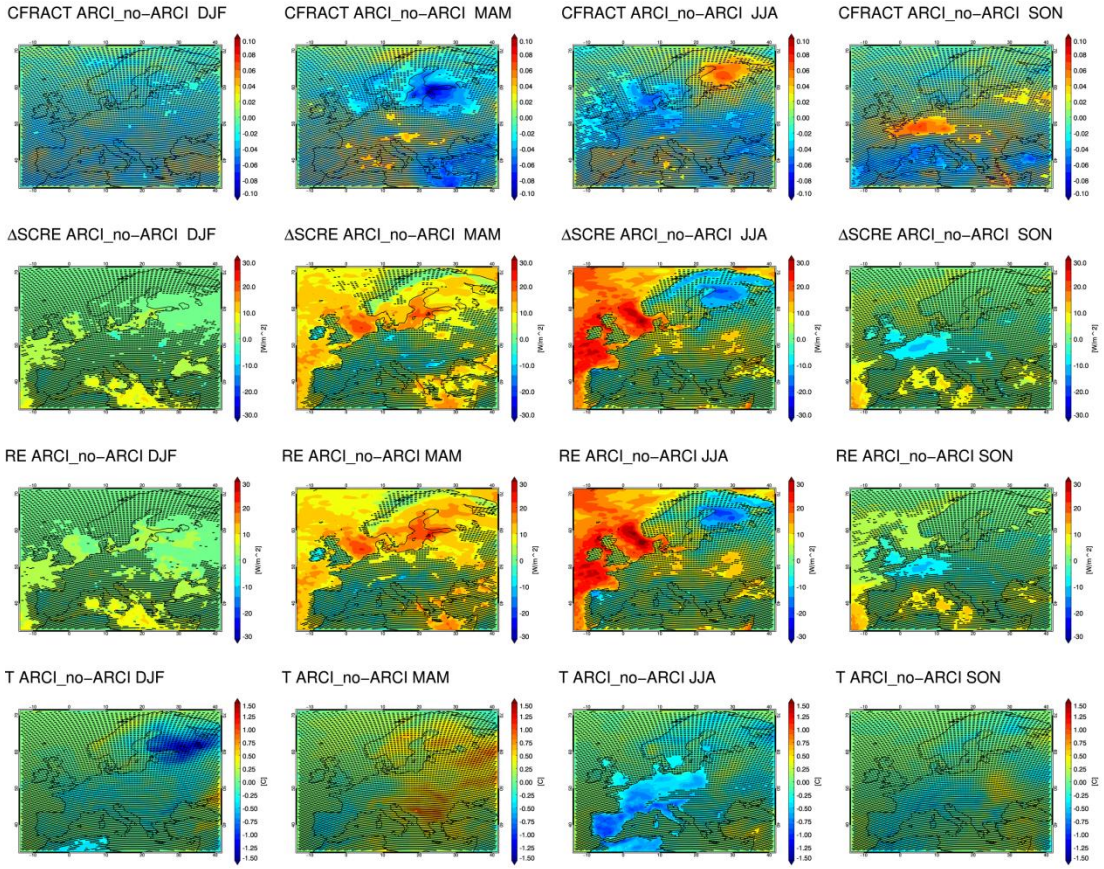

Fig. 31: Differences between simulations ARCI_no and ARCI for total cloud fraction (CFRACT) (first row), cloud forcing (ΔSCRE) (second row), net shortwave radiation at the surface (radiative effect -RE) (third row) and near surface temperature (T) (bottom row). Stippling indicates the areas that are NOT statistically significant 95% level, according to the Mann-Whitney non parametric test.

Table 12: Domain averaged differences between simulations ARCI_no and ARCI regarding total cloud fraction (CFRACT), shortwave down welling radiation at the surface (RSDS), shortwave down welling radiation at the surface over the sea and temperature (T). For all seasons.

	Winter	*Spring*	*Summer*	*Autumn*
CFRACT (%)	0	-1	0	1
RSDS (%)	7	6	4	1
RSDS over SEA (%)	10	8	9	7
Temperature (^{o}C)	0,0	0,3	0,0	-0,1

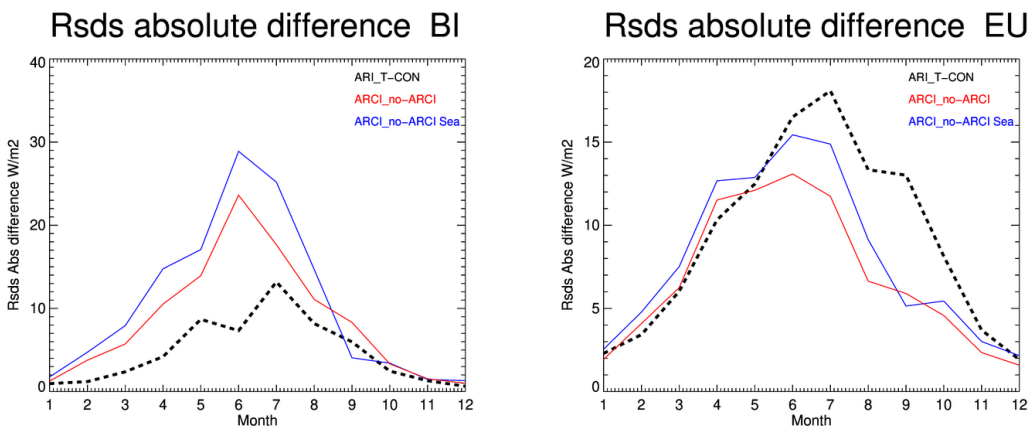

Fig. 32: Domain averaged absolute difference on shortwave down welling radiation at the surface (Rsds) between simulations ARCI_no and ARCI (red line) over the British Isles (BI) and the European domain (EU). For each month. The difference only above the sea is also presented (blue line). Moreover the difference ARI_T-CON is also presented (black dashed line) to enable comparison with the impact of aerosol-radiation interactions. Mind the different scale for the two regions.

1.5.4 Cloud cover scheme sensitivity

1.5.4.1 Introduction

Aerosol tend to affect radiation amount through their direct effect and cloudiness through their semi-direct and indirect effects. However cloudiness is among the most important factors that affect the climate and can be affected by other parameterizations such as the convection scheme and the cloud parameterization. The cloud parameterization is the scheme that is responsible for calculating the cloud fraction amount in atmospheric models. The produced cloud fraction, among other factors such as liquid water path, is then used by the radiation scheme to calculate radiation levels. Since we have seen the cloud fraction changes induced by aerosol implementation, it would be interesting to estimate the impact of cloud scheme selection on cloudiness amount and on other climate variables as well. Such a study would be important on its own, especially because cloud schemes are often overlooked in climate simulations. Furthermore, a comparison with the impact seen in the aerosol sensitivities can help us assess the relative importance of each sensitivity experiment and provide a better context regarding the impact of aerosol in the model.

A cloud parameterization produces cloud fraction amount for each grid cell and at each vertical model level. There is a variety of methods used for this calculation, the most common ones use relative humidity (RH) thresholds or probability density functions (pdf) for saturation (Quaas, 2012). Cloud parameterizations also have different degrees of complexity. The simpler ones produce only either fully covered or cloud-free skies over a specific grid cell. The more advanced ones can produce intermediate degrees of cloud fraction at different model levels for a grid box.

1.5.4.2 Methodology

The control simulation CON in the aerosol sensitivity used the Xu-Randall method to parameterize cloud fraction (option icloud=1 in the namelist). This method relies on relative humidity (RH), the saturation of water vapor and the mixing ratios of cloud and ice water (Xu and Randall, 1996). We have also conducted another simulation, named icloud3, identical with CON in every aspect but with the only difference being the cloud scheme. In this case the scheme uses a method based on Sundqvist et al. (1989) (icloud=3 in the namelist) that relies on a RH threshold that depends on grid cell size.

It is important to note that after the cloud scheme has produced cloud fraction at each model level, the total cloud fraction is calculated by a separate algorithm that combines the values of each model level. The method used can definitely have an impact on the results. However in our study both CON and icloud3 use the same method, that is the maximum-random overlap.

We compare CON and icloud3 to assess the impact of the cloud scheme selection. Also we present results of the comparison ARI_T-CON to compare the importance of cloud scheme selection to the inclusion of aerosol-radiation interactions in the model. Furthermore we calculate the bias of the simulations to see which scheme is closer to the observed data. Analysis mainly focuses on the total cloud fraction (CFRACT) but also temperature near the surface, shortwave down welling radiation at the surface (Rsds) and longwave down welling radiation at the surface (Rlds) are examined.

The CLARA-A1 satellite dataset is used to evaluate total cloud fraction as well as longwave radiation at the surface (Rlds). For shortwave radiation (Rsds) the SARAH dataset is used whereas temperature is evaluated against the E-OBS v16 dataset. Description of each dataset can be seen at section E Observational data.

1.5.4.3 Results

We have seen that control simulation CON in general overestimates cloudiness (section 1.5.2.3) and the same is true for icloud3. Both simulations produce considerably larger cloud fraction amount than the satellite data over almost the entire domain and for most seasons except summer (Fig. 33, first two rows). Averaged for the domain of study the cloudiness overestimation is similar and ranges usually between 20 to 30% but for summer it becomes considerably smaller: 12% for CON and 1% for icloud1 (Table 13). In general icloud3 produces less cloud fraction than CON and thus the overestimation for icloud1 is slightly reduced. In summer both simulations present a pattern of CFRACT overestimation for central and northern Europe whereas for the south an underestimation is present for both schemes, a mild one for CON (less than -10%) that becomes considerably larger with the use of the Xu-Randall method in icloud1 and can reach -30% over extended parts of the Mediterranean. We must always consider however that relative bias in summer can be inflated due to small cloud fraction amounts. Another common feature seen in both simulations is the large biases over mountainous areas. This is probably attributed to the average resolution (~50km) of the simulations that is not sufficient to properly resolve the small-scale and complex interaction between orography and cloud formation.

The bias patterns of the two simulations are quite similar showing almost the same spatial correlation against the CLARA dataset for each season Fig. 34. However CON presents slightly smaller variability improving the matching with the satellite data in this respect. Both simulations have their best correlation with CLARA for summer (0.93) and their worst in winter (0.75).

Moreover the behavior of the bias in relation to the cloud fraction amount of the CLARA dataset is very similar (Fig. 35). For example in winter both simulations have overestimation in almost all cloud fraction amounts of the satellite dataset, with the largest biases seen in the medium values of CFRACT (0.4-0.5) while a declining of large biases is seen as we move towards large (>0.7) cloud fraction values. In summer both simulations have an underestimation of small to medium CFRACT values (0.1-0.5) that turns to overestimation in larger (0.5-0.9) cloud fraction amounts.

To sum up, we see that the two simulations present very similar CFRACT bias patterns and amounts. Both tend to overestimate cloud fraction. However the selection of cloud parameterization can have an impact on bias, especially on summer where the magnitude of the bias changes is the largest.

The cloud fraction differences (icloud1-CON) between the two schemes are small, usually around -0.05 (scale of 0 to 1) whereas in some cases they can exceed -0.1, for example over central Europe in summer (Fig. 33, third row). In relative values domain averaged differences are between -1% to -2% for most seasons (table). For summer however we have both the largest difference (-0.05) and largest relative difference (-13%) in cloud fraction amount. Domain averaged differences are always negative, therefore as said before, icloud1 presents consistently smaller CFRACT amounts that CON throughout the year. This is especially true for summer where the entire domain present smaller cloud fraction in icloud1 with the differences having the indication of statistical significance. However for the rest seasons, there areas with significant cloudiness increase for icloud1, for example winter and spring over Scandinavia.

A really important finding is the intense impact the cloud fraction changes have on the shortwave radiation at the surface (Rsds). Rsds is hugely impacted with icloud1 presenting larger Rsds amounts than CON (icloud3) due to the decreased cloudiness. The domain averaged Rsds increase ranges between +16% and +18% for all seasons. This is much larger (2 to 4 times) than the impact of aerosol-radiation interactions on Rsds (around -4% to -8%), excluding ARI_Mv1urban that has comparable but still slightly smaller impact on shortwave radiation. There are even specific areas where icloud1 has an increase of +30% in shortwave radiation.

Rsds biases are also impacted. The control simulation CON presents Rsds underestimation for all seasons probably because of the large cloudiness overestimation. The increase of shortwave radiation in icloud1 reduces this underestimation in autumn whereas in all other seasons we have a complete change in bias sign with an overestimation of Rsds being present.

It is interesting that icloud1 has both shortwave radiation and cloud fraction overestimation for all seasons except autumn. This is probably a matter of calibration of the cloud and radiation schemes of the model. Different domains and conditions might have different calibration needs. Moreover it must be reminded here, that the cloud fraction (CLARA) and shortwave radiation (SARAH) data used for evaluation belong to two different satellite datasets, something that could partially explain the above discrepancy.

Near surface temperature is also heavily impacted by the change in radiation fluxes. Domain averaged changes are between 0.4 and -0.8^{o}C whereas at grid point level changes greater than 1.5 ^{o}C are seen. This impact far surpasses the one seen in the aerosol sensitivities when aerosol-radiation interactions were enabled. This true even for the ARI_Mv1urban simulation with the highly absorbing aerosol that had a more intense impact on many variables. The largest difference between CON and icloud1 is seen in winter over Scandinavia and northeastern Europe with icloud1 being colder at -1.4 ^{o}C on average. In general for icloud1, temperature decreases in winter and autumn and increases in spring and summer compared to CON. Over large areas the changes have the indication of statistical significance, especially in winter and summer.

These intense changes in temperature also affect temperature bias. CON generally underestimates temperature, thus icloud1 increases this underestimation in winter and autumn and improves it in spring and summer. An extreme impact on bias is seen over northern Europe in winter where icloud1 presents the largest negative temperature decrease. As a result the already cold bias of -1.2^{o}C in CON over Scandinavia considerably worsen in icloud1 to -2.6^{o}C.

A very interesting feature is that icloud1 is clearly colder than CON for winter and autumn, despite allowing more shortwave radiation to reach the surface due to the less cloudiness it presents. This might seem physically inconsistent. However we must also take into account that clouds can also impact longwave radiation. Clouds can absorb the longwave radiation coming from the earth and re-emit a considerable portion of it back to the surface, resulting in near surface temperature increase. When down welling longwave radiation at the surface (Rlds) is analyzed, we see that it decreases around -2 to-3% for all seasons in icloud1. This is consistent with the cloudiness decrease seen in icloud1 since we expect that less clouds will absorb and re-emit a smaller longwave radiation amount back at the surface. This Rlds decrease may sound small but it can be especially important in winter over northern Europe where the shortwave radiation amount is very small. The general Rlds decrease seen in cloud1 helps to counteract the widespread Rsds increase observed, something that can affect temperature. Indeed when the change in the overall radiation budget at the surface is calculated (net shortwave + net longwave) it matches quite well with the changes in temperature. For example the cooling seen in winter for icloud1 is attributed to the considerable decrease in the overall radiative budget that is especially pronounced over northern Europe. In this case the longwave radiation decrease is prevailing over the shortwave radiation increase. Conversely, for summer and spring the increase in the radiation budget leads to warming at the surface. However autumn is a peculiar case. A general temperature decrease is happening despite a positive change in the radiation

budget at the surface. This indicates that other factors, such as changes in the atmospheric circulation or in the sensible and latent heat fluxes might play an important role in this case.

Besides the difference in total cloud fraction, it is important to assess the differences of the two schemes at the various cloud levels up in the atmosphere. Clouds at different altitudes can have quite different characteristics. For example higher clouds do not heavily reduce the incoming solar radiation but can effectively interact with earth's longwave radiation trapping it into the atmosphere.

As a final summary, it is clear that the change of the cloud parameterization had a very strong impact on many variables. Besides cloud fraction, shortwave and longwave radiation at the surface as well as temperature were intensely affected. It is impressive the impact was in most cases considerably higher than the effect on aerosol implementation in the model. We can conclude that the cloud parameterization is a very important one in the model and proper attention needs to given in the selection of the proper scheme.

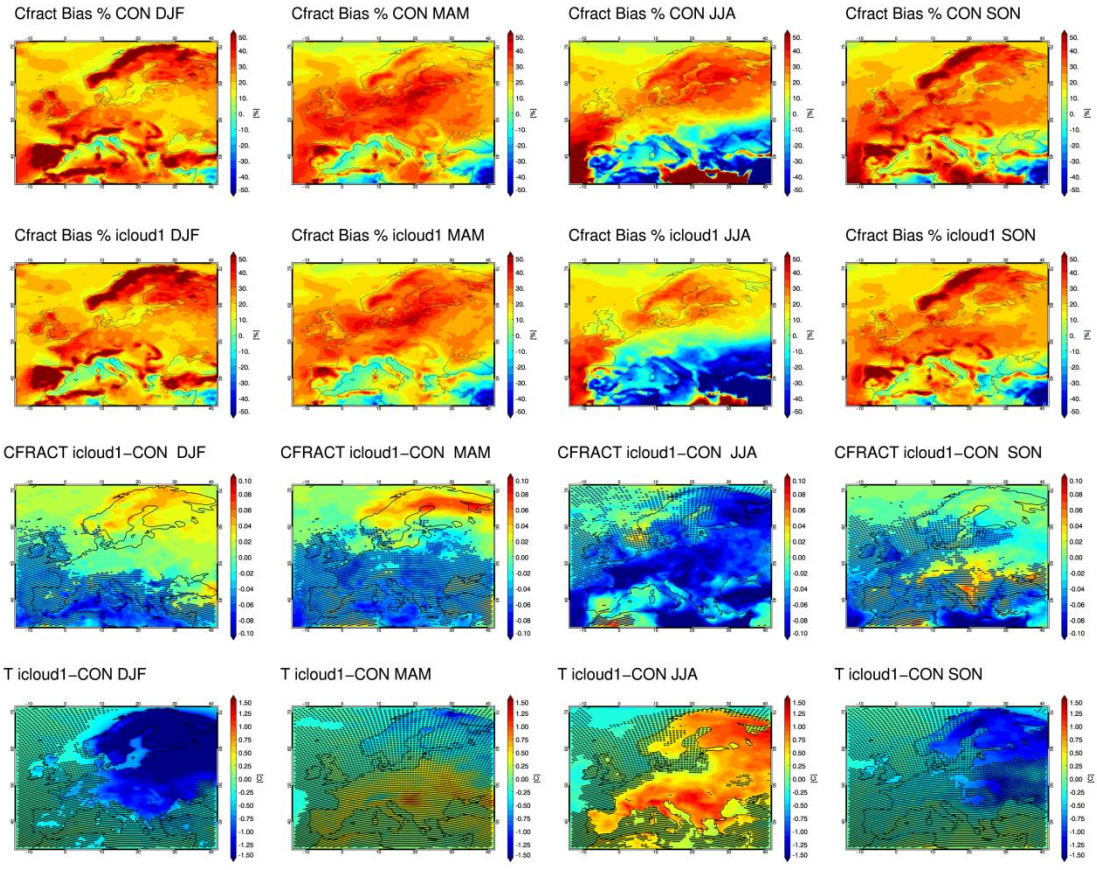

Fig. 33: Total cloud fraction relative bias against the CLARA-A1 data set for control simulation CON (top row) and icloud1 (second row). Cloud fraction difference (third row) and temperature difference (bottom row) between the two simulations (icloud1-CON) with stippling indicating where the differences are NOT significant at the 0.05 level with the Mann-Whitney test. For all seasons.

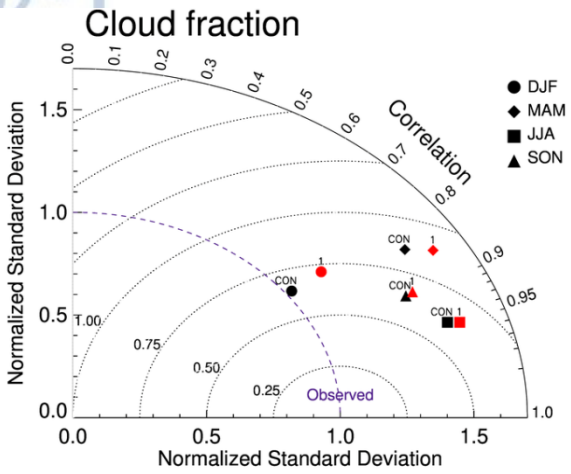

Fig. 34: Spatial Taylor diagram for total cloud fraction (CFRACT) comparing the control simulation (black) and icloud1 (red) for all seasons against the CLARA satellite dataset.

Table 13: Domain averaged relative bias for total cloud fraction (CFRACT), shortwave (Rsds) and longwave down welling radiation at the surface (Rlds) and simple bias for temperature. For all seasons.

Bias

	Winter		***Spring***		***Summer***		***Autumn***	
	icloud3	icloud1	icloud3	icloud1	icloud3	icloud1	icloud3	icloud1
CFRACT (%)	28	26	25	22	12	1	27	24
RSDS (%)	-7	10	-10	6	-8	4	-18	-8
RLDS(%)	6	2	4	2	2	0	4	2
Temperature (°C)	-0.6	-1.5	-1.8	-1.7	-0.5	0.1	-0.1	-0.6

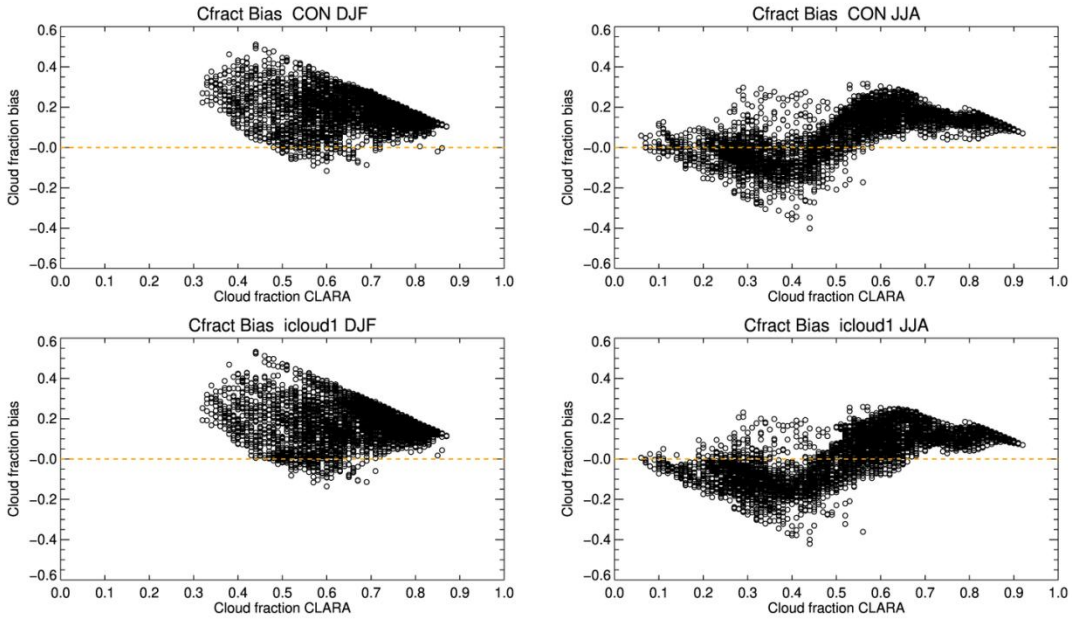

Fig. 35: Cloud fraction (CFRACT) bias against the CLARA dataset in relation to the cloud fraction of the CLARA dataset. For control simulation CON (top) and icloud1 (bottom). For winter (left) and summer (right).

2. PART2-Historical and Rcp8.5 simulations

2.1 Overview

PART1 of this study examined the sensitivity of the model regarding the introduction of aerosol effects as well as the effective radii communication and cloud scheme selection. All the simulations were forced using ERA-Interim reanalysis data and spanned a period of 5 years.

In this section we conduct longer simulations of 30 years for a historical period (1971-2000) and a future period (2021-2050) enabling in the model aerosol-radiation interactions. This time the model is driven by the CESM1 global climate model, using data that have been bias corrected. Moreover the simulation of the future period is performed using the Rcp8.5 scenario. A series of experiments using either a static aerosol field or a time evolving aerosol field is conducted. We use the same aerosol data set that was used for the global simulations of CESM1, while the aerosol-radiation interactions are enabled through the option aer_opt=2 which has been described in section 1.2.

Aim of Part2 of this study is:

a) To assess the impact of aerosol-radiation interactions more robustly based a longer time period
b) To assess the impact of aerosol-radiation interactions using time evolving aerosol in the trends of several variables and especially on the climate change signal.

Outline

Firstly we describe the global model and aerosol data used. Then we present the simulations conducted. A brief evaluation of the Historical simulations is given in section 2.7. The assessment of aerosol-radiation interactions based on a 30year period is given in section 2.9. The impact of aerosol-radiation interactions on the trends or several variables and on the signal of climate change for the historical period is given in section 2.8. An analysis for the future projections is given at section 2.10.

2.2 The global model-CESM1

The global model used for driving the WRF regional climate model is NCAR's Community Earth System Model (CESM1) used in Climate Model Intercomparison Program 5 (CMIP5). It is a state-of-the-art global climate model that has coupled atmosphere, ocean, land, and sea ice component models. It uses the CAM4.0 NCAR Community Atmosphere Model atmospheric model that can enable prescribed aerosols to interact with radiation. CAM4.0 is the sixth generation of the NCAR atmospheric GCM.
The CESM1 data used in this study are bias corrected data according to the method described in (Bruyère et al., 2014). This method corrects the mean bias of the GCM but also lets the weather and climate variability to change. The mean bias is corrected using the ERA-Interim reanalysis data from 1985-2005. Bias correction is performed in all the variables that

are needed by WRF to generate boundary conditions: temperature, geopotential height, relative humidity, sea surface temperature, mean sea level pressure and zonal and meridional wind.
Spatial resolution of the CESM1 data used is 1.25 degrees in longitude and 0.94 degrees in latitude whereas 26 vertical pressure levels are present. Temporal resolution is six hours.

2.3 Aerosol data

For both our Historical and Rcp8.5 simulations with time evolving aerosol we use the exact same aerosol dataset (regarding total AOD) that the driving model CESM1 used for the respective simulations that took part in CMIP5. Since both the RCM and the GCM that provides the boundary conditions rely on the same aerosol dataset we believe this improves the physical consistency of the conducted simulations.

The CCESM1 model uses the CAM4 atmospheric model. Earlier versions of CAM used considerable simplifications regarding aerosol-radiation interaction treatment. CAM2 had only a uniform aerosol background (AOD of 0.15) whereas CAM3 used a static climatology of sulfate, sea-salt, carbonaceous and dust aerosol. The CAM4 version uses a tropospheric aerosol climatology of monthly mean aerosol mass that evolves with time. It uses the same main aerosol categories used in CAM3. However in CAM4 some of the categories are divided even further thus the dataset contains ten aerosol categories: sea salt, four size related types of dust, sulfates, new and aged black carbon, hydrophobic and hydrophilic organic carbon.

The aerosol used in the historical experiments of the CESM1 used for bias correction have been produced by the incorporating updated emission inventories in the CAM-Chem coupled atmosphere-chemistry model for the period 1850-2000 (Lamarque et al., 2010). We use the total AOD of the same aerosol field for the historical simulations (1971-2000) of this study. Similarly, CESM1 used for its future projections an aerosol field coming from CAM-Chem simulations for the period 2000-2100 using the emissions of the different Representative Concentration Pathways (RCPs) (Lamarque et al., 2011). In the future projections of this study (2021-2050) we use the total AOD of the same aerosol field.

Both for the historical and future simulations of this study we use the same total aerosol optical depth that CESM1 used for its respective simulations. We provide it in WRF through the aer_opt=2 option, in order to enable aerosol-radiation interactions. The rest aerosol properties are parameterized using the “rural” aerosol type (see section 1.2).

2.4 Model set up

For both the Historical and Rcp8.5 simulations we use the exact same model set up. We use the Weather Research and Forecasting Model (WRF) version 3.8.1 with the ARW core (Skamarock et al. 2008, Power et al. 2018), the same model and version used in the sensitivity study of PART1.

All the PART2 simulations are forced by the CESM1 bias corrected data (Bruyère et al., 2014).

Model domain is the same as in the sensitivity study of PART1. It covers Europe between 25N-75N and 40W-75E with a resolution of 0.44^{o} (~50km) following the EURO-CORDEX specifications (Giorgi and Gutowski, 2015). We use 44 vertical levels, a higher number than the one used in the sensitivity study of PART1 (31 levels). This is because the CESM1 data reach 10hPa at the top of the atmosphere thus higher in the atmosphere than the ERA-Interim (50hPa) used in PART1. Each group of simulations (Historical, Rcp8.5) covers a period of 30years and uses 3 years as spin up time. The Historical simulations cover the period 1971-2000 (spin up 1968-1970) while the Rcp8.5 cover the period 2021-2050 (spin up 2018-2020).

The simulations are all conducted with the exact same model setup while they differ only in the aerosol fields used (see section 2.5). The basic model parameterizations used are:

The RRTMG (Iacono et al., 2008) radiation scheme for both shortwave and longwave radiation simulation. The CLM4 (Lawrence et al., 2011; Oleson et al., 2010) land surface model. The MYNN surface layer scheme and the MYNN2 (Nakanishi and Niino, 2006) boundary layer scheme. The Kain-Fritsch cumulus scheme (Kain, 2004). The Xu-Randall method (Xu and Randall, 1996) for estimating fractional cloud cover ("icloud=1" option in the namelist). Sub-grid cloud fraction interaction with radiation is enabled with the "cu_rad_feedback" option enabled (Alapaty et al., 2012). Finally we use the Thompson microphysics scheme (Thompson et al., 2008) in all simulations (not the Thompson aerosol-aware scheme).

The above model setup has some changes compared to the set up used in the sensitivity study of PART1. We have chosen the new model set up since it seems to improve some of the biases seen in the old one. The differences are: We use the MYNN surface layer scheme instead of the revised-MM5, the MYNN2 boundary layer instead of the Yonsei University scheme and the Kain-Fritsch cumulus scheme instead of the Grell-Freitas scheme. Finally we use option icloud=1 (Xu-Randall method) to estimate cloud fraction instead of icloud=3 (Sundqvist method) since we have seen in our sensitivity study (section 1.5.4) that it lowers the cloud fraction overestimation.

2.5 Simulations conducted

All simulations use the Thompson 2008 microphysics scheme that does not enable aerosol-cloud interactions. Only aerosol-radiation interactions are enabled through the aer_opt=2 option (see section 1.2). For both the Historical and Rcp8.5 simulations with time evolving aerosol we use the exact same aerosol dataset (regarding total AOD) that the driving model CESM1 used for the respective simulations in the context of CMIP5.

We have conducted three Historical simulations covering the period 1971-2000.

1. Simulation HisNo does not have any aerosol interactions.
2. Simulation HisAer uses the original time evolving aerosol used in the CESM1 Historical runs.
3. Simulation HisStatic uses an aerosol field that has no year-to-year variability, derived by the CESM1 time evolving aerosol. We average the time evolving aerosol of CESM1 over the period 1971-2000 keeping the spatial and monthly variability. In

essence we have constructed a monthly mean (12 fields-one for each month) climatology of the time evolving aerosol dataset that has the same average aerosol optical depth with the time evolving historical dataset. We refer to this static in time (on a year-to-year basis) aerosol dataset as the Static dataset.

We have conducted two scenario Rcp8.5 simulations covering the period 2021-2050.

1. Simulation RcpAer uses the original time evolving aerosol used in the CESM1 Rcp8.5 runs.
2. Simulation RcpStatic uses a static in time aerosol field. It is the same field used in simulation HisStatic, derived by averaging the time evolving aerosol of CESM1 over the period 1971-2000 keeping the spatial and monthly variability. With RcpStatic we have a simulation of a future period that has the same mean AOD with the Historical run.

We see that there are simulations using time evolving aerosol have the term "Aer" in their names whereas those featuring a static in time mean AOD field have the term "Static" in their names.

Table 14: Simulation conducted for PART2 of this study and information about aerosol treatment. The Historical runs are depicted with pale green header. The Rcp8.5 scenarios are depicted with pale purple header.

Simulation	HisNo	HisAer	HisStatic	RcpAer	RcpStatic
Mp scheme	Thompson 2008	Thompson 2008	Thompson 2008	Thompson 2008	Thompson 2008
Aerosol option	-	aer_opt=2	aer_opt=2	aer_opt=2	aer_opt=2
Aerosol source	-	CESM1 time evolving	CESM1 static	CESM1 time evolving	CESM1 static
Aerosol type	-	"rural"	"rural"	"rural"	"rural"
Aerosol interacting	-	**radiation**	**radiation**	**radiation**	**radiation**

with

The goal of conducting these simulations

By evaluating simulations HisAer, HisStatic and HisNo: To assess the coupling between the CESM1 bias corrected data and WRF.

By comparing simulations HisAer and HisNo: To assess the impact of aerosol interactions over the 30year historical period. This will provide a more robust result than the 5year sensitivity studies.

By comparing simulations HisAer and HisStatic: To assess the impact of time evolving aerosol on trends in some main variables (e.g. radiations and temperature) versus the impact of a static aerosol field.

By analyzing RcpAer: To identify the simulated climate of the future 2021-2050 period and detect the trends and climate change signal.

By comparing RcpAer and RcpStatic: To assess the impact of time evolving aerosol (decreasing concentrations) on the simulated future climate compared to a static aerosol field that has the same mean AOD with the historical period.

2.6 Aerosol Optical Depth

We present in this section a short analysis of the aerosol data, specifically the total aerosol optical depth at 550nm (AOD), used in the historical and Rcp8.5 simulations.

In Fig. 36 (left) we present the total aerosol optical depth at the visible range of the CCM4 aerosol data set over the model domain, covering the entire historical period of 1850-2005 and the future period of 2005-2100. For the future period AOD is depicted for the Rcp 4.5, 6.0 and 8.5 scenarios. It is clear that for the broader historical period AOD has an intense increasing trend until the mid 1970s early 1980s. From that time and on the trend is reversed and AOD decreases rapidly with time. This behavior is expected and has been described in observational studies ((Streets et al., 2006). It is attributed to the reduction of anthropogenic aerosol concentrations (Vestreng et al., 2007). The strict regulations regarding aerosol emissions in Europe have affected aerosol concentrations reducing their numbers and resulting in decreasing trends (Wild, 2009). Thus for the future period all the Rcp scenarios present decreasing AOD trends, however less intense compared to the one seen in the 1980-2005 time frame. The Rcp8.5, the one we use in this study, has the largest AOD reduction for the period 2021-2050 compared to the other two emission scenarios.

We must note here that the spikes of sudden increases in AOD during the historical 1850-2005 period are the result of volcanic eruptions. The impact of such eruptions on the total

AOD is impressive. There are cases that the AOD of the entire model domain more than doubles after a large eruption. Volcanic eruptions are also present in the 1971-2000 period (Fig. 36-right) used in the historical simulations of this study and thus their impact on AOD is fully taken into account. For example the large spike in SOD seen in the early 1990s is caused by the eruption of Mt. Pinatubo in 1991. This eruption had the largest ejection of aerosol in the stratosphere in the 20th century and intensely affected radiation and temperature worldwide causing a cooling at the surface of 0.5 to 0.6 ^{o}C in the Northern Hemisphere (McCormick et al., 1995).

In Fig. 36-right we present the temporal evolution of AOD for the simulations conducted in PART2, both historical and Rcp8.5. It is clear that simulations HisStatic and RcpStatic have the same AOD field that has a static average value through time. In both historical and Rcp8.5 simulations with time evolving aerosol, HisAer (1971-2000) and RcpAer (2021-2050), the trends are negative, resulting in decreasing AOD with time. It is characteristic that this decreasing trend is not only present regarding domain averages but it is also detected on the times series at grid point level for the biggest part of the domain. Fig. 37 presents the trend coefficient calculated as the slope of a least-squares fit on the yearly mean time series over each grid point for the historical period 1971-2000 (left) and the Rcp8.5 scenario 2021-2050 (right). It is evident that for the main European domain used in the analysis (Fig. 37) the AOD trend is negative (blue color) thus decreasing. Only some areas of the wider model domain, over North Africa and the Central Atlantic ocean, present increasing (deep red) AOD trends in the period 1971-2000 whereas in the 2021-2050 they are even less spatially extensive.

More information about the trends of the time evolving aerosol used in the historical HisAer simulation are given in section 2.8.2.

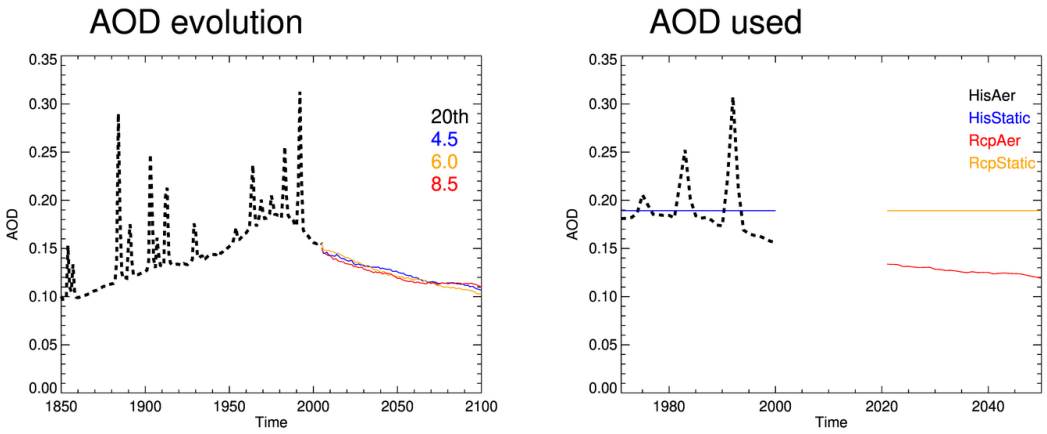

Fig. 36: Left: Aerosol optical depth (AOD) evolution during the entire historical 1850-2005 period and for three Rcp scenarios covering the period 2005-2100. Right: AOD temporal evolution for the simulations conducted in PART2, both historical and Rcp8.5. Both plots cover the entire model domain.

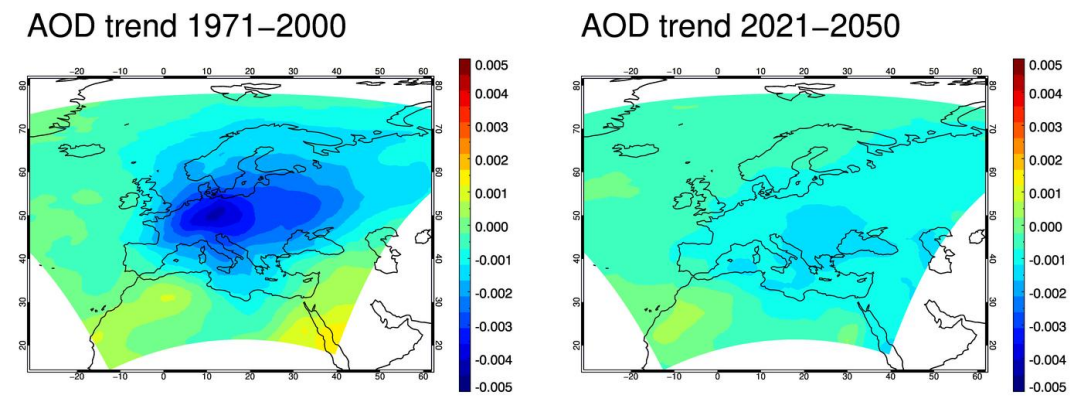

Fig. 37: Aerosol optical depth (AOD) trend coefficient for the periods 1971-2000 and 2021-2050 using yearly mean time series over each grid point over the model domain. The trend coefficient is the slope of a linear fit to each time series using the least-squares method.

In order to put the CESM1 aerosol used in PART2 into context we present in the yearly average AOD for the Static aerosol field, the Historical and Rcp8.5 fields both in the beginning and the end of each period as well as for the aerosol climatologies used in the sensitivity study in PART1 and the Seviri satellite data set (2004-2008 period average). We see that the Static field is close to the Macv1 and MACC mean values as well as close to the Historical data set in the beginning of the period (1971). On a seasonal basis it presents smaller domain averaged AOD than both MACC and Macv1 for all seasons except for summer (0.25). The Tegen climatology on the other hand has the smallest AOD among the climatologies (0.13) with its value being very close to the Rcp8.5 mean AOD. Therefore a user interested only in mean AOD could chose the Tegen climatology to represent aerosol for the simulation of a future period. Moreover, the use of the Static field in the future period (simulation RcpStatic) provides the model with a mean AOD (0.19) considerably larger than that of the Rcp8.5 scenario. The Static fields also presents a seasonal variability, with an average AOD of 0.12 in winter, 0.20 in spring, 0.26 in summer and 0.17 in autumn.

Table 15: Mean aerosol optical depth (AOD) for the Static aerosol field, the Historical and Rcp8.5 fields both in the beginning and end of each period as well as for the aerosol climatologies used in the sensitivity study in PART1 and the Seviri satellite data set (mean for the period 2004-2008).

STATIC	*Historical* 1971	*Historical* 2000	*Rcp8.5* 2021	*Rcp8.5* 2050	*Tegen*	*Macv1*	*MACC* (2004-2008)	*Seviri* (2004-2008)
0,19	0,18	0,16	0,13	0,12	0,13	0,22	0,21	0,27

Spatially the CCM4 aerosol (historical, future and Static) present the same basic behavior like the one seen in the climatologies used in the sensitivity study of PART1. Fig. 38 presents the

Static AOD field and Rcp8.5 field for each season as well as the climatologies of MACv1 and Tegen. We see that the Static field is very similar to the spatial pattern of the MACv1 climatology. However the Static field has a much stronger AOD (exceeding 0.6 in places) over North Africa in summer. This intense AOD over North Africa is the largest among all the datasets examined and only Seviri has a few spots of comparable intensity. Moreover as is the case with MACv1, the Static lacks the intense AOD maximum seen in winter over Eastern Europe in the Seviri satellite dataset. The Rcp8.5 field has a much milder AOD than all the other datasets, indicative of the decreasing AOD trend. The largest part of the European continent presents quite low AOD values (below 0.15) for all seasons without any considerable seasonal variability. It is characteristic that in summer the AOD maximum over North Africa decreases both in intensity and extent whereas the secondary maximum over central Europe is completely gone. The Tegen climatology is the closest to the Rcp8.5 in terms of AOD magnitude, even though Tegen presents larger AOD values over extended parts of eastern and southeastern Europe.

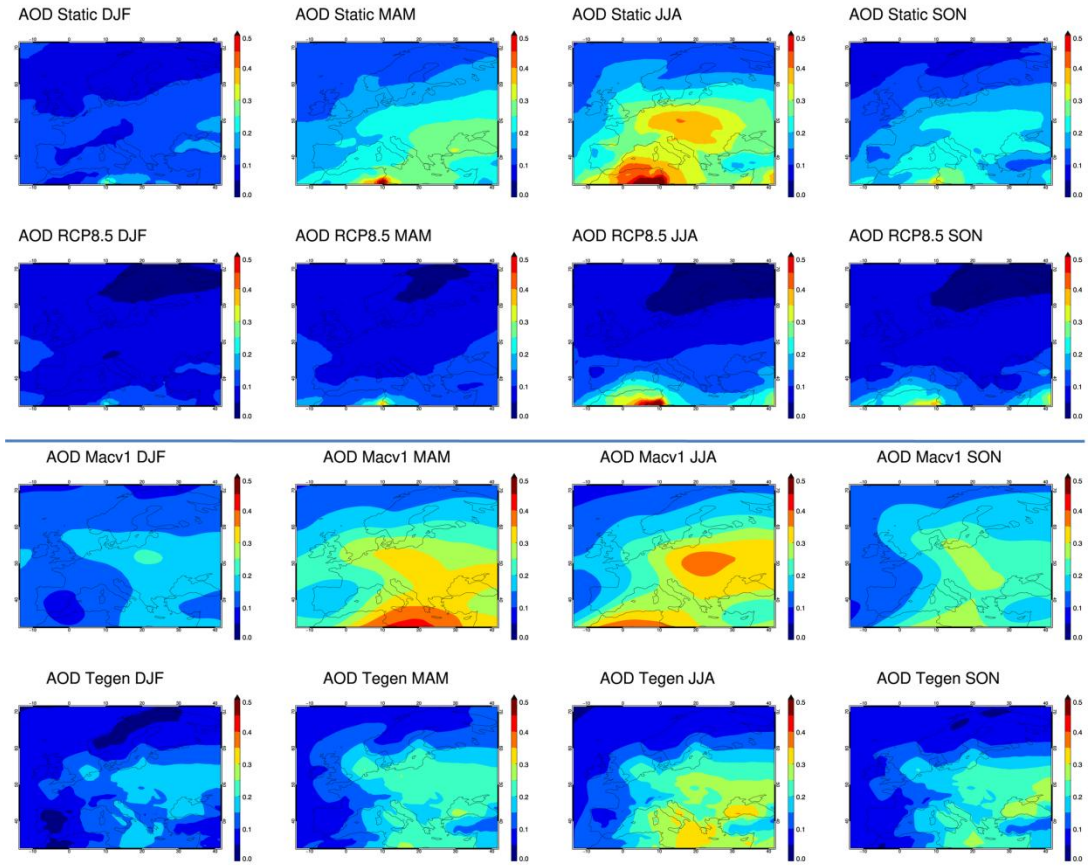

Fig. 38: Seasonal aerosol optical depth (AOD) for the Static field (first row) and the Rcp8.5 field (second row) that are used in PART2. For comparison, the bottom two rows present the aerosol optical depth fields of the MACv1 climatology (third row) and the Tegen climatology (bottom row) that were used in the sensitivity study of PART1..

2.7 Evaluation-Historical simulations

In this section we present the evaluation of the historical simulations. We examine near surface temperature (T), precipitation (Pr), shortwave radiation at the surface (Rsds) and its direct normalized component (DNI) and total cloud fraction (CFRACT). The purpose is to assert the degree of success that our simulations exhibit in simulating the historical climate over Europe.

Here we perform a basic evaluation of the historical runs. Since bias differences between the simulations are small we present plot only for HisNo (no aerosol) and HisAer (transient aerosol). Temperature and precipitation are compared against the E-OBS v19 observational dataset. Rsds and DNI are compared against the SARAH satellite dataset and CFRACT is compared against the CLARA-A1 satellite dataset. Since all the satellite datasets used have data after 1983 evaluation against the satellite data covers the period 1983-2000.

An analysis of the trends of the historical simulations and of the observational data is performed in the next section (2.8). Even though it could be considered as part of the overall evaluation, we choose to present it in a separate section since we mainly focus on the aerosol-radiation interactions impact on the trends.

2.7.1 Summary

In general the biases seem to be reduced compared to the CON simulation in the sensitivity study of PART1 and are constrained compared to other biases seen in the bibliography for both GCMs and RCMs over Europe. This indicates that both the current model setup of WRF as well as the coupling with the CESM1 bias corrected data is successful. The ability of the historical simulations to correctly simulate the climate of Europe makes the results of the Rcp8.5 scenarios more robust. The bias differences between the historical simulations are small indicating that aerosol treatment is not one of the main causes of bias.

2.7.2 Temperature

In general there is a good agreement between the historical simulations and E-OBS. Domain averaged biases are less than 1^{o}C for all seasons and this behavior is also seen for most of the Prudence subregions as well. Only EA and FR in summer have stronger biases, around 1.5 ^{o}C.

There are seasons where the domain averaged bias is very small (winter, autumn and even spring) but this happens because of error compensation between positive and negative values. If we examine the absolute bias we see that domain averages are close to 1 ^{o}C for winter and summer and around 0.6 to 0.7 ^{o}C for spring and autumn. Therefore the magnitude of error is pretty much comparable for all seasons. Moreover the absolute bias is also constrained usually below 1 ^{o}C for most subregions and seasons. The absolute bias

metric is more indicative of the error magnitude since it does not take into account the sign of the bias, thus it does not suffer from sign compensation.

The historical runs are clearly warmer than E-OBS in summer, with this overestimation happening all over the domain. For the rest seasons there is not a clear specific tendency of the bias. In autumn a small overestimation is present for most subregions except Scandinavia. In winter and spring positive and negative biases are seen over the domain. However characteristic is a large area over eastern Europe where the simulations are cooler than the observational data (underestimation).

Compared to the control simulation CON from PART1, the historical simulations have smaller biases. Some of the strong biases of CON, like the underestimation over central and north Europe in spring (-2.3^{o}C) and the underestimation over Scandinavia in winter (-1^{o}C) are decreased or are completely gone in the historical simulations. For example the winter cold bias over Scandinavia, characteristic of many WRF simulations, is altered to a small warm bias (0.4^{o}C) in the historical runs. In terms of absolute bias however the values are comparable to CON in winter, autumn and summer but there are considerably better in spring (0.7 instead of 1.8 ^{o}C).

Overall the performance is quite good compared with CON and with other studies over Europe. There are simulations, especially with WRF than present much larger biases in temperature, especially in winter over northern Europe (sometimes exceeding 3^{o}C) (García-Díez et al., 2015).

Finally it must be noted that the differences between the historical simulations are very small. The pattern of temperature bias is almost identical whereas the magnitude of bias is very similar. Domain or subdomain averages usually do not differ more than 0.1 ^{o}C. The use of aerosol-radiation interactions does not necessarily reduce the temperature bias compared to HisNo. In cases of negative bias in HisNo (e.g. Scandinavia and the Alps in spring) the introduction of aerosol-radiation interactions leads to bias increase since it produces further cooling.

Table 16: Temperature bias (C) for the historical simulations against Eobs19. For all seasons and all subregions including the EU region. Last row presents the absolute bias for the EU region.

	DJF			MAM			JJA			SON		
	HisNo	HisAeros	HisStatic	HisNo	HisAeros	HisStatic	HisNo	HisAeros	HisStatic	HisNo	HisAeros	HisStatic
BI	0,6	0,5	0,6	0,4	0,2	0,1	0,3	0,3	0,2	0,4	0,2	0,2
IP	0,2	0,0	0,0	0,3	0,1	0,0	0,7	0,5	0,5	0,4	0,2	0,2
FR	0,6	0,4	0,5	1,0	0,7	0,6	1,5	1,3	1,2	1,0	0,7	0,6
ME	0,3	0,1	0,2	0,6	0,2	0,1	1,4	1,2	1,0	1,0	0,6	0,5
SC	0,4	0,3	0,4	-0,5	-0,7	-0,7	0,6	0,4	0,2	-0,5	-0,7	-0,7
AL	0,1	-0,2	-0,1	-0,5	-0,8	-0,9	1,1	0,9	0,8	0,7	0,4	0,4
MD	-0,3	-0,5	-0,5	0,1	-0,1	-0,2	1,0	0,6	0,7	0,1	-0,1	0,0
EA	-0,5	-0,7	-0,4	-0,2	-0,7	-0,8	2,2	1,6	1,5	0,7	0,2	0,1
EU	0,0	-0,1	0,0	0,0	-0,3	-0,4	1,1	0,8	0,7	0,3	0,0	0,0
Absolute Bias												
EU	0,9	1,0	0,9	0,6	0,6	0,7	1,4	1,1	1,1	0,7	0,6	0,6

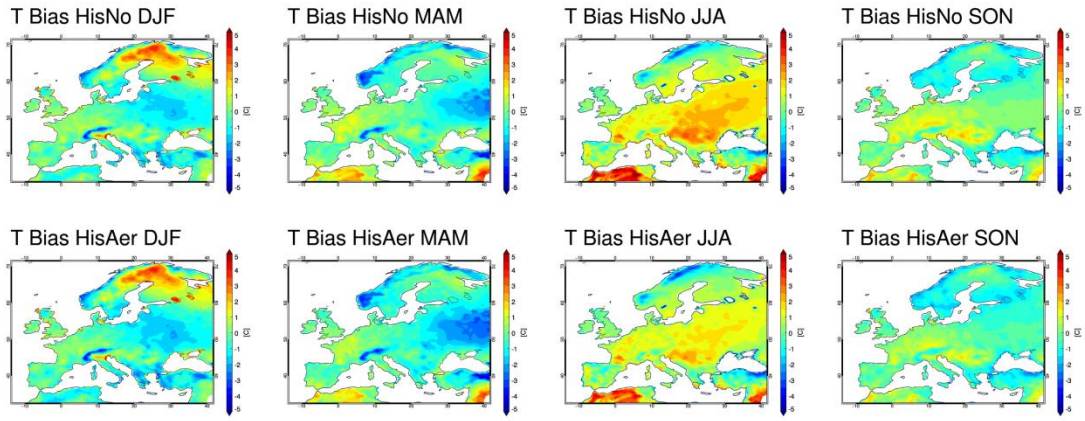

Fig. 39: Temperature bias for the historical simulations, HisAer (top) and HisStatic (bottom). For all seasons.

2.7.3 Precipitation

As is the case with temperature, precipitation bias pattern and magnitude is very similar, almost identical for all historical simulations. Thus all the historical simulations present in essence the same behavior.

In general biases are not very strong, as seen in the context of other studies over Europe (Kotlarski et al., 2014). We can say that there is a nice agreement between the historical simulations and E-OBS. Some large biases are present over extended areas in several cases but nothing particularly important to indicate large errors in simulating the physical mechanisms of precipitation. The historical simulations of this study present considerably better bias results compared to many other WRF simulations over Europe, that are even driven by reanalysis data (García-Díez et al., 2015).

In general the historical runs are more wet than E-OBS. Precipitation is considerably overestimated almost all over the domain in winter and spring (27% to 37% domain averages) and less in autumn (11%). On the other hand, in summer bias does not have a specific tendency. There is a large zone covering west, central and eastern Europe with underestimation, moderate in relative bias (-10 to -20%) but considerable if expressed in mm/day (-0.15 to -0.44 mm/day). Areas of southern Europe over the Mediterranean region and the Iberian Peninsula have precipitation overestimation in summer. However the large relative bias (+47% in MD) is inflated due to the small precipitation amount in this region and season. For MD during summer, bias in mm/day is quite small (0.07 mm/day) but the absolute Bias is definitely not negligible (0.28 mm/day) indicating sign compensation for the simple bias.

We also examine the mean absolute bias. The mean absolute bias is 0.5 to 0.6 mm/day in winter and spring, 0.4 mm/day in autumn and 0.3 mm/day in summer. Therefore we see that the error in precipitation does not deviate that much on a seasonal basis, as was the case in relative bias. Moreover the mean absolute bias is very similar to all historical simulations, regardless of aerosol implementation.

The control simulation CON in PART1 had a similar behavior regarding the pattern and direction of the bias. However it presented more intense biases in several areas like the winter overestimation over EA and summer overestimation in MD and overestimation over the Balkans. In essence the historical runs have similar pattern but more mild biases compared to CON. We must always remember that CON extends only for 5 years on a different time period, making comparisons difficult. We can state however that we have an indication that the model setup in PART2 might be improving bias magnitude.

Table 17: Precipitation relative bias (%) for the historical simulations against Eobs19. For all seasons and all subregions including the EU region. Last two rows present the bias in mm/day and the absolute bias in mm/day for the EU region.

	DJF			MAM			JJA			SON		
%	HisNo	HisAeros	HisStatic	HisNo	HisAeros	HisStatic	HisNo	HisAeros	HisStatic	HisNo	HisAeros	HisStatic
BI	2	2	3	9	11	13	-5	-8	-4	-5	-4	-3
IP	9	9	7	47	43	42	46	33	34	5	7	10
FR	1	0	0	22	19	22	0	-7	-9	-1	1	1
ME	15	16	15	17	17	19	-6	-14	-13	8	8	13
SC	46	48	48	42	42	46	5	0	5	19	18	18
AL	27	23	27	33	32	34	-1	-7	-10	12	9	13
MD	19	19	18	50	48	51	46	47	36	11	13	8
EA	41	38	38	37	34	37	-15	-18	-19	9	16	14
EU	27	27	27	38	35	37	6	1	2	9	11	11
mm/day												
EU	0,29	0,29	0,28	0,53	0,51	0,55	-0,03	-0,12	-0,10	0,09	0,12	0,11
Absolute Bias mm/day												
EU	0,56	0,57	0,57	0,57	0,53	0,56	0,31	0,33	0,33	0,38	0,40	0,40

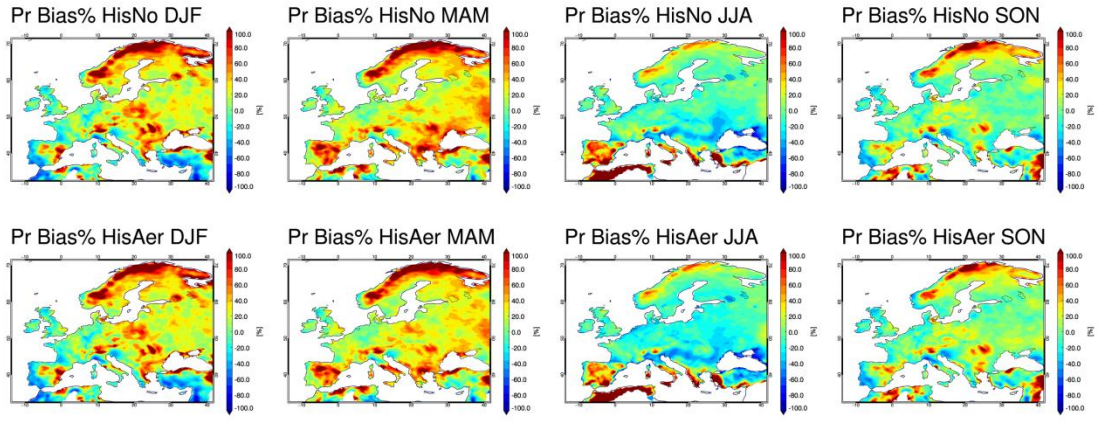

Fig. 40: Precipitation relative bias for the historical simulations, HisAer (top) and HisStatic (bottom). For all seasons.

2.7.4 Total cloud fraction (CFRACT)

Total cloud fraction is evaluated against the CLARA satellite dataset for the period 1983-2000.

Bias pattern and magnitude is again almost identical for the historical simulations for all seasons.

Simulated total cloud fraction has good agreement with the satellite data. Bias and relative bias domain averages are quite small. This is of course up to a point due to error compensation between positive and negative values. However absolute bias not very big as well. Domain averaged absolute relative bias is largest for summer, around 18%, and ranges between 7 to 10% for the rest seasons. Absolute bias is larger for summer and winter at 0.07, and becomes 0.05 for autumn and spring.

The spatial pattern of the bias presents both areas with over and underestimation and has some basic characteristics: 1) An overestimation of cloud fraction over Scandinavia and northeastern Europe in winter. 2) An overestimation over the Iberian Peninsula, more prominent in summer and autumn. 3) An underestimation of cloudiness over the southeastern part of the domain covering parts of eastern Mediterranean, around the Black Sea and the Balkans. This is more prominent during summer with MD and EA having averages of -20% and the relative bias exceeding -50% over extended areas of Greece and Turkey. The relative values are somewhat inflated due to the small cloudiness amount present in this area during summer. However the bias (scale -1 to 1) magnitude is also large (between -0.1 and -0.3), larger than all other areas of Europe in summer, clearly indicating a local deficit of cloudiness amount over the examined area. Interestingly this underestimation is not present over the Black Sea itself, but over the surrounding areas. The historical simulations have cloud fraction amounts that do not differ much between the Black Sea and the surrounding areas. On the other hand the CLARA dataset clearly has a sharp contrast in cloud fraction between the Black Sea and the land areas around it, with that over the sea having less CFRACT amount. Algorithms that produce the satellite datasets, tend to treat points over land and over the sea differently, and this manifests in the cloud fraction of the CLARA dataset. This situation clearly affects the bias spatial pattern over the region keeping it quite smaller over the water area of the Black Sea.

Compared to other studies over Europe, the historical simulations have considerably smaller biases. Several WRF hindcast simulations (Katragkou et al., 2015) presented larger and spatially more extensive CFRACT underestimation over southern Europe in summer (e.g. exceeding -50% over the entire south Europe) and more prominent overestimation over north Europe in winter.

Finally the setup of the CON simulation in PART1 that used ERA-Interim boundaries produced larger biases and tended to generally overestimate cloudiness amount. The new model setup in the historical simulations seems to help simulate more realistic cloud fraction values. The use of a different cloud fraction scheme (using the Xu-Randall method in historical instead of Sundqvist in CON) has probably a positive impact on cloud fraction biases (see section 1.5.4).

Table 18: Total cloud fraction (CFRACT) relative bias (%) for the historical simulations against CLARA satellite dataset. For all seasons and all subregions including the EU region. Last three rows present the absolute relative bias, the bias (scale -1 to 1) and the absolute bias for the EU region.

	DJF			MAM			JJA			SON		
%	HisNo	HisAeros	HisStatic	HisNo	HisAeros	HisStatic	HisNo	HisAeros	HisStatic	HisNo	HisAeros	HisStatic
BI	1	1	1	0	0	1	0	1	2	1	1	1
IP	4	5	5	12	12	11	13	15	13	16	16	17
FR	3	3	2	5	4	4	2	0	-2	9	8	8
ME	4	3	4	1	1	2	-4	-7	-5	-1	-1	-1
SC	11	11	11	8	7	8	8	7	8	8	8	8
AL	0	0	0	1	0	1	-4	-6	-8	2	3	3
MD	-13	-12	-13	-2	-1	-2	-20	-19	-20	-8	-5	-5
EA	10	9	9	1	1	2	-24	-22	-22	0	2	1
EU	3	3	3	2	2	2	-8	-8	-8	1	2	2
Bias	0,03	0,03	0,02	0,01	0,02	0,02	-0,02	-0,02	-0,02	0,01	0,02	0,02
Absolute Bias EU	0,07	0,07	0,07	0,05	0,05	0,05	0,07	0,07	0,07	0,05	0,05	0,05
Absolute bias % EU	10	10	10	7	7	7	17	17	18	8	8	8

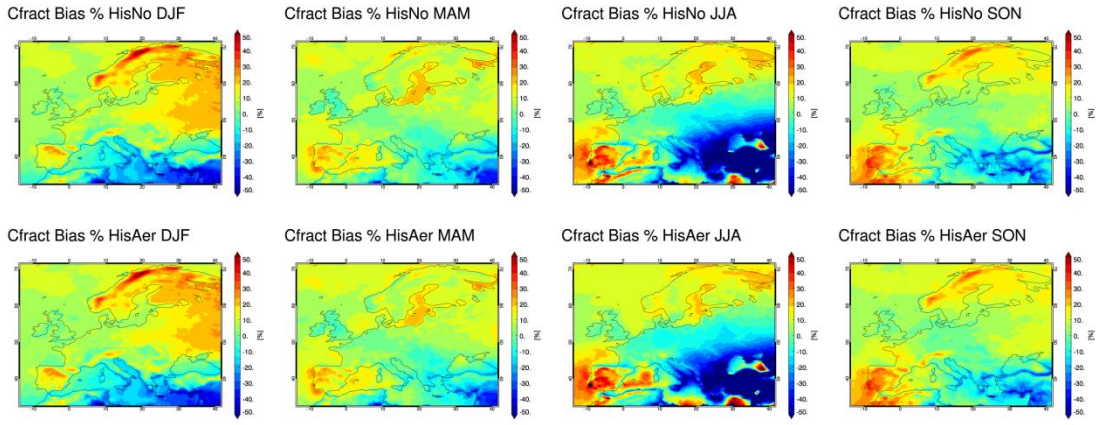

Fig. 41: Total cloud fraction (CFRACT) relative bias for the historical simulations, HisAer (top) and HisStatic (bottom). For all seasons.

2.7.5 Shortwave radiation at the surface (Rsds)

Shortwave down welling radiation at the surface (Rsds) is evaluated for the period 1983-2000 against the SARAH satellite data set.

In general agreement with the satellite data is good. However for all seasons the historical simulations overestimate Rsds. It is characteristic that domain averaged relative bias (and bias in W/m^2) is always positive and the same is true for all the subdomain averages as well. Thus spatially the overestimation is total. Over the entire domain only a very small number of grid points have slightly negative biases. Therefore the introduction of aerosol-radiation interactions, which decrease Rsds amount, lead to bias improvement compared to the historical simulation HisNo that has no aerosol.

In terms of relative bias this overestimation is larger in winter (29%) and in spring (18%). Interestingly for these two seasons large biases are more pronounced over mountainous areas like the Alps and southwest Norway. Simple bias however (expressed in W/m^2) is larger during summer and spring (around 30 W/m^2) due to the larger amount of solar radiation reaching the surface. Domain averages of bias and absolute bias are identical, indicating the total Rsds overestimation over the domain.

The values of the relative bias can be considered quite good even when compared against WRF hindcast simulations driven by reanalysis data. In the study of (Katragkou et al., 2015) all the WRF simulations (period 1990-2008) had worse Rsds relative biases, especially in winter, against the ISCCP satellite dataset.

Moreover it is impressive that the underestimation of Rsds seen in control simulation CON of PART1 is completely reversed to total overestimation in the historical simulations. The model setup and especially cloud scheme selection, icloud=1 (see section 1.5.4), has an intense impact of radiation levels. The tendency and sign of the bias might differ drastically but the absolute bias between CON and historical is quite similar and only differs considerably in autumn with the historical simulations having the better metric (10 W/m^2 instead of 17 W/m^2 for CON).

Finally it must be noted that the prominent biases in cloud fraction described in the previous paragraph (e.g. underestimation in southeastern Europe during summer) do not seem to have an impact on the Rsds biases. It is characteristic that there areas over north and eastern Europe in winter that are considerably overestimating both cloud fraction and shortwave radiation. Situations like this usually are attributed to the calibration of the model, specifically of the radiation scheme and how it is adjusted to work with a given cloud fraction amount.

Table 19: Shortwave down welling radiation at the surface (Rsds) relative bias (%) for the historical simulations against SARAH satellite dataset. For all seasons and all subregions including the EU region. Last two rows present the bias in W/m^2 and the absolute bias in W/m^2 for the EU region.

	DJF			MAM			JJA			SON		
%	HisNo	HisAeros	HisStatic	HisNo	HisAeros	HisStatic	HisNo	HisAeros	HisStatic	HisNo	HisAeros	HisStatic
BI	27	22	22	25	20	19	21	16	15	16	12	12
IP	14	9	9	11	7	8	10	4	4	9	4	3
FR	21	16	16	19	15	15	19	14	14	13	8	8
ME	30	25	25	28	21	21	29	23	21	27	19	18
SC	49	44	43	28	23	22	22	19	17	24	18	17
AL	42	36	36	31	26	25	18	12	12	18	11	11
MD	25	19	20	18	12	12	11	3	3	14	6	6
EA	39	35	35	30	23	22	27	19	18	25	15	15
EU	34	29	29	24	18	18	19	13	12	18	12	11
Bias W/m^2												
EU	15	13	13	40	30	29	43	28	27	17	10	10
Absolute Bias W/m^2												
EU	15	13	13	40	30	29	43	28	27	17	10	10

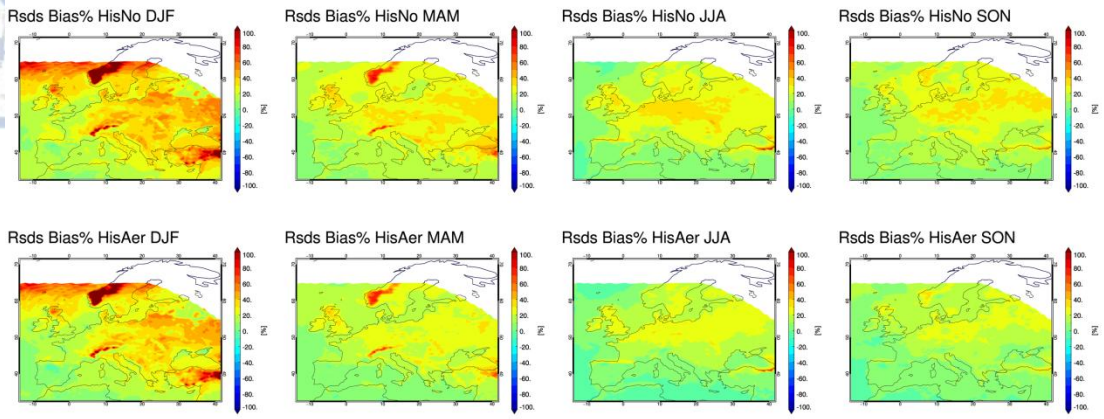

Fig. 42: Shortwave down welling radiation at the surface (Rsds) relative bias for the historical simulations, HisAer (top) and HisStatic (bottom). For all seasons.

2.7.6 Direct normalized irradiance (DNI)

Shortwave direct normalized irradiance at the surface (DNI) is evaluated for the period 1983-2000 against the SARAH satellite data set.

Simulation HisNo

The no aerosol simulation HisNo has considerably larger biases than the two simulations with aerosol-radiation interactions and presents a complete overestimation of DNI. The domain averaged relative biases are strong and range from 30% to 54% depending on season. Due to the total overestimation the absolute relative biases are almost identical. It is characteristic that at grid point level the bias exceed 50% at a large part of the domain for all seasons. However this is especially pronounced in summer over almost the entire continental Europe.

Simulations with aerosol-radiation interactions

For HisAer and HisStatic the relative bias against SARAH satellite dataset is less than 10% regarding domain averages for all seasons. However the small domain averages are a result of error compensation since both strong positive and negative biases exist. The domain averaged absolute relative bias is clearly larger, ranging from 9% in autumn up until 20% in winter where the largest relative error is present. If the absolute bias (W/m^2) is examined summer is the season with the largest domain averaged error (32 to 36 W/m^2) which is 2-3 times larger than the average bias seen for the other seasons. However the larger radiation levels in summer definitely contribute to the enlarged absolute bias detected.

The spatial pattern of the relative bias has some prominent features. A strong negative bias (underestimation) is seen in winter over an extended area at the northeastern part of the domain. This underestimation exceeds 50% over extensive areas. Interestingly it is not seen in any other season. Also in winter, a strong positive bias (overestimation) is present over the southeastern part of the domain. For the rest seasons positive biases continue to be present over parts of this area, mainly over land, but are much less pronounced. In summer a large zone of positive biases covers almost the entire domain over land above 40^o in

latitude (in essence the middle and northern part of the domain). Interestingly, this strong positive bias is especially pronounced over the eastern-northeastern part of Europe, the same area that has the strong negative bias in winter. Finally it is interesting to note that sea areas have in many cases a different bias behavior than the land areas close to them. For example the Mediterranean Sea and has negative biases in all seasons except winter, whereas extensive land areas around the Mediterranean (southern France, Italy, Greece and Turkey) have positive biases. This behavior is more prominent in summer.

Conclusion

Overall the DNI biases of HisNo are larger than those seen in the control simulation CON of PART1. Moreover CON had a clear tendency for DNI underestimation whereas HisNo clearly overestimates direct radiation. In CON the mean absolute relative bias is around 30% for all seasons whereas for the HisNo ranges from 30 to 54%. When aerosol-radiation interactions are enabled the mean absolute relative bias is clearly improved, ranging from 9% in autumn to 20% in winter in HisAer and HisStatic. Therefore the inclusion of aerosol can have a dramatic impact on the direct normalized radiation bias. Of course whether it improves or worsen the bias always depends on model calibration and the behavior of the model without the aerosol interactions. Finally we must also note that small differences between the historical runs that have aerosol do exist, regarding the bias in DNI. In contrast to the other variables examined these differences are not negligible. This is something we expected since both theoretically and also as we demonstrated in section 1.5.3.4 of the sensitivity study of PART1, DNI is more sensitive to aerosol load. Thus the historical simulations present very similar bias patterns and overall behavior, however differences are seen. Small ones are detected regarding domain averages but on local level they can be more pronounced. For example in Middle Europe (ME) during summer HisAer has a 21% overestimation that drops to 12% in HisStatic.

Table 20: Direct normalized irradiance at the surface (DNI) relative bias (%) for the historical simulations against SARAH satellite dataset. For all seasons and all subregions including the EU region. Last three rows present the absolute relative bias (%), the bias and absolute bias (in W/m^2) for the EU region.

	DJF			MAM			JJA			SON		
%	HisNo	HisAeros	HisStatic	HisNo	HisAeros	HisStatic	HisNo	HisAeros	HisStatic	HisNo	HisAeros	HisStatic
BI	50	12	12	54	22	18	55	18	14	44	11	11
IP	11	-12	-11	16	-10	-9	29	-8	-8	14	-14	-16
FR	29	0	1	32	5	3	46	9	6	22	-8	-10
ME	35	3	2	49	10	7	71	21	12	54	8	3
SC	16	-18	-19	43	9	6	55	21	15	44	5	2
AL	51	19	20	45	12	7	54	9	6	35	-3	-5
MD	42	11	12	35	-1	-2	39	-6	-7	34	-7	-8
EA	7	-19	-20	53	7	4	82	24	19	49	-1	-3
EU	30	-2	-2	43	6	4	54	10	7	39	0	-2
Absolute bias % EU	39	20	20	43	11	9	54	18	15	39	9	9
Bias W/m^2 EU	25	2	2	68	7	4	116	17	11	45	-4	-5
Absolute bias W/m^2 EU	29	13	14	68	17	15	116	36	32	45	11	11

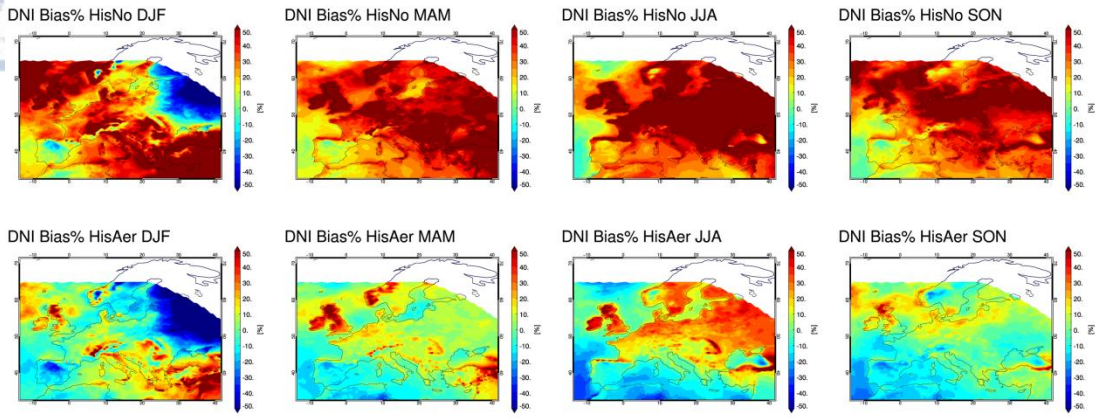

Fig. 43: Direct normalized irradiance at the surface (DNI) relative bias for the historical simulations, HisAer (top) and HisStatic (bottom). For all seasons.

2.8 Trend analysis-Historical simulations

In this section we present an analysis of the trends for all the variables examined in the evaluation (section 2.7) (Rsds, DNI, CFRACT, T, Precipitation) as well as for the time evolving aerosol optical depth of HisAer. We put emphasis on the trend analysis of shortwave radiation at the surface (Rsds) and temperature (T).

The linear fitting is performed with the Theil-Sen method (Theil, 1992; Sen, 1968) that is a non parametric method with resistance to outliers. Statistical significance of the trends is calculated with the non parametric Mann-Kendall test and is identified at the 95% level.

Analysis is performed on a yearly basis. In order to increase the robustness of the results, for shortwave radiation and temperature we also conduct the analysis using monthly mean values after deseasonalizing the time series. Deseasonalization of the monthly means is performed for each month by subtracting from the monthly mean values (time steps =12 x number of years) the mean value for the entire period of study of each respective month. The two different ways of analysis (yearly and monthly) produce in some cases some discrepancies in the intensity of the trends (slopes of the linear regression after being deduced at the same time frame). However the qualitative results are essentially the same, thus increasing the credibility of the conclusions. We primarily present the results of the analysis conducted on a yearly basis.

All variables are analyzed for the full period 1971-2000. However since the satellite data used to evaluate for Rsds, DNI and CFRACT cover only the 1983-2000 period, trend comparison between the satellite data and the historical runs is also performed for the same period regarding these variables.

In order to examine the impact of aerosol on the trends, firstly we examine the trend of the time evolving aerosol used for the HisAer simulation. We remind that the HisStatic

simulation uses an AOD field with monthly variations that present no year to year variability and thus no trend.

2.8.1 Summary

The use of realistic time evolving aerosol (with decreasing AOD over time) in a historical simulation leads to significant positive trends in shortwave radiation at the surface (Rsds) with direct normalized irradiance (DNI) being affected with even greater intensity. This effect on Rsds is in accordance with observational studies over Europe. The use of a static in time aerosol field fails to simulate the increasing shortwave radiation trend. We are confident that the decreasing aerosol optical depth is the cause of the shortwave radiation increasing trend and not a decrease in the cloud fraction amount over time. The positive shortwave radiation trend seen in HisAer leads to an intensification of the positive temperature trend in HisStatic, further enhancing the climate change signal. The use of the SARAH and CLARA satellite data for trend analysis is problematic.

2.8.2 Aerosol optical depth

Firstly we analyze the trends of the time evolving aerosol of the HisAer simulation.

Table 21 presents the slopes of the linear regression for two periods, 1983-2000 and 1971-2000 for all subdomains. The larger the magnitude of the slope (the absolute value) the greater the intensity of the trend is.

Table 21: Slope of the linear regression regarding aerosol optical depth for simulation HisAer. For periods 1983-2000 (top) and 1971-2000 (bottom). For all subdomains including the EU region. Negative trends are depicted with blue color cells while positive trends with orange color cells. Bold fonts are used to depict trends that are statistically significant at the 95% level.

1983-2000

	EU	BI	IP	FR	ME	SC	AL	MD	EA
HisAer	**-3,6**	**-1,7**	**-2,9**	**-3,6**	**-5,7**	**-3,8**	**-5,8**	**-3,9**	**-5,6**

1971-2000

	EU	BI	IP	FR	ME	SC	AL	MD	EA
HisAer	**-2,2**	**-1,2**	-1,0	**-2,3**	**-3,9**	**-2,1**	**-3,3**	**-2,2**	**-3,1**

x 10^{-3} /year

The negative trend of AOD is clear for both periods. It is characteristic that the trends are negative for all subdomains including the EU domain. Moreover all the trends are statistically significant with the only exception being the Iberian Peninsula during the greater 1971-2000 period.

Overall the trend during the 1983-2000 period is more negative than the one during the 1971-2000 period. This is the case not only for the EU domain but for all the subdomains as

well. This is to be expected since the decrease of AOD started in the mid 70s to early 80s, as seen in Fig. 36.

The steepest decrease for both periods is seen over Middle Europe (ME) and the Alps (AL).

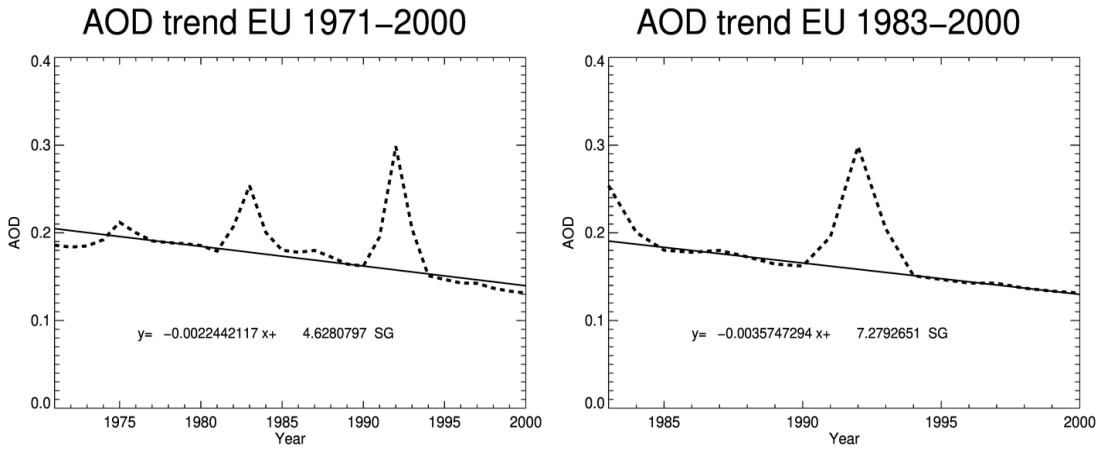

Fig. 44: Aerosol optical depth and linear regression line using the Theil-Sen method over the EU region. For the full period 1971-2000 (left) and period 1983-2000 (right).

2.8.3 Shortwave radiation at the surface

The overall period 1971-2000

Simulation HisStatic, with the static aerosol field, presents no specific trend in shortwave radiation at the surface (Rsds) (Table 22). On the other hand the use of time evolving aerosol in HisAer clearly leads to an increasing trend in Rsds. We have seen that shortwave down welling radiation at the surface is directly impacted by aerosol-radiation interactions (section 1.5.3.2). Aerosol introduction leads to Rsds decrease due to scattering and absorption. Smaller AOD levels mean less Rsds reduction. Thus the decreasing trend of AOD leads to an increasing trend in Rsds levels.

It is characteristic HisAer has clear positive trends for the EU region and all subdomains, with the trends being statistically significant for most cases (EU region and 6 out of 8 subdomains). HisStatic on the other hand does not have a single case with significant trend and the slope magnitudes are quite smaller. Finally, there seems to be a connection between the magnitude of the decreasing AOD trend and the magnitude of the increasing trend in radiation. For example Middle Europe (ME) and the Alps (AL) have at the same time the largest negative trend in AOD and the most positive trend in Rsds. The British Isles (BI) on the other hand have the smallest AOD negative trend and also a non significant negligible trend in shortwave radiation.

Period 1983-2000

In general, the overall picture for the 1983-2000 period is also very similar, for both HisAer and HisStatic. However, in HisAer the increasing trend over Europe has intensified doubling in magnitude (2.9 W/m^2 per decade), whereas intensification is seen for half of the

subregions as well. This is in accordance with the so called "brightening" effect seen over Europe. An increasing trend in Rsds has been widely observed over Europe from the mid 1980s (Norris and Wild, 2007) and has been named the brightening. This is a main result of this study: the use of realistic time evolving AOD in a historical simulation leads to an increasing trend in shortwave radiation at the surface and thus to the simulation of the brightening seen in this period by many observational studies. The use of static in time AOD field completely fails to simulate this observed brightening effect. We are confident that the significant increasing trend in Rsds seen in HisAer (and not in HisStatic) is not the result of a decreasing trend in cloudiness amount. This is because both HisAer and HisStatic have a very similar behavior regarding total cloud fraction tendency over time (section 2.8.5). Therefore we can attribute the simulated brightening effect to the decreasing aerosol load with more confidence. The RCM study of Nabat et al., (2014), also clearly indicated that only the use of transient aerosol reproduced the observed brightening while a static in time AOD field failed to do so. When using transient aerosol, this study produced an increase of 3.2 W/^{2} per decade over Europe for the period 1980-2009.

Observational studies

The brightening trend over Europe in our study is 2.9 W/m^2 per decade when transient aerosols are used in simulation HisAer. The observational study of Wild (2009) presents a similar decreasing trend of 3.3 W/m^2 per decade, using 133 stations over Europe for the period 1985-2005. Previously, Norris and Wild, (2007) had found a trend of 1.4 W/m^2 per decade over Europe for 1987-2002 using a smaller number of sites. Observational studies also indicate increase in the solar radiation over most of the subregions of Europe. For example over the Iberian Peninsula and positive 4 W/m^2 per decade increase has been observed for the period 1980-2000 (Sanchez-Lorenzo et al., 2007), a trend that is close to the one (3 W/m^2 per decade) seen in our study HisAer. Similarly in Scandinavia a trend around 1.6 to 2 W/m^2 per decade has been observed (Stjern et al., 2009; Wild, 2009), a value that also HisAer matches closely. Therefore, it is clear, that the introduction of transient aerosol in HisAer helps to simulate the brightening, and thus present a better match with observations, especially during the period 1983-2000.

Period 1983-2000 and comparison against satellite data

The brightening effect is present in the SARAH satellite dataset. However it is less extensive both spatially and in magnitude than the situation seen in HisAer. SARAH has positive Rsds trends for the EU region as well as for all the subregions. The trends are statistically significant for three subregions, Iberian Peninsula (IP), Scandinavia (SC) and Mediterranean (MD). For these three subregions the trend of HisAer is close to that of SARAH. In general, the trend sign and magnitude of HisAer is much closer to SARAH than that of HisStatic, which in essence presents no trend at all. This is the case for the EU domain and for 6 out of the 8 subregions.

Discussion about the SARAH satellite product

The problem is that we cannot truly rely on SARAH for trend analysis. On the one hand, it has been estimated that SARAH presents an uncertainty of 0.1 W/m^{2}year, that is considered

to be quite small for a satellite dataset (Müller et al., 2015). On the other hand SARAH, despite its accuracy, is a product of extensive modeling of the atmospheric processes including many assumptions and simplifications. In order to calculate shortwave radiation at the surface it assumes a slightly modified MACC aerosol optical depth climatology, that is static in time, in order to calculate the aerosol direct effect. Therefore it cannot account for the decreasing tendency of AOD observed, regarding aerosol-radiation interactions. Thus the increasing trend in Rsds seen in SARAH is not attributed to the decreasing aerosols and their interaction with radiation. However the decreasing AOD observed can have an impact on cloudiness through the indirect and semi-direct aerosol effects. SARAH takes clouds into account by using the variable of effective cloud albedo (CAL) to calculate Rsds amounts. The larger the CAL is, the more reflective the clouds are, leading to smaller shortwave radiation levels at the surface. Therefore it is possible that the increasing trend in Rsds seen is some subregions in the SARAH dataset is attributed to a decrease in the effective cloud albedo over time. We have calculated the trends of CAL for the period 1983-2000 for SARAH. The tendency of CAL change is positive for the EU regions and most subregions, something that could not explain the increasing Rsds tendency. However for two subregions, the Iberian Peninsula (IP) and the Mediterranean (MD), there is a statistically significant negative CAL trend. Moreover, these two subregions also present statistically significant Rsds increasing trends. Therefore we have an indication that for the subregions of IP and MD the decrease of CAL over time, possibly due to aerosol semi-direct and indirect effect, impacts Rsds levels and tendency. It seems that these two subregions are quite sensitive to semi-direct effect and aerosol-cloud interactions. To conclude, we content that the SARAH dataset cannot be used with credibility as a reference dataset for trend analysis in the context of this study. This is true not only for Rsds but for its direct normalized component (DNI) as well, as we will see in the following paragraph. The positive trends in shortwave radiation at the surface seen in several subregions cannot be attributed to the decreasing impact of aerosol direct effect. However for two subregions the Rsds increasing trend could be possibly linked to the semi-direct and indirect effects that are impacting the effective cloud albedo.

Table 22: Slope of the linear regression (W/m^2 year) regarding shortwave down welling radiation at the surface for the historical simulations (both periods) and the SARAH satellite dataset (1983-2000 only). For periods 1971-2000 (top) and 1983-2000 (bottom). For all subdomains including the EU region. Negative trends are depicted with blue color cells and positive trends with pale orange color cells. Bold fonts are used to depict trends that are statistically significant at the 95% level.

1971-2000

	EU	BI	IP	FR	ME	SC	AL	MD	EA
HisAeros	**0,14**	0,06	0,12	**0,13**	**0,29**	**0,12**	**0,22**	**0,16**	**0,13**
HisStatic	0,03	-0,05	0,07	0,00	0,09	0,02	0,12	0,07	0,01

1983-2000

	EU	BI	IP	FR	ME	SC	AL	MD	EA
HisAeros	**0,29**	0,02	**0,30**	0,05	0,26	0,21	**0,29**	**0,31**	0,22
HisStatic	0,05	-0,16	0,05	-0,24	-0,09	0,04	0,08	0,10	0,12
Sarah	0,15	0,03	**0,31**	0,05	0,17	**0,18**	0,04	**0,33**	0,04

Table 23: Slope of the linear regression regarding effective cloud albedo (CAL) (10^{-3}) for the SARAH satellite dataset (1983-2000 only). For all subdomains including the EU region. Negative trends are depicted with blue color cells and positive trends with pale pink color cells. Bold fonts are used to depict trends that are statistically significant at the 95% level.

1983-2000

	EU	BI	IP	FR	ME	SC	AL	MD	EA
Sarah	0,7	1,1	**-1,2**	0,8	0,8	**2,8**	0,7	**-1,6**	1,4

X10^{-3}

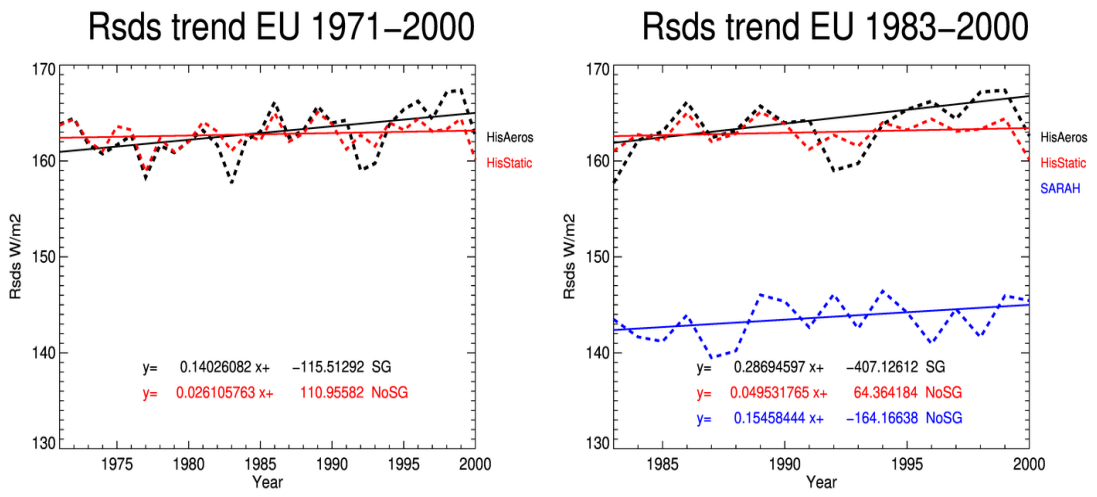

Fig. 45: Shortwave down welling radiation at the surface (Rsds) (dashed line) and linear regression line (solid line) using the Theil-Sen method over the EU region. For the full period 1971-2000 (left) and period 1983-2000 (right). For the historical simulations and SARAH satellite dataset (1983-2000 only). Black is used for HisAer, red for HisStatic and blue for SARAH.

2.8.4 Direct Normalized Irradiance

The impact of the time evolving aerosol used in HisAer is also evident in the direct normalized irradiance (DNI) and is even larger than that for Rsds. In HisAer, the decreasing AOD trend leads to a strong increasing trend in DNI. This is something we theoretically expected. DNI is intensely increased not only because of the overall Rsds increase, but also because the ratio of direct/diffuse radiation increases due to the decrease in aerosol optical depth and thus aerosol direct effect. We have seen in section 1.5.3.4 of the sensitivity study the strong impact that aerosol-radiation interactions have on DNI.

The overall period 1971-2000

There is a clear positive trend for HisAer. All the subregions including the EU region present increasing trends in DNI. The trend is significant for the EU region and for 6 out of 8 subregions. In most cases these trends are considerably larger (2-3 times) compared to those seen in Rsds. HisStatic on the other hand has also positive trends for most subregions but none is statistically significant and are of much smaller magnitude than those seen in HisAer. As was the case for Rsds, Middle Europe (ME) and the Alps (AL) have the most positive trend in DNI since they also present the largest negative trend in AOD. To conclude, the inclusion of time evolving aerosol in HisAer leads to a clear brightening in Rsds and an even more intense effect in DNI.

Period 1983-2000 and comparison against satellite data

In HisAer the trends of all subdomains become even more positive in the period 1983-2000 compared to the overall 1971-2000 period. This is in accordance with the intensification of the AOD negative trend seen in the period 1983-2000. HisStatic again does not present a specific trend tendency of statistical significance. Interestingly however the same is true for the SARAH satellite data set. For SARAH none of the subregions presents a statistically significant increasing trend in DNI whereas some even present decreasing tendencies. SARAH seems to miss completely the expected brightening in DNI. The lack of a time evolving decreasing AOD in the SARAH product seems to be even more problematic regarding trend analysis of the direct normalized irradiance.

Table 24: Slope of the linear regression (W/m^2 year) regarding direct normalized irradiance at the surface for the historical simulations (both periods) and the SARAH satellite dataset (1983-2000 only). For periods 1971-2000 (top) and 1983-2000 (bottom). For all subdomains including the EU region. Negative trends are depicted with blue color cells and positive trends with pale pink color cells. Bold fonts are used to depict trends that are statistically significant at the 95% level.

1971-2000

	EU	BI	IP	FR	ME	SC	AL	MD	EA
HisAeros	**0,55**	0,18	0,26	**0,48**	**0,95**	**0,58**	**0,98**	**0,71**	**0,72**
HisStatic	0,09	-0,08	0,10	-0,01	0,17	0,08	0,23	0,24	0,02

1983-2000

	EU	BI	IP	FR	ME	SC	AL	MD	EA
HisAeros	**1,35**	0,43	**1,28**	0,91	**1,43**	**1,65**	**1,81**	**1,65**	**1,59**
HisStatic	0,18	-0,12	0,14	-0,45	0,03	0,29	0,15	0,37	0,22
Sarah	0,04	0,17	0,40	-0,14	0,04	0,32	-0,61	0,29	-0,18

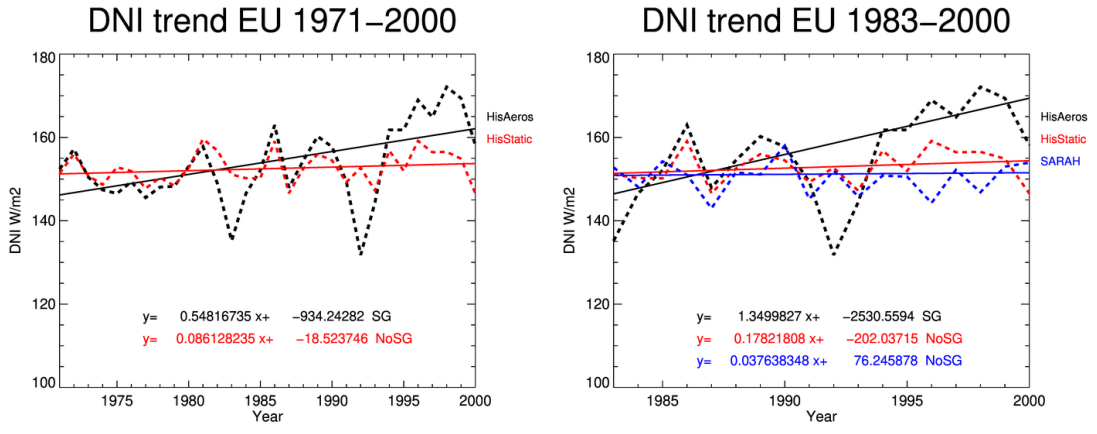

Fig. 46: Direct normalized irradiance at the surface (DNI) (dashed line) and linear regression line (solid line) using the Theil-Sen method over the EU region. For the full period 1971-2000 (left) and period 1983-2000 (right). For the historical simulations and SARAH satellite dataset (1983-2000 only). Black is used for HisAer, red for HisStatic and blue for SARAH.

2.8.5 Total cloud fraction

The overall period 1971-2000

Both historical simulations have a tendency of cloud fraction decrease over time for the EU region and most of the subregions. This is more widespread in HisStatic since only one subregion has an increasing tendency. However, for both simulations results are not statistically significant (only in ME for HisStatic). The slopes of linear regression (tendency magnitude) do not differ much between simulations for the subregions and are very close for the EU region. To better understand the tendency magnitude for the EU region, we have calculated that the decreasing linear regression leads to a -0.5% cloud fraction decrease per decade. The study of Bartók et al. (2017) found that the regional climate EURO-CORDEX simulations of 0.44^{o} resolution did not have a trend in cloud fraction over Europe for the period 1975-2005. The 0.11^{o} simulations however did present a decreasing trend in cloudiness, around -0.15% per decade. The global model simulations of CMIP5 presented a slightly larger decreasing trend, around -0.32% per decade.

Period 1983-2000 and comparison against satellite data

We use the CLARA satellite dataset as a reference. This dataset has been evaluated against observational data regarding the stability of its accuracy over time with satisfactory results that were better than the intended requirements (Karlsson et al., 2013). However the stability of the accuracy does not necessarily mean a good matchup of the cloud fraction tendencies over time. Moreover truly homogenous observational datasets suitable for trend analysis, regarding cloud amount, are hard to find. Therefore we use the CLARA dataset not as a solid reference dataset for trend analysis but only in order to get a general idea of its temporal behavior and tendencies. We want to identify whether this general behavior matches that of the historical runs and possibly detect any large deviations that could be of suspicious origins either in CLARA or in the historical runs.

Interestingly both historical simulations intensify their decreasing tendencies in cloud fraction compared to the 1971-2000 period, in the EU region and most subregions. However still the tendencies are not of statistical significance.

The CLARA dataset has a very similar behavior to the historical simulations. It is characteristic that both historical runs and CLARA have a decreasing tendency in EU and for the same 6 subregions whereas for the British Isles (BI) and France (FR) a positive increasing tendency is present. In most cases the tendency magnitude (slope of linear regression) is quite close for all datasets. The only trend of statistical significance is seen over the Alps (AL) in HisAer. Strong decreasing trends are seen in all datasets (historical and CLARA) in the Mediterranean (MD) and Eastern Europe (EA) subregions.

How does cloud fraction tendency impact shortwave radiation trends?

The fact that both historical simulations present a similar behavior regarding cloud fraction change over time is a very important result. A decreasing CFRACT tendency could potentially affect shortwave radiation (Rsds) tendency. For example the slightly positive Rsds tendency

seen in HisStatic could be the result of the negative cloud fraction tendency present. On the other hand the negative Rsds tendency seen in the British Isles (BI) could be connected with the positive tendency in CFRACT present in this subregion. However, we see that the cloud fraction tendency does not change in a specific direction in HisAer compared to HisStatic. Therefore we are confident that the significant increasing Rsds trends (the brightening effect) seen in HisAer (and not in HisStatic) are not due to the change in cloud fraction but can be attributed even more robustly to the decreasing aerosol optical depth over time.

Table 25: Slope of the linear regression (10^{-4} / year) regarding total cloud fraction (CFRACT) for the historical simulations (both periods) and the CLARA satellite dataset (1983-2000 only). For periods 1971-2000 (top) and 1983-2000 (bottom). For all subdomains including the EU region. Negative trends are depicted with blue color cells and positive trends with pale orange color cells. Bold fonts are used to depict trends that are statistically significant at the 95% level.

Total cloud fraction

1971-2000

	EU	BI	IP	FR	ME	SC	AL	MD	EA
HisAeros	-3,8	1,6	-0,7	4,0	-4,0	1,1	-6,0	-7,9	-5,3
HisStatic	-3,7	2,5	-2,4	-0,7	**-6,5**	-1,1	-7,9	-10,0	-3,8

1983-2000

	EU	BI	IP	FR	ME	SC	AL	MD	EA
HisAeros	-10,4	8,3	-15,2	9,3	-11,2	-9,7	**-8,4**	-13,3	-15,8
HisStatic	-9,7	4,7	-8,0	8,5	-12,8	-8,9	-7,8	-15,6	-15,9
Clara	-8,4	0,9	-15,8	1,2	-6,0	-15,5	-17,1	-18,9	-13,1

x10^{-4} /year

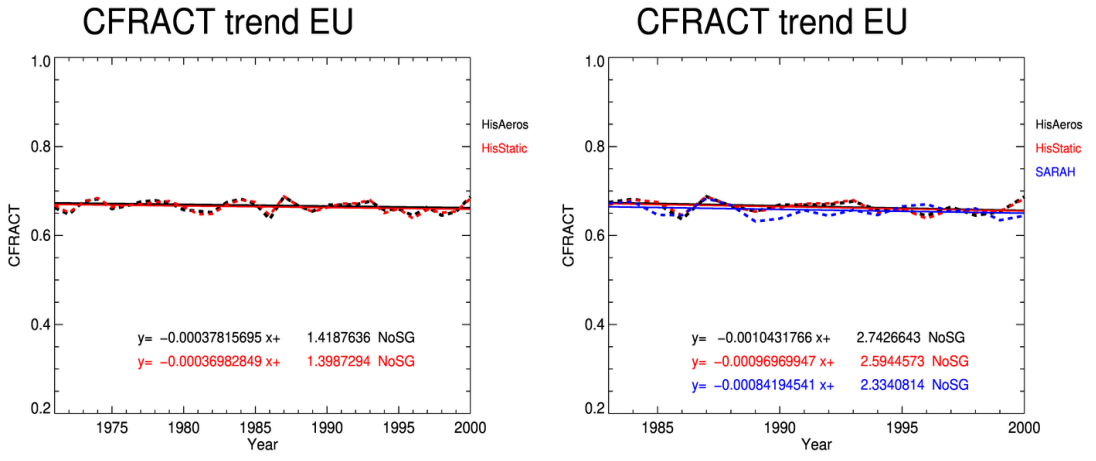

Fig. 47: total cloud fraction (CFRACT) (dashed line) and linear regression line (solid line) using the Theil-Sen method over the EU region. For the full period 1971-2000 (left) and period 1983-2000 (right). For the historical simulations and CLARA satellite dataset (1983-2000 only). Black is used for HisAer, red for HisStatic and blue for SARAH.

2.8.6 Temperature

We conduct the analysis only for the entire 1971-2000 period, since the E-OBS dataset, used as an observational dataset, covers this entire period completely. We also use a

homogenized version of the E-OBSv19 dataset. Since this is a homogenized dataset, we consider it a more robust observational dataset for trend analysis, but we also use the plain E-OBS dataset as an additional reference.

Temperature clearly presents increasing trends for all historical simulations as well as for the E-OBS observational dataset and its homogenized version. This is in accordance with the expected climate change signal. It is characteristic that temperature trends are in all cases positive, and in most cases statistically significant. The EU region has statistically significant temperature trends in the historical runs and in both E-OBS datasets. The same is true for most subregions (6 out of 8) in HisStatic and both E-OBS. However in HisAer the trends in all subregions are significant. Moreover, the homogenized E-OBS dataset has slightly larger trends in almost all subregions than the plain unhomogenized version.

It is evident that HisAer has a more intense positive temperature trend than HisStatic. In HisAer the intensity of the trend is higher for the EU region (0,034 ^{o}C/year than 0,028 ^{o}C/year) and for 6 out of the 8 subregions. In order to better understand the magnitude of the trend intensification we have calculated the temperature increase expected by each linear regression after a period of 30 years for the EU region. The warming is 1.02 ^{o}C for HisAer, 0.84 ^{o}C for HisStatic, 0.94 ^{o}C for E-OBS and 0.99 ^{o}C for the homogenized E-OBS. Calculated trends over Europe based on the CRU dataset for the period 1977-2001 present a similar picture, with the temperature change usually ranging between 0.75 ^{o}C and 1.5 ^{o}C after 30 years for the biggest part of the continent (Jones and Moberg, 2003).

We have already seen that the trends in Rsds become more positive in HisAer compared to HisStatic for the EU region and for all subregions. Therefore we have a strong indication that the increasing and significant trend in shortwave radiation at the surface (Rsds) seen in HisAer enhances the positive trend in temperature compared to HisStatic. Moreover it is characteristic that the more positive the trend in Rsds becomes in HisAer compared to HisStatic the more intensely the trend of temperature is enhanced in HisAer. Only two subregions (IP, SC) seem not increase their positive trends in temperature despite the intensification of the trend in shortwave radiation.

One of the major conclusions of this study is that the use of time evolving realistic aerosol in a historical simulation enhances the increasing trend of temperature and potential climate change signal. The intensification of temperature trend due to the use of transient aerosol has also been shown in the study of Nabat et al. (2014) for the period 1980-2012. In that study the simulation with transient aerosol presented a trend of 0,035 ^{o}C/year, quite close to the one seen in HisAer of our study for the 1971-2000 period.

Finally the trend magnitude (slope of linear regression) of HisAer is closer to that of E-OBS for the EU region and half (4) of the subregions. This does not provide a definitive conclusion, but it gives us the indication that the use of realistic time evolving aerosol in a historical simulation can improve trend matching with the E-OBS and especially the E-OBS homogenized observational dataset.

Table 26: Slope of the linear regression (10^{-2} °C/ year) regarding near surface temperature for the historical simulations, the E-OBSv19 observational dataset and the E-OBSv19 (EobsHOM-bottom row) homogenized observational dataset. For the period 1971-2000. For all subdomains including the EU region. Negative trends are depicted with blue color cells and positive trends with pale orange color cells. Bold fonts are used to depict trends that are statistically significant at the 95% level.

	EU	BI	IP	FR	ME	SC	AL	MD	EA
HisAeros	**3,4**	**2,6**	**3,2**	**4,9**	**5,0**	**3,5**	**4,4**	**2,7**	**3,9**
HisStatic	**2,8**	**2,2**	**3,3**	**3,9**	3,4	**3,6**	**3,7**	**2,6**	2,5
Eobs	**3,2**	**2,6**	**5,8**	**4,7**	**4,2**	3,5	**4,0**	**3,8**	2,6
EobsHOM	**3,3**	**2,7**	**6,1**	**5,0**	**4,4**	3,5	**4,5**	**3,7**	2,6

°C x10^{-2} /year

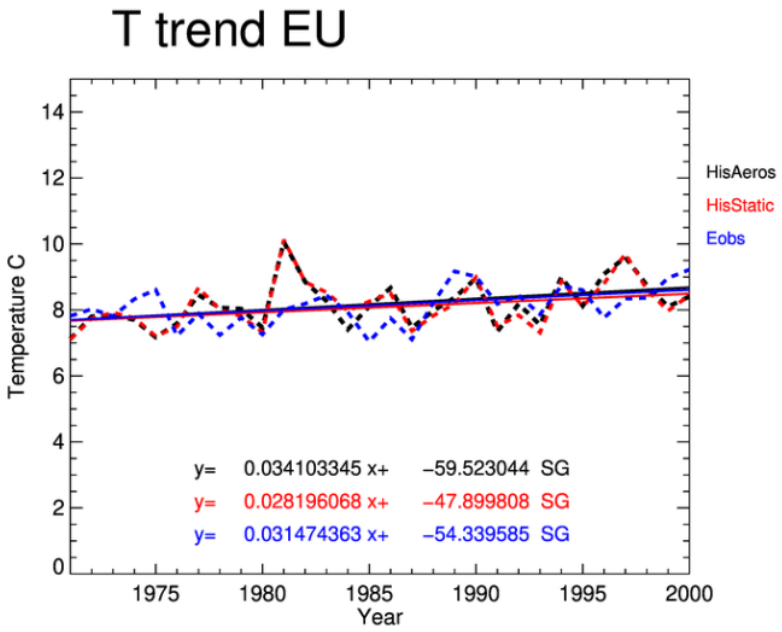

Fig. 48: Near surface temperature (T) (dashed line) and linear regression line (solid line) using the Theil-Sen method over the EU region and the period 1971-2000. For the historical simulations and E-OBS observational dataset. Black is used for HisAer, red for HisStatic and blue for E-OBS.

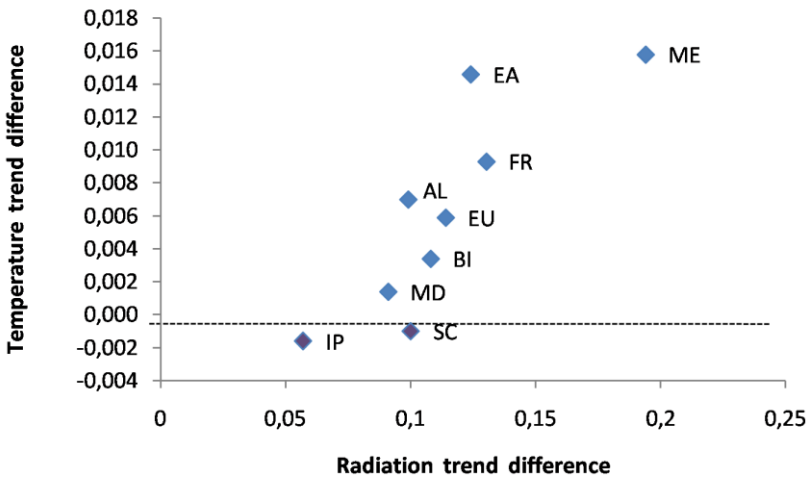

Fig. 49: Scatter plot of slope of linear regression difference between the historical simulations (HisAer-HisStatic) regarding the trends in shortwave radiation at the surface (Rsds - x axis) and near surface temperature (T - y axis). For the EU region and all subregions.

2.8.7 Precipitation

We conduct the analysis for the entire 1971-2000 period, since the E-OBS dataset covers this entire period completely.

Precipitation does not present a clear trend over time in the historical runs. We can say however that there is a tendency for precipitation reduction for both simulations. The EU region and most of the subregions have decreasing tendencies for both HisAer and HisStatic but only one subregion presents statistical significance in each simulation. Moreover the use of a realistic and decreasing aerosol optical depth dataset in HisAer does not impact the precipitation trend on a specific direction compared to HisStatic. The slopes of linear regression are quite close for both historical runs and do not differ systematically in HisAer compared to HisStatic.

The E-OBS observational dataset presents increasing and statistically significant trends for the EU region and two subregions. On the other hand two subregions (ME and MD) present significant decreasing trends of considerable intensity. In order to better grasp the magnitude of the trend: If we follow the linear regression calculated for the EU region, it leads to a 5% precipitation increase after a 30 year period. In comparison the historical runs lead to a -4% decrease in precipitation.

The Alps (AL) is a subregion where the two historical runs have their most intense decreasing trends (significant in HisAer) a situation that is not seen in the observational data that present a negligible positive tendency in this area. Similar behavior between the historical simulation and E-OBS is seen in the Iberian Peninsula (IP), Middle-Europe (ME) and the Mediterranean (MD), all subregions with large negative trends. However for the Mediterranean subregion the simulations fail to capture the considerably larger intensity of precipitation decrease seen over time in E-OBS. Moreover the simulations do not capture at all the very strong positive trend seen in the observations over the British Isles (BI). In

general no simulation has a considerably better matching with the E-OBS observational dataset.

Table 27: Slope of the linear regression (10^{-3}x(mm/day) / year) regarding precipitation for the historical simulations and the E-OBS observational dataset. For the period 1971-2000. For all subdomains including the EU region. Negative trends are depicted with blue color cells and positive trends with pale pink color cells. Bold fonts are used to depict trends that are statistically significant at the 95% level.

1971-2000

	EU	BI	IP	FR	ME	SC	AL	MD	EA
HisAeros	-2,3	-3,1	-8,7	4,4	-5,6	-2,7	**-12,2**	-3,5	0,3
HisStatic	-2,6	-1,0	-7,8	4,3	**-6,8**	-1,9	-10,3	-4,6	0,9
Eobs	**2,7**	**17,4**	-6,6	8,0	**-9,7**	**9,5**	0,1	**-12,5**	0,1

(mm/day)x 10^{-3} /year

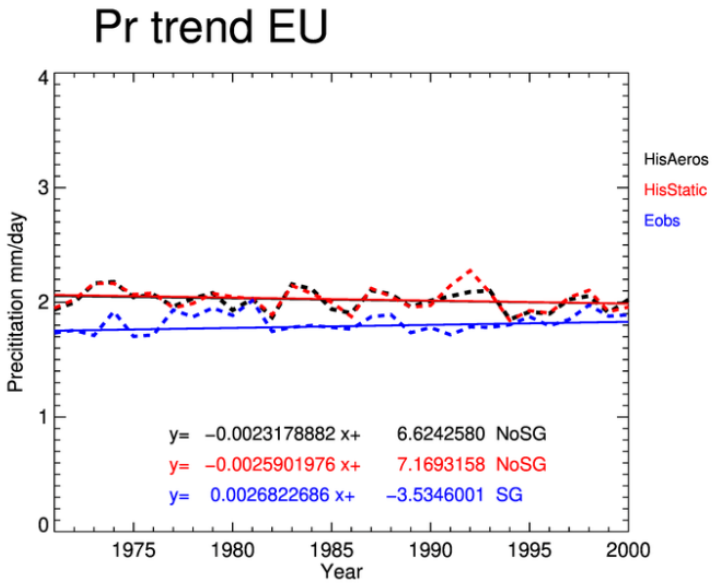

Fig. 50: Precipitation (Pr) (dashed line) and linear regression line (solid line) using the Theil-Sen method over the EU region and the period 1971-2000. For the historical simulations and E-OBS observational dataset. Black is used for HisAer, red for HisStatic and blue for E-OBS.

2.9 Aerosol impact- Historical

In this section we explore the aerosol-radiation interaction impact for the period 1971-2000 of the historical runs. We conduct an analysis similar to that of the sensitivity study in PART1 (section 1.5.3). Simulations HisAer (transient aerosol) and HisStatic (static in time aerosol) are compared to HisNo that has no aerosol effects at all. The use of 30 year period provides even more robust results compared to the sensitivity study (5 year period) and provides a

more credible report about the aerosol-radiation interaction impact on the European climate.

It must be reminded here, that simulations HisAer and HisStatic have the same mean aerosol optical depth over the 30year period. Results between them differ only slightly. Thus we only present plots for the HisAer-HisNo comparison, whereas results for the HisStatic-HisNo comparison are included in the tables of this section.

2.9.1 Summary

Qualitatively, aerosol-radiation interactions for the historical simulations have a similar impact to that seen in the sensitivity study of PART1. Shortwave radiation at the surface is decreased and this leads to a surface cooling. Cloud forcing again becomes less negative and partially constrains the radiation decrease at the surface. Changes in the general circulation are very small however in some cases, like autumn over the Black Sea and the Balkans, they can be persistent and have a small impact in cloudiness and precipitation. In general the impact is quite similar to the one seen in the sensitivity study of PART1, with the change in the cloud forcing being however slightly smaller in the historical simulations.

2.9.2 Clear-sky shortwave radiation

Clear-sky shortwave radiation at the surface (CRsds) is reduced over the entire domain throughout the year. The relative decrease is quite similar for all seasons with domain averaged values between -5 to -6%. At a subdomain level the decrease is also stable and ranges between -4 to -8%.

The direct radiative effect (DRE) of aerosol is calculated as the difference in net clear-sky shortwave radiation at the surface (netCSw) between an aerosol simulation and the HisNo experiment. The DRE is negative and domain averages range from -4 W/m^2 in winter to -17 W/m^2 in summer. The DRE is of statistical significance (0.05 level) almost over the entire domain for all seasons. Spatial correlation of the DRE with the aerosol optical depth field is negative as expected and quite high for all seasons with the correlation coefficient being -0.74 in winter, -0.87 in spring and highest in summer, -0.95, and autumn, -0.94.

The ratio of DRE per unit of AOD (W/m^2/AOD) is very similar to the one seen it the sensitivity simulations of PART1 that used the second aerosol-radiation option (aer_opt=2) and the "rural" aerosol type to parameterize single scattering albedo (Table 7). Thus, the decrease of clear-sky radiation per unit of AOD is -32W/m^2 in winter, -60W/m^2 in spring, -65W/m^2 in summer and -50W/m^2 on an annual basis.

2.9.3 All sky shortwave radiation

Shortwave radiation at the surface is also reduced almost over the entire domain. The relative decrease ranges between -4 to -6% regarding domain averages, slightly smaller than the one seen in clear-sky radiation. At subdomain level the relative decrease has a very similar range. The largest decrease in radiation is seen over Eastern Europe (EA) in autumn, and reaches -8%.

The radiative effect of aerosol (RE, difference in netRsds) is clearly negative and domain averages range between -4 W/m^2 in winter to -14 4 W/m^2 during summer. At subdomain level the largest RE is seen over the Mediterranean (MD) in summer, where large AOD values and large radiation amounts coexist. Statistical significance is present all over the domain in summer and most part of the domain for the rest seasons. Spatial correlation of the radiative effect with AOD is high but slightly smaller than that of the direct radiative effect. Correlation coefficient is lower in winter (-0.65), stronger in spring (-0.83) and summer (-0.86) and highest in autumn (-0.92).

2.9.4 Overall radiation budget

The overall radiation budget at the surface (net shortwave + net longwave) also decreases extensively over the domain and for all seasons (Table 29), after aerosol-radiation interactions are introduced in the historical simulations. Decrease ranges from -2W/m^2 in winter to -12W/m^2 in summer. However, the relative decrease is largest in winter (-30%) due to the small radiation amounts present in this season. For the rest seasons, a decrease around -7% is seen in spring and summer and around -15% in autumn. The largest decrease of the radiation budget (-19W/m^2) is seen in the Mediterranean (MD) during summer, where also the largest shortwave radiative effect (RE) is seen. However, the relative decrease is only around -9%, very similar to that of all other subregions during summer and spring.

Interestingly, the overall radiation budget decrease is slightly smaller that the decrease in net shortwave radiation at the surface (RE), as was the case in the sensitivity study of PART1. Therefore, the negative change in the net shortwave radiation is slightly constrained by a small increase (0.1 to 2 W/m^2) in the net longwave radiation at the surface.

2.9.5 Direct and diffuse radiation

Direct normalized irradiance decreases over the entire domain for all seasons with the decrease being of statistical significance. Domain averaged relative decrease is similar for all seasons, around -26 to 30% whereas comparable decrease (-20 to -35%) is seen for the different subdomains.

On the other hand diffuse radiation is increased extensively over the entire domain throughout the year. Differences are of statistical significance all over the domain whereas the domain averaged relative increase is smallest in winter (9%), increases in spring and autumn (22 to 25%) and becomes largest in summer (55%). The large discrepancies between seasons are connected to the fact that cloudiness amount, which affects diffuse radiation, is also quite different. Total cloud fraction is larger in winter (0.78) and lowest in summer (0.51). Thus in winter the extensive cloudiness increases diffuse radiation considerably by itself and the addition of aerosols does not have a dramatic impact. In summer on the other hand the smaller cloud fraction amount leaves a large part of the direct radiation to reach the surface and the addition of aerosol can heavily impact it and lead to a larger relative increase in diffuse radiation.

Table 28: Radiative effect (RE), direct radiative effect (DRE) and change in cloud forcing (ΔSCRE) (W/m^2) calculated as the difference from simulation HisNo. First two rows: Domain averaged differences for simulations HisAer and HisStatic. Bottom rows: Subdomain averaged differences for HisAer.

	RE				DRE				ΔSCRE			
EU domain	DJF	MAM	JJA	SON	DJF	MAM	JJA	SON	DJF	MAM	JJA	SON
HisAeros	-2,2	-8,7	-13,4	-5,7	-3,9	-12,0	-16,8	-7,5	1,7	3,3	3,4	1,8
HisStatic	-2,1	-8,8	-13,8	-5,9	-3,8	-12,0	-16,8	-7,9	1,7	3,2	3,0	2,0
HisAeros *Subdomain*												
BI	-1	-6	-11	-3	-3	-9	-14	-5	2	3	3	2
IP	-4	-9	-15	-7	-5	-12	-17	-9	2	3	2	2
FR	-2	-7	-13	-6	-5	-11	-16	-8	3	4	4	2
ME	-2	-9	-15	-6	-4	-11	-20	-8	2	3	6	2
SC	-1	-7	-9	-2	-2	-9	-14	-5	1	3	5	2
AL	-3	-8	-14	-7	-4	-12	-20	-9	2	5	6	2
MD	-5	-12	-20	-10	-6	-15	-21	-11	2	3	1	1
EA	-2	-10	-16	-7	-4	-13	-21	-9	2	3	4	1

Table 29: Change (W/m^2) and relative change (%) from simulation HisNo of the overall radiation budget at the surface (net shortwave + net longwave). First two rows: Domain averaged differences for simulations HisAer and HisStatic. Bottom rows: Subdomain averaged differences for HisAer.

	Overall radiation budget							
	difference (W/m^2)				relative difference (%)			
EU domain	DJF	MAM	JJA	SON	DJF	MAM	JJA	SON
HisAeros	-2,1	-7,8	-11,8	-4,4	-34	-8	-7	-14
HisStatic	-2,0	-7,9	-12,1	-4,6	-32	-8	-7	-15
HisAeros *Subdomain*								
BI	-2	-6	-9	-3	-8	-6	-6	-21
IP	-3	-8	-14	-6	-13	-6	-7	-9
FR	-2	-7	-11	-5	-100	-6	-6	-12
ME	-2	-8	-13	-4	-18	-7	-8	-17
SC	-1	-6	-8	-2	-2	-8	-6	-1900
AL	-3	-7	-13	-6	-63	-7	-8	-13
MD	-4	-12	-19	-9	-25	-8	-9	-13
EA	-2	-8	-13	-4	-55	-8	-9	-14

Table 30: Relative difference (%) from simulation HisNo for shortwave radiation at the surface (Rsds), direct normalized irradiance (DNI) and diffuse radiation (DIF). First two rows: Domain averaged differences for simulations HisAer and HisStatic. Bottom rows: Subdomain averaged differences for HisAer.

	Rsds				DNI				DIF			
EU domain	DJF	MAM	JJA	SON	DJF	MAM	JJA	SON	DJF	MAM	JJA	SON
HisAeros	-4,0	-4,8	-5,5	-5,8	-26,1	-26,1	-29,1	-28,8	9,1	21,8	55,7	25,1
HisStatic	-4,1	-4,9	-5,7	-5,9	-26,7	-26,6	-29,6	-29,1	9,2	22,2	56,3	25,4
HisAeros *Subdomain*												
BI	-4	-4	-5	-4	-24	-21	-26	-23	7	12	16	12
IP	-4	-4	-6	-5	-19	-22	-29	-25	17	26	67	29
FR	-4	-4	-5	-6	-22	-23	-28	-27	10	19	35	21
ME	-5	-5	-6	-7	-25	-28	-34	-32	7	21	38	21
SC	-4	-5	-4	-5	-31	-25	-25	-27	3	12	19	10
AL	-3	-4	-6	-6	-19	-24	-31	-30	12	22	54	30
MD	-4	-5	-7	-7	-21	-27	-33	-31	21	38	119	51
EA	-3	-6	-7	-8	-24	-30	-35	-35	6	24	65	29

2.9.6 Cloud fraction

Cloud fraction is not strongly changed by the implementation of aerosol-radiation interactions. Domain averaged differences are small and less than 0.007 (scale 0 to 1). These small number are not due to compensation between positive and negative differences seen over the domain since the mean absolute difference is also quite small and ranges between 0.04 and 0.09. The largest absolute differences are seen in summer (0.08) and autumn (0.09). The relative difference is also small and is largest in autumn at around 1%. At subdomain level differences rarely exceed 1%. Some exceptions are the mountainous region of the Alps in summer (-2.5%) and autumn (+2%) and the Mediterranean subregion (MD) in autumn (+3%). In general no specific direction of cloud fraction change is observed except for autumn where a cloudiness amount increase is seen (domain average 0.07 and 1%) for almost all subdomains. Significant changes are spatially very limited. The only case of extensive statistically significant changes at the 0.05 level is seen also in autumn over part of the Balkans and the Mediterranean subregion and also north of the Black Sea. Other studies over Europe have shown cloud fraction reduction (Nabat et al., 2015a).

Table 31: Total cloud fraction (CFRACT) difference (left columns), absolute difference (middle columns) and relative difference (%) (right columns) from simulation HisNo. First two rows: Domain averaged differences for simulations HisAer and HisStatic. Bottom rows: Subdomain averaged differences for HisAer.

	CFRACT difference (mm/day)				CFRACT absolute difference (mm/day)				CFRACT relative difference (%)			
EU domain	DJF	MAM	JJA	SON	DJF	MAM	JJA	SON	DJF	MAM	JJA	SON
HisAeros	0,0	0	0,001	0,007	0,004	0,005	0,008	0,009	0,1	0,0	0,3	1,3
HisStatic	0,0	0,002	0,001	0,005	0,003	0,006	0,008	0,007	0,0	0,2	-0,2	0,9
HisAeros *Subdomain*												
BI	-0,002	0	0,009	0,002	0,004	0,004	0,009	0,004	-0,3	-0,1	1,2	0,2
IP	0,003	0,003	0,003	0,002	0,005	0,004	0,006	0,006	0,6	0,4	1,0	0,4
FR	-0,006	-0,002	-0,006	0,004	0,006	0,005	0,008	0,007	-0,7	-0,3	-1,2	0,6
ME	-0,002	0	-0,008	0	0,003	0,006	0,011	0,005	-0,3	0,0	-1,3	0,0
SC	-0,001	-0,001	0	0,001	0,002	0,005	0,007	0,004	-0,1	-0,2	0,0	0,2
AL	-0,004	-0,005	-0,013	0,013	0,005	0,006	0,013	0,014	-0,5	-0,7	-2,4	2,1
MD	0,004	0,001	0,001	0,017	0,006	0,005	0,006	0,017	0,7	0,2	0,7	3,7
EA	-0,004	-0,002	-0,004	0,008	0,005	0,005	0,008	0,009	-0,5	-0,3	-1,1	1,4

2.9.7 Cloud forcing

Interestingly the cloud forcing becomes less negative (positive ΔSCRE) thus clouds allow more shortwave radiation to reach the surface. This was also the case in the sensitivity study of PART1. In the historical simulations the positive increase in the cloud forcing is slightly smaller than the one seen in the sensitivity study. Domain averaged values range between 1.7 (winter) and 3 W/m^2 (summer and spring) whereas the positive increase in the cloud forcing is so extensive that is seen all over the domain and for all seasons.

The positive change in the cloud forcing helps to constrain the reduction of shortwave radiation at the surface due to the direct aerosol effect and therefore decreases the magnitude of the overall radiative effect (RE) of aerosols. The fact that cloudiness seems to act in a way that reduces the direct aerosol effect is a major conclusion of this study. The fact that it is encountered in all sensitivity simulations having only aerosol-radiation interactions (ARI group) and, as seen here, also in the longer (30 year) historical simulations increases confidence on this result.

The positive change in cloud forcing (ΔSCRE) is considerable and can substantially counter the direct aerosol effect (DRE). The ΔSCRE is especially important in winter where it amounts for 44% of the DRE value. For the rest seasons it has still substantial impact being up to 27% of DRE in spring, 20% in summer and 24% in autumn.

The change in the cloud forcing seems to have a very weak negative spatial correlation with the AOD field for spring (-0.12), summer (-0.25) and autumn (-0.3). For winter however a positive and a slightly stronger correlation is seen (0.40) indicating a weak tendency of positive cloud forcing forming over areas with large AOD values.

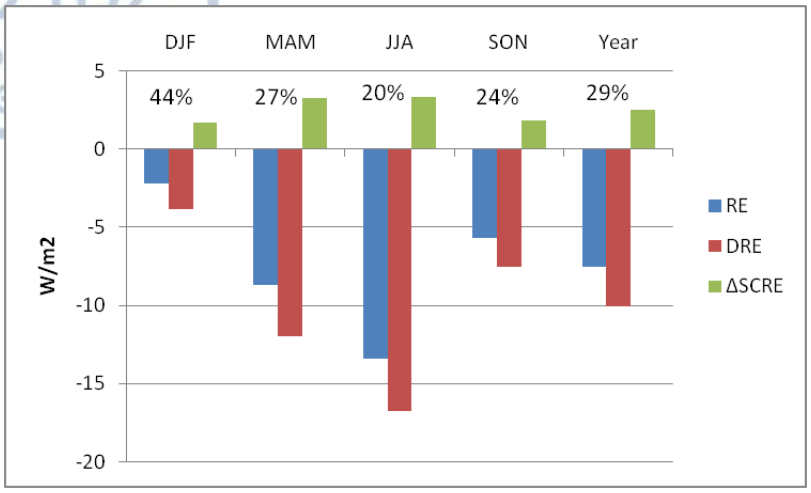

Fig. 51: Domain averaged radiative effect (RE), direct radiative effect (DRE) and difference in cloud forcing (ΔSCRE) for simulation HisAer, calculated against simulation HisNo. The percentages in black fonts indicate the % ratio of ΔSCRE/DRE.

2.9.8 Temperature

Temperature is decreased due to the overall decrease in shortwave radiation at the surface (Rsds). This cooling is seen for all seasons and over most part of the domain. Domain averaged decrease is 0.1°C in winter and between 0.2 and 0.25°C for the rest seasons. If only points over land are considered the cooling is slightly larger, 0.14°C for winter and between 0.32 and 0.38°C for the rest seasons. This is to be expected since sea surface temperature is prescribed in the simulations. At subdomain level the largest cooling is seen in Eastern Europe having an average of -0.6 °C for all seasons except winter. Indeed the strongest cooling is seen over the Balkans, Eastern Europe and north of the Black Sea throughout the year except winter, with a decrease of up to 1 °C seen at grid point level. For the above areas and seasons the cooling also presents statistical significance.

If both land and sea points are considered, spatial correlation of temperature change with the radiative effect is positive as expected but poor, with coefficients ranging between 0.15 to 0.30 depending on season. However if only land points are taken into account the spatial correlation is considerably higher and correlation coefficient is 0.71 to 0.73 for all seasons except autumn where it becomes 0.52.

For spring and autumn the maximum of cooling is spatially very close to the radiative effect maximum which in turn is collocated with the AOD maximum over continental Europe that lies over the Balkans, Black Sea and Eastern Europe for both seasons. In summer however the maximum of temperature decrease is also over the Balkans and north of the Black Sea despite the fact that the AOD maximum is moved to the west towards central Europe. This happens because the radiative effect remains largest over the Balkans, Eastern Europe and the Black Sea. Over central Europe a considerable positive change in the cloud forcing (+6W/m^2 for Middle Europe domain, ME) constrains the overall shortwave radiation decrease and consequently the induced cooling.

Table 32: Temperature difference (°C) from HisNo over both sea and land points (left side) and over only land points (right side). First two rows: Domain averaged changes for simulations HisAer and HisStatic. Bottom rows: Subdomain averaged differences for HisAer.

	T				T land only			
EU domain	DJF	MAM	JJA	SON	DJF	MAM	JJA	SON
HisAeros	-0,1	-0,2	-0,3	-0,2	-0,1	-0,3	-0,4	-0,3
HisStatic	0,0	-0,3	-0,3	-0,2	-0,1	-0,4	-0,5	-0,4
HisAeros *Subdomain*								
BI	-0,1	-0,1	0,0	-0,1	-0,1	-0,2	-0,1	-0,2
IP	-0,1	-0,1	-0,2	-0,2	-0,2	-0,2	-0,2	-0,3
FR	-0,1	-0,2	-0,1	-0,2	-0,2	-0,3	-0,2	-0,3
ME	-0,2	-0,3	-0,2	-0,4	-0,2	-0,4	-0,3	-0,4
SC	0,0	-0,1	-0,2	-0,2	-0,1	-0,2	-0,2	-0,2
AL	-0,2	-0,3	-0,2	-0,3	-0,2	-0,3	-0,2	-0,3
MD	-0,1	-0,1	-0,2	-0,1	-0,2	-0,3	-0,5	-0,2
EA	-0,2	-0,5	-0,6	-0,5	-0,2	-0,6	-0,6	-0,6

2.9.9 Precipitation

Precipitation is not considerably affected by the introduction of aerosol-radiation interactions. In winter and spring domain averaged relative change is very small, less than 1% and no specific direction of precipitation change is detected. A larger impact is seen in summer where both HisAer and HisStatic present a domain averaged decrease (-3.5% and -2.7% respectively) that is also present in almost all subdomains. The decrease is mild but is of statistical significance over a large area covering central Europe and parts of North Eastern Europe and the Balkans. On the other hand, in autumn both historical simulations present a general increase in precipitation (2.4% and 1.5%) that can also be seen in most subdomain averages. The largest increase is seen over the subdomain of Eastern Europe (EA) (6.5% in HisAer). This is part of the wider area including the Balkans and a region over the Black Sea that exhibit a mild precipitation increase that is of statistical significance over several grip points. In all cases however, statistically significant cases cover only a fraction of the overall domain. The sensitivity simulations of PART1 present a similar general behavior with a decrease in summer and an increase during autumn.

Interestingly if we consider the absolute difference from HisNo in mm/day we see that the domain averaged change in precipitation is not very dissimilar for the different seasons. It is 0.06 mm/day in winter, 0.08 in spring and 0.09 in summer and autumn. Other studies over Europe have shown a However only in summer (decrease) and (autumn) the change presents a more clear direction with precipitation reduction. In contrast, the RCM study of Schultze and Rockel (2018) that covered 60 years over Europe presented precipitation reduction throughout the year. In general the spatial field of precipitation changes is somewhat patchy, with small blocks of similar magnitude changes scattered over the domain. However it is considerably less patchy than the field of precipitation changes seen in the sensitivity study of PART1. Those simulations covered a much smaller period of 5 years. Thus it seems that the patchy differences seen in the sensitivities where indeed

mainly due to internal model variability. This internal variability when averaged for considerably larger periods of time, as is the case with the historical simulations, is considerably smoothened.

Table 33: Precipitation difference (mm/day) (left columns), absolute difference (mm/day) (middle columns) and relative difference (%) (right columns) from simulation HisNo. First two rows: Domain averaged differences for simulations HisAer and HisStatic. Bottom rows: Subdomain averaged differences for HisAer.

	Pr difference (mm/day)				Pr absolute difference (mm/day)				Pr relative difference (%)			
EU domain	DJF	MAM	JJA	SON	DJF	MAM	JJA	SON	DJF	MAM	JJA	SON
HisAeros	0,02	-0,01	-0,06	0,04	0,06	0,08	0,09	0,09	0,6	-0,7	-3,6	2,4
HisStatic	0,01	0,01	-0,04	0,02	0,06	0,08	0,09	0,1	0,0	0,6	-2,7	1,5
HisAeros *Subdomain*												
BI	0	0,03	-0,04	0,03	0,05	0,05	0,06	0,06	-0,1	1,7	-1,7	1,3
IP	0	-0,05	-0,06	0,03	0,05	0,09	0,06	0,08	0,6	-2,3	-8,3	1,9
FR	-0,01	-0,05	-0,11	0,06	0,05	0,06	0,12	0,09	-0,8	-1,9	-5,7	2,7
ME	0,01	0	-0,15	0,02	0,03	0,05	0,17	0,06	0,7	0,3	-7,3	0,6
SC	0,05	0,02	-0,09	-0,02	0,06	0,07	0,12	0,08	1,6	0,2	-4,0	-0,2
AL	-0,07	-0,04	-0,16	-0,06	0,12	0,09	0,18	0,2	-3,0	-1,3	-5,4	-1,8
MD	0,02	0	-0,01	0,05	0,08	0,08	0,04	0,13	1,2	0,9	1,6	2,0
EA	-0,03	-0,05	-0,08	0,1	0,05	0,1	0,14	0,11	-2,1	-2,0	-3,7	6,5

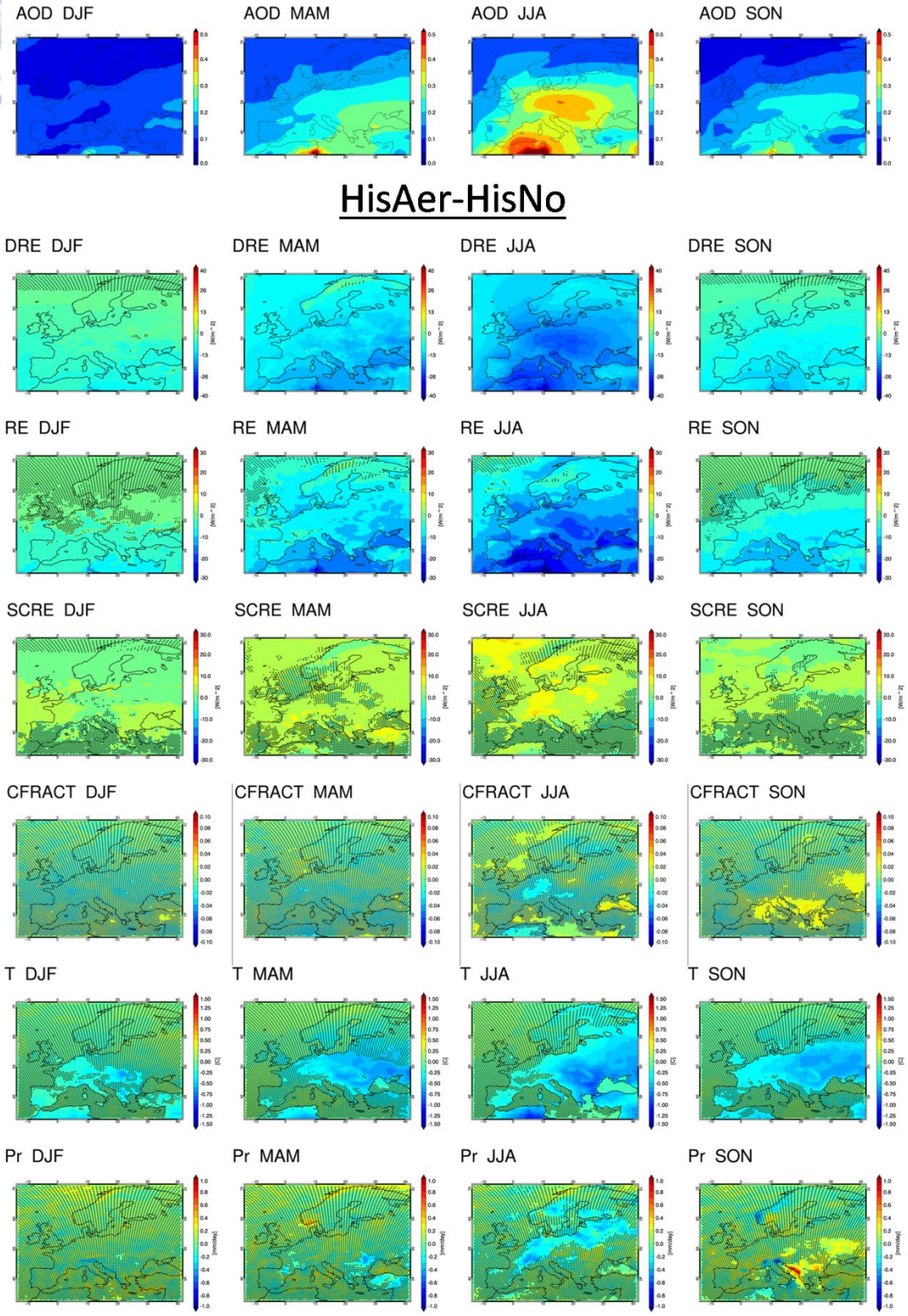

Fig. 52: Top row: Mean seasonal aerosol optical depth at 550nm of the historical period (the same for HisAer and HisStatic). From second row and on: Difference between simulations HisAer and HisNo regarding net CRsds at the surface (DRE, direct radiative effect), net Rsds at the surface (RE, radiative effect), cloud forcing at the surface (SCRE), total cloud fraction (CFRACT), temperature (T) and precipitation (Pr). Stippling indicates the areas where the differences are NOT significant at the 0.05 level with the Mann-Whitney test.

2.9.10 Wind field

The general circulation on a seasonal basis is almost identical for all historical simulations, either with aerosol-radiation interactions (HisAer, HisStatic) or without any aerosol treatment (HisNo). This is the case for both wind direction and wind speed and also for all the pressure levels examined at 850hPa, 700hPa, 500hPa and 300hPa. Thus the introduction of aerosol does not change the general behavior of the circulation.

However if we compare the aerosol including simulations against HisNo some distinct wind anomalies created after the introduction of aerosol-radiation interactions can be identified. Fig. 54 depicts the wind direction and speed change with arrows and the meridional (v) wind component speed change with colors. In autumn and in simulation HisAer, a cyclonic wind anomaly covers most part of Europe with its center over Eastern Europe and seen at the 850hPa. It becomes more clearly formed and the v-wind speed change stronger as we move towards the upper levels, and is present at the 300hPa level. The center of the anomaly is very close to the maximum cooling seen at the near surface temperature. Moreover a small but statistically significant cloud fraction and precipitation increase is seen over the Balkans and north of the Black Sea indicating a possible connection to the circulation change. A very similar cyclonic anomaly in autumn was also encountered in the same region in the sensitivity simulations of PART1. Interestingly in HisStatic, this anomaly also exists, but it is weaker and its center shifted towards western Europe and thus not collocated with the maximum of cooling. The cyclonic anomalies during autumn in both HisAer and HisStatic are collocated with a decrease in geopotential height at all pressure levels examined, indicating a clear tendency to circulation change.

Another cyclonic anomaly is seen in HisStatic during spring, at that too is stronger and more well formed at the upper pressure levels. However this is almost nonexistent in simulation HisAer. On the other hand an anticyclonic anomaly over south Scandinavia in HisAer (mainly at the upper levels) during summer is not present in HisStatic. Despite the two simulations having the same mean aerosol optical depth we see that anomalies in the wind circulation from HisNo can have differences. This indicates a considerable sensitivity of the changes in the wind field. It must be reminded again however that the mean seasonal circulation pattern is almost identical in the historical simulations. Therefore the circulation anomalies fail to considerable impact the circulation pattern. Finally the only anomaly that can be connected to some impact of cloudiness and precipitation is the cyclonic one seen in autumn.

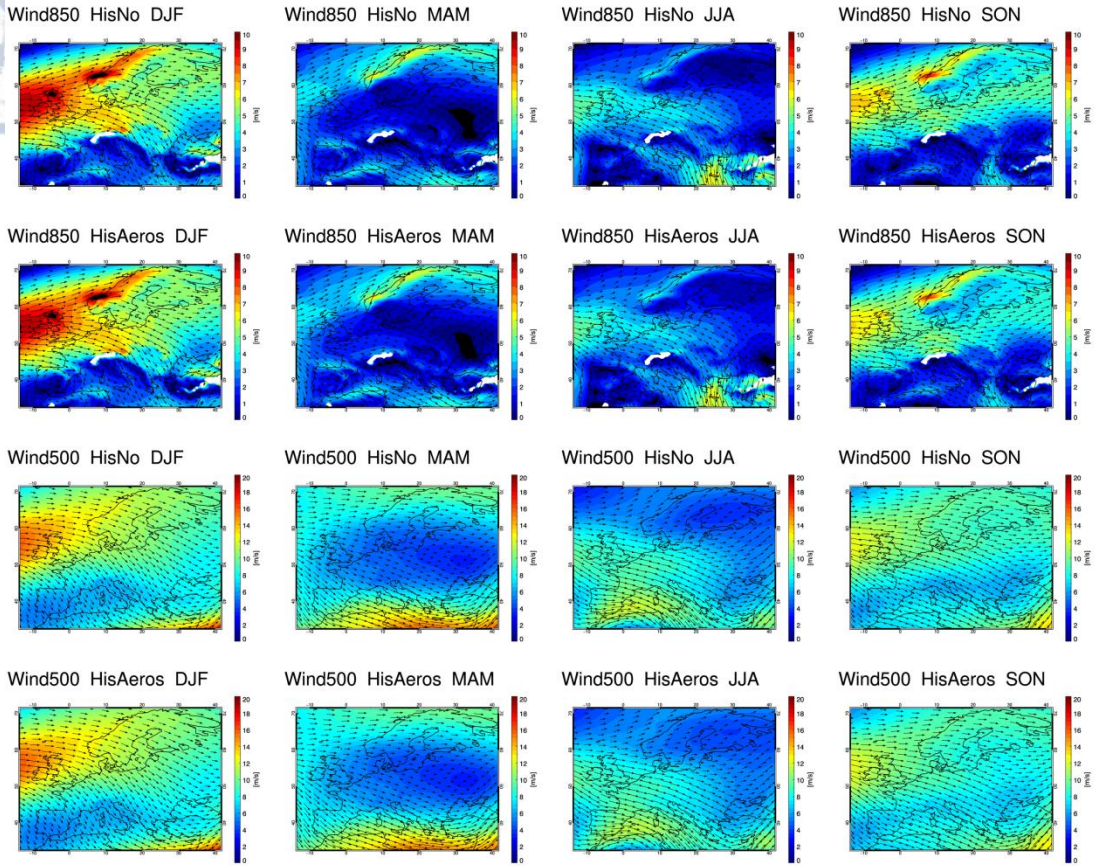

Fig. 53: Wind field (arrows) and wind speed (colors) for simulations HisNo and HisAer. For the 850hPa pressure level (first two rows) and the 500hPa pressure level (bottom two rows). For all seasons.

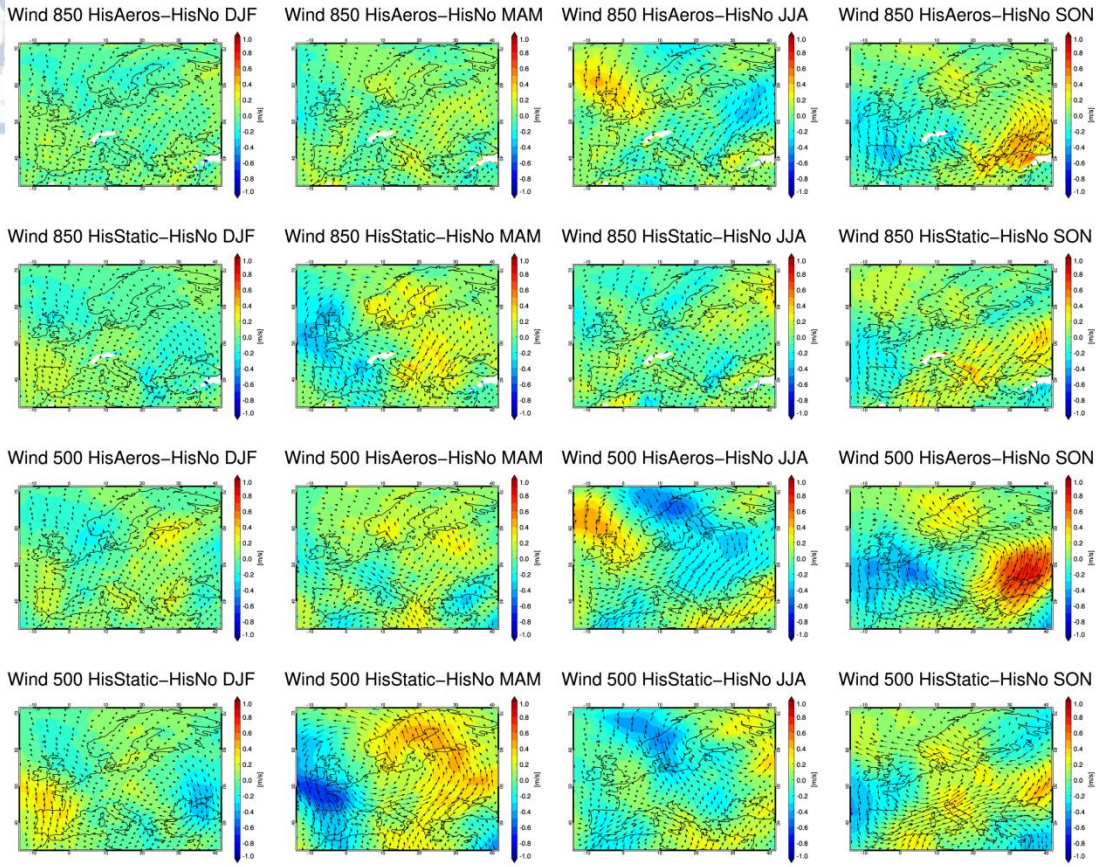

Fig. 54: Difference from HisNo regarding the wind field (arrows) and the magnitude of the meridional (v) wind component (colors) for simulations HisAer and HisStatic. For the 850hPa pressure level (first two rows) and the 500hPa pressure level (bottom two rows). For all seasons.

2.10 Rcp8.5 Future scenarios

In this section we present an analysis of the simulations RcpAer and RcpStatic for the future period 2021-2050. Aim is to detect the changes compared to the historical period and also detect the differences between the future simulations since they implement different aerosol datasets. First we present a comparison against the simulated historical period, 1971-2000, regarding the mean values of the period and the distribution of the mean daily values. We use simulation HisAer as a reference for the historical period because it is the most physically consistent simulation since it implements realistic aerosol optical depth that decreases with time. Then we present the trends detected in the future projections and again present comparison against those seen in HisAer.

2.10.1 Aerosol Optical Depth

We have already seen (Table 15) that simulation RcpStatic uses the same mean AOD with the historical simulation HisAer. On the other hand RcpAer uses a time evolving aerosol field that has smaller AOD than the historical period and consequently is smaller than RcpStatic

for the entire future period. This AOD decrease in RcpAer is large and extends over the entire European continent (Fig. 55). Compared to HisAer the maximum of AOD decrease is seen over central and eastern Europe and is largest in summer where it can even exceed 0.3. Besides the smaller AOD, the aerosols of RcpAer have a decreasing tendency over time that is of statistical significance. On a seasonal basis the AOD decrease is larger in autumn and summer and smaller in winter (Table 34). However the overall decrease of AOD over time in RcpAer is considerably weaker than that seen in HisAer (-0.7x10^{-3}/year compared to 2.2 x10^{-3}/year) during the historical period.

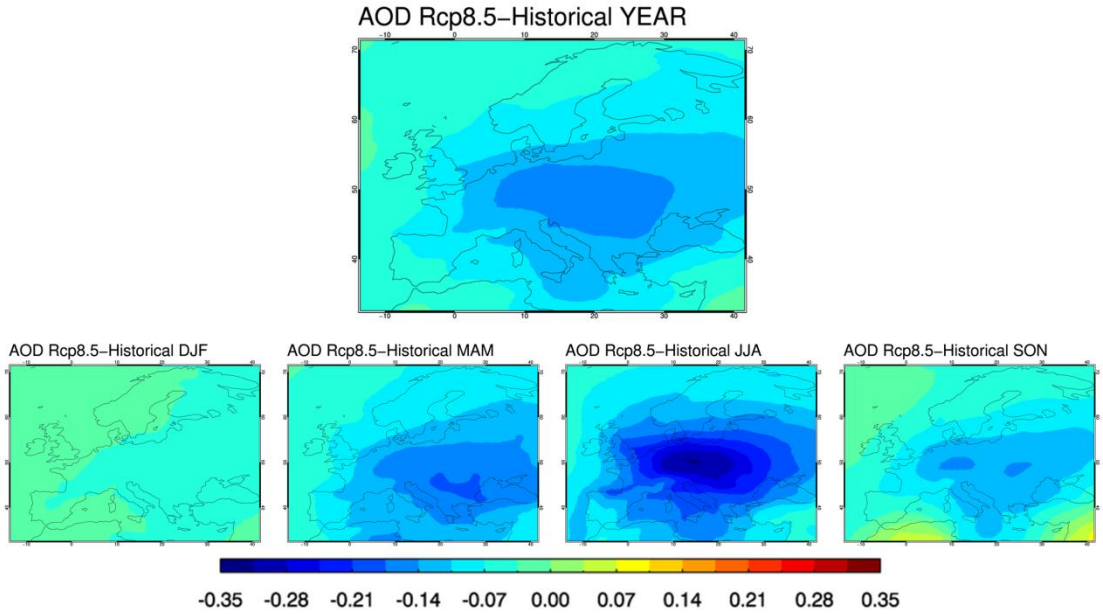

Fig. 55: Aerosol optical depth difference between simulation RcpAer of the future period 2021-2050 and simulation HisAer of the historical period 1971-2000. For the entire year (top) and the various seasons (bottom).

Table 34: Slope of the linear regression (10^{-3} /year) regarding aerosol optical depth for simulation RcpAer over the EU region. For period 2021-2050. Negative trends are depicted with blue color cells and positive trends with pale pink color cells. Bold fonts are used to depict trends that are statistically significant at the 95% level.

	AOD				
RcpAer	Year	Winter	Spring	Summer	Autumn
2021-2050	**-0,73**	-0,3	-0,76	-0,87	-0,95

2.10.2 Shortwave radiation at the surface

Simulation RcpAer clearly presents larger shortwave radiation amounts at the surface compared to the historical period (HisAer). The lower aerosol optical depth used in RcpAer leads to an Rsds increase around 4W/m^2 (3%) on average over the EU region (Table 35) while this decrease is of statistical significance over the biggest part of the domain (Fig. 56). On a seasonal basis the Rsds change in winter is negligible whereas the largest relative increase is seen in summer (3.5%) and autumn (3%). Only for summer however the Rsds change is statistically significant over an extended area. Moreover the maximum of Rsds

increase in summer and autumn lies over central Europe and the Balkans and spatially is quite close to the AOD maximum something that is not the case for spring.

On the other hand, simulation RcpStatic does not have any meaningful differences from the historical period. A very small decrease (-0.6%) is detected on average. The aerosol of RcpStatic have the same mean AOD with the aerosol used in HisAer, thus Rsds levels are not impacted. This is further proof that the lower AOD in RcpAer is the reason for the detected radiation decrease.

We have also calculated the effect of clouds in radiation (SCRE) and how much it differs in the future compared to the historical period (Fig. 57). Since clouds reduce radiation at the surface their effect is negative. Thus a negative difference between the future and the historical period means an increase in the effect of clouds that in turn could lead to a decrease in radiation at the surface and vice versa. We see that SCRE changes are not usually significant. There are however several interesting cases. In spring the large increase in shortwave radiation over south Europe, the Mediterranean sea and North Africa is partially attributed to the significant decrease in the radiative effect of clouds that works along with the decrease in aerosol optical depth. Oppositely an increase in the effect of clouds over central Europe leads to the overall decrease of shortwave radiation overpowering the decrease of aerosol. Finally in summer a small significant increase in the cloud effect is seen over central Europe. Its effect however is totally negated by the large decrease in AOD seen in this season and area that leads to the intense radiation increase at the surface. This further highlights the impact of AOD decrease during summer.

Table 35: Shortwave radiation at the surface (Rsds) mean difference (W/m^2) between simulations for the future period 2021-2050 (RcpAer, RcpStatic) and simulation HisAer for the historical 1971-2000 period. Mean annual differences (first column) and seasonal differences for all subregions including the EU region. Last row presents the relative difference (%) for the EU region.

	Year		DJF		MAM		JJA		SON	
	RcpAer	RcpStatic	RcpAer	RcpStatic	RcpAer	RcpStatic	RcpAer	RcpStatic	RcpAer	RcpStatic
BI	2,0	-1,9	0,5	0,5	0,1	-4,2	5,7	-3,3	1,5	-0,6
IP	4,8	1,2	0,4	-1,1	10,2	6,4	8,3	1,5	0,4	-2,1
FR	5,3	-0,2	0,1	-1,2	4,7	-0,8	10,6	-0,5	5,6	1,6
ME	5,0	-2,4	0,6	-0,1	-0,2	-6,7	12,7	-4,3	7,0	1,7
SC	2,8	-1,1	0,0	-0,2	0,5	-3,8	8,7	-0,8	1,9	0,4
AL	4,6	-1,4	-1,0	-2,2	1,6	-3,5	12,3	0,5	5,5	-0,2
MD	6,6	0,6	0,5	-1,4	9,4	3,7	11,1	-0,1	5,6	0,4
EA	5,4	-1,6	0,4	-0,6	1,3	-4,3	13,3	-2,0	6,9	0,7
EU	4,2	-0,7	0,3	-0,6	3,8	-1,1	9,1	-1,3	3,5	0,0
EU %	2,6	-0,6	0,5	-0,8	1,8	-0,7	3,5	-0,6	3,0	-0,3

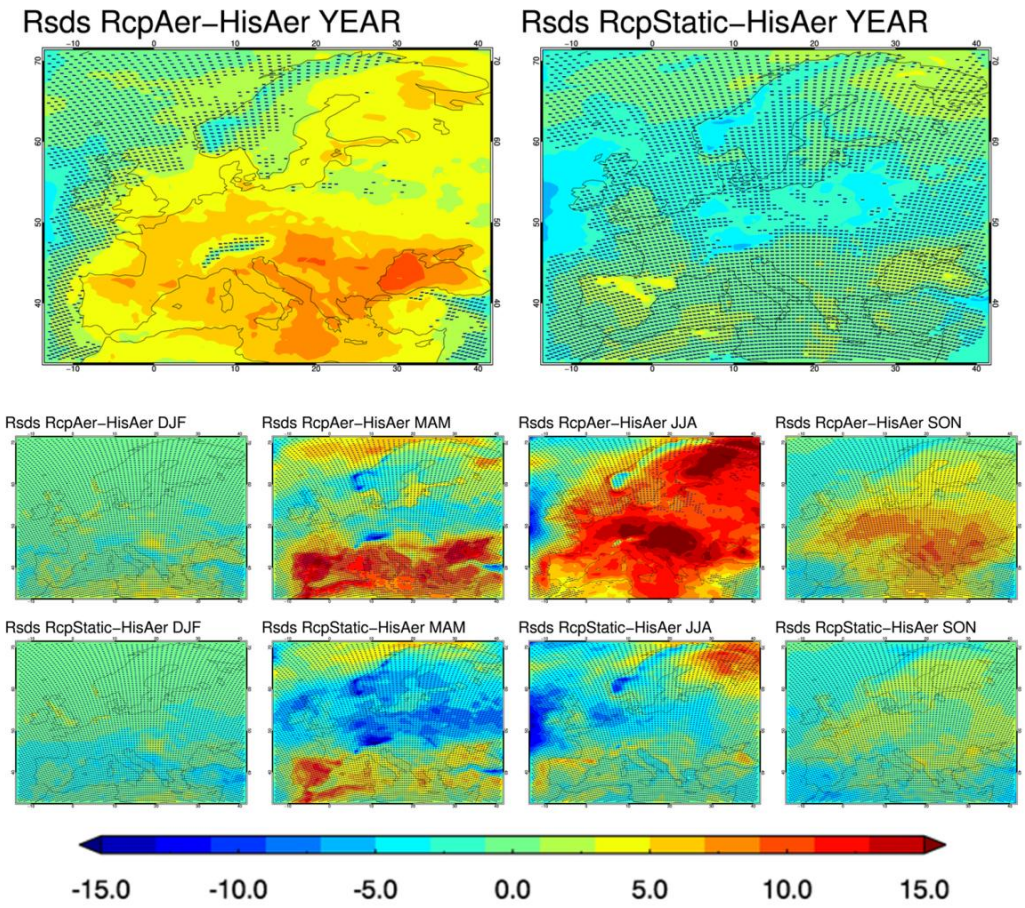

Fig. 56: Shortwave radiation at the surface (Rsds) difference (W/m^2) of the Rcp simulations from the historical simulation HisAer. Large plots at the top: For the entire year. RcpAer at the left and RcpStatic to the right. Smaller plots at the bottom rows: On a seasonal basis. For RcpAer (first row) and RcpStatic (second row).

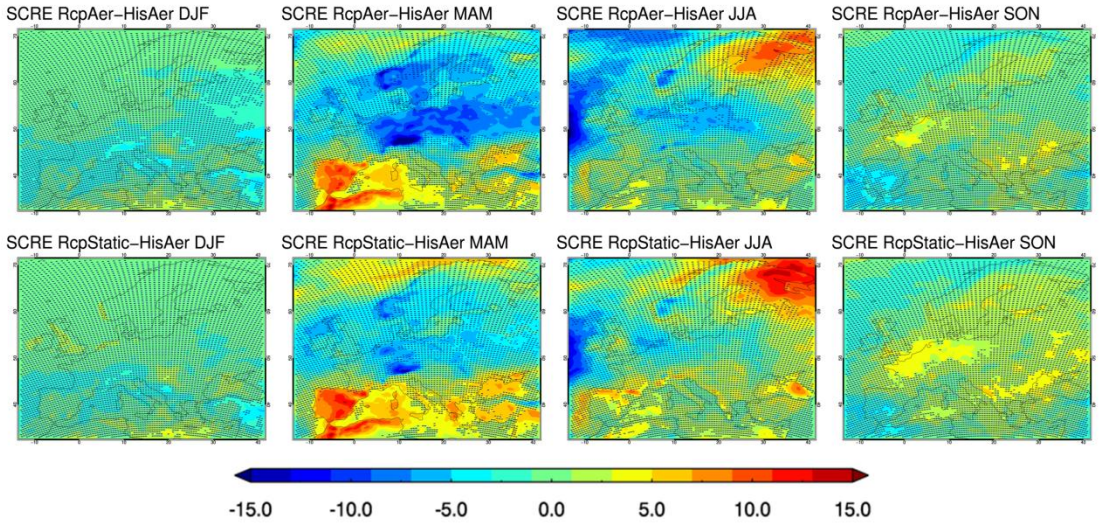

Fig. 57: Cloud radiative effect (SCRE) difference (W/m^2) of the Rcp simulations (2021-2050) from the historical simulation HisAer (1971-2000). Simulation RcpAer at the top row and RcpStatic at the bottom. Negative difference means that the cloud effect on radiation becomes even more negative reducing further shortwave radiation at the surface. Positive difference means that the cloud effect becomes less negative thus tending to increase radiation at the surface.

So far we have seen that the decrease in aerosol optical depth compared to the historical period clearly impacts radiation at the surface for the future period. Yet simulation RcpAer also presents a decreasing trend in aerosol optical depth in the future period 2021-2050. This could potentially lead to an increasing tendency of Rsds over time during the future period. On the other hand we would not expect a similar behavior for RcpStatic since it uses a static in time aerosol field. Interestingly however, results indicate that both Rcp simulations present an increasing trend in shortwave radiation at the surface that is significant on a yearly basis. RcpAer indeed has a slightly more positive trend for the year and all seasons except spring indicating that the decreasing trend in AOD does have some effect. This is more evident if we look at the Clear-sky shortwave radiation at the surface (CRsds). CRsds is not affected by cloudiness change and thus is more directly impacted by changes in the aerosol load. RcpAer does have a small increasing trend on a year to year basis and for all seasons however it is considerably lower than the positive trend seen in Rsds and thus does not explain it fully. RcpStatic on the other hand has a small decreasing tendency, completely in contrast to the positive trend seen in Rsds. To investigate further we also calculated the trends in the cloud radiative effect (SCRE). The trend in SCRE is positive and of statistical significance on a yearly basis for both Rcp simulations. Furthermore the trend magnitude is considerably larger than the one seen in CRsds and is very close to the trend magnitude seen in the overall Rsds. Therefore the increasing trend in shortwave radiation seen in both Rcp simulations during the future period is mainly attributed to cloudiness letting more radiation to reach the surface over time (positive SCRE trend). Finally the decreasing aerosol trend in RcpAer does have some impact and further enhances the positive Rsds trend. However it is definitely not the main cause. This is especially true in RcpAer during summer where the large positive trend in radiation is attributed almost entirely to the change of cloud radiative effect and marginally to the decreasing AOD over time. It might seem peculiar that in the historical period we observed a much more intense impact on Rsds trend by the decreasing AOD trend of HisAer. It must be noted though that the negative AOD trend in the historical period was considerably stronger, about three times larger (-0.7×10^{-3}/year compared to 2.2×10^{-3}/year) thus leading to a more pronounced effect.

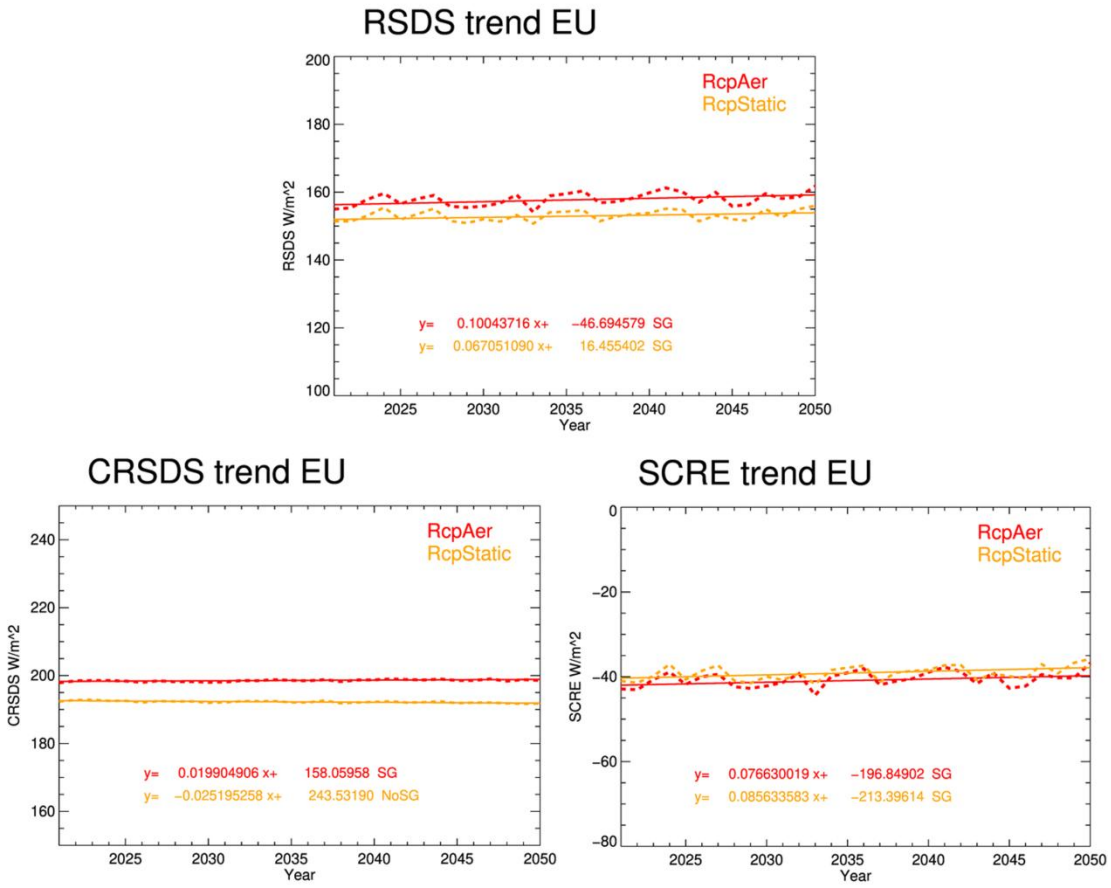

Fig. 58: Shortwave radiation at the surface (Rsds - top), Clear-sky shortwave radiation at the surface (CRsds – bottom left) and Cloud radiative effect (SCRE – bottom right) over the EU region and the period 2021-2050. Variable values are depicted with dashed line whereas the linear regression line using the Theil-Sen method is depicted with solid line. Red is used for RcpAer and orange for RcpStatic.

Table 36: Slope of the linear regression (W/m^2 /decade) regarding shortwave radiation at the surface (Rsds – top), cloud effect on radiation at the surface (SCRE – middle) and Clear-sky shortwave radiation at the surface (CRsds – bottom). For the period 2021-2050 and the EU region. Negative trends are depicted with blue color cells and positive trends with pale pink color cells. Bold fonts are used to depict trends that are statistically significant at the 95% level.

RSDS

2021-2050	Year	Winter	Spring	Summer	Autumn
RcpAer	**1,0**	0,3	**1,1**	1,1	0,9
RcpStatic	**0,7**	0,2	**1,3**	0,1	0,7

SCRE

2021-2050	Year	Winter	Spring	Summer	Autumn
RcpAer	**0,8**	0,2	0,8	1,0	0,5
RcpStatic	**0,9**	0,4	**1,3**	0,5	**1,0**

CRSDS

2021-2050	Year	Winter	Spring	Summer	Autumn
RcpAer	**0,2**	0,1	**0,3**	0,1	**0,4**
RcpStatic	-0,3	-0,1	-0,2	-0,1	-0,2

2.10.3 Temperature

Mean annual temperature is clearly increased in the future period 2021-2050 compared to the historical period 1971-2000 (Fig. 59). It is characteristic that both future projections present an increase of mean annual temperature that is statistically significant all over the domain. The detected warming usually ranges between 1-2^{o}C and is more intense over the eastern part of the domain. For the EU region averaged warming is 1.5 ^{o}C for RcpAer and 1.3 ^{o}C for RcpStatic (Table 37). For the rest subregions largest warming is seen for Eastern Europe (EA) (1.9 ^{o}C - 1.6 ^{o}C), while smallest warming is seen for the British Isles (0.9-0.8 ^{o}C). This more intense warming over the eastern part of Europe has also been detected in other EURO-CORDEX simulations for the period 2071-2100 and both Rcp4.5 and Rcp8.5 scenarios (Jacob et al., 2014). The warming of the future climate in Europe is also clearly described by CMIP5 global climate models (McSweeney et al., 2015). In general RcpAer presents a more intense warming than RcpStatic. The smaller aerosol optical depth in RcpAer seems to have a clear impact on future warming through the decrease of shortwave radiation at the surface. An extra increase of temperature due to the reduction of aerosol load in the future is also presented in the GCM study of Xu et al., (2018).

On a seasonal basis a widespread warming is also detected, however differences between seasons do exist. Winter is the season with the less intense warming, around 1^{o}C for both future projections regarding EU region averages, whereas the largest increase is seen in summer and autumn (1.7-1.5 ^{o}C) (Table 37). Temperature increase is again slightly larger in RcpAer compared to RcpStatic for all seasons except spring. Moreover the warming is statistically significant for RcpAer over the entire domain for all seasons, except some small areas in northern France and Britain in spring. On the other hand, RcpStatic does have an extended area of non significant warming over the eastern part of the domain in autumn and two zones of non significant warming over central and eastern Europe in winter and spring. Thus the use of realistic aerosol (lower AOD in RcpAer compared to RcpStatic) clearly leads to a more intense warming and also increases the significance of temperature change on a seasonal basis.

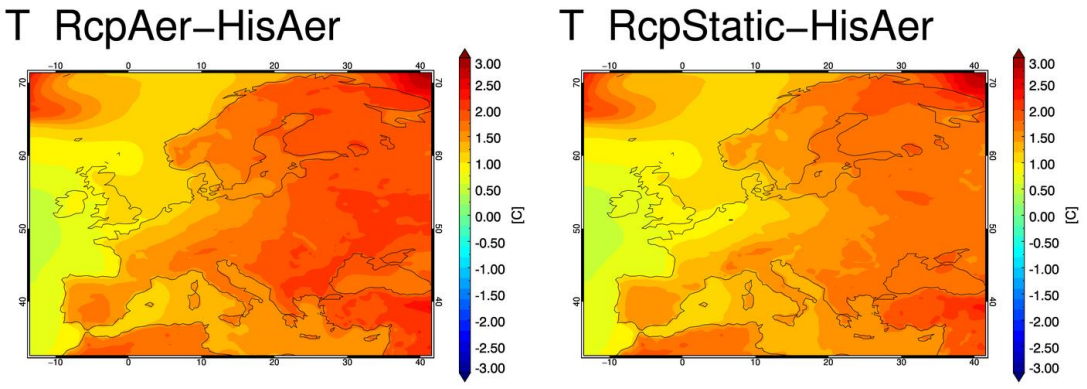

Fig. 59: Mean annual temperature difference between simulations for the future period 2021-2050 (RcpAer-left, RcpStatic-right) and simulation HisAer for the historical 1971-2000 period. Stippling indicates areas that are not of statistical significance at the 95% level according to the Mann-Whitney non parametric test.

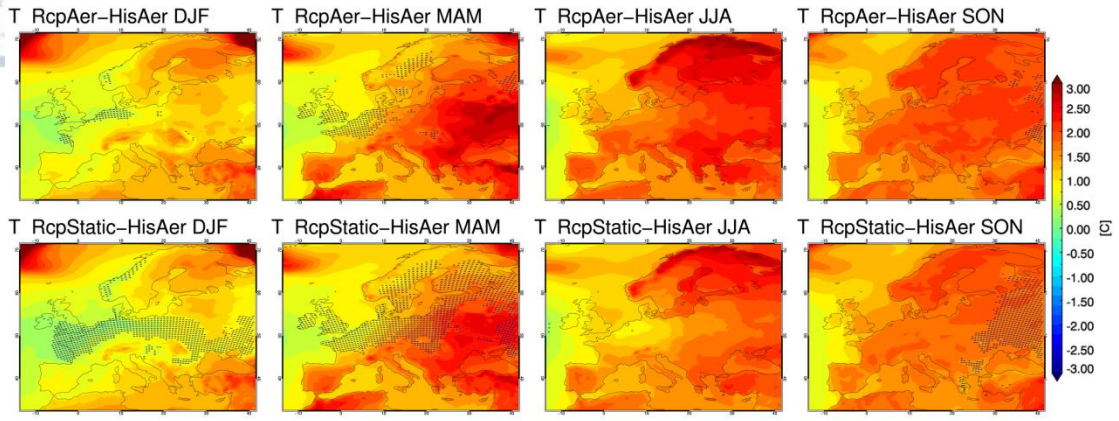

Fig. 60: : Mean seasonal temperature difference between simulations for the future period 2021-2050 (RcpAer-left, RcpStatic-right) and simulation HisAer for the historical 1971-2000 period. Stippling indicates areas that are not of statistical significance at the 95% level according to the Mann-Whitney non parametric test.

Table 37: Mean temperature difference between simulations for the future period 2021-2050 (RcpAer, RcpStatic) and simulation HisAer for the historical 1971-2000 period. Mean annual differences (first column) and seasonal differences for all subregions including the EU domain.

	Year		DJF		MAM		JJA		SON	
	RcpAer	RcpStatic	RcpAer	RcpStatic	RcpAer	RcpStatic	RcpAer	RcpStatic	RcpAer	RcpStatic
BI	0,9	0,8	0,6	0,5	0,8	0,7	1,1	1,0	1,2	1,2
IP	1,3	1,3	0,8	0,8	1,5	1,4	1,5	1,4	1,5	1,4
FR	1,2	1,0	0,6	0,4	1,0	0,9	1,5	1,2	1,6	1,5
ME	1,4	1,1	0,8	0,6	1,3	1,1	1,6	1,1	1,8	1,7
SC	1,6	1,5	1,2	1,0	1,4	1,3	2,1	1,8	1,9	1,8
AL	1,6	1,5	1,2	1,0	1,7	1,6	1,8	1,5	1,9	1,7
MD	1,5	1,4	1,2	1,1	1,5	1,5	1,7	1,5	1,7	1,6
EA	1,9	1,6	1,1	0,9	2,2	2,0	2,1	1,6	2,0	1,7
EU	1,5	1,3	1,0	0,9	1,4	1,4	1,7	1,5	1,7	1,6

Difference between RcpAer and RcpStatic

Now we examine in more detail the differences in temperature between the two Rcp simulations. As said before, the aerosol dataset implemented has a clear impact on temperature since RcpAer is in general warmer than RcpStatic. The smaller AOD of RcpAer leads to less shortwave radiation at the surface thus impacting temperature and further enhancing the warming of the future period. RcpAer presents increased temperature for the largest part of the domain and for all seasons (Fig. 61). Usually for most seasons the temperature difference ranges around 0.1 to 0.2 ^{o}C with the averages for the subregions and the EU region having similar values. Interestingly, considerably larger positive differences are seen in summer when warming in RcpAer is usually above 0.3 ^{o}C and in extended areas of central and eastern Europe it even exceeds 0.5 ^{o}C. Moreover the temperature increase is

statistically significant over the biggest part of continental Europe, the only season to present such a behavior.

We have also calculated the ratio of temperature difference between the Rcp simulations (RcpAer-RcpStatic) to the overall warming seen in RcpAer compared to the historical period (RcpAer-HisAer). This expresses the relative importance of the warming due to the introduction of realistic aerosol compared to the overall future warming seen in RcpAer. The aerosol impact is considerable since the use of realistic aerosol can explain on average 9% of the overall warming in the EU region. For winter and summer this percentage is even greater, around 14%. A large impact is also seen on several subregions. The most prominent example is central Europe (ME and FR subregions) in winter and summer with the time evolving aerosol being responsible for 30% of the overall warming of RcpAer.

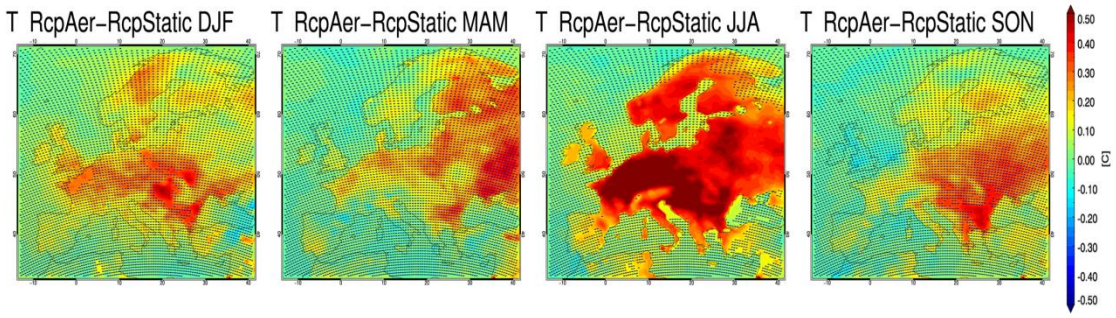

Fig. 61: Temperature difference between RcpAer and RcpStatic for all seasons. For the period 2021-2050. Stippling indicates areas that are not of statistical significance at the 95% level according to the Mann-Whitney non parametric test.

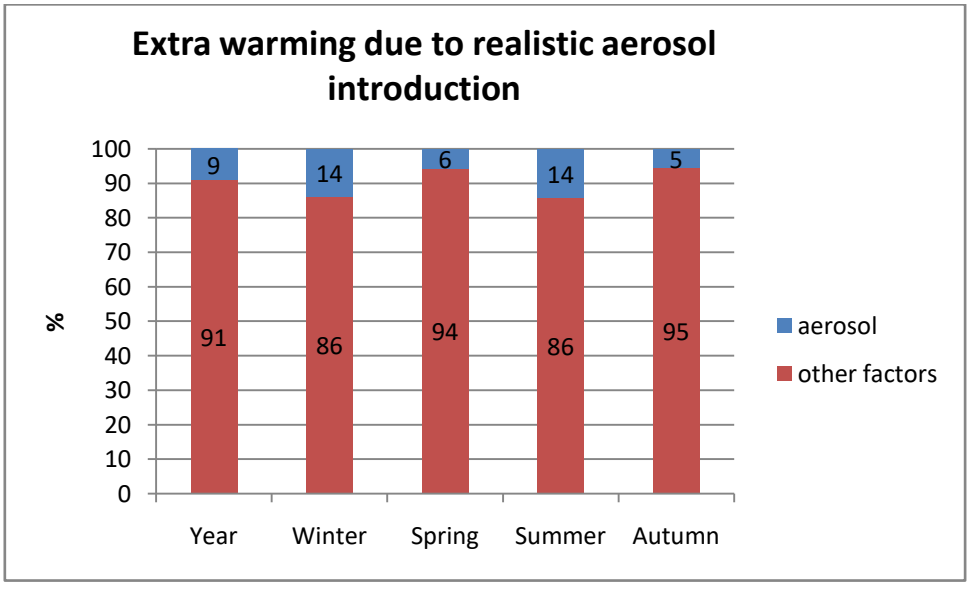

Fig. 62: Mean percentage of the overall warming (blue+red) seen in the future period 2021-2050 in RcpAer that is explained by the introduction of realistic time evolving aerosol (blue). For the EU region. In essence the blue values are the metric: (RcpAer-RcpStatic)/(RcpAer-HisAer)*100.

Changes in the distribution

Interestingly, when we examine the probability density function plots of mean daily temperature (Fig. 63-top two rows) we see that the shape of the distribution is almost identical between the Rcp simulations and the historical HisAer for all seasons. The warming of the future period is evident since the Rcp simulations are shifted towards larger temperatures. However all the features of the distributions (width, number of peaks etc.) remain essentially the same. A similar picture is seen in the box plots (Fig. 63-bottom two rows). The main width of the distribution, given by the interquantile range, remains unchanged. The quantiles though are shifted towards larger values. Regarding the outliers, the Rcp simulations also present a shift towards larger values. This shift is especially pronounced in Spring and mainly in Winter regarding the outlier values at low temperatures. It is characteristic that HisAer presents temperatures that reach down to -45 ^{o}C in Winter whereas both Rcp simulations do not exceed values of -35^{o}C.

In order to better study the behavior of the different parts of the temperature distribution we have constructed the daily mean q-q plots for the Rcp simulations using HisAer as a reference (Fig. 64-top). We have calculated twenty percentile classes (0-5, 5-10…,95-100) and depict the mean value of each percentile class. It is characteristic that the mean value for each percentile class is larger in the Rcp simulations compared to HisAer for all seasons. This clearly confirms that the warming affects the entire distribution of temperature. In general, the warming compared to the historical period does not seem to deviate substantially for the different percentile classes. In order to capture this more clearly we have plotted the differences in mean daily temperature between the Rcp simulations and the historical HisAer for each percentile class (Fig. 64-bottom). Indeed for most percentile classes the shift towards larger temperatures is quite similar usually not deviating more than half a degree. For the majority of classes it ranges between 1 to 1.5 ^{o}C in winter, 1.5 to 2 ^{o}C in autumn and summer and between 1.2 to 2 ^{o}C in spring. On the other hand a more intense warming is encountered in the first couple percentiles in spring and autumn that can exceed 2.5 ^{o}C, corresponding to the shift of the outlier values seen in the box plots for these two seasons at low temperatures. In winter however, the first percentile class has a moderate warming, not much larger than the rest classes, that does not explain the large shift in outlier values towards larger temperatures seen in the box plot. It must be reminded here that for each class a mean value is calculated. If the number of outliers with a large shift is small then this information is probably lost in the averaging. The largest shift is seen in very low values around -30 ^{o}C. Indeed the number of these values is very small compared to overall number of daily values in the first percentile (0-5%), being only 0.18% of the first percentile class in HisAer, 0.04% in RcpAer and 0.06% in RcpStatic. Therefore the averaging of the first class cannot be substantially affected by the large shift seen in these very few cases.

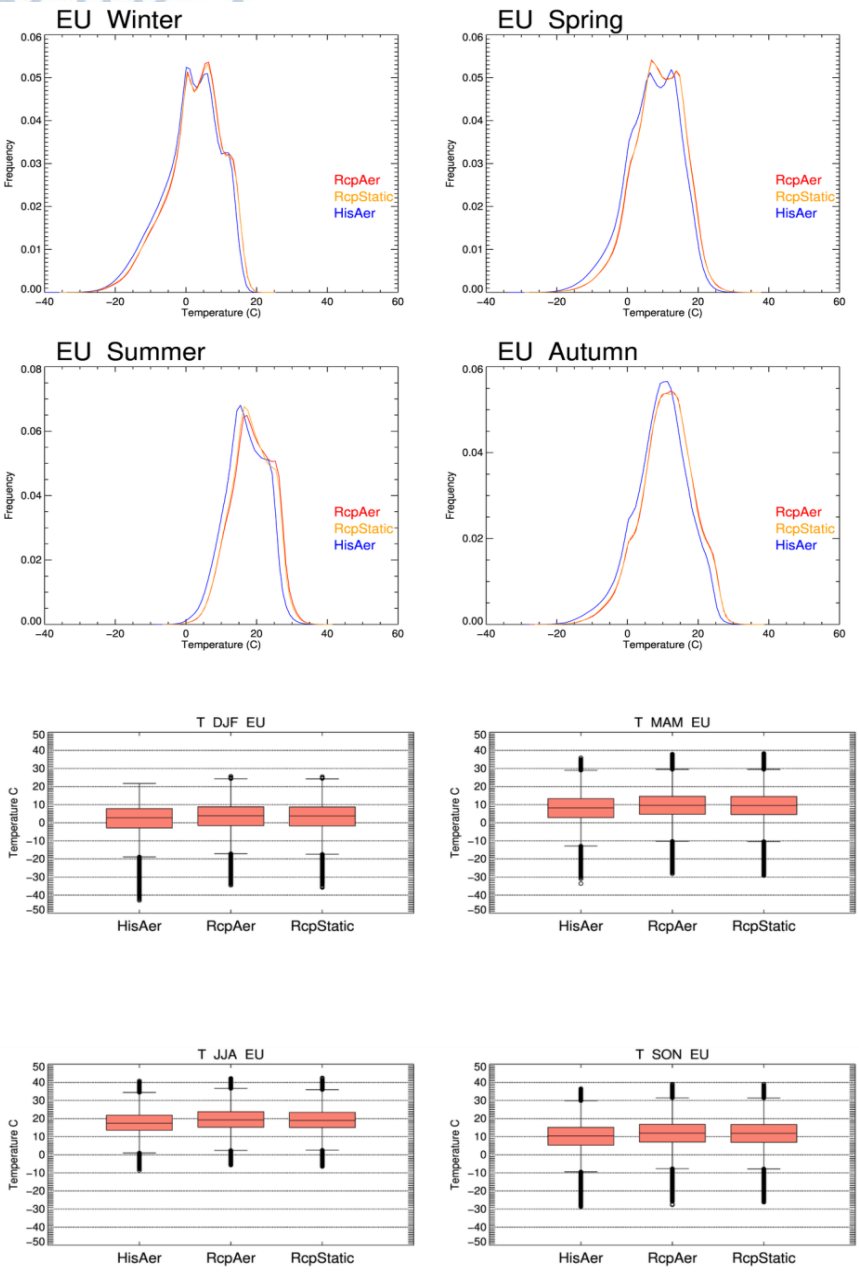

Fig. 63: Probability density functions (top two rows) and box plots (bottom two rows) regarding daily mean temperature for historical simulation HisAer (1971-2000) and future simulations RcpAer and RcpStatic (2021-2050). For all seasons.

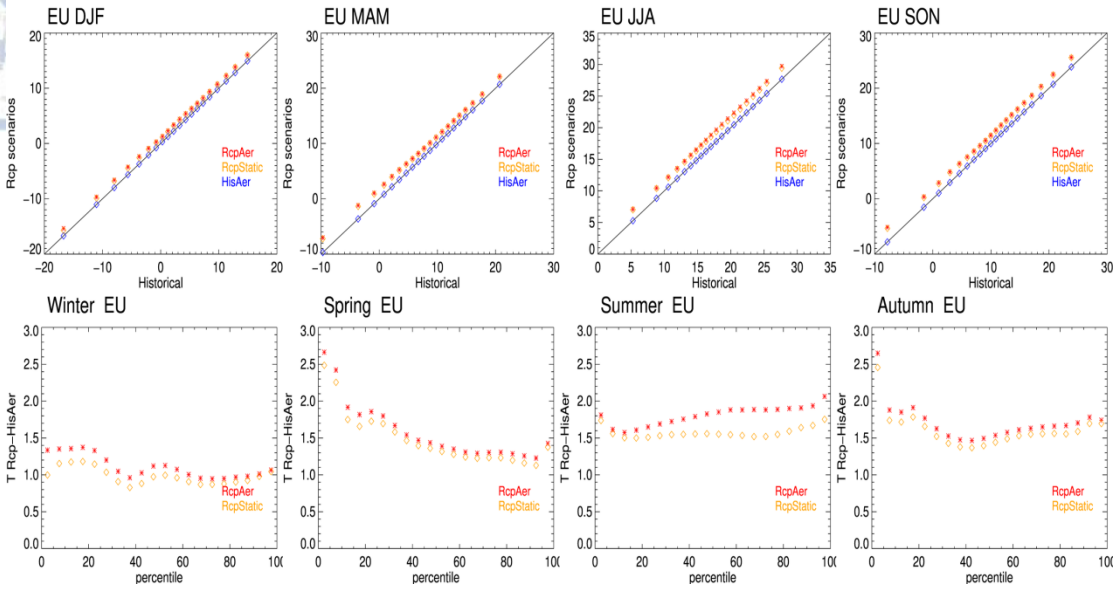

Fig. 64: Top row: Q-Q plots for daily mean temperature (°C) for RcpAer (red), RcpStatic (orange) and HisAer (blue). For all seasons. Bottom row: The temperature difference of each Rcp simulation from the historical simulation HisAer for each percentile class. Red for RcpAer-HisAer and orange for RcpStatic-HisAer.

Trends

The temperature tendency in the future period is clearly positive. Analysis of mean yearly values reveals increasing and statistically significant trends for both Rcp simulations in the EU region and all the subregions (Table 38). The most intense trend is seen in Eastern Europe (EA) whereas the weakest trend is seen in the British Isles (BI). The trend magnitude in the EU region is $3{,}4 \times 10^{-2}$ °C/year for both Rcp simulations and is exactly the same with trend detected in HisAer for the historical period 1971-2000. Compared to the historical period (HisAer) the future period presents in general less intense trends over central Europe (ME, FR, AL) whereas a stronger trend is seen in Eastern Europe (EA).

Differences in trend intensity do exist between the Rcp simulations. However a substantial impact of the aerosol dataset cannot be identified. The future simulations have the same trend magnitude for the EU region, whereas RcpAer has larger trends only in half of the subregions. We expected the decreasing aerosol in RcpAer to lead to more positive trends in temperature compared to RcpStatic. However if we analyze the trend behavior on a seasonal basis a clear difference is seen on the summer temperature (Table 38, Fig. 65). The seasonal trends have been estimated by using the mean value of each season for each year. Interestingly, compared to RcpStatic simulation RcpAer presents slightly less intense trends for the EU region in winter and spring and a clearly less positive trend in autumn. However in summer, the trend magnitude in RcpAer is clearly larger ($4{,}1$ to $3{,}1 \times 10^{-2}$ °C/year). The same can be said for the majority of the subregions. However we have seen that the shortwave radiation trend in summer is mainly affected by the trend in cloud radiative effect. Thus we can conclude that the larger Rsds trend in RcpAer clearly impacts summer temperature trend intensifying the temperature increase during the future period. However this cannot be attributed to the aerosol decrease. Finally, we must not be confused by the fact that

RcpAer is clearly warmer than RcpStatic for the future period but at the same time it does not present larger increasing trends in temperature. RcpAer is warmer because it uses considerably smaller AOD for the entire future period that leads to less shortwave radiation at the surface. The temperature trend on the other hand is controlled by the Rsds trend which in turn is impacted by the AOD tendency in time but mainly as we saw in the previous section by the tendency of cloud radiative effect.

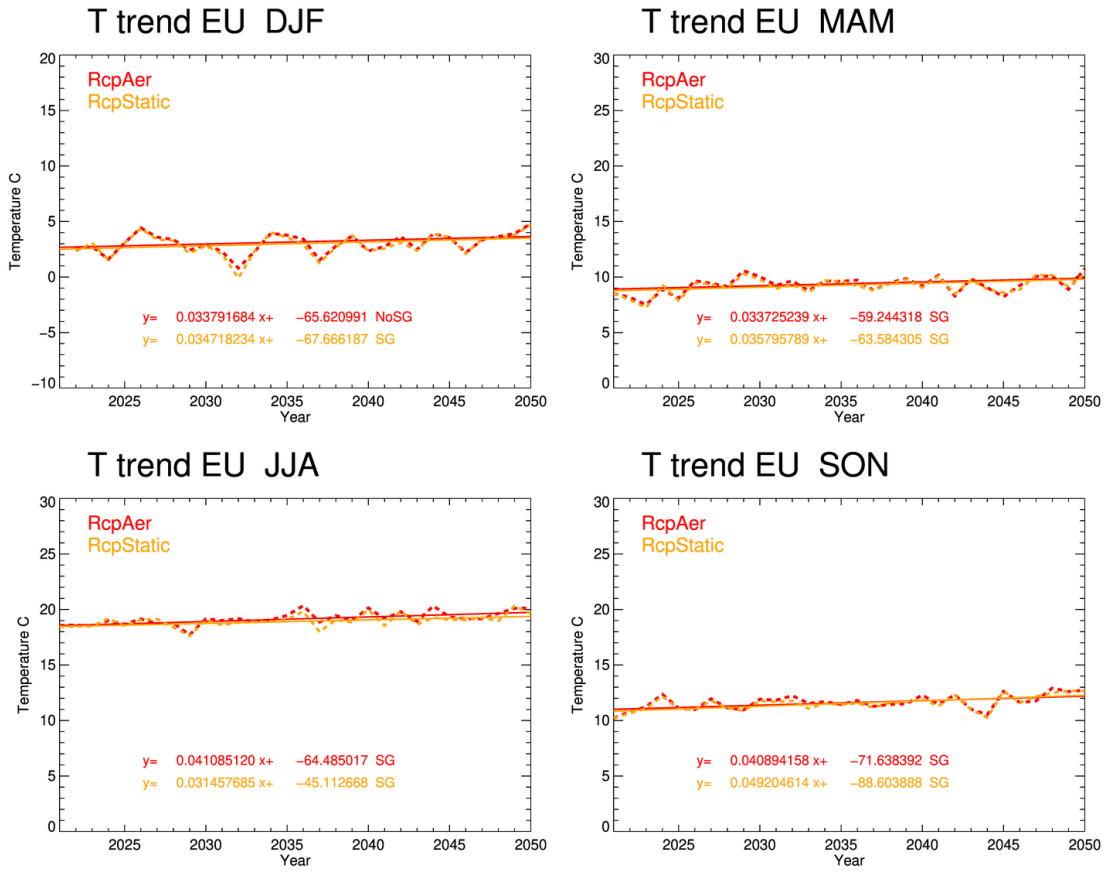

Fig. 65: Seasonal mean temperature (dashed line) and linear regression line (solid line) using the Theil-Sen method over the EU region and the period 2021-2050. For the Rcp simulations RcpAer (red) and RcpStatic (orange).

Table 38: Slope of the linear regression (10^{-2} °C /year) regarding yearly mean temperature (top three rows) and seasonal mean temperature for the Rcp simulations. For the period 2021-2050 and for all subdomains including the EU region. For the yearly mean temperature data for the historical simulation HisAer (period 1971-2000) are also presented to facilitate comparison between the two periods. Negative trends are depicted with blue color cells and positive trends with pale pink color cells. Bold fonts are used to depict trends that are statistically significant at the 95% level.

Year

	EU	BI	IP	FR	ME	SC	AL	MD	EA
RcpAer	**3,4**	**2,5**	**3,4**	**2,6**	**3,0**	**3,7**	**2,8**	**2,8**	**5,1**
RcpStatic	**3,4**	**2,3**	**3,5**	**3,2**	**3,0**	**3,9**	**3,4**	**2,7**	**4,7**
HisAer	**3,4**	**2,6**	**3,2**	**4,9**	**5,0**	**3,5**	**4,4**	**2,7**	**3,9**

Winter

	EU	BI	IP	FR	ME	SC	AL	MD	EA
RcpAer	3,4	2,8	2,0	0,8	2,7	**8,6**	0,6	1,8	4,9
RcpStatic	**3,5**	2,3	2,0	0,3	2,6	**9,2**	1,5	0,8	3,8

Spring

	EU	BI	IP	FR	ME	SC	AL	MD	EA
RcpAer	**3,4**	**2,3**	2,2	1,6	2,4	1,6	3,3	**4,5**	4,9
RcpStatic	**3,6**	**2,5**	3,9	4,0	3,0	1,7	5,5	**4,6**	**5,2**

Summer

	EU	BI	IP	FR	ME	SC	AL	MD	EA
RcpAer	**4,1**	**2,3**	**5,0**	**5,5**	**4,3**	**5,4**	**4,7**	**3,2**	**6,0**
RcpStatic	**3,1**	2,2	**5,5**	**6,2**	2,7	2,7	3,1	**2,9**	4,4

Autumn

	EU	BI	IP	FR	ME	SC	AL	MD	EA
RcpAer	**4,1**	**2,3**	**4,8**	**4,1**	**5,1**	4,4	**4,7**	**2,9**	**7,4**
RcpStatic	**4,9**	2,3	**4,7**	3,8	**4,6**	**4,6**	**4,5**	**2,8**	**8,9**

2.10.4 Precipitation

Precipitation on an annual basis does not present clear and significant changes in the 2021-2050 period compared to the historical simulation HisAer (1971-2000). The pattern of annual differences is very similar for both Rcp8.5 simulations with statistically significant changes seen in limited cases (Fig. 66): a statistically significant increase is seen over the Alps (+7%, +0.19 mm/day for RcpAer), over eastern-northeaster Europe (+9%, +0.15 mm/day for RcpAer) and over extended parts of Scandinavia (+4%, 0.07 mm/day for RcpAer). In general both Rcp simulations present a slight domain averaged increase compared to HisAer that is slightly larger in RcpAer. Moreover, an increase is seen mainly over the central and northern-northeastern part of Europe, whereas the southern part presents spots of precipitation reduction. This spatial pattern of precipitation change is qualitatively quite similar to some recent high resolution (12km) EURO-CORDEX simulations for the period 2071-2100 and both Rcp4.5 and Rcp8.5 scenarios (Jacob et al., 2014).

On a seasonal basis an increase is seen in winter and a decrease in autumn. However the most spatially extensive statistically significant changes are seen in spring, with an increase over Eastern Europe and parts of Scandinavia (+0.3mm/day,+16% for RcpAer) whereas a precipitation decrease is seen over the entire Iberian Peninsula (-4.6 mm/day, -24%). Moreover the mountainous part of the Alps presents a significant increase for all seasons except summer.

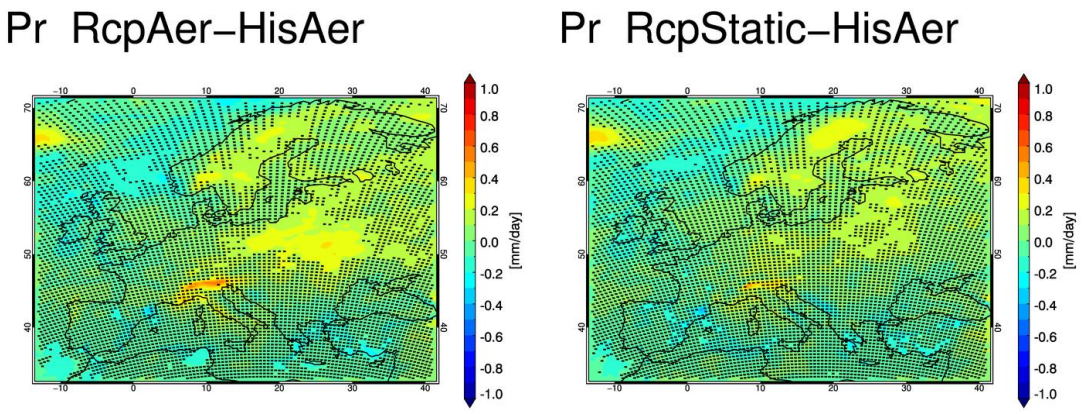

Fig. 66: Mean annual precipitation difference between simulations for the future period 2021-2050 (RcpAer-left, RcpStatic-right) and simulation HisAer for the historical 1971-2000 period. Stippling indicates areas that are not of statistical significance at the 95% level according to the Mann-Whitney non parametric test.

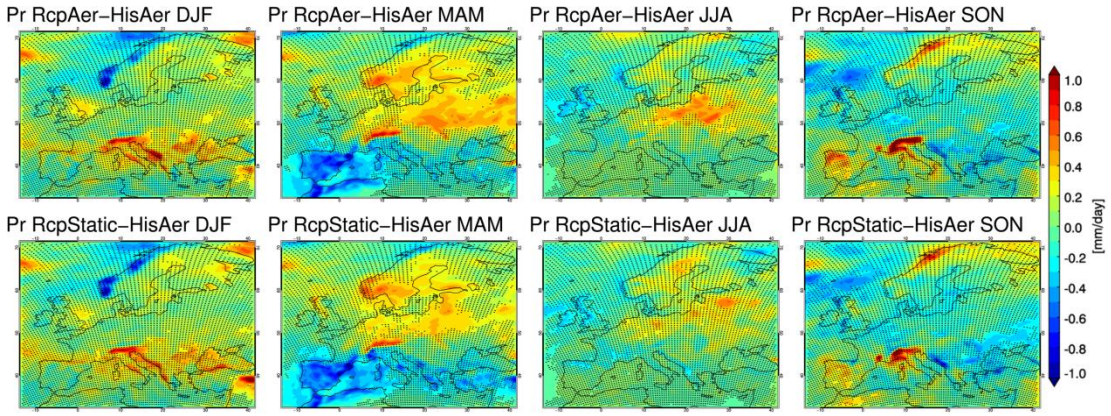

Fig. 67: Mean seasonal precipitation difference (mm/day) between simulations for the future period 2021-2050 (RcpAer-left, RcpStatic-right) and simulation HisAer for the historical 1971-2000 period. Stippling indicates areas that are not of statistical significance at the 95% level according to the Mann-Whitney non parametric test.

Table 39: Mean precipitation difference (mm/day) (top rows) and relative difference (%) (bottom rows) between simulations for the future period 2021-2050 (RcpAer, RcpStatic) and simulation HisAer for the historical 1971-2000 period. Mean annual differences (first column) and seasonal differences for all subregions including the EU domain.

	Year		DJF		MAM		JJA		SON	
mm/day	RcpAeros	RcpStatic	RcpAeros	RcpStatic	RcpAeros	RcpStatic	RcpAeros	RcpStatic	RcpAeros	RcpStatic
BI	-0,07	-0,06	0,04	0,03	0,01	0,07	-0,19	-0,19	-0,17	-0,15
IP	-0,05	-0,08	0,04	0,05	-0,46	-0,47	0,01	-0,03	0,2	0,14
FR	-0,02	-0,02	0,08	0,09	-0,07	-0,07	-0,08	-0,09	0	-0,03
ME	0,07	0,08	0,07	0,07	0,26	0,26	0,13	0,14	-0,18	-0,16
SC	0,07	0,07	-0,03	-0,01	0,25	0,24	0,07	0,11	-0,01	-0,05
AL	0,19	0,12	0,35	0,37	0,06	-0,02	0,03	-0,09	0,33	0,23
MD	-0,01	-0,04	0,2	0,22	-0,26	-0,32	0	-0,03	0,03	-0,02
EA	0,15	0,08	0,21	0,19	0,3	0,18	0,25	0,13	-0,14	-0,17
EU	0,02	0,01	0,08	0,09	0,01	-0,01	0,03	0,01	-0,04	-0,07
relative %										
BI	-2	-2	3	2	0	3	-10	-10	-5	-4
IP	-4	-5	1	2	-24	-25	9	7	12	9
FR	-1	-1	4	4	-3	-3	-6	-6	0	-2
ME	4	4	4	3	13	13	7	7	-8	-7
SC	4	4	2	3	16	16	3	6	-1	-2
AL	7	5	16	17	0	-2	1	-4	11	9
MD	-1	-3	11	12	-17	-21	5	-1	2	-1
EA	9	5	15	14	16	10	14	7	-8	-10
EU	1	0	6	6	1	-1	3	1	-1	-3

Difference between RcpAer and RcpStatic

Both Rcp simulations have a very similar behavior regarding precipitation. The spatial pattern of precipitation differences (RcpAer-RcpStatic) presents no points with statistical significance if calculated from monthly mean values. If we use daily values, small areas with significant changes are seen only in spring and summer (Fig. 68). In spring an increase over the Balkans and north of the Black Sea is seen. In summer there is a spatially more extensive area with significant increase over eastern Europe whereas a significant decrease over parts of Scandinavia is present. Interestingly the domain averaged precipitation is larger (1.5 to 2%) in RcpAer compared to RcpStatic in all seasons except winter (Table 40). The same is also true for most subregions. We have seen from the sensitivity study of PART 1 (section 1.5.3.8) that the inclusion of aerosol-radiation interactions leads to a small precipitation reduction in summer and spring. Therefore the larger AOD of RcpStatic is possibly affecting precipitation amount leading to small reductions.

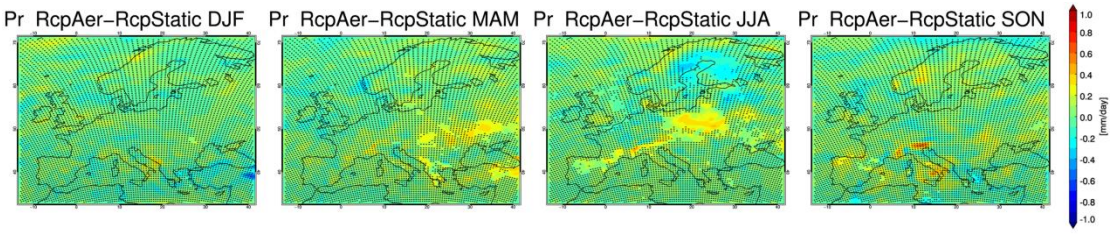

Fig. 68: Precipitation difference (mm/day) between RcpAer and RcpStatic for all seasons. For the period 2021-2050. Stippling indicates areas that are not of statistical significance at the 95% level according to the Mann-Whitney non parametric test using daily values.

Table 40: Domain averaged precipitation differences (mm/day) and relative difference (%) between RcpAer and RcpStatic (RcpAer-RcpStatic) for all seasons. For the period 2021-2050.

mm/day	DJF	MAM	JJA	SON
EU	-0.01	0.02	0.02	0.03
relative %				
EU	-0.51	1.56	2.27	1.44

Changes in the distribution

The changes in the probability density function plots of mean monthly and mean daily values are small regarding the entire domain. They can be more pronounced at a subdomain level, especially for Eastern Europe (EA) and the Iberian Peninsula (IP) in spring (Fig. 69) where the statistically significant changes are seen. It is visible that there is a systematic shift towards larger precipitation values in Eastern Europe during spring for the two Rcp simulations. On the contrary there is a clear shift towards smaller precipitation amounts in the Iberian Peninsula, especially concerning low precipitation values below 1 mm/day that present a considerable increase in frequency.

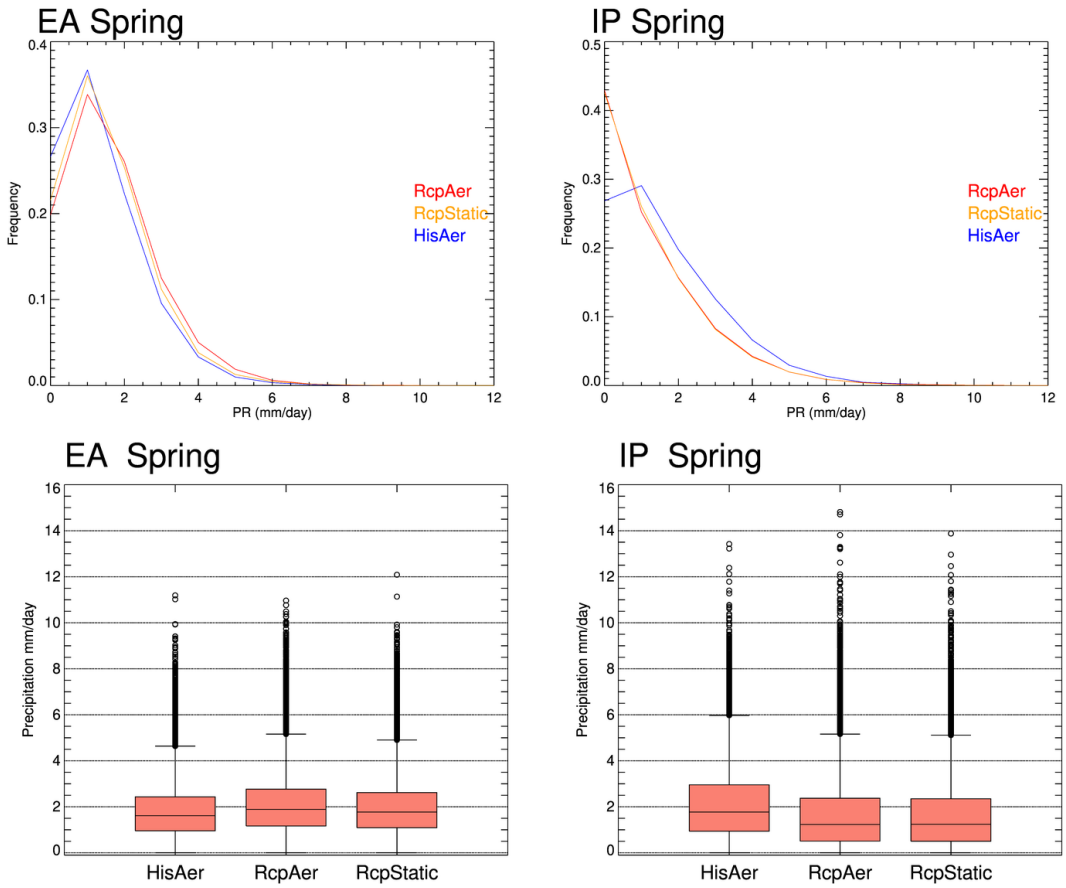

Fig. 69: Probability density functions (top two rows) and box plots (bottom two rows) regarding monthly mean precipitation (mm/day) for historical simulation HisAer (1971-2000) and future simulations RcpAer and RcpStatic (2021-2050). For the subdomains of Eastern Europe (EA) (left) and the Iberian Peninsula (IP) (right) in spring.

Now we consider the Rcp simulations differences from HisAer for twenty percentile classes (0-5, 5-10…,95-100) of precipitation monthly values. We see that over the domain the decrease in autumn is happening in almost all percentiles whereas in winter an increase is seen in almost all percentiles. Interestingly in all seasons an increase is seen in the last percentile class (95-100 indicating a strengthening of the largest precipitation amounts on a monthly level (Fig. 70). The same behavior is seen if daily values are considered. For the two areas of particular interest in spring: The increase in Eastern Europe is happening in all percentiles and is also more pronounced in the last percentile class. Finally, in the Iberian Peninsula the observed decrease is present in all percentiles.

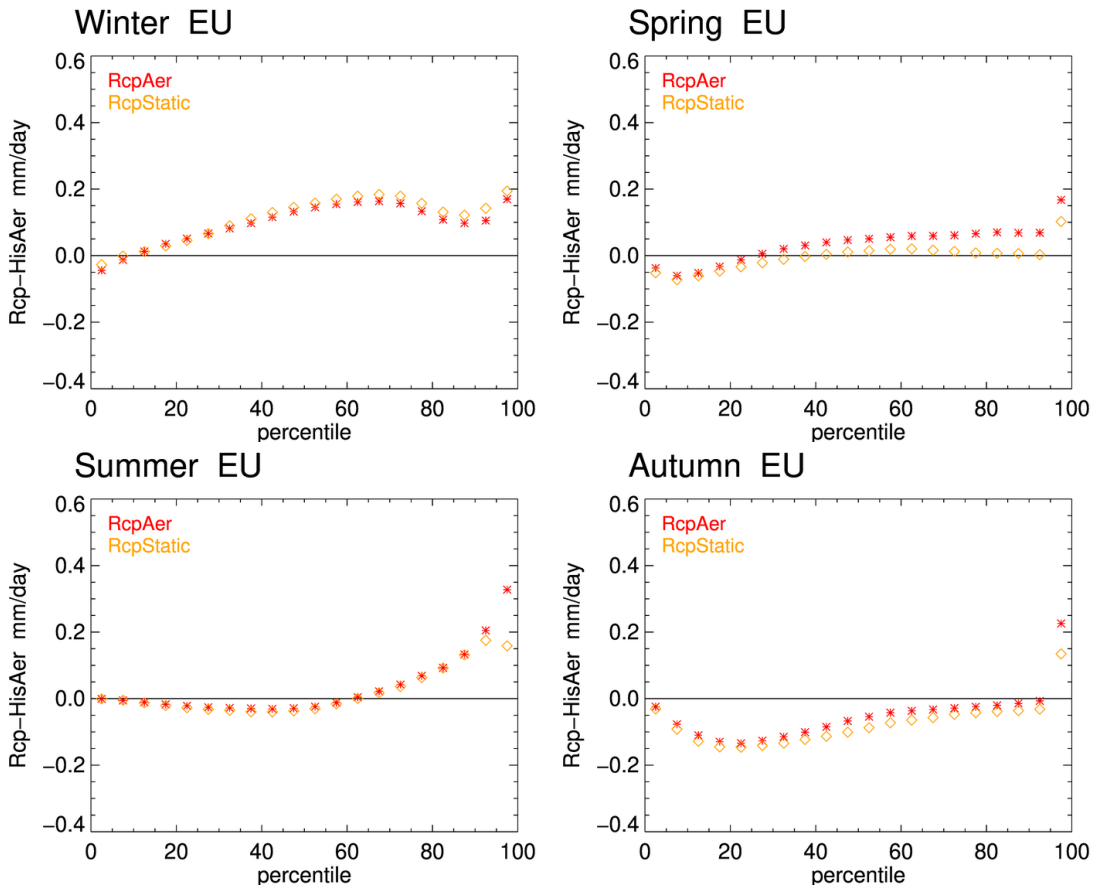

Fig. 70: The precipitation difference (mm/day) of each Rcp simulation from the historical simulation HisAer for each percentile class, regarding monthly values. All grid points of the EU domain are considered. Red for RcpAer-HisAer and orange for RcpStatic-HisAer.

Trends

In the future period 2021-2050, domain (EU) averaged precipitation presents a decreasing tendency for all seasons as well as on a yearly basis (Fig. 71, Table 41). This decreasing trend is also seen for most subregions both on a yearly and a seasonal basis.

However the trends are almost always not significant at the 95% level. Yet at the 90% level some statistically significant trends exist. On a yearly basis significant trends are seen in the Iberian Peninsula (IP) and France (FR) for RcpAer and for the EU domain and France (FR) for

RcpStatic. On a seasonal basis only RcpAer shows a significant reduction over the British Isles (BI) in spring and summer and over the Iberian Peninsula (IP) in autumn. The latter has the strongest trend (-22.7x10^{-3} (mm/day)/year) detected, including all subregions and seasons.

The future trends for the Rcp simulations do not differ much from the trends seen on a yearly basis for the historical HisAer simulation (1971-2000). HisAer also presents a decreasing trend for the domain and most subregions. However a considerable difference is seen for the France (FR) subregion, since HisAer has a small increasing trend whereas both Rcp simulations have considerably stronger decreasing trends that are statistically significant.

Finally, between the Rcp simulations themselves there are not systematic differences in trend intensity and sign. The larger AOD of RcpStatic does not seem to considerably impact the trend behavior.

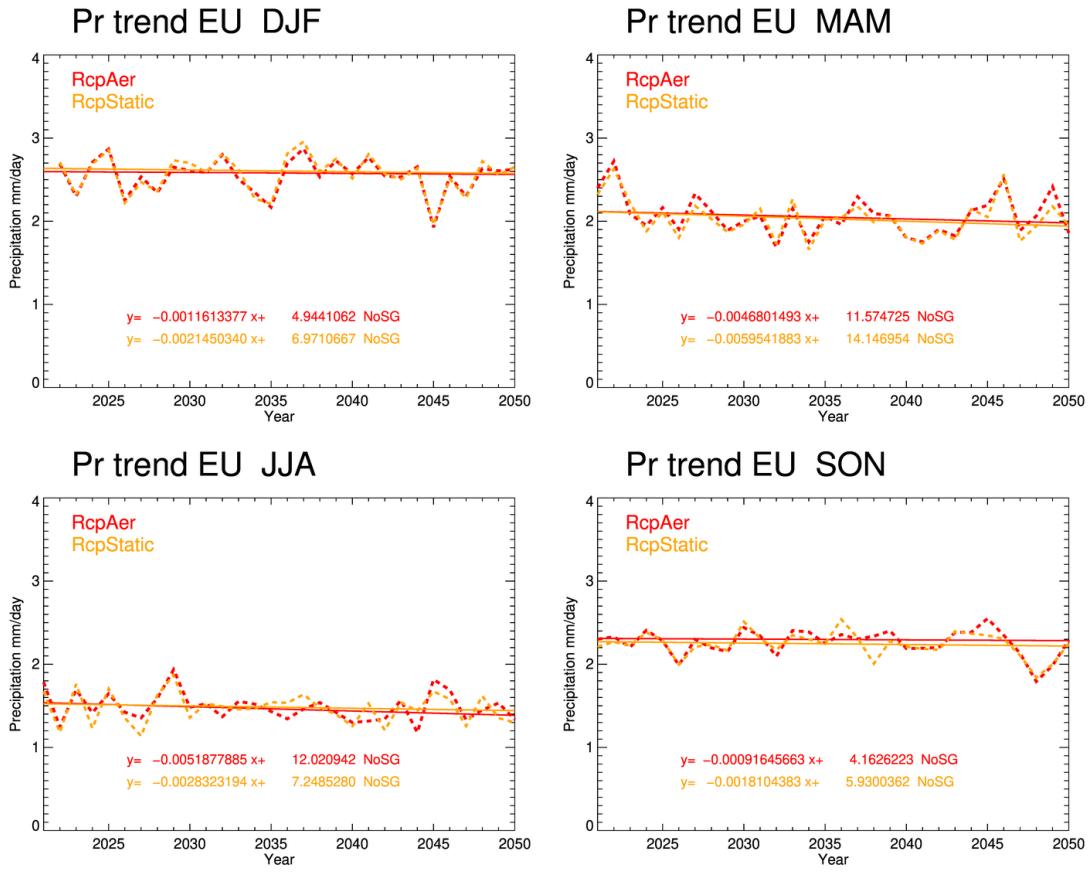

Fig. 71: Seasonal mean precipitation (dashed line) and linear regression line (solid line) using the Theil-Sen method over the EU region and the period 2021-2050. For the Rcp simulations RcpAer (red) and RcpStatic (orange).

Table 41: Slope of the linear regression (10^{-3}x(mm/day)/year) regarding yearly mean precipitation (top three rows) and seasonal mean precipitation for the Rcp simulations. For the period 2021-2050 and for all subdomains including the EU region. For the yearly mean precipitation data for the historical simulation HisAer (period 1971-2000) are also presented to facilitate comparison between the two periods. Negative trends are depicted with blue color cells and positive trends with pale pink color cells. Bold fonts are used to depict trends that are statistically significant at the 90% level.

Year

	EU	BI	IP	FR	ME	SC	AL	MD	EA
RcpAer	-3,1	-3,8	**-10,9**	**-13,4**	-4,8	3,6	-10,5	-9,1	-0,7
RcpStatic	**-4,2**	-7,7	-9,9	**-12,5**	-3,6	4,0	-9,6	-9,4	-6,1
HisAer	-2,3	-3,1	-8,7	4,4	-5,6	-2,7	**-12,2**	-3,5	0,3

Winter

	EU	BI	IP	FR	ME	SC	AL	MD	EA
RcpAer	-1,2	-1,3	-12,9	-12,0	-1,8	7,4	-5,5	-0,9	1,4
RcpStatic	-2,2	-3,5	-12,6	-16,5	-0,3	12,8	-7,3	-6,1	-1,1

Spring

	EU	BI	IP	FR	ME	SC	AL	MD	EA
RcpAer	-4,7	**-12,1**	-9,5	-12,3	-0,4	10,6	2,2	-12,2	2,7
RcpStatic	-6,0	-6,0	-13,3	-8,9	1,6	6,2	-0,8	-21,5	-4,6

Summer

	EU	BI	IP	FR	ME	SC	AL	MD	EA
RcpAer	-5,2	**-12,6**	-2,6	-9,2	-4,5	-6,7	-22,4	-3,4	0,4
RcpStatic	-2,8	-9,1	-2,0	-4,2	-12,1	-4,0	0,1	-3,0	1,6

Autumn

	EU	BI	IP	FR	ME	SC	AL	MD	EA
RcpAer	-0,9	1,8	**-22,7**	-14,0	-9,4	4,4	-18,0	-3,2	-5,1
RcpStatic	-1,8	-4,8	-7,4	-12,7	-17,6	4,0	-21,0	-4,8	-8,1

3. Summary and discussion

The purpose of this study is to assess the impact of aerosol on regional climate simulations over the European domain. We use different aerosol datasets and different modeling options to enable aerosol-radiation and aerosol-cloud interactions in the simulations. We assess mainly the impact of aerosol-radiation interactions (direct and semi-direct effects) and also describe how aerosol-radiation interactions perform when aerosol-cloud interactions are also present.

Aerosol impact

We have seen both from the sensitivity study (2004-2008 period) and the historical simulations (1971-2000) that the impact of aerosol-radiation interactions is considerable on many aspects of the climate. As expected, radiation is more prominently impacted. Clear-sky radiation is significantly reduced all over the domain and the same is true for shortwave radiation. Moreover, the net shortwave radiation at the surface (radiative effect RE) as well as the overall radiation budget at the surface (net shortwave and longwave) are also negative. Spatial correlation between the AOD field and the radiative effect is high (0.6 to 0.9).

The Impact on the direct and diffuse components of shortwave radiation (Rsds) is considerably stronger than that for Rsds. Direct (and direct normalized, DNI) radiation is strongly reduced while diffuse is greatly increased. Therefore, because of the opposite impact on its components, the overall impact on Rsds is constrained. With the introduction of aerosol-radiation interactions the distribution of direct/diffuse ratio changes greatly in favor of the diffuse component and diffuse becomes usually larger than direct radiation. Unfortunately most modeling studies usually explore only the overall shortwave radiation (Rsds) and rarely the direct and diffuse components. This is despite the fact that the direct component is a far more important factor in solar applications than Rsds.

Temperature is another variable that is considerably affected by aerosol-radiation interactions. A cooling is seen over the domain due to the reduction in radiation. This cooling is more intense over land, partly because of the lower thermal capacity of land compared to sea and partly because our simulations lack an ocean model component and rely on prescribed seas surface temperature. Domain averaged cooling can reach -0.5^{o}C depending on season, however on grid point level the temperature reduction can be considerably stronger and reach -1.5 ^{o}C near the maxima of shortwave radiation decrease. The temperature reduction at the surface is moderately spatially correlated with the AOD field as well as with the spatial pattern of radiative effect (RE). The maxima of cooling usually are collocated or close to the maxima of RE. This was not the case in two RegCM studies over Europe (Zanis, 2009; Zanis et al., 2012). Emphasis is given to the fact that temperature is also affected higher in the atmosphere. Cooling is easily seen at the 800hPa level over spots of strong surface cooling. However considerable cooling can be detected also in the middle to upper troposphere, in cases reaching the 400hPa level. This type of cooling is

probably related to the semi-direct aerosol effect and changes in cloudiness. It is interesting that the modeling study of (Schultze and Rockel, 2018) presented a shallow cooling near the surface and heating at the higher levels, something that resulted in the overall stabilization of the atmosphere which in turn led to the decrease of cloud fraction and precipitation. There are instances of such a behavior in our study when aerosol-radiation interactions are enabled, over specific places and seasons (e.g. in summer) however this is not an overall behavior. An exception is the simulation with ultra absorbing aerosol, ARI_Mv1urban, which presents a very intense warming of the middle troposphere accompanied by a strong and shallow surface cooling.

Precipitation is not clearly affected throughout the year in a systematic way by enabling aerosol-radiation interactions. However, most of the ARI group of simulations present small domain averaged precipitation decrease (-2 to -5%) in spring and summer. The lack of an ocean model in our simulations is probably a limitation to study impact on precipitation to its full extent. Since the sea surface temperature cannot change due to the reduction of radiation, evaporation and thus atmospheric humidity may not be reduced to a degree that could cause precipitation reduction. A modeling study that used a coupled atmospheric-ocean model found reduced precipitation and cloud fraction because of the reduced atmospheric humidity (Nabat et al., 2015a). Another modeling study over Europe (Schultze and Rockel, 2018) that covered a long 60 year period, also found precipitation reduction that was attributed to the stabilization of the atmosphere. In our study, the spatial pattern of precipitation change with aerosol introduction is quite patchy in the sensitivity simulations, with small spots of precipitation increase and decrease scattered over the domain. This indicates that internal model variability plays a strong role in the precipitation results. Interestingly, the spatial pattern of precipitation changes is much smoother is the historical simulations, that spanned for a much longer time period (30 years). Probably averaging over a larger period of time has smoothing results for the internal model variability. Moreover, since the historical simulations have some changes in the model parameterizations used (e.g. convection scheme, cloud fraction option etc.) and this could also be partially responsible for the smoother spatial variability of precipitation change.

One major conclusion of this study is that the introduction of aerosol-radiation interactions clearly leads to increased cloud forcing at the surface. This means that cloudiness reacts in a way that lets more radiation to reach the surface due to the semi-direct aerosol effect. This happens due to change in cloud fraction amount and/or due to change in cloud properties. However, since changes in the cloud fraction are constrained, the positive change in cloud forcing (ΔSCRE) must be mainly attributed to a change in the cloud properties and particularly to the decreased reflectivity of clouds. It is impressive that the change in cloud forcing is positive for all ARI simulations, for all seasons and almost over the entire domain. The positive ΔSCRE counteracts up to a degree the direct aerosol effect, constraining the reduction of shortwave radiation at the surface. The role of the semi-direct effect is very important since it take values that range between 20% to 45% (historical) (20-60% in the sensitivities) of the direct aerosol effect, thus being a considerable part of the overall radiative effect at the surface (17-40%). A positive semi-direct shortwave forcing over Europe is also seen in the study of Nabat et al. (2015) that was attributed to the decrease of cloud fraction amount.

A quite interesting result is that in some cases distinct changes have been observed in the general circulation patterns. These changes are definitely not strong. The wind pattern on a seasonal basis is almost identical before and after the introduction of aerosol-radiation interactions. However in some cases, clear anomalies in the wind patterns are seen in both the lower and upper troposphere. The most prominent example is the area in the Balkans and north of the Black Sea in autumn, where a cyclonic anomaly forms close to the area of intense surface cooling. This anomaly is also accompanied by an increase in vertical velocity, cloud fraction, liquid water path and precipitation, indicating that it has an impact on local climate. In general there is a tendency of cyclonic anomalies to form close to areas of strong cooling at the surface.

Implementation of aerosol-radiation interactions in an environment where aerosol-cloud interactions are also present, behaves qualitatively in a similar way to the implementation of only aerosol-radiation interactions. Shortwave radiation is reduced at the surface which leads to an overall cooling. However with both aerosol-radiation and aerosol-cloud interactions enabled, the reduction of shortwave radiation at the surface (and of its direct and diffuse components) is smaller. This is because the change in the cloud forcing (ΔSCRE) is slightly more positive for all seasons and constrains to a larger degree the shortwave radiation decrease. The ΔSCRE now ranges between 25% and 80% of the direct aerosol effect (DRE). Therefore, we have a strong indication that the indirect aerosol effect is further enhancing in our simulations the semi-direct aerosol effect, leading to stronger positive cloud forcing.

Aerosol introduction does not necessarily leads to the improvement of bias. The main biases in most variables examined in both the sensitivity studies and the historical simulations do not drastically change with aerosol introduction, indicating that aerosol representation is not the main cause of bias. Direct normalized irradiance (DNI) is however an exception, since it is highly impacted by aerosol and enabling aerosol-radiation interactions can strongly alter the bias. However the bias in a certain variable, even in DNI, seems to be mainly regulated by the overall characteristics of the simulations, including the initial and boundary conditions and of course the selection of physics parameterization and their tuning and overall model calibration. Therefore whether bias is improved or not with aerosol introduction depends on the state of the bias when aerosol are not present in the simulation. A prime example is seen in the sensitivity simulations for shortwave radiation at the surface (and in DNI) where the bias negative in the control simulation without aerosol and it worsens when introducing aerosol-radiation interactions since they tend to decrease shortwave radiation at the surface.

The role of single scattering albedo (SSA) that defines aerosol absorptivity is very important. First of all, the simulation with ultra absorbing aerosol, ARI_Mv1urban, has the strongest impact among all other sensitivity simulations with aerosol-radiation interaction for all variables examined. It must be noted however that the SSA values of this simulation are unrealistically absorbing (Rodríguez et al., 2013; Tombette et al., 2008; Witte et al., 2011) so ARI_Mv1urban is treated as an idealized experiment that showcases the effects of extremely absorbing aerosols. Interestingly however, the role of SSA is evident in the other simulations featuring more realistic absorption. We have seen that two sensitivity simulations (ARI_Mv1

and ARI_Mv1full) featuring the exact same AOD (MAC-v1) but different SSA fields presented in some cases considerable differences between them (for example temperature in spring and direct radiative effect in summer). It is characteristic that in some of these cases the above simulations had a more similar aerosol impact with simulations that had a different AOD field but very similar SSA values, rather than with the partner simulation with the same AOD but with differentiated aerosol absorptivity. Moreover, we have seen that the first aerosol-radiation interaction option (aer_opt=1) which uses the Tegen climatology produces similar shortwave radiation reduction with the simulations that use the MAC-v1 and MACC aerosol datasets and use the "rural" aerosol type to parameterize the rest aerosol properties, despite the Tegen climatology having lower AOD values. This is because the aerosol of Tegen are more absorbing, leading to a larger radiation reduction per unit of AOD (W/m^2/AOD).

Finally, we have seen that the use of different aerosol datasets (Tegen, MAC-v1, MACC and the CESM1 aerosol) did not lead to dramatic changes on domain averaged values regarding all the variables examined. After all, all the aerosol datasets have a similar spatial pattern of and seasonal behavior again regarding domain averages. However, at a subregional level and even more at a grid point level, there can be large spatial and seasonal differences between the aerosol datasets. This leads to strong differences over these smaller spatial scales. Thus, selection of a proper dataset is important and can have a strong difference. Therefore users are advised to use the newest and most up-to-date aerosol datasets available, as has been recommended by other studies as well (Schultze and Rockel, 2018; Zubler et al., 2011a).

Aerosol options in WRF model

All the aerosol-radiation interaction options tested in the Weather Research and Forecasting Model produce physically consistent results. As expected, shortwave radiation at the surface and its direct component are reduced while diffuse radiation increases. The first aerosol option (aer_opt=1) is a ready-to-use option that can enable aerosol-radiation interactions based on the climatology of Tegen. The Tegen dataset is 3-D meaning that it has values also in the upper troposphere levels, thus there is no need for the parameterization of the vertical aerosol profile. Moreover, Tegen has lower AOD compared to the newer products tested (MAC-v1, MACC). However, the smaller SSA values (more absorbing aerosol) the first aerosol option produces, lead to a similar reduction of shortwave radiation at the surface with the simulations that use larger AOD but have less absorbing aerosol. The second aerosol option (aer_opt=2) uses an external aerosol field provided by the user. Implementation of this option is relatively easy, with the only technical problem being the preparation of the intended aerosol field in a file with a specific WRF-compatible format. The parameterization of single scattering albedo (SSA), asymmetry factor (ASY) and Angstrom exponent based on the "rural" aerosol type provides realistic more realistic results over the European domain. On the other hand, the "urban" aerosol type is extremely absorbing and over Europe it can be useful only in idealized experiments with unrealistically strong aerosol absorptivity. The use of a prescribed vertical profile of AOD in the second

aerosol option seems adequate to simulate the shortwave radiation reduction at the surface. However, in order to fully assess the semi-direct aerosol effect, a prescribed vertical profile could be problematic. The vertical profiles of the first and second aerosol options, as well as the profile produced by the Thompson aerosol-aware scheme, do of course have some similar basic characteristics but also present differences, such as the number of AOD maxima and the height that these are observed. However the impact seen at the troposphere, for variables such cloud fraction and temperature, presents very similar characteristics in both aerosol-radiation interaction options (aer_opt=1 and 2). In essence, what seems to be more impactful to changes higher in the troposphere is the aerosol absorptivity and not the vertical AOD profile.

The Thompson aerosol aware microphysics scheme offers an easy and computationally low cost way to implement interactive aerosol in the WRF model. Moreover, aerosol interaction with radiation can also be enabled, thus including the full spectrum of aerosol effects (aerosol-radiation-cloud interactions). Implementation of this scheme is straightforward, with only some steps required at the preprocessing stage (WPS) of WRF realization in order to prepare aerosol initial and boundary conditions. Even though it explicitly predicts aerosol number concentrations, the aerosol aware scheme is not a fully detailed prognostic aerosol scheme. It relies on some major simplifications such as the categorization of aerosol into only two broad types (water friendly and ice friendly) and the use of an artificial emission flux (based on initial AOD and a mean wind speed value) only for the water-friendly type. In essence, it does not try to forecast the aerosol field in the most precise way, but its purpose is to generate an aerosol field that on the long term approximates the GOCART climatology while on the short term is free to change according to the atmospheric conditions. However, the AOD field generated by the scheme in the sensitivity study during the 2004-2008 period has an abnormal AOD maximum over Eastern Europe consistently seen throughout the year and overall large AOD domain averaged values. This AOD maximum is not seen in any other aerosol dataset used including the two satellite datasets examined. The vertical AOD profile generated by the scheme presents the expected basic characteristics such as an AOD maximum at the lower troposphere and an exponential decrease at higher altitudes. However it produces an AOD maximum that is closer to the surface compared to the profiles of the second (aer_opt=2) and especially the first (aer_opt=1) aerosol options. The stability of the aerosol concentrations over the long term seems adequate. Over the 5 year period covered by the simulations with the aerosol-aware scheme a very small negative trend was detected for the water-friendly aerosol concentrations and a slightly larger negative trend for the ice-friendly aerosol, probably attributed to the lack of an emission field for the ice-friendly aerosol type. Overall, AOD produced a slight decreasing trend that leads to a -1.5% AOD reduction after a 5 year period (plus 1 year spin up time). This is definitely adequate for the simulation of such a time span of several years. However, for much longer simulations (e.g. spanning decades) a decreasing AOD trend of the magnitude observed in our simulations could be problematic since it could lead to considerable AOD reduction during the simulation. Finally, the use of the aerosol-aware scheme required a very small computational cost increase, with time for realization increasing only by ~10%, compared to the Thompson 2008 (Thompson et al., 2008) microphysics scheme. This is a huge advantage compared to systems that describe aerosols with more complexity such as the Weather

Research and Forecasting Model with Chemistry (WRF-Chem) which requires massively larger computational cost.

Cloud cover scheme

Our study highlights the importance of the cloud cover scheme. This scheme is responsible for the production of cloud fraction amount at each grid point. Cloud fraction is not just a diagnostic variable but can be actively used by the radiation scheme and thus has the ability to severely impact radiation amounts. In our study we used two cloud cover schemes, one based on Sundqvist et al. (1989) (icloud=3 option) and the other based on Xu and Randall (1996) (icloud=1 option). Both schemes presented overestimation of cloud fraction for all seasons, while for summer an underestimation over southern Europe was seen. The icloud1 scheme consistently produced smaller cloud fraction amounts, something that improved the overestimation throughout the year, but also led to an increase of cloudiness underestimation in summer over southern Europe. The differences in the produced cloud fraction between the two schemes had a large impact on shortwave radiation at the surface (Rsds). It is characteristic that it exceeded the impact of aerosol-radiation interaction implementation in the model. The difference in domain averaged Rsds was around 16% to 18% for all seasons, much larger (2 to 4 times) than the impact of aerosol-radiation interactions (around 4% to 8%). The differences in shortwave radiation also considerably impacted near surface temperature with domain averaged changes between 0.4 and 0.8^{o}C, also larger than the impact seen by aerosol-radiation interactions. It is important to note however, that the impact of the cloud cover scheme also depends on the radiation scheme used. In our study we used the RRTMG radiation scheme, which makes use of the cloud fraction amount, among other variables such as liquid water path, to estimate radiation amounts. A different radiation scheme could have a different approach for the use of the cloud fraction amount. For example, the Dudhia (1989) radiation scheme assumes only cloud fraction that is either 0 or 1 (cloud-free or overcast sky), thus the impact of a more advanced cloud fraction option could be minimal. Moreover, the impact of the cloud cover scheme might heavily depend on the simulation spatial resolution, since higher resolution could reduce the uncertainty of sub-grid scale cloudiness. Furthermore, the choice of the cumulus (convection) scheme and the boundary layer scheme might also interfere with the cloud cover scheme impact, since some of these schemes can produce their own sub-grid scale cloudiness and modify the final cloud fraction (only in the case of icloud=1). To conclude, despite their potential impacts, the cloud cover schemes are not given any attention in several model evaluation studies (García-Díez et al., 2015; Katragkou et al., 2015; Kotlarski et al., 2014). This study recommends that the cloud cover scheme must be treated as one of the major physics parameterizations of the WRF model.

Historical simulations and Rcp8.5 future simulations

The coupling between WRF and CESM1 was quite successful. Implementation was straightforward since the bias corrected CESM1 data used are offered by NCAR in an easy to use format and cover all the variables needed to drive WRF. The historical simulations have very good evaluation results in the context of other GCM evaluation studies (Cattiaux et al., 2013; McSweeney et al., 2015) as well as compared to RCM modeling studies over Europe (García-Díez et al., 2015; Katragkou et al., 2015; Kotlarski et al., 2014). It is characteristic that bias is improved in most variables compared to the sensitivity simulations driven by reanalysis data. The use of a different model set up in the historical simulations has probably helped in the right direction. For example the use of a different option to parameterize cloud fraction (icloud=1) seems to have reduced the cloudiness overestimation.

We used in both the historical (1971-2000) and Rcp8.5 (2021-2050) simulations the aerosol optical depth (AOD) field that CESM1 used for the respective periods. This aerosol field is the product of chemistry-climate model simulations using an inventory of known and projected emissions (Lamarque et al., 2011, 2010). It is characteristic that both for the historical (after the early 1980s) and the future period the aerosol optical depth presents a decreasing trend over Europe, indicating the decrease of aerosol concentrations, possibly due to the stricter regulations regarding emissions and air quality. It must be noted however, that the decreasing AOD trend in the historical period is considerably stronger than the one seen in the Rcp8.5 future scenario.

A major finding of this study is that transient aerosols do have a considerable impact on trends in shortwave radiation at the surface during the historical period. This is more pronounced after the 1980 when the aerosol optical depth starts decreasing. The use of a realistic aerosol field that has a decreasing trend over time clearly leads to an increasing trend in shortwave radiation (brightening). Moreover a much stronger brightening is seen for the simulated direct normalized irradiance. The brightening of solar radiation over Europe is an observational fact (Wild, 2009) and only the use of time decreasing aerosol enables to simulate it while the use of a static in time aerosol field fails to reproduce it. This has been also the result of the RCM study of Nabat et al. (2014) over Europe and the Mediterranean. Moreover, the study of Bartók et al. (2017) found that EURO-CORDEX regional climate model simulations could not reproduce the brightening of solar radiation over Europe. It is impressive that their ensemble mean trend in radiation was decreasing instead of increasing. This was attributed to the use of static in time aerosol information. On the other hand, global climate models of CMIP5 managed to reproduce the brightening, due to their use of interactive and time varying aerosol. Therefore, aerosol evolution in time can definitely impact the temporal evolution of shortwave radiation at the surface.

The historical simulations clearly present increasing trends for temperature, consistent with the expected climate change warming due to increased greenhouse gases emissions (IPCC AR5). Temperature is also impacted by the increasing trend in shortwave radiation at the surface that takes place to the decreasing aerosol trend. An important finding of this study is that the use of transient, decreasing in time, aerosol leads to a slight but clear enhancement of the already increasing trend in temperature, further intensifying the warming due to the

increased greenhouse gases emissions. Moreover, the use of realistic time evolving aerosol optical depth leads to a small improvement in temperature trend simulation indicating that transient aerosol help to better simulate temperature trends over Europe, a result seen in other studies as well (Van Oldenborgh et al., 2009).

For the main Rcp8.5 simulation of the future climate we used the CESM1 Rcp8.5 aerosol that present considerably smaller AOD values than the ones seen in the historical period. The use of a lower AOD in the future period clearly led to a significant increase in shortwave radiation at the surface (Rsds) compared to the historical period. This increase in Rsds is spatially extensive and is more prominent during summer.

Both Rcp8.5 simulations present an increase of the mean temperature compared to the historical period (1971-2000). Simulation of the future climate (2021-2050) presents a clear warming that ranges between 1^{o}C and 1.7^{o}C regarding domain averages. This warming is stronger during summer and autumn and over Eastern Europe. This strong increase over the eastern part of Europe has also been detected in other simulations over Europe (Jacob et al., 2014).

We have stated, that the use in the future period of a weaker AOD field, clearly lead to an increase of shortwave radiation at the surface. This increase in Rsds also impacts temperature leading to further warming. Therefore another major finding of this study is that expected decrease of AOD in the future over Europe, leads to an intensification of the overall warming of this regions. This extra warming due to the lower future AOD can be considerable, and amounts between 5% (in autumn) and 14% (winter and summer) of the overall detected warming of the future period compared to the historical one.

The Rcp8.5 aerosols of CESM1 also present a decreasing AOD trend during the future period. This decreasing trend does impact the trend in shortwave radiation, slightly intensifying the already positive Rsds trend seen when a static aerosol field is used, however the impact is not as strong as the one seen in the historical period. This is because the decreasing AOD trend in the future period is considerably weaker.

As said above, both Rcp8.5 simulations, either using the time decreasing aerosol or a static in time aerosol field present increasing trends in shortwave radiation for the future period. Interestingly, this positive trend in shortwave radiation is mainly attributed to a positive trend in cloud forcing. Therefore, in both Rcp8.5 simulations, clouds tend to let more radiation to reach the surface over time and this leads to an increasing trend in shortwave radiation. The use of decreasing aerosol over time only helps to slightly intensify this trend.

Finally, regarding future precipitation, there is no clear behavior of change throughout the year, compared to the historical period for the entire domain. However an increase is seen for the central and north-northeast part of Europe, whereas southern Europe presents a tendency to reduce precipitation amount. Similar results are also seen in other simulations over Europe (Jacob et al., 2014). On a seasonal basis, significant changes are seen mainly in spring, where again an increase of future precipitation over Eastern Europe is seen and a decrease over the Iberian Peninsula and parts of the Mediterranean.

4. Conclusions

- All the aerosol-radiation interaction options of the WRF model used in this study presented physically consistent results.
- The Thompson aerosol-aware microphysics scheme is a valuable tool that can implement interactive aerosol and thus aerosol-cloud interactions in the model with negligible computational cost. Its use on prolonged climate simulations however must be examined with caution.
- The cloud cover scheme can have a very strong impact on many climatic variables. It must be treated as one of the major physics parameterizations in the WRF model.
- Introduction of aerosol-radiation interactions leads to:
  - Considerable decrease of shortwave radiation at the surface, a much stronger decrease in direct radiation and a strong increase in diffuse radiation.
  - A cooling over the domain is seen that can be strong over areas of intense radiation reduction. Temperature changes are not only constrained at the surface but are also seen higher in the troposphere.
  - Changes in the general circulation pattern are constrained, however in specific areas and seasons specific circulation anomalies are present and tend to impact the regional climate.
  - Clouds tend to let more radiation to reach the surface due to a decrease in their reflectivity.
- Bias is not necessarily improved with the introduction of aerosol-radiation interactions since it depends on overall model performance and calibration.
- The use of up-to-date and improved aerosol optical depth datasets is recommended. It might not have a large impact on domain averaged values, however at a regional level impact can be considerably larger.
- The coupling of WRF with the global model CESM1 has been quite successful and produced nice evaluation results for the historical simulations.
- Only the use of realistic transient aerosol that decrease over time can produce the radiation increase (brightening) seen over Europe during the historical period.
- The simulations of both the historical (1971-2000) and the future period (2021-2050) present increasing trends in temperature. This is indicative of the warming of the climate.
- The decrease of the aerosol optical depth in the future period leads to an increase in the shortwave radiation at the surface. This impacts temperature further enhancing the warming of the future climate.

To conclude this study, we content that aerosols are an important part of the climate. Aerosol inclusion in a regional climate model is important and deserves our attention since it can strongly impact many aspects of the climatic system and therefore affect the simulated historical, present as well as future climate.

Extented Abstract

The subject of the thesis is to study the effects of atmospheric aerosols on regional climate simulations over Europe with the WRF climate model. We mainly study the interactions of aerosols with radiation (direct and semi-direct effect) while the interactions of aerosols with clouds are also simulated.

The dissertation is divided into two main parts. In the first part, 5-year sensitivity simulations (2004-2008) were performed using different aerosol configurations in the model as well as different datasets of aerosol optical properties. The results showed that the introduction of the aerosol-radiation interaction significantly reduced the shortwave radiation at the surface (-3 to -8%), leading to a decrease in temperature which may well exceed 1 ° C at the regional level. The effect on the direct and diffuse component of the solar radiation is much stronger with a sharp decrease in the direct and a sharp increase in the diffuse component. Minor changes in precipitation and cloud cover were observed and in certain cases parameterization and the communication of radiation and microphysics parameterizations with respect to the radius of cloud particles. Both experiments showed a strong effect on the solar radiation reaching the ground.

In the second part of the thesis, 30 years long simulations were performed with the WRF regional model driven by the global model CESM1, for the historical (1971-2000) and future climate (2021-2050) based on the Rcp8.5 emission scenario. A static in time aerosol field as well as a decreasing in time aerosol field were used. The effect of the aerosol-radiation interactions was similar to that observed in the sensitivity simulations, leading to a decrease in radiation and surface temperature. The use of a realistic aerosol field with a decreasing trend over the historical period has led to an increasing trend of solar radiation at the surface (brightening) which is consistent with observational data. All simulations of the future climate show an increase in temperature over Europe in relation to the historical period. Also, the reduction of the optical depth of the aerosols in the future compared to the historical period leads to increased ground radiation and an intensification of the overall warming.

ΕΛΛΗΝΙΚΗ ΠΕΡΙΛΗΨΗ

Τίτλος διατριβής: Εκτίμηση σφαλμάτων και αβεβαιότητας αλληλεπιδράσεων νεφών-αερολυμάτων-ακτινοβολίας σε κλιματικές προσομοιώσεις περιοχικής κλίμακας.

Συγγραφέας: Βασίλειος Παυλίδης, Φυσικός, MSc: Μετεωρολογία-Κλιματολογία

Περίληψη:

Το αντικείμενο μελέτης της διατριβής είναι οι επιδράσεις των ατμοσφαιρικών αιωρούμενων σωματιδίων (αεροζόλ) σε περιοχικές κλιματικές προσομοιώσεις πάνω από την Ευρώπη με το κλιματικό περιοχικό μοντέλο WRF. Μελετώνται κατά κύριο λόγο οι αλληλεπιδράσεις των αεροζόλ με την ακτινοβολία (direct και semi-direct effect) ενώ προσομοιώνονται και οι αλληλεπιδράσεις των αεροζόλ με τα νέφη.

Η διατριβή χωρίζεται σε δύο κύρια μέρη. Στο πρώτο μέρος πραγματοποιήθηκαν προσομοιώσεις ευαισθησίας διάρκειας 5 ετών (περίοδος 2004-2008) στις οποίες χρησιμοποιήθηκαν διαφορετικές παραμετροποιήσεις των αεροζόλ στο μοντέλο καθώς και διαφορετικά δεδομένα των οπτικών τους ιδιοτήτων. Τα αποτελέσματα έδειξαν ότι η εισαγωγή της αλληλεπίδρασης αεροζόλ-ακτινοβολίας μειώνει σημαντικά την μικρού μήκους κύματος ακτινοβολία στην επιφάνεια (-3 με -8%) οδηγώντας σε μείωση της θερμοκρασίας η οποία σε περιοχικό επίπεδο μπορεί να ξεπεράσει και τον 1^{o}C. Η επίδραση στην άμεση και την διάχυτη συνιστώσα της ηλιακής ακτινοβολίας είναι αρκετά πιο ισχυρή με έντονη μείωση της άμεσης και έντονη αύξηση της διάχυτης συνιστώσας. Παρατηρήθηκαν μικρές αλλαγές στην βροχόπτωση και την νεφοκάλυψη ενώ σε συγκεκριμένες περιπτώσεις παρατηρήθηκαν κυκλωνικές ανωμαλίες στο πεδίο του ανέμου πάνω από τα σημεία έντονης ψύξης. Στο πρώτο μέρος έγιναν επίσης πειράματα ευαισθησίας που αφορούν την επιλογή της παραμετροποίησης της νεφοκάλυψης καθώς και την επικοινωνία των παραμετροποιήσεων της ακτινοβολίας και της μικροφυσικής όσον αφορά την ακτίνα των νεφοσταγόνων. Και τα δύο πειράματα αυτά έδειξαν έντονη επίδραση στην ηλιακή ακτινοβολία που φτάνει στο έδαφος.

Στο δεύτερο μέρος της διατριβής πραγματοποιήθηκαν μεγαλύτερης διάρκειας προσομοιώσεις 30 ετών με το περιοχικό μοντέλο WRF οδηγούμενο από το παγκόσμιο μοντέλο CESM1, για το ιστορικό (1971-2000) αλλά και για το μελλοντικό κλίμα (2021-2050) με βάση το σενάριο εκπομπών Rcp8.5. Έγινε χρήση στατικού στο χρόνο πεδίου αεροζόλ όσο και πεδίου αεροζόλ με μειωτική τάση. Η επίδραση των αλληλεπιδράσεων αεροζόλ-ακτινοβολίας ήταν παρόμοια με αυτήν που παρατηρήθηκε στις προσομοιώσεις ευαισθησίας οδηγώντας σε μείωση της ακτινοβολίας και της θερμοκρασίας στην επιφάνεια. Η χρήση ρεαλιστικού πεδίου αεροζόλ με μειωτική τάση κατά την ιστορική περίοδο οδήγησε σε μια αυξητική τάση της ακτινοβολίας (brightening) η οποία είναι σε σύμπτωση με τα παρατηρησιακά δεδομένα. Όλες οι προσομοιώσεις του μελλοντικού κλίματος δείχνουν μια αύξηση της θερμοκρασίας πάνω από την Ευρώπη σε σχέση με την ιστορική περίοδο. Επίσης η μείωση του οπτικού βάθους των αεροζόλ στην μελλοντική σε σχέση με την ιστορική περίοδο οδηγεί σε αύξηση της ακτινοβολίας στο έδαφος και σε εντατικοποίηση της συνολικής θέρμανσης.

References

Alapaty, K., Herwehe, J. A., Otte, T. L., Nolte, C. G., Bullock, O. R., Mallard, M. S., Kain, J. S. and Dudhia, J.: Introducing subgrid-scale cloud feedbacks to radiation for regional meteorological and climate modeling, Geophys. Res. Lett., 39(24), 2012GL054031, doi:10.1029/2012GL054031, 2012.

Alexandri, G., Georgoulias, A. K., Zanis, P., Katragkou, E., Tsikerdekis, A., Kourtidis, K. and Meleti, C.: On the ability of RegCM4 regional climate model to simulate surface solar radiation patterns over Europe: An assessment using satellite-based observations, Atmos. Chem. Phys., 15(22), 13195–13216, doi:10.5194/acp-15-13195-2015, 2015.

Bae, S. Y., Hong, S.-Y. and Lim, K.-S. S.: Coupling WRF Double-Moment 6-Class Microphysics Schemes to RRTMG Radiation Scheme in Weather Research Forecasting Model, Adv. Meteorol., 2016, 1–11, doi:10.1155/2016/5070154, 2016.

Baró, R., Palacios-Peña, L., Baklanov, A., Balzarini, A., Brunner, D., Forkel, R., Hirtl, M., Honzak, L., Luis Pérez, J., Pirovano, G., San José, R., Schröder, W., Werhahn, J., Wolke, R., Åabkar, R. and Jiménez-Guerrero, P.: Regional effects of atmospheric aerosols on temperature: An evaluation of an ensemble of online coupled models, Atmos. Chem. Phys., 17(15), 9677–9696, doi:10.5194/acp-17-9677-2017, 2017.

Bartók, B., Wild, M., Folini, D., Lüthi, D., Kotlarski, S., Schär, C., Vautard, R., Jerez, S. and Imecs, Z.: Projected changes in surface solar radiation in CMIP5 global climate models and in EURO-CORDEX regional climate models for Europe, Clim. Dyn., 49(7–8), 2665–2683, doi:10.1007/s00382-016-3471-2, 2017.

Basart, S., Pérez, C., Cuevas, E., Baldasano, J. M. and Gobbi, G. P.: Aerosol characterization in Northern Africa, Northeastern Atlantic, Mediterranean Basin and Middle East from direct-sun AERONET observations, Atmos. Chem. Phys., 9(21), 8265–8282, doi:10.5194/acp-9-8265-2009, 2009.

Benas, N., Finkensieper, S., Stengel, M., van Zadelhoff, G.-J., Hanschmann, T., Hollmann, R. and Meirink, J. F.: The MSG-SEVIRI-based cloud property data record CLAAS-2, Earth Syst. Sci. Data, 9(2), 415–434, doi:10.5194/essd-9-415-2017, 2017.

Bruyère, C. L., Done, J. M., Holland, G. J. and Fredrick, S.: Bias corrections of global models for regional climate simulations of high-impact weather, Clim. Dyn., 43(7–8), 1847–1856, doi:10.1007/s00382-013-2011-6, 2014.

Cattiaux, J., Douville, H. and Peings, Y.: European temperatures in CMIP5: origins of present-day biases and future uncertainties, Clim. Dyn., 41(11–12), 2889–2907, doi:10.1007/s00382-013-1731-y, 2013.

Christensen, J. H., Carter, T. R., Rummukainen, M. and Amanatides, G.: Evaluating the perfomance of regional climate models: The PRUDENCE project, Clim. Change, 81(6), 1–6, doi:10.1007/s10584-006-9211-6, 2007.

Clerbaux, N., Ipe, A., De Bock Veerle, Urbain, M., Baudrez, E., Velazquez-Blazquez, A., Akkermans, T., Moreels, J., Hollmann, R., Selbach, N., and Werscheck, M.: CM SAF Aerosol Optical Depth (AOD) Data Record - Edition 1, 15 https://doi.org/10.5676/EUM_SAF_CM/MSG_AOD/V001, 2017.

Colarco, P., Da Silva, A., Chin, M. and Diehl, T.: Online simulations of global aerosol distributions in the NASA GEOS-4 model and comparisons to satellite and ground-based aerosol optical depthfile:///C:/Users/PC/Desktop/Φακελοι/PhD/paper/DaSilva_Thompson_aerosol_2018.pdf, J. Geophys. Res. Atmos., 115(14), doi:10.1029/2009JD012820, 2010.

Cusworth, D. H., Mickley, L. J., Leibensperger, E. M. and Iacono, M. J.: Aerosol trends as a potential driver of regional climate in the central United States: Evidence from observations, Atmos. Chem. Phys., 17(22), 13559–13572, doi:10.5194/acp-17-13559-2017, 2017.

Dee, D. P., Uppala, S. M., Simmons, A. J., Berrisford, P., Poli, P., Kobayashi, S., Andrae, U., Balmaseda, M. A., Balsamo, G., Bauer, P., Bechtold, P., Beljaars, A. C. M., van de Berg, L., Bidlot, J., Bormann, N., Delsol, C., Dragani, R., Fuentes, M., Geer, A. J., Haimberger, L., Healy, S. B., Hersbach, H., Hólm, E. V., Isaksen, L., Kållberg, P., Köhler, M., Matricardi, M., Mcnally, A. P., Monge-Sanz, B. M., Morcrette, J. J., Park, B. K., Peubey, C., de Rosnay, P., Tavolato, C., Thépaut, J. N. and Vitart, F.: The ERA-Interim reanalysis: Configuration and performance of the data assimilation system, Q. J. R. Meteorol. Soc., 137(656), 553–597, doi:10.1002/qj.828, 2011.

Dudhia, J.,: Numerical study of convection observed during the Winter Monsoon Experiment using a mesoscale two–dimensional model. *J.* Atmos. Sci., 46, 3077–3107. doi:10.1175/1520-0469(1989)046<3077:NSOCOD>2.0.CO;2PDF, 1989

Dufresne, J.-L., Gautier, C., Ricchiazzi, P. and Fouquart, Y.: Longwave Scattering Effects of Mineral Aerosols, J. Atmos. Sci., 59(12), 1959–1966, doi:10.1175/1520-0469(2002)059<1959:LSEOMA>2.0.CO;2, 2002.

Forkel, R., Werhahn, J., Hansen, A. B., McKeen, S., Peckham, S., Grell, G. and Suppan, P.: Effect of aerosol-radiation feedback on regional air quality – A case study with WRF/Chem, Atmos. Environ., 53, 202–211, doi:10.1016/j.atmosenv.2011.10.009, 2012.

Forkel, R., Balzarini, A., Baró, R., Bianconi, R., Curci, G., Jiménez-Guerrero, P., Hirtl, M., Honzak, L., Lorenz, C., Im, U., Pérez, J. L., Pirovano, G., San José, R., Tuccella, P., Werhahn, J. and Žabkar, R.: Analysis of the WRF-Chem contributions to AQMEII phase2 with respect to aerosol radiative feedbacks on meteorology and pollutant distributions, Atmos. Environ., 115, 630–645, doi:10.1016/j.atmosenv.2014.10.056, 2015.

García-Díez, M., Fernández, J. and Vautard, R.: An RCM multi-physics ensemble over Europe: multi-variable evaluation to avoid error compensation, Clim. Dyn., 45(11–12), 3141–3156, doi:10.1007/s00382-015-2529-x, 2015.

Ginoux, P., Chin, M., Tegen, I., Prospero, J., Holben, B., Dubovik, O., and Lin, S.-J.: Sources and distributions of dust aerosols simulated with the GOCART model, Journal of Geophysical

Research Atmospheres, 106, 20 255–20 273, 33, https://doi.org/10.1029/2000JD000053, 2001

Giorgi, F. and Gutowski, W.J., J.: Regional Dynamical Downscaling and the CORDEX Initiative, Annual Review of Environment and Resources, 40, 467–490, https://doi.org/10.1146/annurev-environ-102014-021217, 2015.

Grell, G. A. and Freitas, S. R.: A scale and aerosol aware stochastic convective parameterization for weather and air quality modeling, Atmos. Chem. Phys., 14(10), 5233–5250, doi:10.5194/acp-14-5233-2014, 2014.

Gutiérrez, C., Somot, S., Nabat, P., Mallet, M., Gaertner, M. Á. and Perpiñán, O.: Impact of aerosols on the spatiotemporal variability of photovoltaic energy production in the Euro-Mediterranean area, Sol. Energy, 174(March), 1142–1152, doi:10.1016/j.solener.2018.09.085, 2018.

Hansen, J., Sato, M. and Ruedy, R.: Radiative forcing and climate response, J. Geophys. Res. Atmos., 102(D6), 6831–6864, doi:10.1029/96JD03436, 1997.

Haylock, M. R., Hofstra, N., Klein Tank, A. M. G., Klok, E. J., Jones, P. D. and New, M.: A European daily high-resolution gridded data set of surface temperature and precipitation for 1950-2006, J. Geophys. Res. Atmos., 113(20), doi:10.1029/2008JD010201, 2008.

Haywood, J., Office, U. K. M. and Boucher, O.: Estimates of the Direct and Indirect Radiative Forcing Due To Tropospheric Aerosols : a Review, , (1999), 513–543, 2000.

Hofstra, N., Haylock, M., New, M. and Jones, P. D.: Testing E-OBS European high-resolution gridded data set of daily precipitation and surface temperature, J. Geophys. Res. Atmos., 114(21), doi:10.1029/2009JD011799, 2009.

Hogan, R. J. and Illingworth, A. J.: Deriving cloud overlap statistics from radar, Q. J. R. Meteorol. Soc., 126(569), 2903–2909, doi:10.1256/smsqj.56913, 2000.

Hong, S.-Y., Noh, Y. and Dudhia, J.: A New Vertical Diffusion Package with an Explicit Treatment of Entrainment Processes, Mon. Weather Rev., 134(9), 2318–2341, doi:10.1175/MWR3199.1, 2006.

Hubanks, P., Platnick, S., King, M. and Ridgway, B.: MODIS atmosphere L3 gridded product algorithm theoretical basis document Collection 6.0 & 6.1 Version 4.4, Tech. Rep. ATBD-MOD-30, NASA, 2019.

Huszar, P., Miksovsky, J., Pisoft, P., Belda, M. and Halenka, T.: Interactive coupling of a regional climate model and a chemical transport model: evaluation and preliminary results on ozone and aerosol feedback, Clim. Res., 51(1), 59–88, doi:10.3354/cr01054, 2012.

Iacono, M. J., Delamere, J. S., Mlawer, E. J., Shephard, M. W., Clough, S. A. and Collins, W. D.: Radiative forcing by long-lived greenhouse gases: Calculations with the AER radiative transfer models, J. Geophys. Res. Atmos., 113(13), 2–9, doi:10.1029/2008JD009944, 2008.

IPCC, 2014: *Climate Change 2014: Synthesis Report. Contribution of Working Groups I, II and III to the Fifth Assessment Report of the Intergovernmental Panel on Climate Change* [Core Writing Team, R.K. Pachauri and L.A. Meyer (eds.)]. IPCC, Geneva, Switzerland, 151 pp.

IPCC, 2007: *Climate Change 2007: Synthesis Report. Contribution of Working Groups I, II and III to the Fourth Assessment Report of the Intergovernmental Panel on Climate Change* [Core Writing Team, Pachauri, R.K and Reisinger, A. (eds.)]. IPCC, Geneva, Switzerland, 104 pp.

Jacob, D., Petersen, J., Eggert, B., Alias, A., Christensen, O. B., Bouwer, L. M., Braun, A., Colette, A., Déqué, M., Georgievski, G., Georgopoulou, E., Gobiet, A., Menut, L., Nikulin, G., Haensler, A., Hempelmann, N., Jones, C., Keuler, K., Kovats, S., Kröner, N., Kotlarski, S., Kriegsmann, A., Martin, E., van Meijgaard, E., Moseley, C., Pfeifer, S., Preuschmann, S., Radermacher, C., Radtke, K., Rechid, D., Rounsevell, M., Samuelsson, P., Somot, S., Soussana, J.-F., Teichmann, C., Valentini, R., Vautard, R., Weber, B. and Yiou, P.: EURO-CORDEX: new high-resolution climate change projections for European impact research, Reg. Environ. Chang., 14(2), 563–578, doi:10.1007/s10113-013-0499-2, 2014.

Ji, Z., Kang, S., Zhang, Q., Cong, Z., Chen, P. and Sillanpää, M.: Investigation of mineral aerosols radiative effects over High Mountain Asia in 1990–2009 using a regional climate model, Atmos. Res., 178–179, 484–496, doi:10.1016/j.atmosres.2016.05.003, 2016.

Jimenez, P. A., Hacker, J. P., Dudhia, J., Haupt, S. E., Ruiz-Arias, J. A., Gueymard, C. A., Thompson, G., Eidhammer, T. and Deng, A.: WRF-SOLAR: Description and clear-sky assessment of an augmented NWP model for solar power prediction, Bull. Am. Meteorol. Soc., 97(7), 1249–1264, doi:10.1175/BAMS-D-14-00279.1, 2016.

Jiménez, P. A., Dudhia, J., González-Rouco, J. F., Navarro, J., Montávez, J. P. and García-Bustamante, E.: A Revised Scheme for the WRF Surface Layer Formulation, Mon. Weather Rev., 140(3), 898–918, doi:10.1175/MWR-D-11-00056.1, 2012.

Jin, J., Miller, N. L. and Schlegel, N.: Sensitivity Study of Four Land Surface Schemes in the WRF Model, Adv. Meteorol., 2010, 1–11, doi:10.1155/2010/167436, 2010.

Johnson, B. T., Shine, K. P. and Forster, P. M.: The semi-direct aerosol effect: Impact of absorbing aerosols on marine stratocumulus, Q. J. R. Meteorol. Soc., 130(599), 1407–1422, doi:10.1256/qj.03.61, 2004.

Jones, P. D. and Moberg, A.: Hemispheric and Large-Scale Surface Air Temperature Variations: An Extensive Revision and an Update to 2001, J. Clim., 16(2), 206–223, doi:10.1175/1520-0442(2003)016<0206:HALSSA>2.0.CO;2, 2003.

Kain, J. S.: The Kain–Fritsch Convective Parameterization: An Update, J. Appl. Meteorol., 43(1), 170–181, doi:10.1175/1520-0450(2004)043<0170:TKCPAU>2.0.CO;2, 2004.

Karlsson, K. G. and Hollmann, R.: Validation Report, Cloud Products, CM SAF Cloud, Albedo, Radiation dataset, AVHRR-10 based, Edition 1 (CLARA-A1), Tech. rep., Satellite Application Facility on Climate Monitoring, https://doi.org/10.5676/EUM_SAF_CM/CLARA_AVHRR/V001, 2012.

Karlsson, K. G. and Johansson, E.: On the optimal method for evaluating cloud products from passive satellite imagery using CALIPSO-CALIOP data: Example investigating the CM SAF CLARA-A1 dataset, Atmos. Meas. Tech., 6(5), 1271–1286, doi:10.5194/amt-6-1271-2013, 2013.

Karlsson, K. G., Riihelä, A., Müller, R., Meirink, J. F., Sedlar, J., Stengel, M., Lockhoff, M., Trentmann, J., Kaspar, F., Hollmann, R. and Wolters, E.: CLARA-A1: A cloud, albedo, and radiation dataset from 28 yr of global AVHRR data, Atmos. Chem. Phys., 13(10), 5351–5367, doi:10.5194/acp-13-5351-2013, 2013.

Katragkou, E., Garciá-Diéz, M., Vautard, R., Sobolowski, S., Zanis, P., Alexandri, G., Cardoso, R. M., Colette, A., Fernandez, J., Gobiet, A., Goergen, K., Karacostas, T., Knist, S., Mayer, S., Soares, P. M. M., Pytharoulis, I., Tegoulias, I., Tsikerdekis, A. and Jacob, D.: Regional climate hindcast simulations within EURO-CORDEX: Evaluation of a WRF multi-physics ensemble, Geosci. Model Dev., 8(3), 603–618, doi:10.5194/gmd-8-603-2015, 2015.

Kedia, S., Cherian, R., Islam, S., Das, S. K. and Kaginalkar, A.: Regional simulation of aerosol radiative effects and their influence on rainfall over India using WRFChem model, Atmos. Res., 182, 232–242, doi:10.1016/j.atmosres.2016.07.008, 2016.

Koch, D. and Del Genio, A. D.: Black carbon semi-direct effects on cloud cover: Review and synthesis, Atmos. Chem. Phys., 10(16), 7685–7696, doi:10.5194/acp-10-7685-2010, 2010.

Komkoua Mbienda, A. J., Tchawoua, C., Vondou, D. A., Choumbou, P., Kenfack Sadem, C. and Dey, S.: Impact of anthropogenic aerosols on climate variability over Central Africa by using a regional climate model, Int. J. Climatol., 37(1), 249–267, doi:10.1002/joc.4701, 2017.

Kotlarski, S., Keuler, K., Christensen, O. B., Colette, A., Déqué, M., Gobiet, A., Goergen, K., Jacob, D., Lüthi, D., Van Meijgaard, E., Nikulin, G., Schär, C., Teichmann, C., Vautard, R., Warrach-Sagi, K. and Wulfmeyer, V.: Regional climate modeling on European scales: A joint standard evaluation of the EURO-CORDEX RCM ensemble, Geosci. Model Dev., 7(4), 1297–1333, doi:10.5194/gmd-7-1297-2014, 2014.

Lamarque, J., Kyle, G. P., Meinshausen, M., Riahi, K., Smith, S. J., van Vuuren, D. P., Conley, A. J. and Vitt, F.: Global and regional evolution of short-lived radiatively-active gases and aerosols in the Representative Concentration Pathways, Clim. Change, 109(1–2), 191–212, doi:10.1007/s10584-011-0155-0, 2011.

Lamarque, J. F., Bond, T. C., Eyring, V., Granier, C., Heil, A., Klimont, Z., Lee, D., Liousse, C., Mieville, A., Owen, B., Schultz, M. G., Shindell, D., Smith, S. J., Stehfest, E., Van Aardenne, J., Cooper, O. R., Kainuma, M., Mahowald, N., McConnell, J. R., Naik, V., Riahi, K. and Van Vuuren, D. P.: Historical (1850-2000) gridded anthropogenic and biomass burning emissions of reactive gases and aerosols: Methodology and application, Atmos. Chem. Phys., 10(15), 7017–7039, doi:10.5194/acp-10-7017-2010, 2010.

Lawrence, D. M., Oleson, K. W., Flanner, M. G., Thornton, P. E., Swenson, S. C., Lawrence, P. J., Zeng, X., Yang, Z.-L., Levis, S., Sakaguchi, K., Bonan, G. B. and Slater, A. G.: Parameterization improvements and functional and structural advances in Version 4 of the

Community Land Model, J. Adv. Model. Earth Syst., 3(1), n/a-n/a, doi:10.1029/2011MS00045, 2011.

McCormick, M. P., Thomason, L. W. and Trepte, C. R.: Atmospheric effects of the Mt Pinatubo eruption, Nature, 373(6513), 399–404, doi:10.1038/373399a0, 1995.

McSweeney, C. F., Jones, R. G., Lee, R. W. and Rowell, D. P.: Selecting CMIP5 GCMs for downscaling over multiple regions, Clim. Dyn., 44(11–12), 3237–3260, doi:10.1007/s00382-014-2418-8, 2015.

Mehta, M., Singh, R., Singh, A., Singh, N. and Anshumali: Recent global aerosol optical depth variations and trends — A comparative study using MODIS and MISR level 3 datasets, Remote Sens. Environ., 181, 137–150, doi:10.1016/j.rse.2016.04.004, 2016.

Mooney, P. A., Mulligan., F. J. and Fealy, R.: Evaluation of the sensitivity of the weather research and forecasting model to parameterization schemes for regional climates of europe over the period 1990-95, J. Clim., 26(3), 1002–1017, doi:10.1175/JCLI-D-11-00676.1, 2013.

Mueller, R. and Träger-Chatterjee, C.: Brief accuracy assessment of aerosol climatologies for the retrieval of solar surface radiation, Atmosphere (Basel)., 5(4), 959–972, doi:10.3390/atmos5040959, 2014.

Müller, R., Pfeifroth, U., Träger-Chatterjee, C., Trentmann, J. and Cremer, R.: Digging the METEOSAT treasure-3 decades of solar surface radiation, Remote Sens., 7(6), 8067–8101, doi:10.3390/rs70608067, 2015.

Nabat, P., Somot, S., Mallet, M., Sanchez-Lorenzo, A. and Wild, M.: Contribution of anthropogenic sulfate aerosols to the changing Euro-Mediterranean climate since 1980, Geophys. Res. Lett., 41(15), 5605–5611, doi:10.1002/2014GL060798, 2014.

Nabat, P., Somot, S., Mallet, M., Sevault, F., Chiacchio, M. and Wild, M.: Direct and semi-direct aerosol radiative effect on the Mediterranean climate variability using a coupled regional climate system model, Clim. Dyn., 44(3–4), 1127–1155, doi:10.1007/s00382-014-2205-6, 2015a.

Nabat, P., Somot, S., Mallet, M., Michou, M., Sevault, F., Driouech, F., Meloni, D., Di Sarra, A., Di Biagio, C., Formenti, P., Sicard, M., Léon, J. F. and Bouin, M. N.: Dust aerosol radiative effects during summer 2012 simulated with a coupled regional aerosol-atmosphere-ocean model over the Mediterranean, Atmos. Chem. Phys., 15(6), 3303–3326, doi:10.5194/acp-15-3303-2015, 2015b.

Nakanishi, M. and Niino, H.: An Improved Mellor–Yamada Level-3 Model: Its Numerical Stability and Application to a Regional Prediction of Advection Fog, Boundary-Layer Meteorol., 119(2), 397–407, doi:10.1007/s10546-005-9030-8, 2006.

Norris, J. R. and Wild, M.: Trends in aerosol radiative effects over Europe inferred from observed cloud cover, solar “dimming,” and solar “brightening,” J. Geophys. Res., 112(D8), D08214, doi:10.1029/2006JD007794, 2007.

Van Oldenborgh, G. J., Drijfhout, S., Van Ulden, A., Haarsma, R., Sterl, A., Severijns, C., Hazeleger, W. and Dijkstra, H.: Western Europe is warming much faster than expected, Clim. Past, 5(1), 1–12, doi:10.5194/cp-5-1-2009, 2009.

Oleson, K. W., Lawrence, D. M., Gordon, B., Flanner, M. G., Kluzek, E., Peter, J., Levis, S., Swenson, S. C., Thornton, E., Dai, A., Decker, M., Dickinson, R., Feddema, J., Heald, C. L., Lamarque, J., Niu, G., Qian, T., Running, S., Sakaguchi, K., Slater, A., Stöckli, R., Wang, A., Yang, L., Zeng, X. and Zeng, X.: Technical Description of version 4 . 0 of the Community Land Model (CLM), , (April), 2010.

Péré, J. C., Bessagnet, B., Mallet, M., Waquet, F., Chiapello, I., Minvielle, F., Pont, V. and Menut, L.: Direct radiative effect of the Russian wildfires and its impact on air temperature and atmospheric dynamics during August 2010, Atmos. Chem. Phys., 14(4), 1999–2013, doi:10.5194/acp-14-1999-2014, 2014.

Platnick, S., et al.: MODIS Atmosphere L3 Monthly Product. NASA MODIS Adaptive Processing System, Goddard Space Flight Center, USA: http://dx.doi.org/10.5067/MODIS/MOD08_M3.006, 2015

Powers, J. G., Klemp, J. B., Skamarock, W. C., Davis, C. A., Dudhia, J., Gill, D. O., Coen, J. L., Gochis, D. J., Ahmadov, R., Peckham, S. E., Grell, G. A., Michalakes, J., Trahan, S., Benjamin, S. G., Alexander, C. R., Dimego, G. J., Wang, W., Schwartz, C. S., Romine, G. S., Liu, Z., Snyder, C., Chen, F., Barlage, M. J., Yu, W. and Duda, M. G.: The weather research and forecasting model: Overview, system efforts, and future directions, Bull. Am. Meteorol. Soc., 98(8), 1717–1737, doi:10.1175/BAMS-D-15-00308.1, 2017.

Qian, Y. and Giorgi, F.: Interactive coupling of regional climate and sulfate aerosol models over eastern Asia, J. Geophys. Res. Atmos., 104(D6), 6477–6499, doi:10.1029/98JD02347, 1999.

Qian, Y., Ruby Leung, L., Ghan, S. J. and Giorgi, F.: Regional climate effects of aerosols over China: modeling and observation, Tellus B, 55(4), 914–934, doi:10.1046/j.1435-6935.2003.00070.x, 2003.

Quaas, J.: Evaluating the “critical relative humidity” as a measure of subgrid-scale variability of humidity in general circulation model cloud cover parameterizations using satellite data, J. Geophys. Res. Atmos., 117(9), 1–10, doi:10.1029/2012JD017495, 2012.

Ramanathan, V., Crutzen, P. J., Kiehl, J. T. and Rosenfeld, D.: Atmosphere: Aerosols, climate, and the hydrological cycle, Science (80-.)., 294(5549), 2119–2124, doi:10.1126/science.1064034, 2001.

Rodríguez, E., Kolmonen, P., Sundström, A.-M., Sogacheva, L., Virtanen, T. and de Leeuw, G.: Satellite study over Europe to estimate the single scattering albedo and the aerosol optical depth, in AIP Conference Proceedings, vol. 1531, pp. 196–199., 2013.

Ruiz-Arias, J. A., Dudhia, J., Santos-Alamillos, F. J. and Pozo-Vázquez, D.: Surface clear-sky shortwave radiative closure intercomparisons in the Weather Research and Forecasting model, J. Geophys. Res. Atmos., 118(17), 9901–9913, doi:10.1002/jgrd.50778, 2013.

Ruiz-Arias, J. A., Dudhia, J. and Gueymard, C. A.: A simple parameterization of the short-wave aerosol optical properties for surface direct and diffuse irradiances assessment in a numerical weather model, Geosci. Model Dev., 7(3), 1159–1174, doi:10.5194/gmd-7-1159-2014, 2014.

Sanchez-Lorenzo, A., Brunetti, M., Calbó, J. and Martin-Vide, J.: Recent spatial and temporal variability and trends of sunshine duration over the Iberian Peninsula from a homogenized data set, J. Geophys. Res., 112(D20), D20115, doi:10.1029/2007JD008677, 2007.

Sarangi, C., Kanawade, V. P., Tripathi, S. N., Thomas, A. and Ganguly, D.: Aerosol-induced intensification of cooling effect of clouds during Indian summer monsoon, Nat. Commun., 9(1), 3754, doi:10.1038/s41467-018-06015-5, 2018.

Schultze, M. and Rockel, B.: Direct and semi-direct effects of aerosol climatologies on long-term climate simulations over Europe, Clim. Dyn., 50(9–10), 3331–3354, doi:10.1007/s00382-017-3808-5, 2018.

Schulz, J., Albert, P., Behr, H.-D., Caprion, D., Deneke, H., Dewitte, S., Dürr, B., Fuchs, P., Gratzki, A., Hechler, P., Hollmann, R., Johnston, S., Karlsson, K.-G., Manninen, T., Müller, R., Reuter, M., Riihelä, A., Roebeling, R., Selbach, N., Tetzlaff, A., Thomas, W., Werscheck, M., Wolters, E. and Zelenka, A.: Operational climate monitoring from space: the EUMETSAT Satellite Application Facility on Climate Monitoring (CM-SAF), Atmos. Chem. Phys., 9(5), 1687–1709, doi:10.5194/acp-9-1687-2009, 2009.

Sen, P. K.: Estimates of the Regression Coefficient Based on Kendall's Tau, J. Am. Stat. Assoc., 63(324), 1379–1389, doi:10.1080/01621459.1968.10480934, 1968.

Da Silva, N., Mailler, S. and Drobinski, P.: Aerosol indirect effects on summer precipitation in a regional climate model for the Euro-Mediterranean region, Ann. Geophys., 36(2), 321–335, doi:10.5194/angeo-36-321-2018, 2018.

Skamarock, W. C., Klemp, J. B., Dudhi, J., Gill, D. O., Barker, D. M., Duda, M. G., Huang, X.-Y., Wang, W. and Powers, J. G.: A Description of the Advanced Research WRF Version 3, Tech. Rep., (June), 113, doi:10.5065/D6DZ069T, 2008.

Solmon, F., Mallet, M., Elguindi, N., Giorgi, F., Zakey, A. and Konaré, A.: Dust aerosol impact on regional precipitation over western Africa, mechanisms and sensitivity to absorption properties, Geophys. Res. Lett., 35(24), L24705, doi:10.1029/2008GL035900, 2008.

Solmon, F., Elguindi, N. and Mallet, M.: Radiative and climatic effects of dust over West Africa, as simulated by a regional climate model, Clim. Res., 52(1), 97–113, doi:10.3354/cr01039, 2012.

Squintu, A. A., van der Schrier, G., Brugnara, Y. and Klein Tank, A.: Homogenization of daily ECA&D temperature series, Int. J. Climatol., 1–25, doi:10.1002/joc.5874, 2019.

Stjern, C. W., Kristjánsson, J. E. and Hansen, A. W.: Global dimming and global brightening-an analysis of surface radiation and cloud cover data in northern Europe, Int. J. Climatol., 29(5), 643–653, doi:10.1002/joc.1735, 2009.

Streets, D. G., Wu, Y. and Chin, M.: Two-decadal aerosol trends as a likely explanation of the global dimming/brightening transition, Geophys. Res. Lett., 33(15), L15806, doi:10.1029/2006GL026471, 2006.

Sundqvist H., Berge E., Kristjánsson. J. E., 1989. Condensation and cloud parameterization studies with a mesoscale numerical weather prediction model, Mon. Weather Rev., 117, 1641–1657.

Tegen, I., Hollrig, P., Chin, M., Fung, I., Jacob, D. and Penner, J.: Contribution of different aerosol species to the global aerosol extinction optical thickness: Estimates from model results, J. Geophys. Res. Atmos., 102(D20), 23895–23915, doi:10.1029/97JD01864, 1997.

Theil, H.: A rank-invariant method of linear and polynomialregression analysis. Springer, Netherlands. doi:10.1007/978-94-011-2546-8_20, 1992

Thompson, G. and Eidhammer, T.: A Study of Aerosol Impacts on Clouds and Precipitation Development in a Large Winter Cyclone, J. Atmos. Sci., 71(10), 3636–3658, doi:10.1175/JAS-D-13-0305.1, 2014.

Thompson, G., Field, P. R., Rasmussen, R. M. and Hall, W. D.: Explicit Forecasts of Winter Precipitation Using an Improved Bulk Microphysics Scheme. Part II: Implementation of a New Snow Parameterization, Mon. Weather Rev., 136(12), 5095–5115, doi:10.1175/2008MWR2387.1, 2008.

Tombette, M., Chazette, P., Sportisse, B. and Roustan, Y.: Simulation of aerosol optical properties over Europe with a 3-D size-resolved aerosol model: comparisons with AERONET data, Atmos. Chem. Phys., 8(23), 7115–7132, doi:10.5194/acp-8-7115-2008, 2008.

Tuccella, P., Menut, L., Briant, R., Deroubaix, A., Khvorostyanov, D., Mailler, S., Siour, G. and Turquety, S.: Implementation of Aerosol-Cloud Interaction within WRF-CHIMERE Online Coupled Model: Evaluation and Investigation of the Indirect Radiative Effect from Anthropogenic Emission Reduction on the Benelux Union, Atmosphere (Basel)., 10(1), 20, doi:10.3390/atmos10010020, 2019.

Vestreng, V., Myhre, G., Fagerli, H., Reis, S. and Tarrasón, L.: Twenty-five years of continuous sulphur dioxide emission reduction in Europe, Atmos. Chem. Phys., 7(13), 3663–3681, doi:10.5194/acp-7-3663-2007, 2007.

Wild, M.: Global dimming and brightening: A review, J. Geophys. Res., 114(1), D00D16, doi:10.1029/2008JD011470, 2009.

Witte, J. C., Douglass, A. R., da Silva, A., Torres, O., Levy, R. and Duncan, B. N.: NASA A-Train and Terra observations of the 2010 Russian wildfires, Atmos. Chem. Phys., 11(17), 9287–9301, doi:10.5194/acp-11-9287-2011, 2011.

Xu, Y., Lamarque, J. and Sanderson, B. M.: The importance of aerosol scenarios in projections of future heat extremes, , 393–406, doi:10.1007/s10584-015-1565-1, 2018.

Xu, K.-M., Randall, D. A.,: A semiempirical cloudiness parameterization for use in climate models. J. Atmos. Sci., 53, 3084-3102, 1996

Zanis, P.: A study on the direct effect of anthropogenic aerosols on near surface air temperature over Southeastern Europe during summer 2000 based on regional climate modeling, Ann. Geophys., 27(10), 3977–3988, doi:10.5194/angeo-27-3977-2009, 2009.

Zanis, P., Ntogras, C., Zakey, A., Pytharoulis, I. and Karacostas, T.: Regional climate feedback of anthropogenic aerosols over Europe using RegCM3, Clim. Res., 52(1), 267–278, doi:10.3354/cr01070, 2012.

Zubler, E. M., Lohmann, U., Lüthi, D. and Schär, C.: Intercomparison of aerosol climatologies for use in a regional climate model over Europe, Geophys. Res. Lett., 38(15), 1–5, doi:10.1029/2011GL048081, 2011a.

Zubler, E. M., Folini, D., Lohmann, U., Ltühi, D., Schr, C. and Wild, M.: Simulation of dimming and brightening in Europe from 1958 to 2001 using a regional climate model, J. Geophys. Res. Atmos., 116(18), 1–13, doi:10.1029/2010JD015396, 2011b.

Acknowledgments

This research is co-financed by Greece and the European Union (European Social Fund- ESF) through the Operational Programme «Human Resources Development, Education and Lifelong Learning» in the context of the project "Strengthening Human Resources Research Potential via Doctorate Research" (MIS-5000432), implemented by the State Scholarships Foundation (IKY).

We acknowledge the support of the Greek Research and Technology Network (GRNET) High Performance Computing (HPC) infrastructure that provided the computational resources necessary for the model simulations (pr006005_thin). We also acknowledge the IT centre of the Aristotle University of Thessaloniki and its HPC infrastructure.

We acknowledge EUMETSAT for providing the satellite data through the Satellite Application Facility on Climate Monitoring (CM SAF) (www.cmsaf.eu). Moreover we acknowledge the E-OBS dataset from the EU-FP6 project ENSEMBLES (http://ensembles-eu.metoffice.com) and the data providers in the ECA&D project (http://www.ecad.eu) and the use of MAC-v1 aerosol climatology data (ftp://ftp-projects.zmaw.de). We also acknowledge ECMWF (www.ecmwf.int) for providing the ERA-Interim reanalysis data as well as the MACC aerosol data. We acknowledge NASA for providing the MODIS satellite data.

We acknowledge the National Center for Atmospheric Research (NCAR) and all its people that helped in this study. We especially thank Andreas Prein, Cindy Bruyere, James Done and all the people in the C3WE center as well as Greg Thompson, Jimy Dudhia, Pedro Jimenez and Dave Gill.

The author would also like to thank the thesis supervisor Ass.Prof. Eleni Katragkou for the excellent cooperation and the entire supervisory committee for their help and guidance.

I would also like to thank my family and friends for all their support throughout this project.

Finally the author would like to thank he WRF unicorns that helped him to successfully complete this study.

This research is co-financed by Greece and the European Union (European Social Fund- ESF) through the Operational Programme «Human Resources Development, Education and Lifelong Learning» in the context of the project "Strengthening Human Resources Research Potential via Doctorate Research" (MIS-5000432), implemented by the State Scholarships Foundation (IKY)

Ευρωπαϊκή Ένωση
European Social Fund

Operational Programme
Human Resources Development,
Education and Lifelong Learning
Co-financed by Greece and the European Union

ΕΣΠΑ 2014-2020
ανάπτυξη - εργασία - αλληλεγγύη

Το έργο συγχρηματοδοτείται από την Ελλάδα και την Ευρωπαϊκή Ένωση (Ευρωπαϊκό Κοινωνικό Ταμείο) μέσω του Επιχειρησιακού Προγράμματος «Ανάπτυξη Ανθρώπινου Δυναμικού, Εκπαίδευση και Διά Βίου Μάθηση», στο πλαίσιο της Πράξης «Ενίσχυση του ανθρώπινου ερευνητικού δυναμικού μέσω της υλοποίησης διδακτορικής έρευνας» (MIS-5000432), που υλοποιεί το Ίδρυμα Κρατικών Υποτροφιών (ΙΚΥ)

Ευρωπαϊκή Ένωση
Ευρωπαϊκό Κοινωνικό Ταμείο

Επιχειρησιακό Πρόγραμμα
Ανάπτυξη Ανθρώπινου Δυναμικού,
Εκπαίδευση και Διά Βίου Μάθηση
Με τη συγχρηματοδότηση της Ελλάδας και της Ευρωπαϊκής Ένωσης

ΕΣΠΑ 2014-2020
ανάπτυξη - εργασία - αλληλεγγύη